GEOCHEMISTRY AND PETROGENESIS OF PERINTHATTA ANORTHOSITE, NORTHERN KERALA

THESIS SUBMITTED TO THE

COCHIN UNIVERSITY OF SCIENCE AND TECHNOLOGY

IN PARTIAL FULFILMENT OF THE REQUIREMENTS

FOR THE DEGREE OF

DOCTOR OF PHILOSOPHY

IN THE FACULTY OF MARINE SCIENCE

BY

P. SONEY KURIEN

DEPARTMENT OF MARINE GEOLOGY AND GEOPHYSICS
SCHOOL OF MARINE SCIENCES
COCHIN UNIVERSITY OF SCIENCE AND TECHNOLOGY
LAKESIDE CAMPUS, COCHIN – 682 016

MAY 2000

Dedicated to my family

DECLARATION

I, P. Soney Kurien, do hereby declare that the thesis entitled "**Geochemistry and Petrogenesis of Perinthatta Anorthosite, Northern Kerala**" is a genuine record of research work done by me under the supervision of **Dr. C.G. Nambiar**, Reader, Department of Marine Geology and Geophysics, School of Marine Sciences, Cochin University of Science and Technology, Lakeside Campus, Cochin – 682 016. This work has not been previously formed the basis for the award of any degree or diploma of this or any other University or other institute of learning.

Cochin – 16

May 2, 2000

P. SONEY KURIEN

CERTIFICATE

I certify that this thesis, "**Geochemistry and Petrogenesis of Perinthatta Anorthosite, Northern Kerala**" has been prepared by P. Soney Kurien under my supervision and guidance in partial fulfilment of the requirements for the degree of Doctor of Philosophy and no part thereof has been submitted for any other degree.

Cochin – 16.
May 2, 2000

C.G. Nambiar
(Research Supervisor)
Dept. of Marine Geology and Geophysics
School of Marine Sciences
Cochin University of Science and Technology
Cochin – 682 016.

Preface

This report deals essentially with the geochemistry and petrogenesis of Perinthatta anorthosite. The work also addresses the geological setting of the pluton in terms of its field relationships and petrography and the structure and metamorphism of the region and examines its relation with the associated plutons. For the sake of convenience, the thesis is divided into six chapters.

The first chapter gives a general introduction to the topic in terms of regional geology, petrogenetic problem of anorthosites and the objectives and methodology adopted in the work.

The second chapter deals with the structure of the region and the third chapter attempts a synthesis of metamorphism of the northern Kerala.

Chapter IV describes the field aspects and petrography of anorthositic rocks.

The fifth chapter deals with the geochemistry or anorthositic rocks and the petrogenetic interpretations based on this. It also incorporates the mineral chemistry of the anorthositic rocks and thermobarometric calculations and the results of preliminary isotope analysis on the pluton.

The last chapter gives an account of the field, petrographic, geochemical and petrogenetic aspects of other plutonic rocks spatially associated with Perinthatta anorthosite and examines their genetic relationship with the anorthositic rocks.

The summary of the work is given at the end which is followed by a bibliography of cited references and three appendices.

ACKNOWLEDGEMENTS

Contents

Chapter IV. Field relationships and petrography

Chapter V. GEOCHEMISTRY AND PETROGENESIS

Chapter   VI. ASSOCIATED PLUTONS

SUMMARY

BIBLIOGRAPHY

List of Figures

List of Tables

Chapter I

INTRODUCTION

1.1 Regional geology— *Geology of South India with special reference to northern Kerala*

The South Indian shield is regarded as a classic terrain for Precambrian research and has been studied extensively during the last few decades. Many important theories on crustal evolution like granulite genesis at low P_{H_2O} (Janardhan et al, 1979) emerged out of the studies on this terrain. Excellent reviews or compilations of works on the general geological aspects of the Precambrians of South India are available (Naqvi and Rogers, 1987; Radhakrishna et al, 1990; Radhakrishna and Ramakrishnan, 1990 and Radhakrishna, 1993; Mahadevan, 1994). This shield has a triangular shape and this reflects the lines of tectonic separation during break-up of the Gondwana super continent (Drury and Holt, 1980). Some recent geochronological studies show that the southern Indian shield is a mosaic of several crustal blocks (Fig. 1.1) with contrasting geological histories from Middle Archaean to Early Palaeozoic (Harris et al., 1994; Mahabaleshwar et al., 1995; Unnikrishnan-Warrier et al., 1995; Jayananda and Peucat, 1996). The dominant rock types in the southern part of the peninsula include gneisses, charnockites, khondalites, schists and granites (Fig. 1.2).

The major geological unit of the Precambrians of South India is a polyphase 3300 to 2900 Ma old migmatitic gneiss complex which was metamorphosed to granulite facies about 2600 Ma ago with the development of an extensive charnockite-khondalite zone. A still older major granulite forming event was recorded at 3000 Ma (Mahabaleshwar and Peucat, 1988; Jayanada and Peucat, 1996). Later the terrain was dissected by several shear belts and then the terrain was affected by retrogressive metamorphism (Raith et al., 1983). A later Pan-African granulite facies metamorphism was recorded from several locations (Choudhary et al.,1992; Santosh et al., 1992; Bartlett et al., 1995;

1
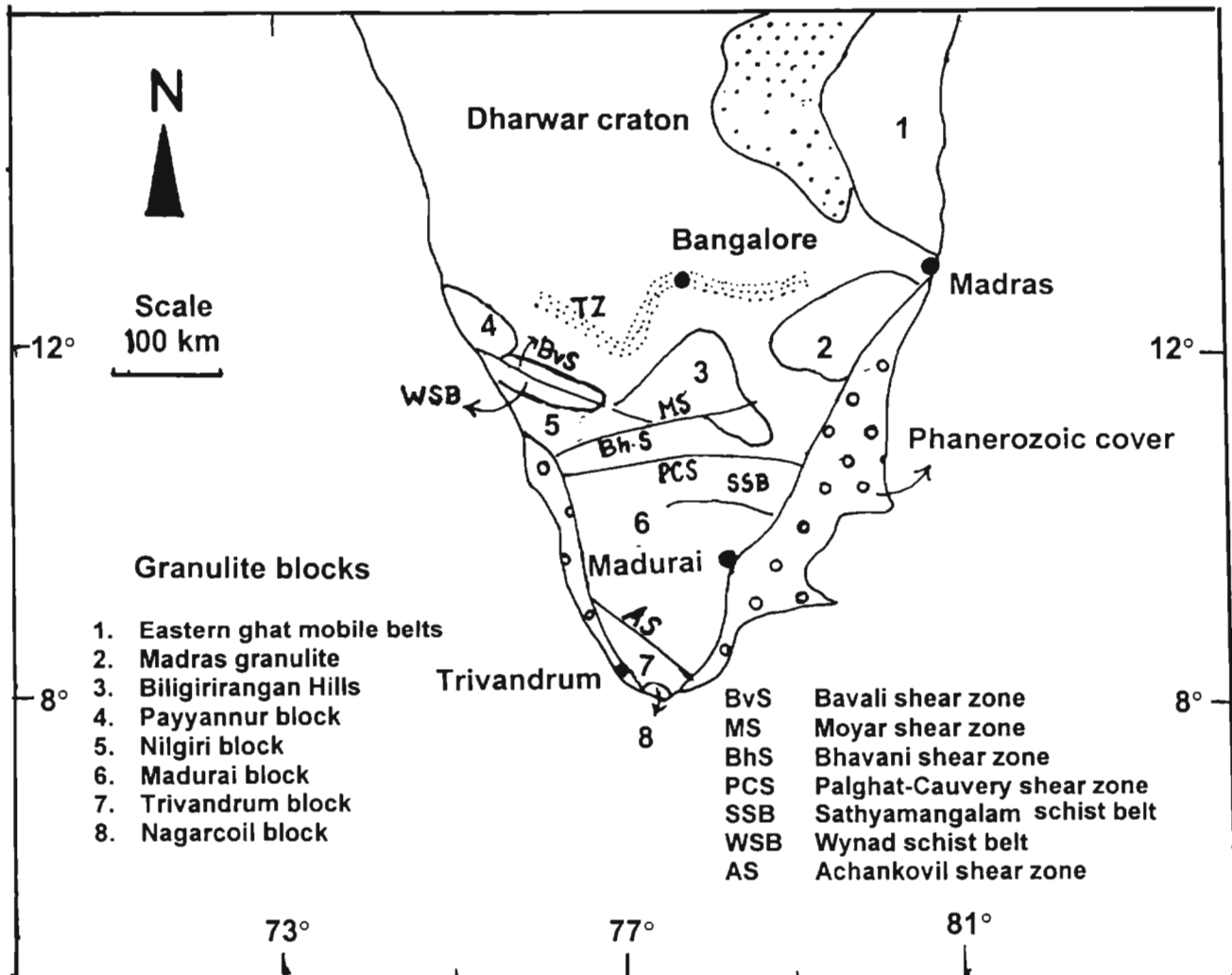
Fig.1.1 Generalized map of southern Peninsular India showing major shear zones and granulite blocks (modified after Gopalakrishna et al.1975; Naqvi and Rogers, 1983; Nambiar, et al., 1992 Unnikrishnan-Warrier et al. 1995; Mohan and Jayananda, 1999)

Scale

50 km

LEGEND

	Mesozoic cover
	Cuddapah Kurnool bsin
	Closepet plutonic belt
	Post-kinematic granitoids
---	Major shear belts

	Dharwars
	Sargurs
	Peninsular gneiss
	Charnockites
	Khondalites

Mangalore
Kannur
Cochin
Madras

Transition zone
Bavali SZ
Moyar SZ
Bhavani SZ
Palghat Cauvery SZ
Achankovil SZ

12°
10°
8°

75°
77°
79°
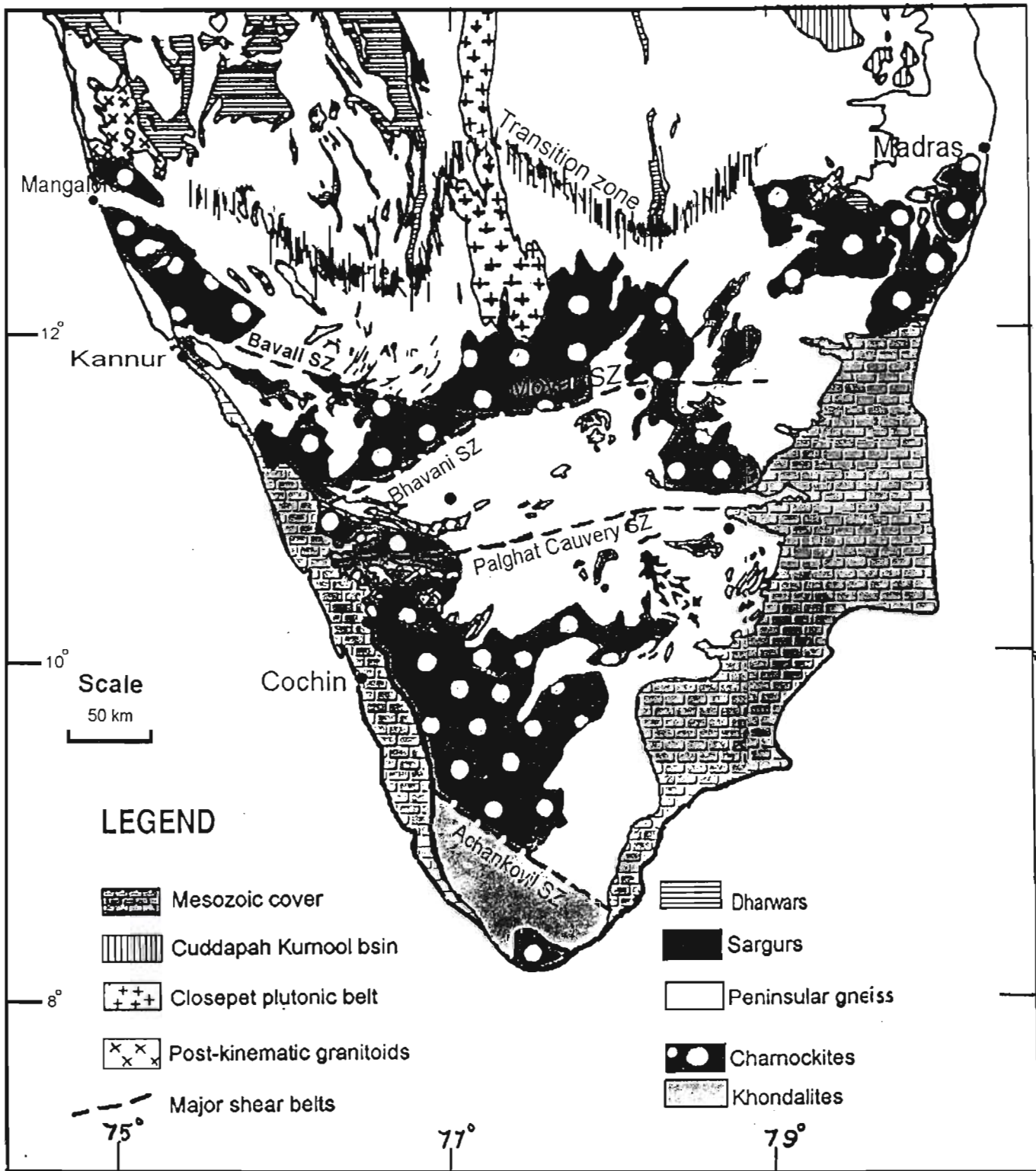
Jayananda et al., 1995). Based on geographic distribution, lithology, geochronologic and isotopic data, southern Indian shield is divided into three principal domains: the Dharwar Craton (DC), Southern Granulite Terrain (SGT) and Eastern Ghats Mobile Belt (EGMB). A transition zone separates the SGT from DC. Geothermobarometric studies across different granulite blocks in southern India show wide ranging P-T conditions of metamorphism (700-1000°C and 5-10kb) as reflected in a series of recent works (Harris et al., 1982; Raith et al., 1988a; Raith et al., 1988b; Touret, 1988; Raith et al., 1990; Ravindra Kumar and Chacko, 1994; Chacko et al., 1996; Rameshwar Rao and Narayana, 1996 and Srikantappa, 1996).

Geographically, the South Indian shield encompasses Kerala, Tamil Nadu, Karnataka, Andhra Pradesh and parts of Orissa, Madhya Pradesh and Maharashtra. Kerala forms the western segment of the Southern Granulite Terrain. The Precambrian rocks of the state essentially include charnockites, khondalites, gneisses and schists. Southern part of the state, south of the Achankovil shear zone, exposes khondalite group of rocks as the main rock type. From north of the Achankovil shear zone up to the southern flank of the Palghat gap, the rocks are predominantly charnockites. Charnockites, mafic granulites, schists and gneisses are exposed in the northern part of Kerala.

The oldest supracrustal rock association in northern Kerala is represented by bands of quartz-mica schists with kyanite, quartz-sericite schist, quartzites, meta-ultramafites and metapyroxenites in various stages of migmatization and is designated as the Wynad Group (Nair, et al.,1976). These high grade schists and ultramafic enclaves occurring as several linear bands and broadly parallel linear belts trending NNW-SSE in parts of Wynad and Kannur (Cannanore) districts. This belt is known as Wynad schist belt and it extends from Sultan's Battery, through Manantoddy to Talipparamba and Payyannur. These schistose rocks are described as equivalent to the Sargur complex of Karnataka. The Vengad group of rocks spread over an area of 300 sq.km in Cannanore district of

Northern Kerala forms a lensoid basin with the longer axis trending NW. The rocks of the Vengad group apparently overlie charnockites, gneisses and high grade schists of Wynad group and consist of schists and quartzites with a conglomerate at the base. Occurrence of conglomerate at Vengad at the base of the schistose formations indicates that the Vengad group of rocks is equivalent to the Dharwar group of Karnataka and has been assigned a Proterozoic age (Nair et al.,1980).

Charnockite is the major rock seen in the northern Kerala (Fig. 1.3). Wynad schist belt separates the charnockites of northern Kerala into a northern and a southern province. Charnockites of these two provinces are different in many aspects like petrography, P-T conditions of metamorphism and geochemistry (Nambiar, 1987).

The northern charnockite province has coarse grained, mostly masssive, felsic charnockites as the dominant rock type. In general, these rocks are dark bluish grey, massive and coarse grained. Retrogression of charnockite to gneisses with hydrous mineral assemblages are rare in the area. The P-T path of this province calculated from a sample of charnockite of the northern province (Nambiar et al., 1989) changes from 860°C, 10.5 kb to 640°C, 6.5kb. Basic granulites which are seen as irregular or lensoid bodies or bands within charnockite form the second important rock type of this province.

Charnockites of the southern province contain enclaves of basic granulite, high-K granulites and hronblende-biotite gneisses (Nambiar et al., 1992). Chemically these charnockites are tonalitic or andesitic. These massive or feebly foliated rocks are cut across in several places by intrusives causing retrogression in the host charnockites. P-T estimates of a sample from the southern charnockite province gave a core and a rim temperature of 860°C and 640°C respectively with the corresponding pressures of 10.5kb and 6kb respectively (Nambiar et al., 1992).

3

Scale

0   10km

Sagur

Virajpet

Mananthavady

Kalpatta

Waying

Tritty

Calicut

Tellicherry

Kannur

Bavali shear

N

A R A B I A N   S E A

Nilleswaram

Payyannur

12° 30'

12° 00'

11° 30'

75° 00'   75° 30'   76° 00'   76° 30'

Dolerite/Gabbro dyke
Granite/Syenite
Anorthosite
Gabbro
Diorite
Quartz-Mica schist & Quartzite
Biotie-Hornblende gneiss
with supracrustal enclaves
Hornblende gneiss
Charnockite
Mafic granulite
Major shear
Minor shear/Fault
Trend lines
State boundary

Two main ages of charnockite formation in South India have been repeatedly reported. First major granulite forming event close to 2.5 Ga was confirmed with new isotope data by Bernard-Griffiths et al.(1987) and Peucat et al.(1989) in Madras granulites and high grade rocks from the transition zone. The second granulite forming event was identified in Madurai and Trivandrum blocks of SGT and this event occurred during Pan-African time close to 0.55 Ga (Choudhary et al., 1992; Santosh et al., 1992; Bartlett et al., 1995; Jayananda et al., 1995). No such data are available regarding the age of the charnockites of the northern Kerala.

Two-pyroxene bearing mafic granulite bands of varying thickness commonly occur as enclaves or bands or as folded, rotated and broken boudins within the charnockites and migmatitic gneisses in various parts. Charnockites in parts of Cannanore, Kozhikode, Malappuram and Thrissur districts of Kerala contain these granulites. In Wynad district also such granulite occurrence is noted in charnockite.

A variety of gneisses occur within the granulite terrain of Kerala, mostly associated with lineaments/faults, zones of migmatization and granite emplacement. Narrow zones of hornblende-biotite gneiss and gneisses of granitic composition are well exposed in parts of Kasaragod district, in the Wynad-Nilambur-Kozhikode region, Attapadi valley, Palghat-gap area and Munnar-Periyar-Thodupuzha-Muvattupuzha region in northern and central Kerala (Narayanaswami, 1976, Nambiar et al., 1989). Some of the gneissic rocks, like those of the areas mentioned above were mostly formed as a result of retrograde metamorphism of charnockites under upper amphibolite to granulite facies conditions (Mahadevan, 1964).

Intrusive phases within the Kerala region includes felsic, mafic and ultramafic bodies and dykes belonging to Lower-Middle Proterozoic age. Late

4

Proterozoic magmatic activity in the northern Kerala is manifested by the emplacement of felsic and alkaline intrusives along major lineaments (Fig. 1.3). The most important granite/syenite bodies in northern Kerala include Ezhimala, Peralimala, Kalpatta and Amabalavayal plutons. Age of Ezhimala granite is 678 Ma (Nair and Vidyadharan, 1982). For Peralimala, an age of ca.750±40 Ma was reported by Santosh et al. (1989). Geochronolgic data of Ambalavayal granite yielded an age of 595±20 Ma (Santosh et al., 1986). Dating of Kalpatta granite based on zircon gave an age of 765 Ma (Odom, 1982) whereas K-Ar dating gave an age of 512±20 Ma (Nair et al., 1985). Mafic and intermediate intrusives of northern Kerala include gabbros, diorites and anorthosites. Important gabbro bodies are from Ezhimala and Kattikkulam. Diorite occurs at Karikkottakkari and Adakkathod. No geochronologic data is available on these igneous rocks.

After the metamorphism and stabilization of the crust, mafic dykes were emplaced during the early-mid-Proterozoic and again during the late Phanerozoic times in the high grade region (Radhakrishna and Mathew, 1995). The oldest dykes in this region are seen in the Agali-Coimbatore dyke swarm. These dykes intruded at ca. 2.0 Ga (Radhakrishna et al., 1995). Dykes in north and central Kerala are of late Phanerozoic age. In north Kerala, the strike of the dykes varies from NW-SE to NE-SW. Their age ranges between 99-129 Ma (Radhakrishna et al., 1995).

Onland sedimentary formation belonging to Neogene period and Quaternary period unconformably overlies Precambrian rocks. The sedimentary sequence can be seen almost all along the coast of Kerala. The best occurrence of such rocks in the northern Kerala is at Cheruvathur.

The granulite facies terrain of southern India is traversed by a set of prominent faults or shears (Katz, 1978). The shear zones are Achankovil shear zone, Noyil-Cauvery shear zone, Moyar-Bhavani shear zone etc (Fig. 1.2). Landsat imagery study over South India conducted by Drury and Holt (1980)

revealed the regional nature of these shear zones. Strike of trendlines show a swing at the vicinity of the shear zones. The swing of the trendlines is from roughly N-S through NE-SW to roughly E-W and then to NE-SW Nilgiri massif. A dextral sense of shear was proposed for most of these shears. Many of these shear zones contain recrystallized cataclastic rocks, foliation and lineation parallel to the shears and diminution of strain away from the zones (Drury et al, 1984). One such fault/lineament trending WNW-ESE is a major feature of the northern Kerala, named after the Bavali river (Nair et al., 1976). The Bavali lineament is considered by some workers as the western extension of the Moyar shear which in turn is a part of the Moyar-Bhavani shear system of Tamil Nadu. But there is a slight change in the trends of the Moyar and Bhavani lineaments. The Wynad schist belt is coinciding with this lineament.

A series of mafic to felsic plutonic rocks are seen spatially associated with the Bavali lineament. These plutonic rocks are Perinthatta anorthosite, Ezhimala gabbro-granophyre complex, Peralimala syenite, Adakkathod diorite, Karikkottakkari diorite, Kattikkulam gabbro, Kalpatta granite and Ambalavayal granite. Among these plutons, Perinthatta anorthosite is important because of the rarity in the occurrence of massif-type anorthosites and Perinthatta anorthosite forms the least studied one in the region. This pluton was emplaced towards the north of the Bavali shear zone. Ezhimala gabbro-granophyre complex, Peralimala syenite, Adakkathod diorite and Karikkottakkari diorite are closely associated with the Perinthatta anorthosite.

1.2 General introduction to anorthosites

Anorthosites are a relatively uncommon rock-type, but have been the focus of research for over a century because of the unique problem they present. In the present usage, the term 'anorthosite' refers strictly to igneous rocks consisting of 90% or more plagioclase. The term 'anorthosite' was introduced by T.S. Hunt in 1863. Anorthosites are formed over the entire range of geologic

6

time although they are dominant in the Archaean and Proterozoic. The anorthosites can be grouped into six basic types as given below (Ashwal, 1993):

1. Archaean (calcic) anorthosite

2. Proterozoic (massif-type) anorthosite

3. Anorthosites in layered mafic complexes

4. Anorthosites of oceanic settings

5. Anorthosite inclusions in other igneous rocks

6. Extra terrestrial anorthosite

Origin of anorthosites is a problem among petrologists. Earlier, a sedimentary origin was proposed for many anorthosites. Now it is known clearly that anorthosites are igneous rocks. Nevertheless, the origin of anorthosites is still not understood completely. The most puzzling feature is the process responsible for the formation of these rocks consisting almost entirely of a single mineral, plagioclase feldspar. There are disagreements regarding the composition of the parental magmas of Proterozoic anorthosites. As most researchers agree that the Proterozoic anorthosite massifs represent the crystallization products of mantle-derived magmas, the massifs can be used as geochemical probes of their late Precambrian upper mantle sources (Leelanandam, 1987). The Proterozoic massif-type anorthosites have been studied for over a century and several review papers are available (Emslie, 1978, 1985; Ashwal, 1982; Morse, 1982 and Leelanandam, 1987).

Archaean megacrystic anorthosites contain equidimensional, calcic plagioclase megacrysts. Commonly the megacrysts have accumulated to form anorthosites and they are seen associated with supracrustal rocks emplaced at relatively shallow levels as elongate sills into mafic lavas, tuffs and/or hypabyssal gabbroic rocks. Well known examples of Archaean megacrystic anorthosites are the Fiskenaesset (West Greenland), Sittampundi (India), Messina (South Africa) etc.

Proterozoic massif-type anorthosites comprise the most voluminous anorthosites on Earth and considerable disagreements still exists as to their origin. The primary minerals of massif-type anorthosite are plagioclase feldspar, high Ca-pyroxenes, low Ca-pyoroxenes, olivine, ferroan ilmenite, titaniferous magnetite and apatite. The composition of plagioclase in anorthositic rocks generally ranges between An_{40} and An_{65} ; however, values as low as An_{15} and as high as An_{90} are not uncommon. Some of the typical features of most massif-type anorthosites as summarised by Ashwal (1990) are given below:

1. Many massifs are intrusive complexes thousands of km^2 in areal extent, with several individual plutonic masses.
2. The dominant rock types include anorthosite, leuconorite, leucogabbro, and/or leucotroctolite.
3. There is usually a minor volume of comagmatic, more mafic material, including norite, gabbro, troctolite, and Fe-Ti oxide-rich rocks, which in some cases form sizeable concentrations of ilmenite/magnetite.
4. Large volumes of mafic or ultramafic rocks are notably absent.
5. There is typically a spatially associated suite of intrusive K-rich plutonic rocks ranging in composition between monzonite and granite.
6. Plagioclase in the anorthositic rocks is generally $An_{50\pm10}$.
7. Anorthositic rocks are typically coarse to very coarse grained.
8. Many massifs contain Al-rich orthopyroxene megacrysts.
9. Massif-type anorthosites are almost entirely a middle Proterozoic phenomenon. No Archaean examples have been reported.

Major occurrences of massif-type anorthosites are found in eastern north America, southern Norway, Angola/Namibia, the Kola peninsula and eastern Siberia. Grenville and adjacent Nain/Churchill provinces of the Canadian shield has the largest concentration of anorthosites on earth. The largest individual massif is the Lac Saint-Jean complex (17,000 Km^2) of Canadian shield.

Proterozoic massif-type anorthosites are mostly found in high grade metamorphic terrains and majority of them are metamorphosed and deformed. Some areas like Nain/Churchill Provinces of Labrador, the Kola Peninsula, the Ukraine and eastern Siberia, the anorthosites have intruded into or through Archaean crust. Moreover, the emplacement of massif-type anorthosites was not restricted to Proterozoic crustal basement.

Country rocks of majority of massif-type anrothosites show amphibolite-granulite facies metamorphism. Country rocks of Harp Lake massif (Labrador) include Archaean granitoid gneisses of upper amphibolite to granullite grade (Emslie, 1980). The Mealy mountains massif is also has the high grade country rocks. There are examples of massif-type anorthosites which emplaced into low grade country rocks. Both the Nain anorthosite complex and the Michikimau intrusion of Labrador are bordered in part by early Proterozoic paragneisses whose metamorphic grade was no higher than greenschist prior to contact metamorphism (Berg 1977 ; Emslie 1980). Thus a broad generalization cannot be made about the metamorphic grade of country rocks of massif-type anorthosites. All metamorphic grades seem to be represented. Both metamorphosed and unmetamorphosed massif-type anorthosites are there. The anorthosite massifs and related mafic intrusions in the Nain Province of Labrador are completely unmetamorphosed and undeformed and retain primary igneous textures, structures and mineralogy (Ashwal and Wooden, 1985).

1.3 Indian anorthosites

Anorthosites are common in India particularly in the southern part of the continent. Most of the Archaean anorthosites are reported from Sargurs and some of them occur as enclaves or fragments in high grade peninsular gneisses. Anorthosites are generallly absent from the younger Dharwar super group. The Chimalpahad anorthosite complex is the largest (~200km^2) layered metamorphosed anorthosite complex of the Precambrian shield of India

(Leelanandam, 1987). In Salem district of Tamil Nadu two layered anorthosite complexes are there viz., the Sittampundi and Bhavani complexes.

Proterozoic massif-type anorthosites are reported from Chilka Lake and Bolangir in Orissa, Bakura in Bengal, Oddanchatram and Kadavur in Tamil Nadu. The Chilka Lake syntectonic composite complex consists of an anorthosite suite and an acidic suite (Leelanandam and Reddy, 1988). This anothosite is intermediate between massif and gravity stratified types. The Bolangir body is confined in between the NE-SW trending Tel lineament and E-W trending Ong lineamnt (Tak, 1983). The border facies is more mafic and fine-grained and exhibits stronger foliation. Geothermobarometric studies by Mukherjee et al. (1986) concluded that 6 kb and 675°C may be very close to the final equilibrium P-T conditions. Bankura is the first anorthosite massif discovered in India (Holland, 1900). Rhythmic banding and layering were observed in it. The complex is associated with intrusive granitic, syenitic and nepheline-syenite rocks (Kumar et al., 1984 and Mukherjee et al., 1984). Kadavur anorthosite is the first Adirondack type of anorthosite reported from Archaean of southern India (Subramaniam, 1956). Sarkar and Bose (1978) identified three units in this anorthosite and they correspond to three major types of anorthosites. Oddanchatram anorthosite is an unmetamorphosed one and its primary igneous textures can be seen. It has all the chemical and mineralogical characters of Proterozoic massif anorthosites (Janardhan and Wiebe, 1985). The Oddanchatram anorthosite was supposed to have been derived from an unusually feldspathic parental magma.

A number of anorthosites are present in Nellore-Gudur area, South India. These anorthosites are Proterozoic massif type and are comparable to that of the Adirondacks of South Central America (Kanungo et al., 1986 and Bhushan et al., 1988). The Kondappalli Layered Complex (KLC) consists dominantly of gabboroic and anorthositic rocks, with subordinate ultramafic rocks (Leelanandam, 1997).

10

In Kerala, Perinthatta anorthosite is the only major occurrence of anorthosite. However, minor occurrences were reported from Kattikkulam gabbro (Nambiar et al., 1982). Anorthosite inclusions are reported from Adakkathod gabbro also (Nambiar, 1987). Lahiri et al. (1975) reported the occurrence of an anorthosite band from Attapadi area. Nambiar (1976) also reported several lenses and bands of anorthosites occurring conformably in charnockite and hornblende gneisses of Attapadi area. A massive gabbro body with minor anorthosite was reported by Vidhydharan et al. (1977) towards south of Kabbani river east of Karrug. This gabbro anorthosite massif is emplaced in the rocks of Wynad Schist Complex near the intersection of Bavali lineament and Kabbani lineament and this anorthosite body is metamorphosed (Nambiar et al., 1982). A minor occurrence of anorthosite was reported by Balachandran et al. (1980) at Kottanjari Parambu near Kerala-Karnataka border and it is similar to Attapadi anorthosites.

1.4 Previous works on Perinthatta anorthosite

The occurrence of Perinthatta anorthosite was first reported by Vidhyadharan et al. (1977) by describing the field aspects of the body, its intrusive nature and the structure of the country rocks and the pluton in brief. Further petrographical data on Perinthatta anorthosite were given by Nambiar et al., 1982. According to them the relict textures like poikilitic and subophitic, presence of zoned feldspar, prismatic inclusions of apatite within plagioclases and pyroxenes clearly show that this anorthosite body was formed by crystallization from a melt. Later some details of the petrology and geochemistry of Perinthatta anorthosite was given by Ravindrakumar (1986). A vaster subjacent extension for the pluton has been envisaged by Nambiar and Devarajan (1993). Preliminary geochemical studies by Gopinathan et al. (1996) has revealed the differentiated nature of the rocks of the pluton. Rajesh et al. (1998) reported the different generations of exsolutions in pyroxenes in the anorthosite and suggested a slow cooling history for it. Gravity surveys over the

Perinthatta anorthosite and adjoining areas precluded the existence of larger mafic bodies in the immediate subsurface region of Perinthatta anorthosite (John Kurian et al., 1999). Moreover, this study revealed the lensoid shape and presence of small isolated cylindrical bodies beneath it probably representing either the mafic/oxide rich portions of the pluton sagged down during crystallization or the individual feeders of the plagioclase rich mushes, which coalesced in the upper crust to give rise to the massif.

1.5 Objectives of the present study

The objectives of the present work are:

- To understand the field setting and petrography of Perinthatta anorthosite;

- To understand the metamorphic and structural aspects of the country rocks of Perinthatta anorthosite;

- To estimate the pressure and temperature from the mineral chemistry of Perinthatta anorthosite;

- To study the geochemistry and thereby to model the petrogenesis of Perinthatta anorthosite; and

- To analyze the petrogenetic relations (if any) between Perinthatta anorthosite and adjacent plutonic rocks;

1.6 Study Area

The study-area for the present work is essentially the Perinthatta and adjacent areas Kannur district of Northern Kerala, which was mapped in detail by examining all the outcrops, quarries, sections etc. Field visits were also made to the main quarries of the plutons associated with the Perinthatta anorthosite like Ezhimala, Karikkottakkari, Peralimala and Adakkathod. Further, to understand the metamorphic conditions of the country rocks of the Perinthatta anorthosite, the whole of the northern part of Kerala (ie., covering Calicut, Wynad, Kannur and southern part of Kasaragod districts) was considered. Similarly, to understand the structural aspects, structural mapping

12

was carried out all along the Bavali shear zone, a linear stretch of nearly 10km width and 100km length extending from Mananthavady to Payyannur (Fig. 1.4).

1.7 Methodology

Various methods and techniques adopted at different stages of the present work are summarized below:

1.7.1 Field study

Extensive field work was carried out for approximately 6 months for detailed mapping of the anorthosite pluton and the adjacent areas. Along with the mapping, fresh samples were collected by visiting all the exposures and quarries for the detailed laboratory investigations. The field relationships of the anorthosite were also studied during the field work. The field work was extended to study and sample the adjacent plutons also. Fresh samples of the country rocks were collected to study the metamorphic conditions of the area. Several traverses were taken across the Bavali shear zone to collect the structural data. Details of the important locations from where samples and other data were collected are given in Appendix-I.

1.7.2 Petrography

About 150 thin sections covering all the rock types were studied for the their petrographic details. Modal analysis of selected samples of anorthosite, associated plutonic rocks and the country rocks were done with the help of a spindle type integrating stage. Micrographs and photomicrographs were prepared using Leitz microscope with photographic attachment. Part of the photomicrographic work was carried at the Department of Geology, University of Kerala.

1.7.3 Chemical analysis of rocks

Selected samples of anorthositic rocks and representative samples from the adjacent plutons were powdered using steel and agate mortars. These
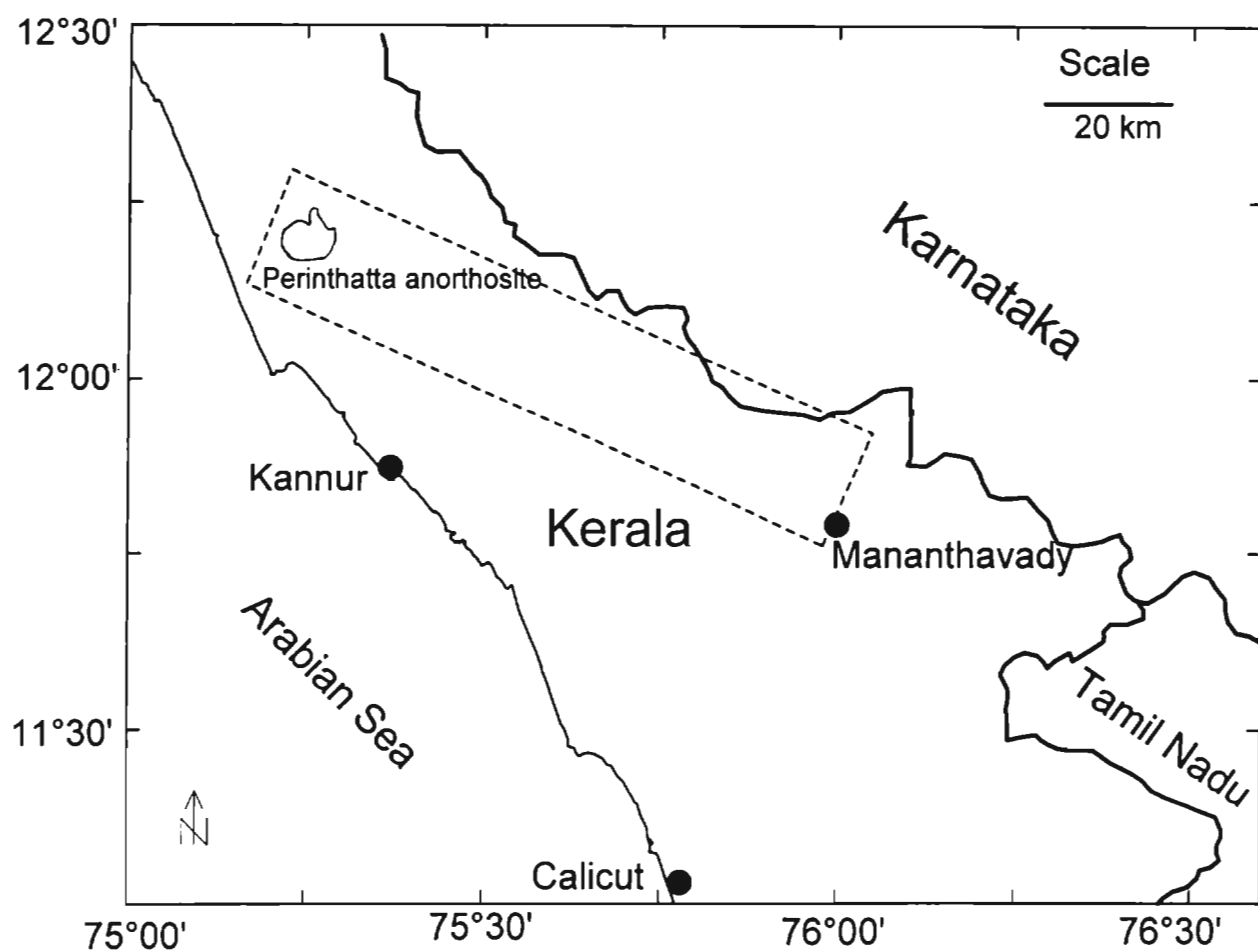
Fig.1.4: Map of northern Kerala showing the location of Perinthatta anorthosite Rectangle represents the area covered for structural study.

samples were analysed for their major, trace and rare earth element concentrations. The analysis were done in National Geophysical Research Institute (NGRI), Hyderabad. XRF method was used for major element analysis and ICP-MS method was used for trace element analysis.

1.7.4 Chemical analysis of minerals

Mineral chemistry of plagioclase, pyroxenes, opaque minerals present in the Perinthatta anorthosite pluton was done by EPMA at NGRI. Mineral chemistry data for metamorphic rocks were obtained by analyzing a few samples at the EPMA unit at Kochi University, Japan.

1.7.5 XRD studies

To confirm the composition of the feldspars in the Perinthatta anorthosite, X-ray powder diffraction method was employed in the case of four samples. This was done by the Seifert (1001) XRD.

1.7.6 Geochronological studies

The anorthosite samples were subjected to preliminary geochronological studies. Plagioclase and pyroxenes were separated by handpicking from coarsely powdered samples. These minerals were then fine powdered using steel and agate mortars. Then Sm-Nd and Pb-Pb methods were used for dating the samples. The Mass Spectrometric analysis for this was done at NGRI.

1.7.7 Data processing and computations

The work involved the calculation of petrochemical parameters, structural formulae of minerals, magma-mixing, trace element models, P-T values corresponding to phase equilibria etc. and preparation of various graphs and illustrations. These works were done using a personal computer with the help of relevant software. For the P-T calculations, a computer program called average P-T method developed by Powell and Holland (1994) was used.

• • •

Chapter II
STRUCTURE

2.1 Introduction

The Perinthatta anorthosite and many other plutons in the northern part of Kerala are spatially associated with a major structure namely, the Bavali shear zone. Thus a detailed understanding of the structural evolution of the Bavali shear zone becomes important in the present study. The nature of shear zone and its role in regional tectonics and magmatism can be deciphered by the structural mapping along the shear zone. Detailed study of structure can be of help in the correlation among the deformational, magmatic and metamorphic events. However, owing to the presence of thick laterite/soil/vegetation cover, the rocks are not well exposed in the area and poses problems for such a detailed structural study. What is attempted here is an analysis based on the field data gathered from the available outcrops and quarries. This chapter starts with a brief review of the previous work followed by field observations pertaining to structures and their analysis.

2.2 Previous work

No detailed study of structure of this area is available till now. Regional structural investigations over the Tellilchery-Manantoddy areas by the Geological Survey of India have revealed the major aspects of structure of the area (Nair et al., 1975). The identification of the main fault system and naming it after Bavali river and describing a variety of folds and faults were also done in the above work. A technical report by Sinha-Roy and Ravindrakumar (1983) was a later work to study the structure of the Bavali fault zone around Peravur and Kelakom. They identified three generations of folds and the occurrence of mylonite and pseudotachylite zones. According to them the area has undergone polyphase deformation accompanied by migmatization and emplacement of plutons. Later the same authors carried out a more detailed study on the pseudotachylites of that area (Sinha-Roy and Ravindrakumar, 1985).

2.3   Structural data from the present work

Field work for collecting the   structural data was mostly confined to the exposures along the Bavali river beds between Mananthavady in the east and Srikantapuram in the west (Fig. 2.1). Thus the study area has a length of almost 100km and a maximum width of 10km. Thick alluvial and sedimentary cover made the data collection impossible along the western extension of shear.

The area for structural study is divided into three sectors viz., eastern, central and western sectors (Fig. 2.1). The eastern sector falls between longitudes 75° 50' and 76° 00' and the central sector falls between long. 75° 40' and long. 75° 50' The Perinthatta anorthosite falls in the western sector and it extends from the coast to the longitude 75° 40'. Though the gross structural aspect is more or less same for all these sectors, in terms of attitudes of certain fabric elements there is variation from sector to sector. The general structural scenario in all the sectors as evident from the deformation styles of compositional layering and other fabric elements is the presence of a few generations of folding, flattening, development of mineral lineations, extreme flattening/shearing with development of stretching lineations and evidences of pure shear.

2.3.1 Eastern Sector

The eastern sector is characterized by approximately 11km long straight course of Bavali river where the best topographic expression of the shear is seen. The western boundary of this sector is near Adakkathod and the eastern boundary is near Mananthavady. Width of the shear zone could not be fixed here because of the lack of sufficient exposures. Towards North and South of the Bavali river, rocks which are not affected by shearing is observed. The major litho unit observed in this sector is hornblende-biotite gneiss.

Regional foliation is the most conspicuous and penetrative planar structural element. This is secondary planar structure which is seen throughout

16

the area of investigation and it is denoted as S_1. The S_1 surfaces are developed by the preferred orientation of prisms of hornblende and biotite flakes.

S_1 surfaces form the dominant planar structural element and their general strike is ESE-WNW. Mylonitic foliation (S_2) is encountered at many locations in the eastern sector. S_2 surfaces dip mostly in the southerly direction. Minor ductile shear planes are observed at Chungam bazar (Fig. 2.2 a). Here these planes strike N82° and are at at an angle to the regional foliation. The sense of shear along these ductile shear zones is sinistral.

Brittle fractures are observed in many locations. At Thalappoya, a brittle fracture cutting the regional foliation trends N60° and it shows a sinistral sense of shear. At Ambayathod, a conjugate set of brittle fractures is observed. One of them trends N150° and the other, N255° (Fig. 2.2 b).

2.3.1.1 Folds

The most widely seen mesoscopic structures in the gneissic exposures studied are folds of different generations.   The earliest generation of fold is designated as F_1 and the later generations are designated as F_2 and F_3 accordingly.

The F_1 are mainly observed on quartzo-feldspathic material and some mafic bands. These are similar folds with thickened hinges and thinned limbs (class 3 of Ramsay, 1967). The limbs are so stretched that they have become parallel to the S_1 surfaces. The hinge area of the F_1 fold is cut by S_1 surfaces and thus they are axial planar to F_1 folds. Generally these are symmetric folds. At a location in Ambayathode F_1 folds on quartzo-feldspathic material are observed. These are highly flattened. Moreover, along the limbs minor S-type folds and at the hinge, M-type folds are observed. The wavelength is around 30cm and amplitude is around 90cm for these folds.
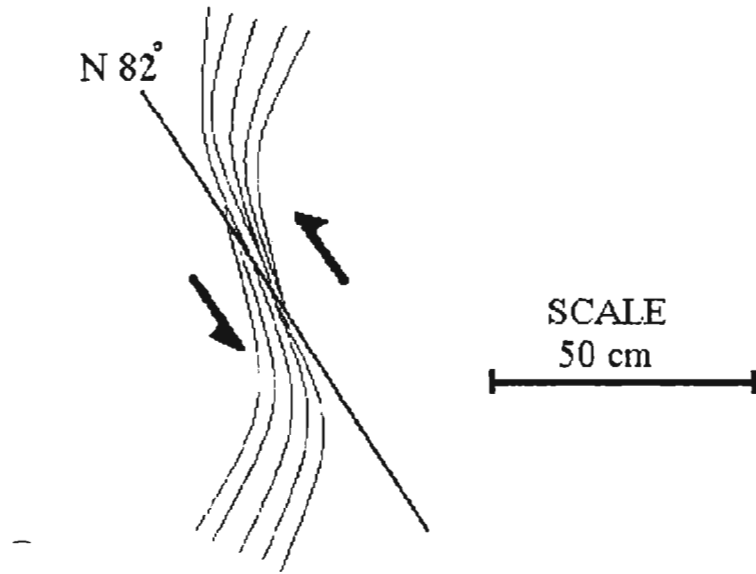
Fig. 2.2 a Field sketch of minor ductile shear (plan view) observed at Chungam bazar (eastern sector).
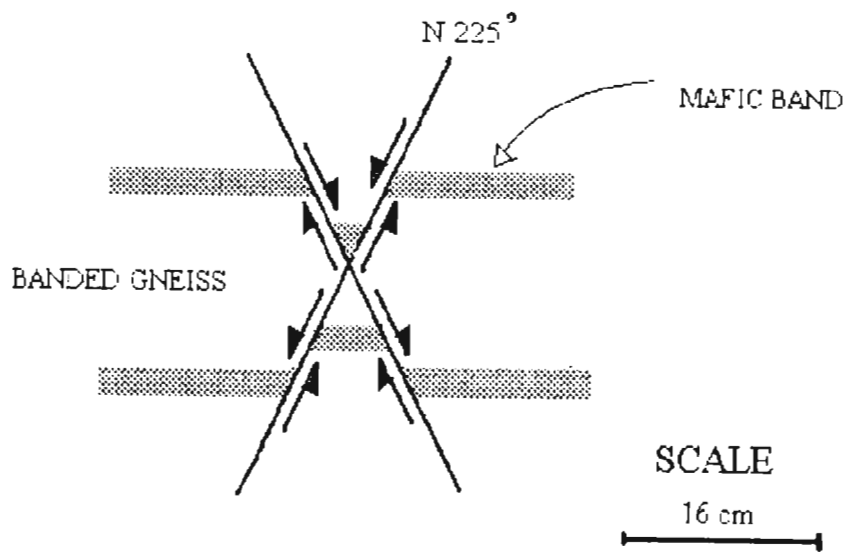
Fig. 2.2 b Field sketch of a conjugate set of brittle fractures (plan view) observed on a river bed exposure at Ambayathod (eastern sector).

The S_1 surfaces are folded to form the F_2 folds. In almost all gneissic outcrops F_2 folds are observed. They are tight to open folds and they do not show thinning along limbs and thickenning along hinges (class 1B of Ramsay, 1967). F_2 folds are observed near Ambayathod where these folds are plunging 55°/N145°. They are asymmetric and S-shaped and their approximate wavelength is 150cm and approximate amplitude is 90cm.

F_2 axial traces are folded by a later episode of folding which can be designated as $\dot{F}_3$. F_3 folds are seen on S_1 and S_2 surfaces as large warves. They do not show thickenning along the hinges and thinning along the limbs (class 1B of Ramsay,1967). F_3 folds are observed south of Palukachi Para in mylonites and biotite gneiss. The wave length is approximately 3m and amplitude is approximately 10cm.

2.3.1.2 Lineation

Both mineral and stretching lineations are observed. Mineral lineation defined by hornblende is seen at a location near Ambayathod. It is seen associated wirh the limbs of folds. This lineation plunges 55° towards N145° and it is parallel to the F_2 fold axis. Another mineral lineation defined by Kyanite is observed at a location north of Tindummal. Here it pitches 55° due 255° on a plane (S_1) that dips N96°/65° southerly. Two sets of stretching lineations are also observed at Tindummal. One of them pitches 30°/N190° on a plane that strikes N110° and dips 35° due SSW. The other one pitches 30° towards N332° on a plane that strikes N290° and dips 5° due NNE.

2.3.1.3 Boudinage

A quartz boudin (7cm long) is observed at Tindummal. It trends N120°. At Ambayathode, boudinage (1 to 7cm long) is noticed along the limbs of F_2 fold. Here pinch and swell structure is also observed.

2.3.2 Central sector

Western boundary of the central sector is 1km west of Manathana and the eastern boundary is close to Adakkathod. In this sector width of shear zone as indicated by the presence of mylonite zone is approximately 4km.

In this sector also S_1 surfaces constitute the dominant planar structural element. Here also S_1 surfaces are developed by the preferred orientation of hornblende prisms and/or biotite flakes. General strike of the foliation is ESE-WNW.

S_2 surfaces are observed in this sector along the river exposures at Aralam, Payancheri, Vilakkode and Palappuzha.. Strike of the mylonitic foliation varies from N110° to N125° In almost all the locations they dip southerly. In this sector, high grade metamorphic minerals like garnet and pyroxenes are seen defining a very crude foliation cutting the F_2 folds. For example, the granulite facies assemblage of opx-cpx-gt is seen overprinting the F_2 folds. This foliation is not well-defined due to the stubby nature of garnet and pyroxenes. However, they trend in an E-W direction.

Minor ductile shear zones (S_3) are observed in this area deflecting the mylontic foliation at Kelakam. At Kuttuppuzha these ductile shears trend N320° and at Aralam, N250°. Crenulation cleavage is also developed parallel to the axial planes of small-scale upright folds defined by S_1. This S_3 surfaces strike N80°. At a location near Kanichar, a ductile shear almost parallel to the former is observed. Both of these shears show a dextral sense of shear.

In almost all the locations small scale brittle fractures of the youngest generations are observed and they are grouped into two sets according to their orientation. One set strikes approximately NE-SW and the other NW-SE (conjugate set of shears). These faults displace regional foliation at many locations. At Kuttuppuzha one brittle fracture striking N190⁰ cuts an F_2 fold

closure with a dextral sense of movement. The sense of shear along these brittle fractures vary depending on which limb of the fold it is observed.

2.3.2.1 Folds

At a location near Kanichattil Kunnu, a F_1 closure is observed. It is observed on a mafic band. It occurs as rootless intrafolial fold (Fig. 2.3 a). Regional foliation is axial planar to it. Another F_1 closure is observed on quartzofeldsapathic material and its axial plane strikes N115° (Fig. 2.3 b). In the central sector, plunge of the F_1 folds is measured at Tondyil and there it plunges 70°/N270°. At a location near Kelakam an F_1 closure is observed which is showing S-type profile. Average wave length is 5cm and average amplitude is 20cm.

F_2 folds are observed on foliation (S_1) in many locations of this sector. At Anungod, an F_2 closure is observed and along the limbs of this fold S, Z-type minor folds are observed (Fig. 2.4 a). This fold is plunging 30° towards N85° E. Near Kelakam a huge closure of F_2 fold is observed with a wavelength of 3m and amplitude 1.5m. They are tight folds (class 1B of Ramsay, 1967). This fold plunges 66° due N335°.

F_3 folds are observed as broad open folds with average wavelength of 45cm and amplitude of 6cm (Fig. 2.4 b). In all the locations they plunge steeply towards north. They are symmetric folds and do not show thickening along hinges and thinning along the limbs.

2.3.2.2 Interference

At a location east of Palappuzha bridge, interference pattern between F_1 and F_2 folds are observed. It is a hook shaped pattern and this was observed in hornblende gneiss (Fig. 2.5 a). In this case the axis of F_2 trends N10°E. Double zig-zag pattern is also observed between F_1 and F_2 folds (Fig. 2.5 b). In a river exposure at Aralam, interference between F_1 and F_3 is observed. It is a dome

and basin type (Fig. 2.5 c). Here the axis of F_1 trends N275°E and that of F_3 is perpendicular to it.

2.3.2.3 Lineation

In the central sector, stretching lineation defined by elongated quartz crystals is observed at a location towards south of Palappuzha bridge.   It plunges 24° due N70°. This is parallel to the strike of F1 fold axial plane. Near Kuttupuzha bridge also the lineation is observed plunging towards N325°. In the same location, mineral lineation defined by hornblende is also noticed.   In this sector both these lineations are parallel. In the western sector both are seen associated with foliation plane.

Another type of lineation observed in the area is the pucker lineation. This is noticed at Aralam area and they are seen along the foliation (S_1) and they pitch towards N73° on a plane that strikes N85° and dips 84° northerly. The pitch of this lineation and the plunge of F_2 folds are coinciding. Stretching lineation defined by quartz is observed along the limbs of F_2 folds found at Anigod palam. This lineation is parallel to the F_2 fold axis. It plunges 30 towards N85°.

Mineral lineation defined by hornblende is noticed at Kelakam where it plunges 75° due N260°.

2.3.2.4 Boudinage and 'pinch and swell structure'

At a location south of Palappuzha bridge pinch and swell structures are observed and they are parallel to the S_1 surfaces (Fig. 2.6). At this location pinch and swell structure is observed on quartzo-feldspathic bands. Their width is 0.5mm and their length is 1 to 2cm. In this location a mafic band is also showing pinch and swell structure.   At Kuttuppuzha also pinch and swell structure is observed. At Anigod palam, small boudins (1 to 2cm long) are observed parallel to foliation. At Kelakam along the river bed exposures, large boudins of quartzo-feldspathic material (20cm to 70cm long and 4 to 25cm wide) are observed.
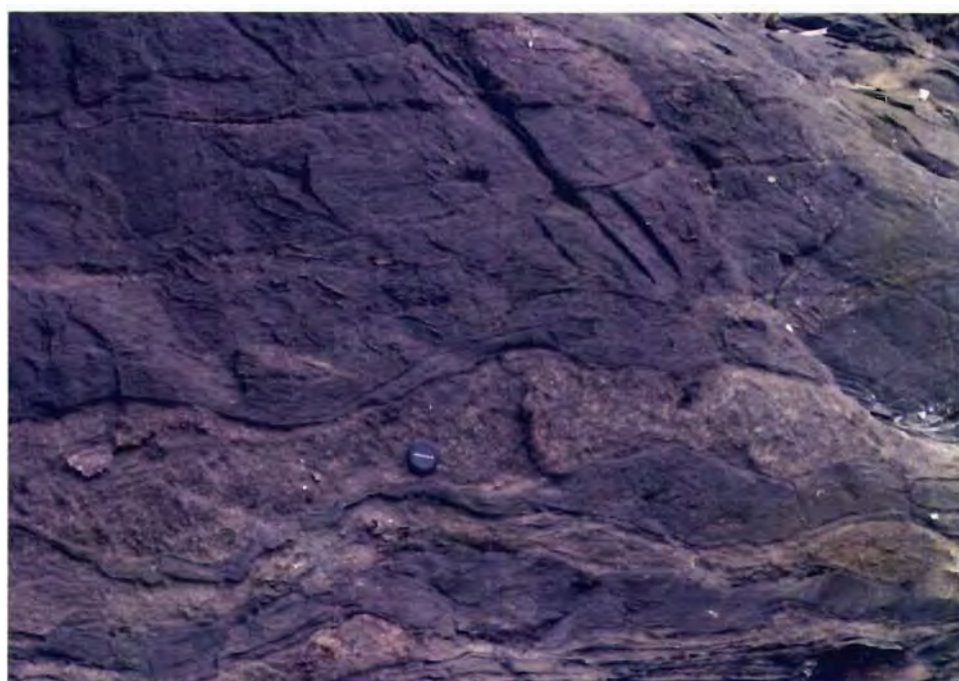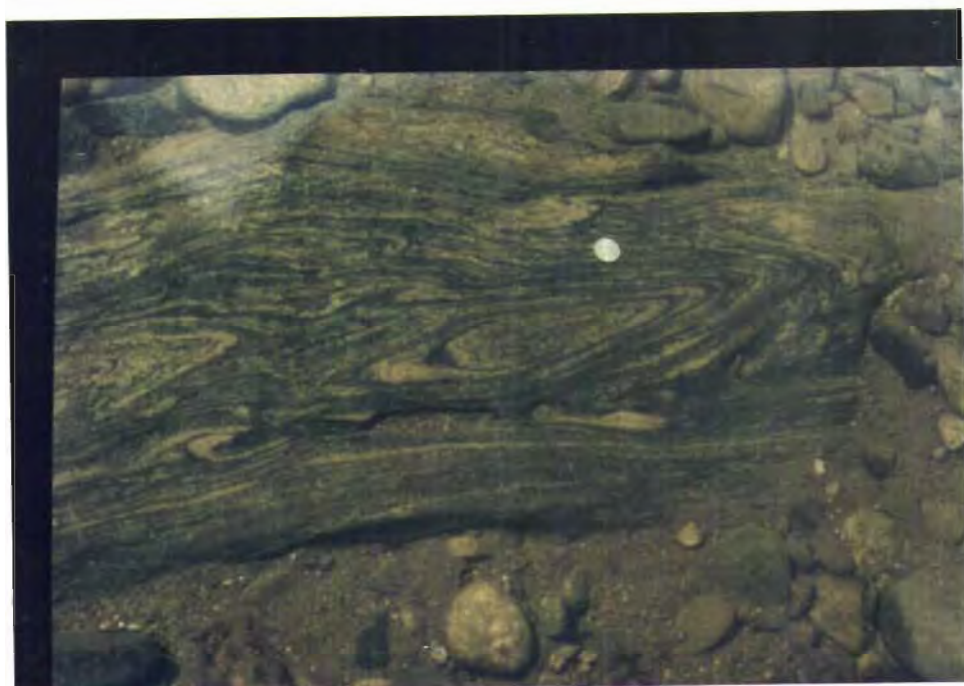
2.3.3 Western sector

The width of the shear zone is approximately 5km as evidenced by the extreme flattening of the fabric elements along this and the occurrence of mylonites. In this sector the general strike of foliation(S_1) is approximately E-W.

S_2 surfaces are represented by mylonitic foliation. In the western sector, mylonitic foliation is observed in locations like Srikandapuram and Kuilur. The S_2 surfaces strikes approximately E-W. In most of the locations dip direction varies from NW to N. In some locations southerly dip is observed.

Small scale ductile shear zones cutting the S_1 surfaces are observed and they trend NNW to SSE and thus they are subparallel to the major shear in the region. The sense of shear associated with most of these shear zones is of sinistral.

In almost all the locations small scale brittle fractures are observed.

2.3.3.1 Folds

The limbs of the F_1 folds are so stretched that they have become parallel to the S_1 surfaces. The hinge area of the folds is cut by S_1 surfaces and thus they became axial planar to F_1 folds. Generally these are symmetric folds, but at a location in the river bed exposures near Kelakam F_1 is asymmetric and it occurs as S-type fold. The wavelength of this fold is 24cm and amplitude is 90cm.

At a location near Kuilur, the F_2 folds occur as Z-type folds. Along the limbs, Z and S-type minor folds are observed and they are so flattened that they became parallel to the regional foliation. In the western sector, wavelength of F_2 fold is approximately 7cm and amplitude is approximately 5cm.

22

At some locations F_3 folds were observed with an approximate wavelength of 3m and amplitude of 20cm.. They are symmetric folds plunging 80° due north.

2.3.3.2 Interference

Interference between different generations are not observed in this sector and that may be due to the lack of sufficient exposures.

2.3.3.3 Lineation

It was not possible to collect good data of lineations from this sector due to the absence of good exposures.

2.3.3.4 Boudinage and 'Pinch and Swell' structure

In the western sector boudinage is rare but pinch and swell structures are seen in some locations.

2.3.4 Mylonite

Mylonite is not seen as a continuous zone and it is more or less restricted to the course of Bavali river. The mylonite is represented by both augen gneiss and banded gneiss. Mylonite is very well developed near Aralam and it grades into hornblende-biotite gneiss on either side. Most of the augens are asymmetric with recrystallized tails showing consistent dextral sense of shearing. On microscope examination it is found that the augen structures are feldspar porphyroclasts. Both K-feldspar and plagioclase form porphyroclasts. K-feldspars include orthoclase and microcline. The ground mass is made up of recrystallized quartz an feldspar. They are fine grained with straight grain boundaries. Sometimes porphyroclasts themselves are made of numerous tiny crystals with straight grain boundaries. Dark coloured bands can be seen in mylonites and they warp around the porphyroclasts. In all these mylonites, the matrix is less than 50% and so they are classed as protomylonites.

23

2.3.4.1 Shear sense indicators

At Amabayathod (eastern sector), along stream-bed outcrops banded gneiss is exposed. In the gneiss some sygmoidal feldspar boudins were noted (Fig. 2.7). A dextral sense of shear is envisaged from their shape. These are found in the mylonite zone. The boudins are 3.5cm long and 2cm wide.

At Kelakom and Kanichar (central sector) sygmoidal feldspar boudins were noted. They also give a dextral sense of shear. Their long axis trends generally trend N120°. At Payyancheri (central sector), near Iritty also feldspar boudins giving a dextral sense of shear were noted.

Oriented sections of mylonite were also studied for shear sense indicators. Because of the recrystallization, the sygmoidal boudins giving shear sense are very rare. In one sample from Aralam, two plagioclase feldspar grains indicate dextral sense of shear (Fig. 2.8 a). Originally, these two grains were part of a single grain. They were broken into two parts due to shearing. The albite twin lamellae in them are exactly matching indicating optical continuity. The broken pieces are displaced in a dextral sense.

Vertical component of the shear is examined in a few oriented thin sections. From a sample near Aralam, two sigmoidal boudins of feldspar were noted (Fig.2. 8 b & c). These give an indication that the northern block has gone up with respect to the southern block.

2.4 Geometrical analysis of folds

The structural data can be used for geometrical analysis of folds. For this purpose, πS_1 diagrams were prepared for three sectors by plotting the S_1 poles in Schmidt equal area net. These poles were contoured using a Kalsbeek counting net. The πS_1 diagrams can be used to study the regional variation in the foliation from sector to sector and to determine the orientation of major folds. F_2 folds are

24
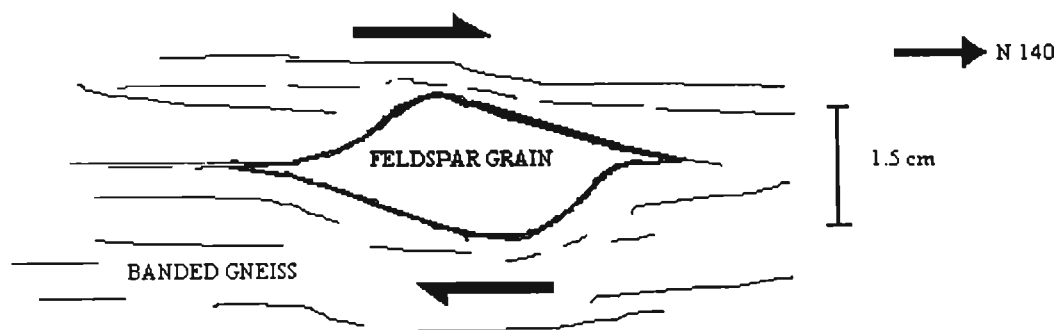
Fig. 2.7 a Field sketch of shear sense indicators (feldspar augens) indicating a dextral sense of shear (plan view) and these are observed in a river side exposure of mylonite at Ambayathode (eastern sector).
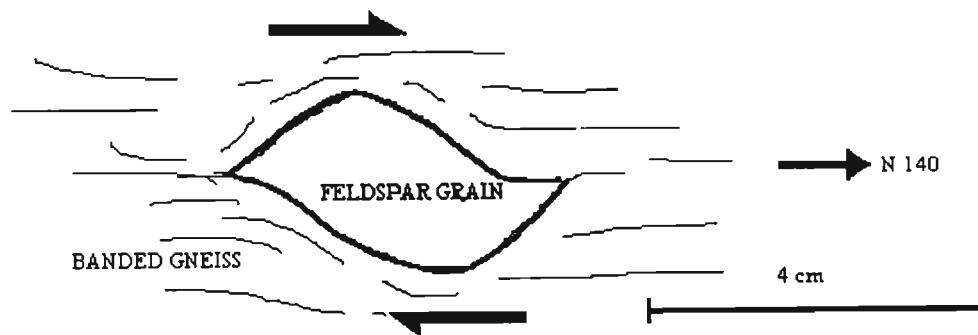
Fig. 2.7 b Field sketch of feldspar augens observed on a sheared granite gneiss at a quarry near Payyancheri, Iritty.
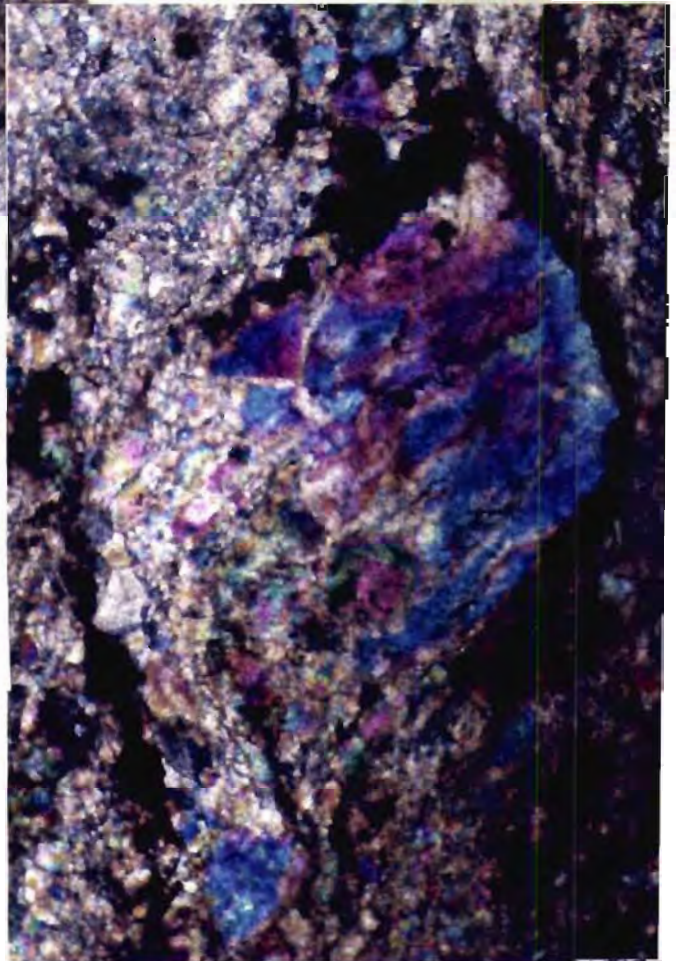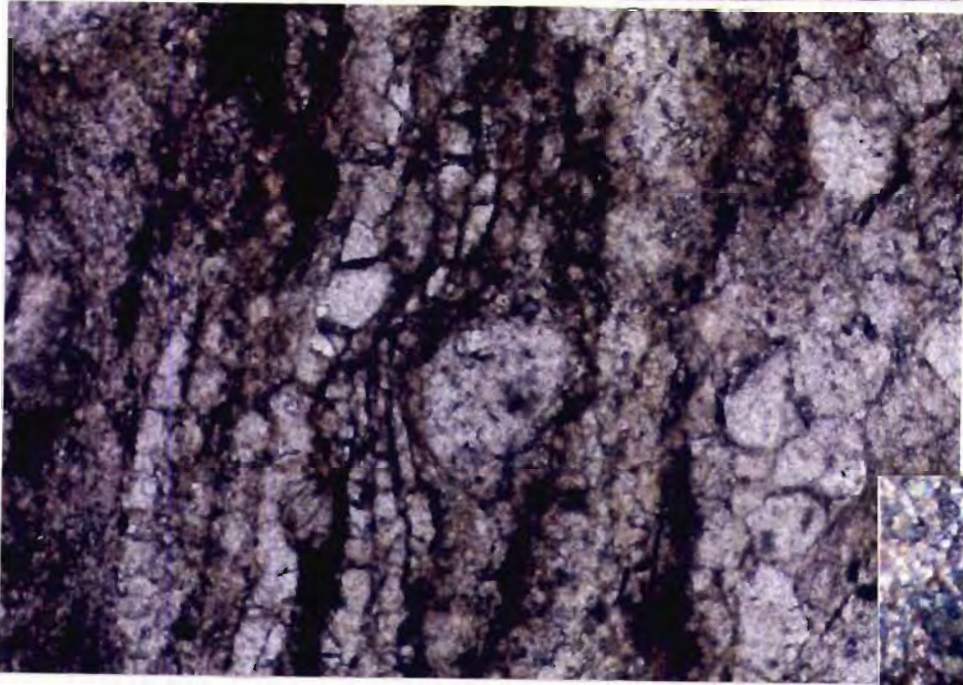
defined by S_1 surfaces and thus poles of the π girdle will give the orientation of F_2 major fold.

In the πS_1 diagram of Eastern sector (Fig. 2.9 a), single maxima is seen and it plunges northerly. The pole to the π girdle plunges 16° / N121°. This is almost similar to the plunge of F_2 minor folds. The modal S_1 plane dips 66°/N204° Elongation of contoured area indicates the effect of F_3 folding.

In central sector also a single maximum is seen and it plunges southerly (Fig. 2.9 b). The pole to the π girdle plunges 30°/N104°. F_2 folds plunge almost in this direction in the central sector. Modal S_1 plane dips 78°/N21°. Elongation of contoured area is lesser than that of eastern sector.

The πS_1 diagram of western sector (Fig. 2.9 c) is characterized by a single maximum which plunges southerly. The pole to the π girdle plunges 30°/N85°. Modal S_1 plane dips 77°/N3°. Elongation of contour is lesser than that of central sector.

2.5 Discussion

Presence of different generations of penetrative planar structures in the area indicates the poly-deformed state of the rock. These deformations have affected all the metamorphic rocks of the area and therefore, primary structures like bedding and igneous layering are not observable. However, certain primary structures have been reported from areas far away from the presently studied areas like Vengad and Icheri. These include the deformed pillow structures and bedding in conglomerate. In other areas, the primary planar surfaces are not distinguishable from S_1 surfaces because of thorough recrystallization of the rocks.

25
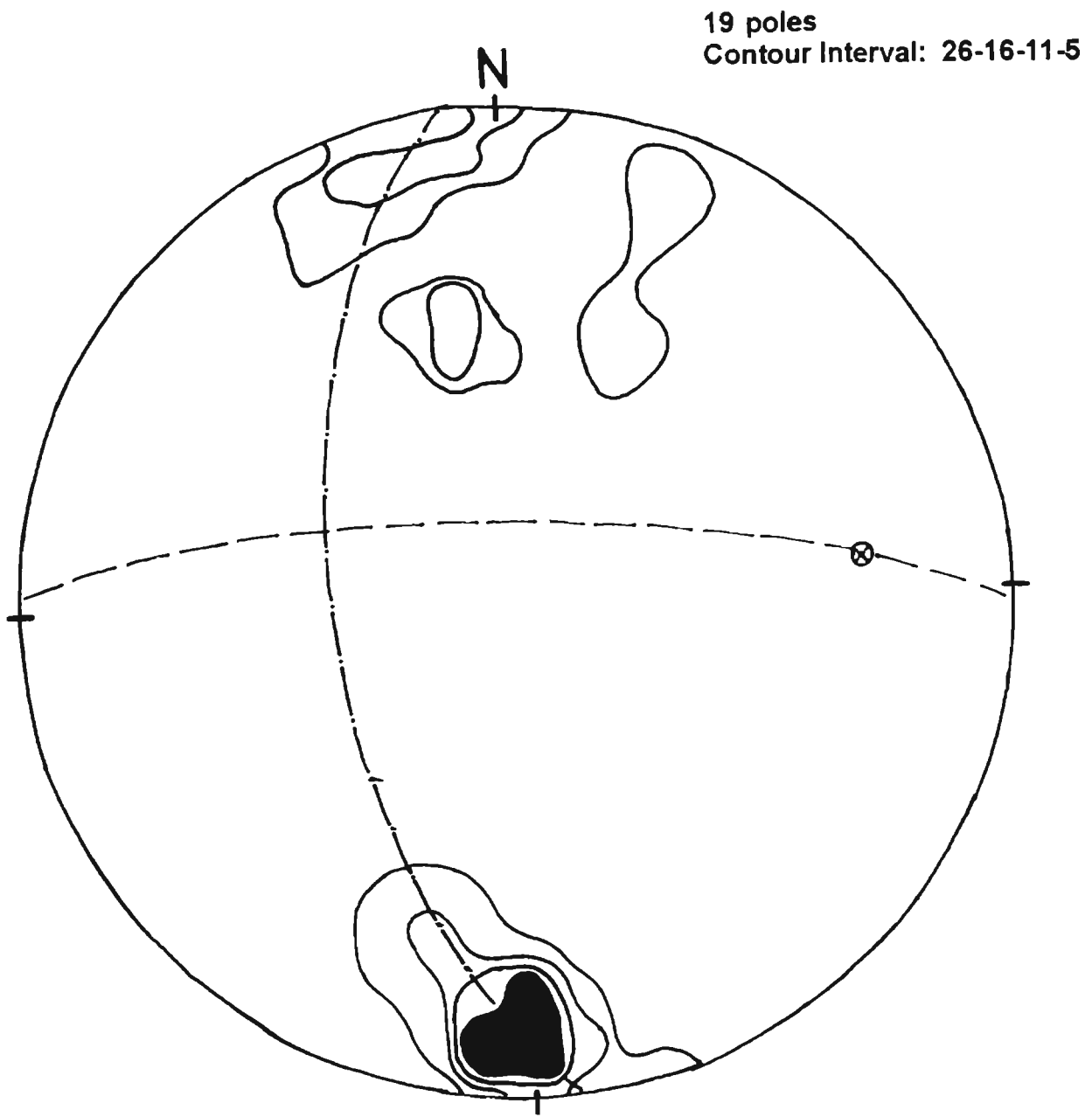
Fig. 2.9 a   π- pole diagrams of foliation planes in the western sector.
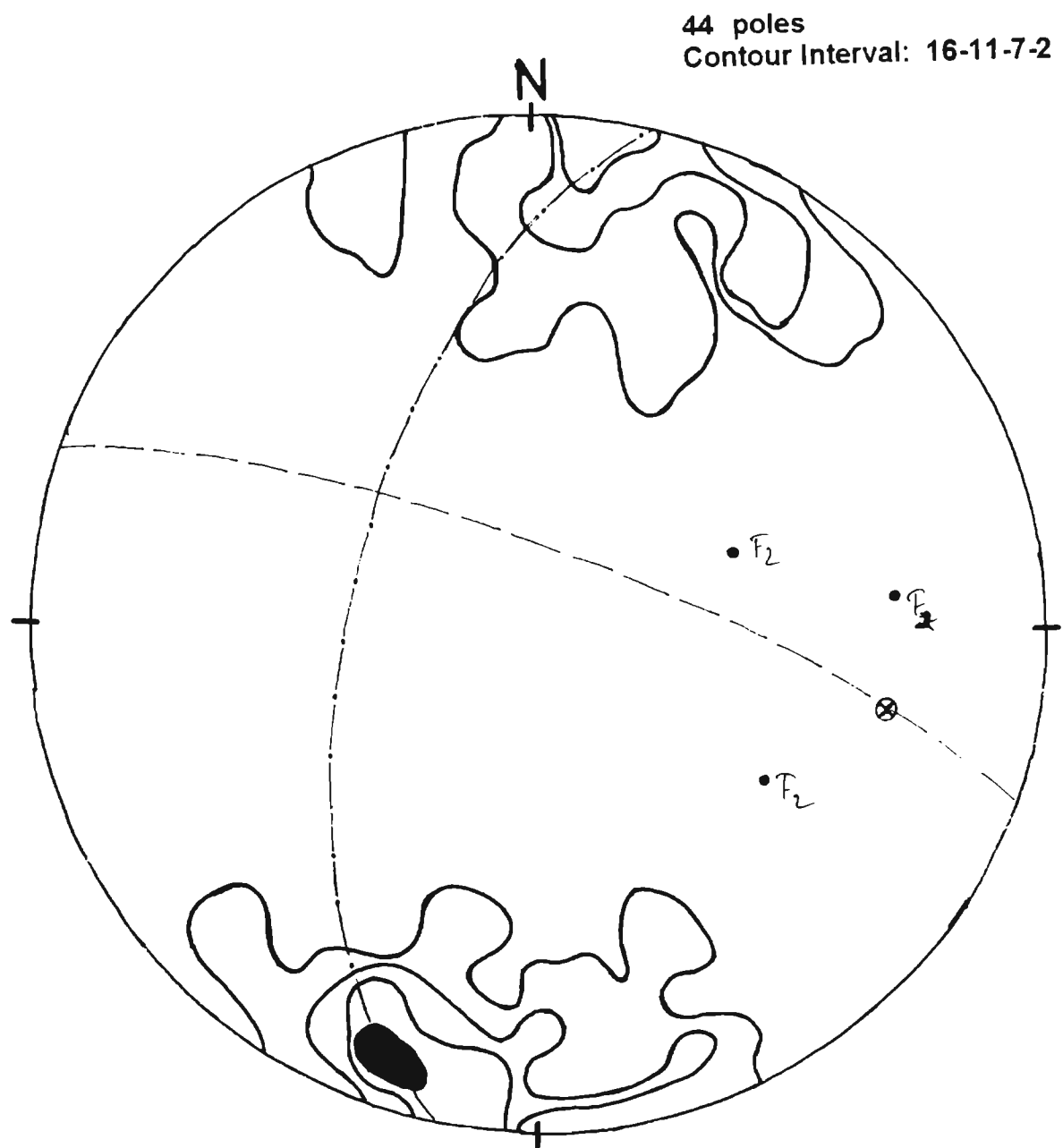
Fig. 2.9 b π- pole diagrams of foliation planes in the central sector.
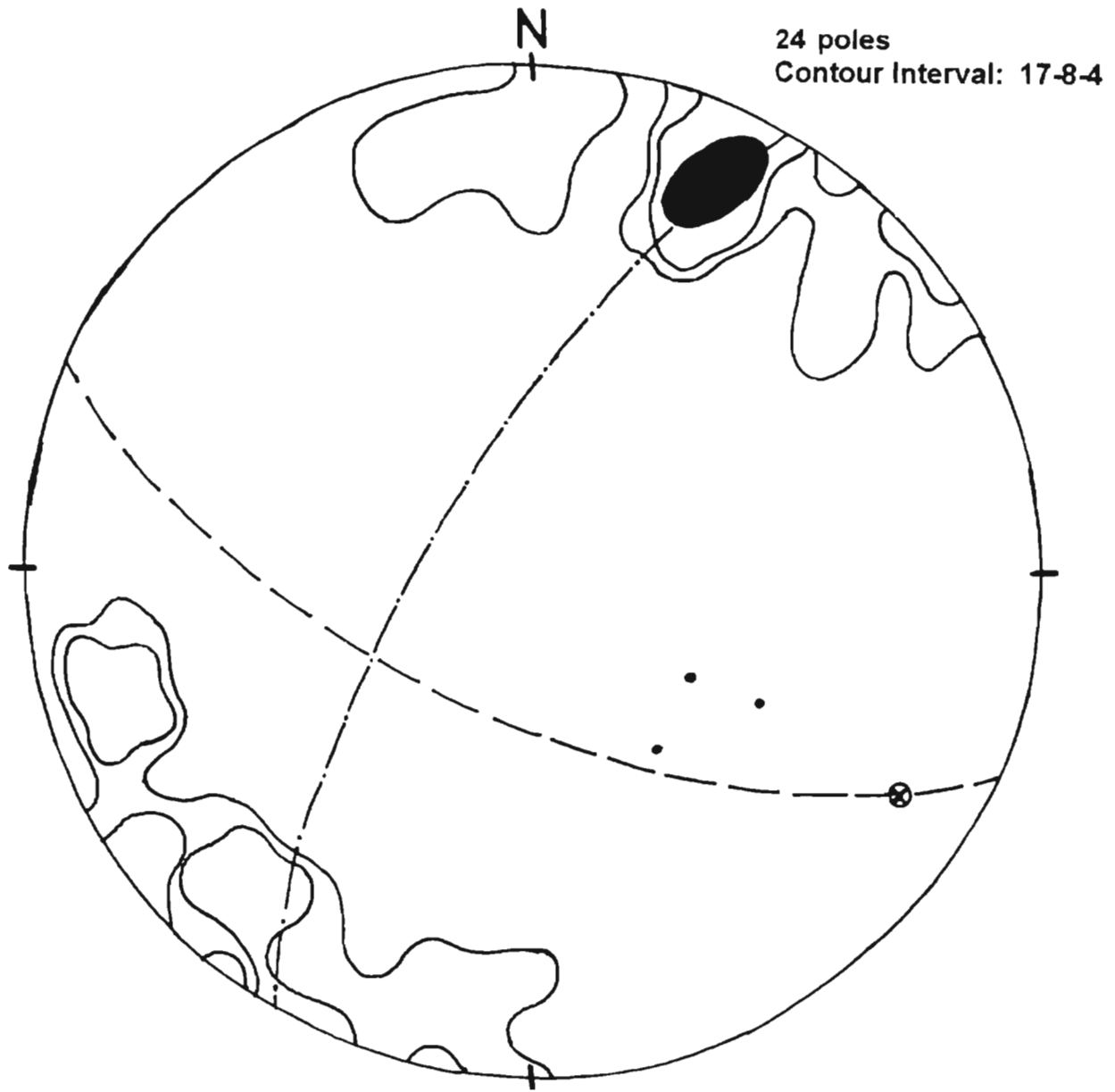
Fig. 2.9 c π - pole diagrams of foliation planes in the eastern sector.

A comparison of the structural data from the three different sectors indicates similar structural evolution but with slight difference in the inferred stress fields and localized differential response depending on the nature of the affected rocks. Another factor which decides the nature of planar and linear structures in a location is its proximity to the major shear zone.

S_1 surfaces show variation in their attitude in all the three sectors due to ployphase deformation. However, the variation is not random; there is gradual change in the variation from western sector to eastern sectors. This can be seen in the πS_1 diagrams. The general strike of the foliation in the western sector is E-W and it varies to ESE-WNW in central and eastern sector. As the regional foliation(S_1) is defined by preferred orientation of hornblende, it can be concluded that metamorphism reached upto amphibolite facies, during deformational episode corresponding to S_1.

The S_1 surfaces are axial planar to the earliest generation of folds (F_1). From this cross-cutting relationship, it can be concluded that the F_1 folding event is younger to the amphibolite facies metamorphism which generated the S_1 surfaces.

The cross-cutting relationship between the foliation defined by high grade minerals and the F_2 folds indicates that, the high grade metamorphism of the granulites seen towards the northern block of the Bavali shear is younger to the F_2 folding event.

In almost all the locations the F_1 folds occur as intrafolial folds while in some other areas they occur as rootless intrafolial folds. This indicates the variation in the degree of flattening. The plunge of the F_1 fold varies even in the adjacent locations and this can be attributed to the effect of later events of folding. The deformation which produced F_1 generation folds was progressive and thus it folded the foliation and thus F_2 folds are observed on S_1 surfaces.

26

Both the regional foliation (S_1) and mylonitic foliation (S_2) are folded to form the F_3 generation folds. These folds plunge towards north wherever they are encountered and this consistency indicates that after F_3 folding there was no major ductile deformational events.

F_3 folds are seen in mylonites as well as in gneisses. In highly mylonitized zones, F_1 and F_2 are very rare. From these observations it can be concluded that the major shearing along the Bavali fault took place after F_1 and F_2 folding events.

There exists a difference in the style of pinch and swell structures and boudinages in various sectors. In the western sector, only pinch and swell structure is observed. In the central sector, mainly boudinage structure is observed. In the eastern sector, both these are present. This indicates a variation in the stress during deformation ie., stress was relatively less where only pinch and swell structure is observed. Towards the central sector, stress was increasing and that is indicated by the presence of fully developed boudinage. In the eastern sector, a moderate stress is inferred from the presence of both boudinage and pinch and swell structures. Such variations in the stress fields are indicated by the style of F_1 folds as discussed earlier.

After F_3 folding event, some minor ductile shearing caused the local development of shear zones cutting the regional and mylonitic foliation. In the western sector, the S_4 shear planes strikes NNW-SSE with a sinistral sense of shear. In the central and eastern sectors the S_4 surfaces are parallel (trending N80°) but with different sense of shearing. In the central sector it is dextral and in eastern sector, sinistral.

This minor ductile shearing is followed by a late stage brittle fracturing at or near surface. Two sets of brittle fractures are noticed. One set strikes

27

approximately NE-SW and other NW-SE. They cut the regional foliation and mylonitic foliation. The brittle fractures are rarely observed in the central sector. Sometimes these two sets of fractures occur together to form conjugate fractures. The sense of shearing is not uniform in the case of brittle faulting.

Study of shear sense indicators in mylonite both in the field and under microscope revealed that the horizontal component of the Bavali shear is of dextral sense. Study of shear sense indicators along the vertical sections indicated that the Bavali shear has dip slip component also. The Bavali shear is considered to be the western extension of Moyar shear and for Moyar shear has a dip slip component (Naha and Srinivasan, 1996). In Bavali shear, the dip slip component of the shear is such that the northern block has moved up with respect to the southern block. Since the general dip of the mylonite foliation is towards south west, the shear zone is of normal type.

From the πS_1 diagrams of the three sectors, orientation of major F_2 fold axis can be determined. In the foliation map, the presence of such a major fold can be seen. Field data of the plunge of F_2 minor folds are generally consistent with the plunge of F_2 major folds determined from πS_1 diagrams. In the central a dispersion of the F_2 fold axis is noted and that may be due to the effect of F_3 fold. In the western sector, the foliation data is very limited due to the lack of exposures. Since the form surface of F_3 fold is also the S_1 surfaces, the elongation of the contoured area indicates the effect of F_3 folds. Their plunge can be towards north or south depending on the limb disposition of the F_2 major fold. F_1 folds are highly appressed with very sharp hinge and so the subparallel limbs will appear as virtually one set of planar surface in πS_1 diagram. Moreover, F_1 and F_2 folds are coaxial folds and F_2 is dominating and overprinting F_1. Thus, from the πS_1 diagrams it is very difficult to identify the effect of F_1 folds separately.

Towards the west of Srikantapuram structural data collection was impossible due to sedimentary/alluvial cover. Nevertheless, not much difference is expected from the general structural aspects in that region. The Perinthatta anorthosite was emplaced towards the north of the Bavali shear and the anorthosite is entirely surrounded by massive charnockite and granulites. Moreover, the anorthosite is not metamorphosed and so it was emplaced after metamorphism. The unmetamorphosed and unfoliated Perinthatta anorthosite shows no evidences of the above mentioned deformational events except some brittle shearing (possibly equivalent to the post F_3 minor shears in the Bavali shears) indicated by pseudotachylite veins. So the Perinthatta anorthosite can be considered as a post-tectonic intrusion. Other intrusives in the region namely Kalpatta granite, Peralimala syenite and Ezhimala igneous complex are also essentially post-tectonic.

• • •

Chapter III
METAMORPHISM

3.1 Introduction

Perinthatta anorthosite is emplaced in the high grade terrain of northern Kerala. Though the area forms a part of the South Indian Granulite terrain of the Precambrian shield, it is not completely covered by granulite facies rocks. Mappable units as well as larger areas are occasionally occupied by lower grade rocks. The Bavali shear zone traverses this terrain in a WNW-ESE direction. On either side of this (towards north and south of this shear zone), the lithology and metamorphism are not same. The region has not been studied in detail for the metamorphic condition except for a few localized works on the petrography of metamorphic rocks or preliminary P-T studies (Nair et al., 1980; Ravindrakumar and Srikantappa, 1987; Nambiar et al., 1989; Nambiar et al.,1992; Krishnaraj et al., 1994; Ravindrakumar and Chacko, 1994a & 1994b and Nair and Nair, 1997).

In the present work the metamorphism of the area is analyzed by
(1) identifying different provinces of metamorphism;
(2) collecting more petrographic data on charnockites and granulites of the province in which Perinthatta anorthosite occurs;
(3) mineral chemistry based calculations of P and T of metamorphism;
(4) province-wise synthesis of the data on metamorphism taking data from previous works also into consideration; and
(5) Comparing the P-T conditions of metamorphism of the area with those of nearby regions.

3.2 Metamorphic provinces

The study area can be divided into five metamorphic provinces based on the dominant metamorphic rock of the area, their mineral assemblage, grade of

30

metamorphism and certain geographical considerations (Fig.3.1), namely,

1. Northern granulite province;
2. Wynad schist belt;
3. Southern charnockite province;
4. Retrogressed charnockite (biotite-hornblende gneiss) province south of Wynad schist belt and north of Calicut; and
5. Vengad basin.

The northern granulite province is essentially composed of charnockite and mafic granulite indicating high grade metamorphism and it encompasses northern part of Kannur (Cannanore) and southern part of Kasaragod districts. The general mineral assemblage of this province is cpx-opx-hbl-gt-fls-ilm-mt-qtz (The expansions of mineral abbreviations used are given Appendix III). The Perinthatta anorthosite is seen emplaced in this province. The second province is a linear stretch extending for about 100km running in a WNW-ESE direction from Mananthavady to south of Payyannur. In this province, hornblende-biotite gneiss forms the main litho unit. In this gneiss several enclaves of high grade schistose rocks are observed and they form the Wynad schist belt coinciding the Bavali shear zone. The general mineral assemblage of the gneisses of this province is gt-bi-hbl-plg-qtz. The schistose rocks of this belt have the assemblages like gt-bi-sill-ky-plg-qtz±rt±cor. In the 3rd province, which essentially occupies the southern parts of Calicut and Wynad districts, charnockite is the major rock unit. In the 4th province, retrogressed charnockite occurs as biotite-hornblende gneiss with relict enclaves of charnockite and granulite. The major formation of the Vengad basin is the schistose and fissile quartz-mica schist consisting of quartz, biotite, magnetite and occasionally zircon and these rocks have not been metamorphosed beyond greenschist facies.

Detailed petrographic study of the rocks of the northern granulite province to which the Perinthatta anrothosite has intruded is given in the following section.
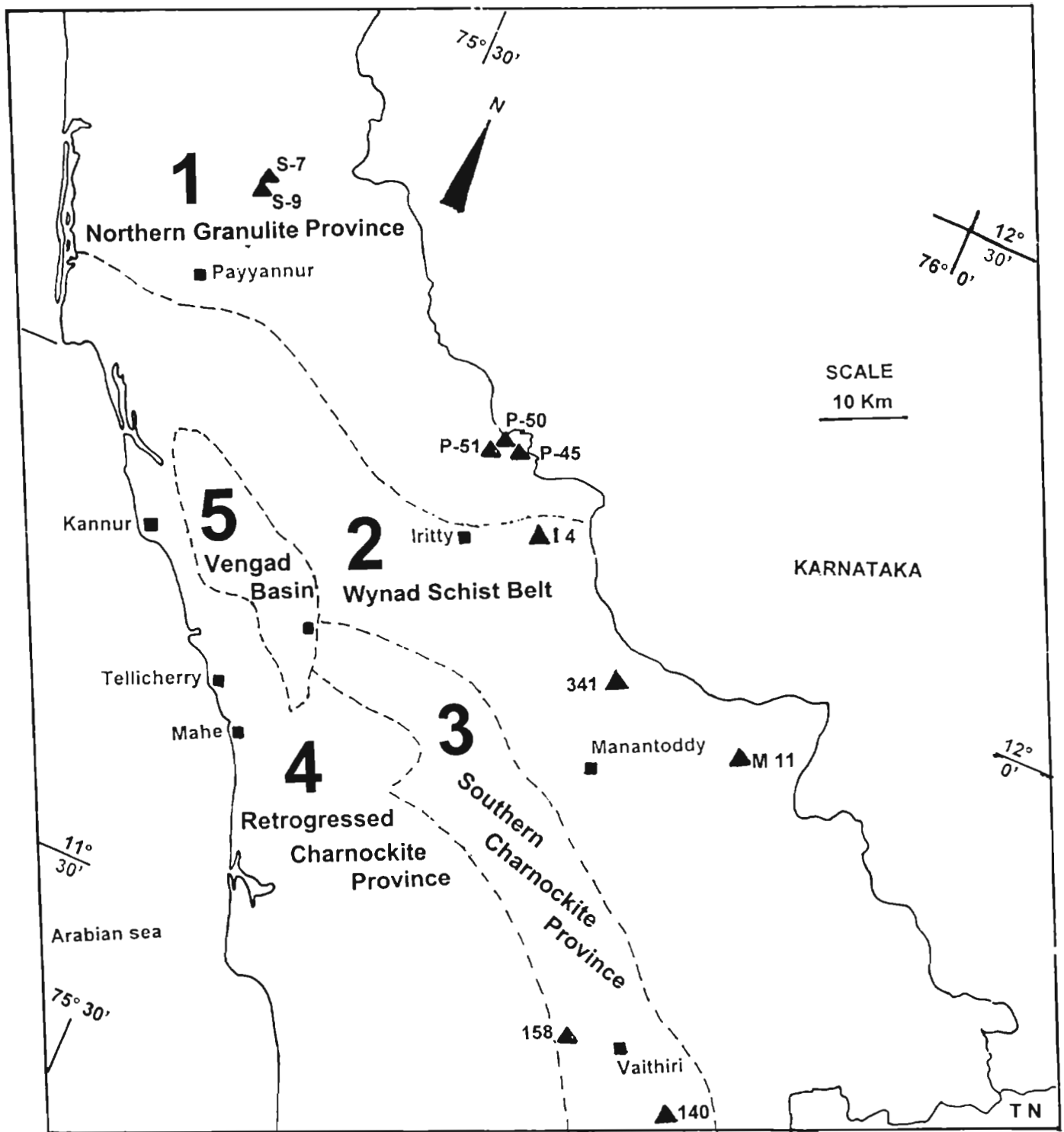
Fig. 3.1   Map of northern Kerala showing the different metamorphic provinces identified in the region around Perinthatta anorthosite. Solid triangles represent the locations of the samples analyzed for geothermobarometric studies with sample numbers.

3.3 Petrography of northern granulite province

Based on mineralogical composition, the entire province can be said to be containing chiefly two rock units namely mafic granulites and charnockites. In the southern part of the province, the major rock unit is pyroxene granulite in which charnockite occurs as concordant bands or lenses or irregular patches. But, in the northern part, charnockite is predominant which has minor enclaves of mafic granulites. Minor occurrences of felsic granulites (quartzofeldspathic garnet granulites) are also seen. The important observations from the study of thin sections of mafic granulites and charnockites of the northern granulite province is given below:

3.3.1. Mafic granulites

Most of the mafic granulite samples show granoblastic texture. Clinopyroxene is the dominant mineral in majority of the granulite samples. Its modal content ranges from 10 to 45%. They are pale bluish in colour and most of them do not show pleochroism. Some clinopyroxenes show faint pleochroism from light green to pale bluish green. In most cases they occur together with orthopyroxene. The clinopyroxene grains show straight grain boundaries and the individual crystals are having almost same size.

Majority of the samples show some amount of retrogression on a thin section level and that is manifested by the alteration of clinopyroxenes to hornblende (Fig.3.2). The alteration is seen along the grain boundaries of clinopyroxene crystals. The grain boundaries become irregular where the alteration is seen. Clinopyroxene crystals show inclusions of quartz, plagioclase and opaques. In one sample (P-50), the clinopyroxene is devoid of any inclusions and in this sample clinpyroxene is slightly pleochroic. In some cases alteration to hornblende is so intense that clinopyroxene occurs as inclusions in hornblende (sample S-5).

Orthopyroxene is very less compared to the abundance of clinopyroxene. Their modal percentage ranges from 5 to 10%. They are distinctly pleochroic with colours changing from pale pink to pinkish yellow or to pale bluish green. In sample (S-5), orthopyroxene is totally absent. Orthpoyroxenes are mostly hypersthene and their size is almost same as that of clinopyroxene crystals. In most cases they show straight grain boundaries with other minerals. In almost all the cases orthopyroxene crystals show alteration along the grain boundaries to hydrous phases like hornblende (Fig.3.3). At places grain boundaries have become curved due to secondary hornblende rims. Orthopyroxene does not occur in the absence of clinopyroxene. Many opaques are usually seen associated with them. In section P-45, garnet is a recrystallization product of orthopyroxene.

Plagioclase is the most dominant felsic mineral in all the granulite samples studied. Its modal percentage ranges from 10 to 35. Plagioclase shows straight grain boundaries and the crystals are of same size as that of mafic minerals and K-feldspar. In one sample (S-5), the plagioclase crystals are smaller than orthoclase crystals. Some plagioclase crystals show bent and kinked polysynthetic twin lamellae. Plagioclase inclusion can be seen in some mafic minerals. The common inclusions found in plagioclase include zircon and opaques.

In many of the samples, K-feldspar is present in very small amounts, but in the sample S-5 orthoclase is present as the most dominant mineral. In sample P-50, orthoclase is totally absent. K-feldspar crystals show straight grain boundaries. K-feldspar occurs in the form of microcline also. Microcline is not present in all the samples. Perthite is a common feature in almost all the samples. Mainly vein type and spindle shaped perthitic lamellae are present. Orthoclase crystals are of same size as those of plagioclase and they show triple-point junctions with other minerals. In sample S-5, uniformity in grain size is not seen and in this sample orthoclase is larger than clinopyroxene and

33
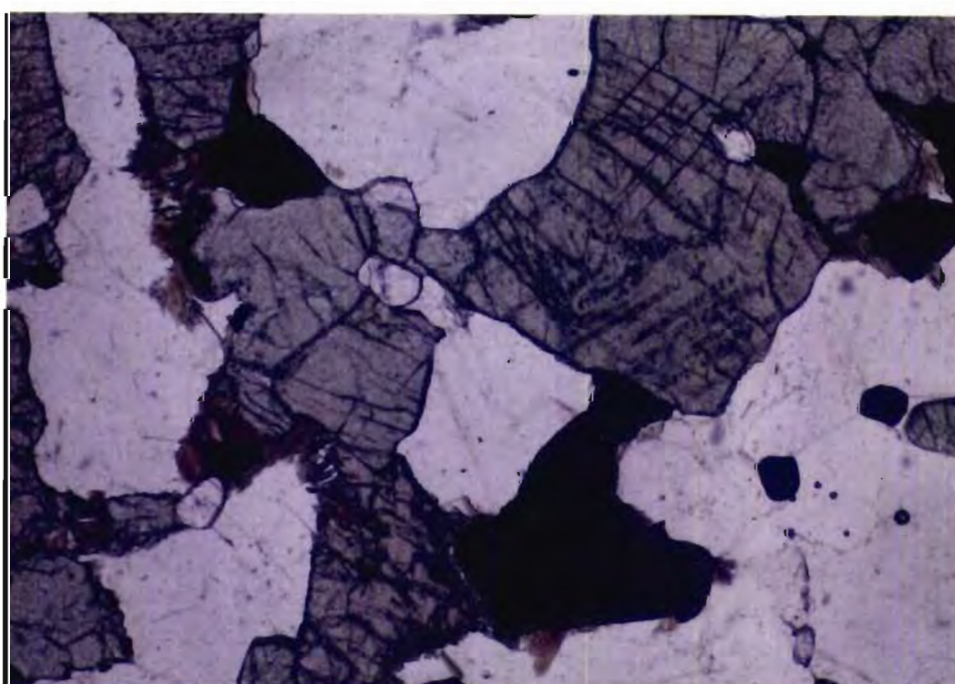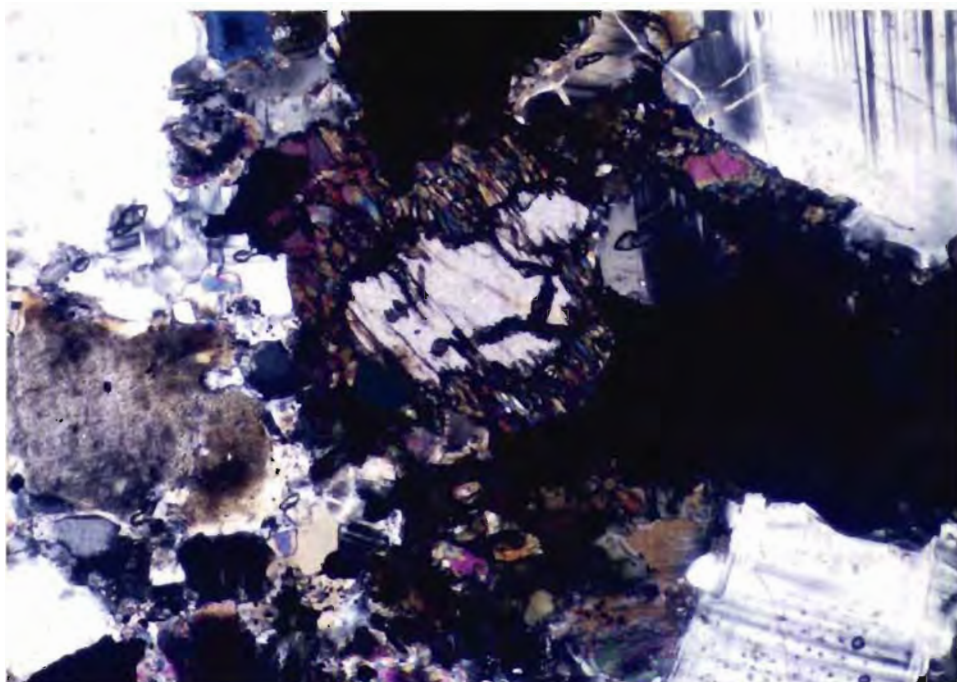
hornblende crystals. Inclusions of quartz and apatite are common. In a few instances orthoclase embays into clinopyroxene crystals.

Quartz is present in all the granulite samples in very little amounts and its modal percentage ranges from 5 to 10. Two generations of quartz grains are observed in most of the thin sections. The older generation is generally larger. Its size is almost same as that of plagioclase and mafic minerals. The younger generation is formed due to recrystallization and they are very small and are characterized by straight grain boundaries with triple point junctions. They occur as discontinuous veins or as pockets. They show wavy extinction also. Sometimes they are smaller than apatite crystals. Some of the quartz crystals show elongation and they are large. In some of the quartz grains zircon inclusions are observed. Some larger quartz crystals have straight grain boundaries with other minerals.

Next to pyroxenes, hornblende is the dominant mafic mineral and it shows pale brownish yellow to pale yellowish green pleochroism. In most of the cases hornblende is the alteration product of other mafic minerals lke pyroxenes. Sometimes they occur as alteration product of opaques which are seen in association with pyroxenes. Usually they occur as small prisms around pyroxene crystals. In sample P-45, hornblende is the alteration product of garnet. In sample S-5, hornblende is the dominant mafic mineral. In this they are anhedral and are of different sizes. Here the hornblende crystals show inclusions of clinopyroxene crystals indicating that they are the retrogression product of clinopyroxene. One clinopyroxene crystal rimmed by hornblende also supporting this observation.

Garnet is present in many cases and in one sample (P-45) good amount of garnet is present. They have irregular grain boundary showing alteration to hornblende along the grain boundaries (Fig.3.4). Alteration to hornblende is common where opaque minerals are seen in association with garnet. The garnet

34

is forming from pyroxenes. The alteration to hornblende is also seen along the fractures of garnet crystals. Small garnet crystals are euhedral with perfect polygonal outline. Inclusions in garnet include apatite, pyroxene, quartz and opaques.

Opaques are the most dominant accessories. They are seen closely associated with mafic minerals. Sometimes the opaques are seen showing alteration to hornblende or biotite. Zircon and apatite also occur as minor accessories in most of the samples.

3.3.2 Charnockite

The charnockites of the area are dark grey coloured and very coarse grained. Occasionally they have the characteristic blue quartz crystals. The mafic minerlas constitute less than 25% in these rocks.

Orthopyroxene is present in all the samples. Its modal percentage varies from 5 to 20. They show vivid pleochroism with colours changing from pale reddish pink to pinkish yellow or to pale bluish green. All the orthopyroxene crysrtals have straight grain boundaries and thus they show triple point junctions with other minerals. Many opaque minerals are seen associated with them. The size of orthopyroxene crystals are same as that of clinopyroxene crystals except in S-15/P where orthopyroxene crystals are as large as 1cm. They are pleochroic and the colour changes from light green to dark green. Fine opaque inclusions are observed in orthopyroxene crystals. In many sections orthopyroxene shows alteration to biotite or hornblende (Fig.3.5).

Clinopyroxene is observed in many of the thin sections and their proportion with other co-existing minerals varies considerably. In thin sections like P-44 and S-6/A clinopyroxene is totally absent. These samples are of highly felsic variety. Size of pyroxene crystals is uniform in all the thin sections except in sample S-15/P in which size of some clinopyroxene crystals reaches upto

1cm. In a location about 5km north of Srikandapuram (P-36) the size of clinopyroxene crystals are very small compared to all other samples. Their proportion is also less. Some clinopyroxene crystals show faint pleochroism from pale pink to pale green. The pleochroism is same in all the sections.

Grain boundaries of clinopyroxene crystals are straight in most cases, but amoeboid boundary is seen in areas where alteration to hydrous phases is intense. Triple-point junctions of grain boundaries are common. In two thin sections (P-25 and P-51) clinopyroxene crystals show polysynthetic twinning. In all the thin sections, opaque minerals can be seen associated with clinopyroxenes. Another important feature of clinopyroxene crystals is the alteration or retrogression to hydrous phases like hornblende and biotite (Fig.3.6). Alteration to hornblende is more frequent than the alteration to biotite. No sign of retrogression is there in some samples like P-51.

Orthoclase feldspar is a major component of all the charnockite samples of this province. The modal content of orthoclase feldspar is in the range of 5-75%. In majority of the thin sections the size the orthoclase crystals are same as that of plagioclase and mafics. Only in a few sections they occur as smaller crystals. In section P-25, orthoclase shows peripheral granulation and thus a bimodal size grouping of orthoclase crystals is observed. In many cases they show straight grain boundaries and triple-point junctions. Sometimes they show amoeboid and irregular boundaries also. Perthitic texture is shown by orthoclase crystals of all the locations. Generally, the exsolved phase occurs as long spindles and rarely as small blebs. Very rarely orthoclase shows Carlsbad twinning.

Plagioclase is an important mineral phase observed in all the charnockite samples. Its modal content varies from 5 to 25%. In most of the sections, the size of plagioclase crystals is almost uniform except in the sample P-44 in which the plagioclase crystals are smaller. The plagioclase crystals have straight grain boundaries with other minerals. In section P-46, intergrowth between quartz and
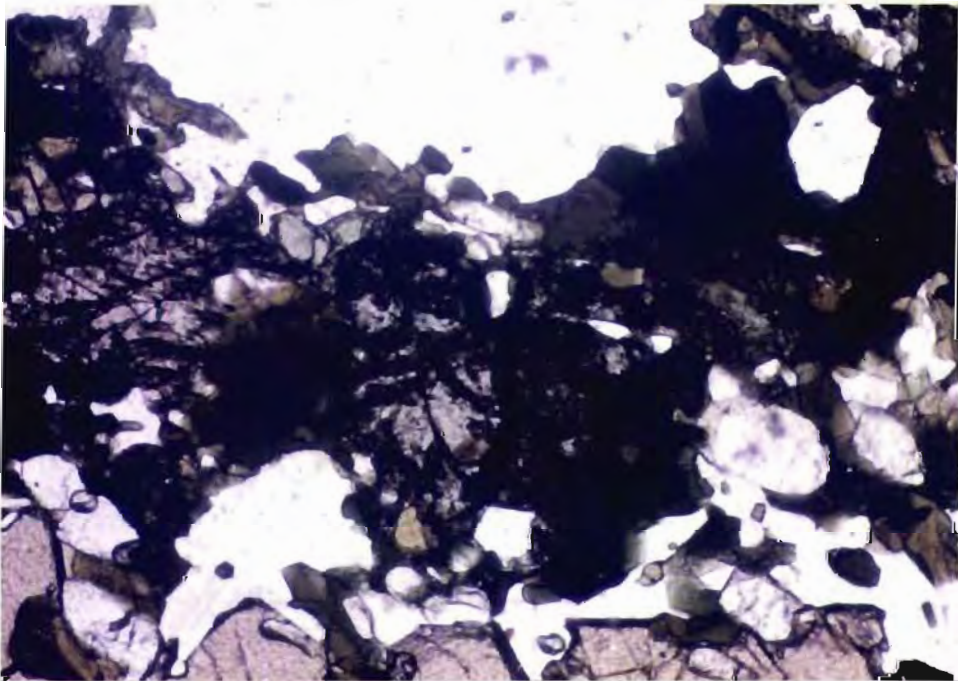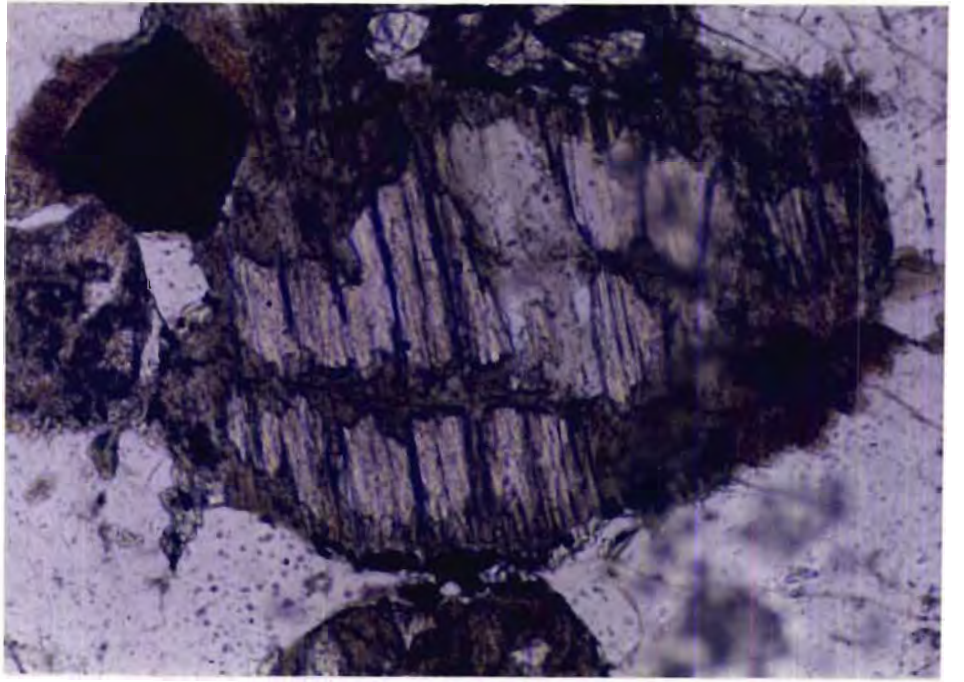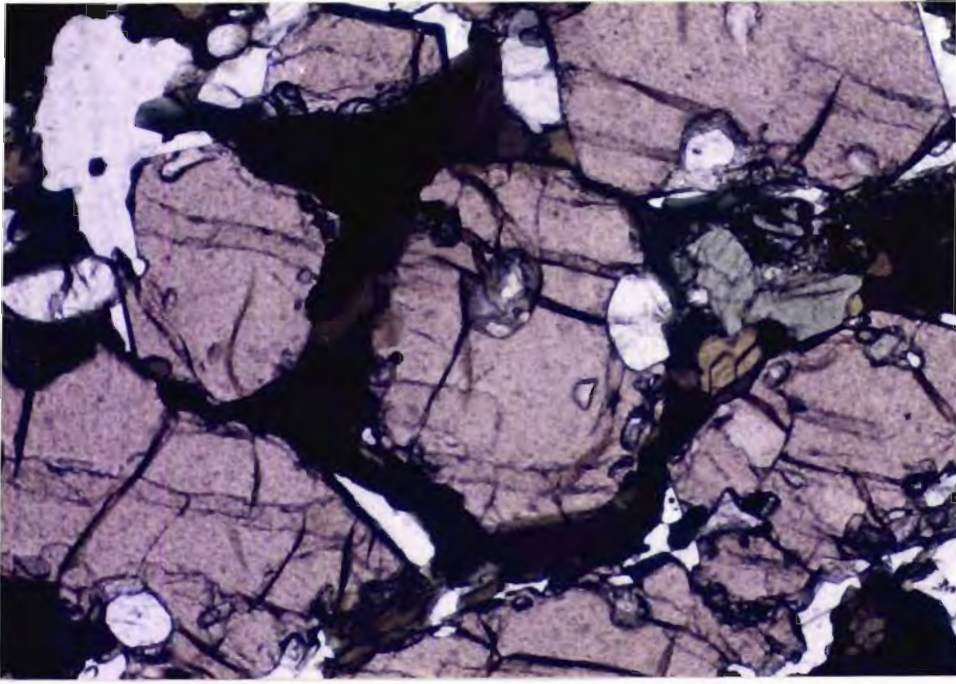
plagioclase can be seen. In rare cases plagioclase crystals show wavy extinction. Polysynthetic twinning is common and in some cases deformed twin lamellae can be observed. In addition to polysynthetic twinning plagioclase in rare cases show pericline twinning. Perthitic texture is shown by some plagioclase grains. The exsolved phase occurs as spots of irregular shape and they are distributed parallel to twin lamellae. Inclusions in plagioclase include zircon, quartz and opaques.

Small amount of microcline is present in almost all the thin sections. They occur along the edges of plagioclase and orthoclase. Some microcline crystals show perthitic blebs in it and these blebs are devoid of cross-hatched twinning. Majority of the microcline is associated with plagioclase crystals.

Quartz is present in all the thin sections and their modal percentage varies considerably (5 to 50). They occur as interstitial to other minerals. Size of quartz crystals sometimes is almost equal to that of other minerals like plagioclase, orthoclase and mafics. In some cases they are finer and show effect of recrystallization. Very elongated quartz crystals are observed in all the thin sections. Recrystallized quartz crystals have straight grain boundaries and the larger crystals have amoeboid grain boundaries. Most of the quartz especially the recrystallized ones show wavy extinction. Apatite and opaque inclusions are noted.

Garnet is observed in a few samples (eg. section P-25). Its modal content is less than 5%. Garnet contains inclusions of apatite, quartz, opaques and pyroxenes. It shows alteration to hornblende. The grain boundaries of garnet crystals are highly irregular.

Hornblende is noticed in many thin sections as a secondary mineral. They are strongly pleochroic and the colours change from pale greenish yellow to green or brownish green. It occurs as tiny crystals around pyroxene, garnet and opaques. Some opaque minerals which are seen in contact with pyroxenes

show alteration to hornblende.   They have straight grain boundaries and sometimes show triple point junctions with other minerals.

Biotite is observed in a few sections (eg. P-44 and S-6/A).   Their size varies and grain boundaries are highly irregular.   They seem to be the alteration product of hornblende.   Quartz and opaque inclusions are observed.   In S-6/A, the biotite shows a crude preferred orientation.   Sometimes biotite is seen around opaque minerals.

3.4 Mineral chemistry

The microprobe data were used to determine the structural formulae of the minerals which were used in the geothermobarometric calculations.   The data is presented with corresponding cation percentages in tables 3.1 to 3.5.   From the structral formulae, variation of composition from core to rim is also studied.   In the following part, an account of the mineral chemistry of the rocks of the northern granulite province is given.

3.4.1 Clinopyroxenes

Clinopyroxenes of both mafic granuliltes and charnockites show only minor compositional variation in different locations.   Calcium endmember content (Wo) does not show any significant variation from core to rim of the grains. It varies from 43mol% to 47mol%. Enstatite (En) content shows slight variation with location in mafic granulite samples (varying from 30 to 38 mol%). Ferrosilite (Fs) content also varies from location to location (varying from 15 to 26 mol%). In individual grains core to rim variation of these components is very little or absent. It reveals that there was no effect of retrogression and that the peak metamorphic condition is preserved.   In charnockite sample also no zoning in clinopyroxenes is observed.

Al content is less than the Al content of Nilgiri and Shevaroy Hills (.09 to 0.23 Al p.f.u). Al content is very much similar to that reported for the highly retrogressed rocks of Bhavani shear zone (0.08 to 0.13 mol%). Ti, Mn an Cr

Table 3.1a Chemical analysis of clinopyroxene, orthopyroxene, ilmenite and magnetite from sample S-7

Mineral	clinopyroxene			orthopyroxene				ilmenite	magnetite
	core	core	rim	core	core	rim	rim		
SiO2	51.45	52.23	52.18	51.79	52.60	52.06	52.76	0.00	0.06
TiO2	0.27	0.21	0.17	0.10	0.04	0.10	0.09	50.61	0.25
Al2O3	2.08	2.39	1.94	1.50	1.29	1.20	1.21	0.02	3.02
Cr2O3	0.03	0.05	0.03	0.02	0.00	0.00	0.00	0.04	0.90
FeO	11.10	10.37	10.81	27.54	27.96	28.25	28.28	48.12	90.26
MnO	0.28	0.33	0.26	0.73	0.73	0.87	0.90	0.50	0.03
MgO	12.18	12.41	12.95	18.54	18.74	18.86	19.21	1.01	0.55
CaO	21.73	22.23	22.18	0.61	0.55	0.43	0.51	0.01	0.00
Na2O	0.65	0.64	0.57	0.01	0.01	0.02	0.00	0.00	0.00
K2O	0.00	0.00	0.00	0.00	0.00	0.00	0.00	0.00	0.00
P2O5	0.00	0.00	0.03	0.00	0.00	0.01	0.01	0.00	0.00
Cations									
Si	1.95	1.95	1.95	1.954	1.972	1.960	1.962	0.000	0.001
Ti	0.01	0.01	0.01	0.003	0.001	0.003	0.003	0.948	0.003
Al	0.09	0.11	0.09	0.068	0.057	0.053	0.053	0.000	0.059
Cr	0.00	0.00	0.00	0.001	0.000	0.000	0.000	0.001	0.012
Fe3+	0.00	0.00	0.00	0.000	0.000	0.000	0.000	0.103	1.248
Fe2+	0.35	0.32	0.34	0.879	0.876	0.890	0.879	0.899	0.000
Mn	0.01	0.01	0.01	0.024	0.023	0.028	0.028	0.011	0.000
Mg	0.69	0.69	0.72	1.055	1.047	1.058	1.064	0.037	0.013
Ca	0.88	0.89	0.89	0.025	0.022	0.017	0.020	0.000	0.000
Na	0.05	0.05	0.04	0.001	0.001	0.001	0.000	0.000	0.000
End members									
En	36	36	37	54	54	54	54		
Fs	18	17	17	45	45	45	45		
Wo	46	47	46	1	1	1	1		

Table 3.1b   Chemical analysis of plagioclase and hornblende from sample S-7.

Mineral	plagioclase				hornblende			
	core	core	rim	rim	core	core	rim	rim
SiO2	60.32	60.92	62.26	60.32	42.87	43.00	43.00	42.70
TiO2	0.01	0.01	0.00	0.02	2.08	1.98	1.74	1.88
Al2O3	26.21	26.23	26.41	26.44	11.70	11.91	11.68	11.90
Cr2O3	0.00	0.05	0.00	0.00	0.05	0.05	0.04	0.11
FeO	0.15	0.06	0.08	0.19	15.78	15.83	16.30	14.01
MnO	0.00	0.01	0.00	0.00	0.15	0.11	0.12	0.19
MgO	0.00	0.03	0.01	0.00	10.88	10.81	11.46	10.81
CaO	7.89	7.57	7.72	8.20	11.42	11.84	11.67	11.72
Na2O	6.64	7.16	6.56	6.24	1.70	1.74	1.68	1.60
K2O	0.47	0.43	0.35	0.46	1.58	1.65	1.53	1.70
P2O5	0.02	0.00	0.01	0.00	0.03	0.02	0.00	0.00
Cations								
Si	2.647	2.653	2.676	2.641	6.679	6.659	6.648	6.716
Ti	0.000	0.000	0.000	0.001	0.244	0.202	0.202	0.222
Al	1.356	1.346	1.338	1.365	2.149	2.175	2.129	2.207
Cr	0.000	0.002	0.000	0.000	0.006	0.006	0.005	0.014
Fe3+	0.000	0.000	0.000	0.000	0.000	0.000	0.000	0.000
Fe2+	0.006	0.002	0.003	0.007	2.056	2.050	2.107	1.843
Mn	0.000	0.000	0.000	0.000	0.020	0.014	0.016	0.025
Mg	0.000	0.001	0.001	0.000	2.526	2.495	2.640	2.534
Ca	0.371	0.353	0.355	0.385	1.906	1.965	1.933	1.975
Na	0.565	0.605	0.547	0.530	0.514	0.326	0.504	0.488
K	0.026	0.024	0.019	0.026	0.314	0.326	0.302	0.341
End members								
An	39	36	39	41				
Ab	59	62	59	56				
Or	2	2	2	3				

Table 3.2a   Chemical analysis of clinopyroxene and orthopyroxene from
sample S-9

Mineral	clinopyroxene			orthopyroxene			
	core	core	rim	core	core	rim	rim
SiO2	52.45	51.27	52.35	52.33	51.54	52.52	52.32
TiO2	0.25	0.25	0.13	0.05	0.05	0.07	0.07
Al2O3	2.49	2.4	1.57	1.07	0.87	0.91	0.91
Cr2O3	0.01	0	0	0.01	0	0	0.03
FeO	11.96	11.92	10.2	28.38	28.78	29.43	28.16
MnO	0.47	0.52	0.36	1.06	1	1.09	1.03
MgO	11.48	11.74	12.34	18.58	17.96	18.02	18.48
CaO	22.08	21.16	22.29	0.56	0.56	0.45	0.59
Na2O	0.78	0.67	0.53	0	0.02	0	0.01
K2O	0	0	0	0	0	0	0
P2O5	0	0.01	0.04	0	0	0.04	0.01
Cations							
Si	1.947	1.942	1.972	1.968	1.97	1.974	1.974
Ti	0.007	0.007	0.004	0.001	0.001	0.002	0.002
Al	0.109	0.107	0.07	0.047	0.039	0.04	0.04
Cr	0	0	0	0	0	0	0
Fe3+	0	0	0	0	0	0	0
Fe2+	0.371	0.378	0.321	0.893	0.92	0.925	0.889
Mn	0.015	0.017	0.011	0.034	0.032	0.035	0.033
Mg	0.635	0.663	0.693	1.041	1.023	1.009	1.039
Ca	0.878	0.859	0.9	0.023	0.023	0.018	0.024
Na	0.056	0.049	0.039	0	0.001	0	0.001
K	0	0	0	0	0	0.002	0
End members							
En	34	35	36	53	52	52	53
Fs	20	20	17	46	47	47	46
Wo	47	45	47	1	1	1	1

Table 3.2b Chemical analysis of plagioclase, hornblende ilmenite and magnetite from sample S-9

	plagioclase				hornblende		ilmenite	magnetite
	core	core	rim	rim	core	rim		
SiO2	62.61	62.08	62.37	62.26	42.44	42.97	0	0.05
TiO2	0	0	0	0	2.07	1.32	48.91	0.22
Al2O3	25.6	25.39	25.83	25.88	11.89	11.85	0	0.49
Cr2O3	0	0.02	0.07	0	0.03	0	0.01	0.02
FeO	0.07	0.18	0.18	0.21	16.7	18.35	48.75	92.92
MnO	0.01	0.02	0	0	0.21	0.22	0.76	0.02
MgO	0.03	0.02	0	0	10.27	10.28	0.87	0.07
CaO	6.73	6.92	7.11	7.36	11.63	11.82	0.04	0
Na2O	6.97	7.14	7.37	7.53	1.49	0.99	0.02	0.03
K2O	0.48	0.46	0.43	0.34	1.84	1.71	0	0
P2O5	0.02	0.01	0	0.05	0.04	0.02	0	0.02
Cations								
Si	2.709	2.7	2.687	2.68	6.632	6.677	0	0.001
Ti	0	0	0	0	0.243	0.154	0.924	0.004
Al	1.306	1.302	1.312	1.313	2.19	2.171	0	0.015
Cr	0	0	0	0	0	0	0	0
Fe3+	0	0	0	0	0	0	0.152	1.975
Fe2+	0.003	0.007	0.006	0.008	2.182	2.385	0.872	0
Mn	0	0.001	0	0	0.028	0.029	0.017	0.001
Mg	0.002	0.001	0	0	2.392	2.381	0.032	0.003
Ca	0.312	0.323	0.328	0.339	1.947	1.968	0.001	0
Na	0.585	0.602	0.616	0.628	0.451	0.298	0.001	0.001
K	0.026	0.026	0.024	0.019	0.367	0.339	0	0
End members								
An	34	34	34	34				
Ab	63	63	64	64				
Or	3	3	2	2				

Table 3.3a   Chemical analysis of clinopyroxene from sample S-45

	core	core	core	core	core	rim	rim	rim
SiO2	52.4	52.06	52.31	52.4	53	52.72	52.94	52.71
TiO2	0.19	0.16	0.2	0.13	0.08	0.1	0.14	0.06
Al2O3	1.73	1.92	1.97	1.84	1.57	1.49	1.41	1.5
Cr2O3	0	0.01	0.05	0	0.04	0.04	0	0.01
FeO	15.81	14.72	14.19	14.62	14.19	13.74	13.57	12.97
MnO	0.28	0.31	0.25	0.15	0.09	0.22	0.2	0.12
MgO	10.53	10.49	10.37	10.8	10.99	10.66	11.17	11.25
CaO	20.08	20.78	21.83	21.32	21.37	22.27	22.2	22.41
Na2O	0.68	0.68	0.84	0.74	0.68	0.69	0.65	0.67
K2O	0	0	0	0	0	0	0	0
P2O5	0.01	0.01	0.03	0	0.07	0	0.01	0
Cations								
Si	1.971	1.966	1.959	1.962	1.977	1.972	1.971	1.97
Ti	0.005	0.005	0.006	0.004	0.002	0.003	0.004	0.002
Al	0.077	0.085	0.087	0.081	0.069	0.066	0.062	0.066
Cr	0	0	0	0	0	0	0	0
Fe3+	0	0	0	0	0	0	0	0
Fe2+	0.497	0.465	0.444	0.458	0.443	0.43	0.423	0.405
Mn	0.009	0.01	0.008	0.005	0.003	0.007	0.006	0.004
Mg	0.59	0.59	0.579	0.603	0.611	0.594	0.62	0.627
Ca	0.81	0.841	0.876	0.855	0.854	0.893	0.886	0.897
Na	0.05	0.05	0.061	0.054	0.049	0.05	0.047	0.049
K	0	0	0	0	0	0	0	0
P	0	0	0	0	0	0	0	0
End members								
En	31	31	30	31	34	31	32	32
Fs	26	25	23	24	23	22	22	21
Wo	43	44	46	45	44	47	46	47

Table 3.3b Chemical analysis of plagioclase, hornblende and ilmenite from sample S-45

Mineral	plagioclase		hornblende		ilmenite	
	core	core	core	rim		
SiO2	64.11	62.83	42.76	43.41	0.02	0
TiO2	0.02	0.01	1.48	1.15	49.1	48.5
Al2O3	24.47	25.17	11.65	11.38	0.01	0.01
Cr2O3	0	0.02	0.03	0.02	0	0.01
FeO	0	0.03	20.55	20.22	51.89	50.67
MnO	0	0.02	0.04	0.07	0.19	0.25
MgO	0	0.01	8.56	8.62	0.5	0.49
CaO	5.28	6.46	11.31	11.52	0.05	0
Na2O	8.1	7.87	2.06	1.89	0.01	0
K2O	0.22	0.24	1.12	1.01	0	0
P2O5	0	0.01	0	0.01	0.01	0.03
Cations						
Si	2.77	2.717	6.421	6.544	0	0
Ti	0.001	0	0.167	0.129	0.908	0.914
Al	1.246	1.283	2.061	2	0	0
Cr	0	0	0.004	0.002	0	0
Fe3+	0	0	0	0	0.183	0.172
Fe2+	0	0.001	2.58	2.52	0.884	0.89
Mn	0	0.001	0.005	0.009	0.004	0.005
Mg	0	0.001	1.915	1.915	0.018	0.018
Ca	0.244	0.299	1.819	1.839	0.001	0
Na	0.679	0.66	0.598	0.545	0	0
K	0.012	0.013	0.215	0.192	0	0
P	0	0				
End members						
An	26	31				
Ab	73	68				
Or	1	1				

Table 3.3c   Chemical analysis of garnet from sample S-45

	core	core	core	rim	rim	rim
SiO2	39.22	39.07	38.86	39.01	38.67	38.66
TiO2	0.04	0.04	0.07	0.03	0.04	0
Al2O3	21.3	21.31	20.98	21.32	21.33	21.11
Cr2O3	0	0	0	0	0.06	0
FeO	30.26	29.55	31.05	29.4	31.75	30.93
MnO	0.95	0.97	1.15	1.14	1.2	1.22
MgO	4.39	4.12	3.29	2.85	2.7	2.55
CaO	6.82	6.78	6.61	7.27	7.14	7.29
Na2O	0.03	0.01	0.02	0	0	0.02
K2O	0	0	0	0	0	0
P2O5	0.02	0.01	0.01	0.01	0	0.01
Cations						
Si	3.014	3.028	3.031	3.052	3.005	3.029
Ti	0.002	0.002	0.004	0.002	0.002	0
Al	1.93	1.947	1.929	1.967	1.954	1.95
Cr	0	0	0	0	0	0
Fe3+	0	0	0	0	0	0
Fe2+	1.945	1.915	2.025	1.924	2.063	2.026
Mn	0.062	0.064	0.076	0.076	0.079	0.081
Mg	0.503	0.476	0.382	0.332	0.313	0.298
Ca	0.562	0.563	0.552	0.61	0.594	0.612
Na	0.004	0.002	0.003	0	0	0.003
K	0	0	0	0	0	0
P	0	0	0	0	0	0
End members						
Al	63	63	67	65	68	67
Gr	18	19	18	21	19	20
Py	16	16	13	11	10	10
Sp	2	2	3	3	3	3

Table 3.4a   Chemical analysis of clinopyroxene, orthopyroxene and ilmenite from sample S-50

Mineral	clinopyroxene				orthopyroxene				ilmenite
	core	core	core	rim	core	core	rim	rim	
SiO2	51.81	51.94	53.29	52.71	52.84	52.9	51.97	53.38	0
TiO2	0.32	0.32	0.25	0.25	0.03	0.04	0.02	0	45.95
Al2O3	3.92	3.59	3.37	3.42	1.84	1.98	1.95	1.45	0.05
Cr2O3	0.02	0	0.01	0.09	0.01	0	0.03	0.01	0.05
FeO	9.44	9.36	9.12	9.03	23.58	24.11	21.28	23.71	53.27
MnO	0.31	0.27	0.29	0.35	0.58	0.67	0.58	0.65	0.17
MgO	12.46	12.5	13.21	12.68	22.27	22.07	21.49	22.46	0.8
CaO	21.61	21.49	22.3	21.99	0.42	0.3	0.4	0.32	0.01
Na2O	1.02	1.05	1.08	1.52	0	0	0.02	0	0
K2O	0	0	0	0	0	0	0	0	0
P2O5	0.02	0.01	0.01	0.01	0	0.01	0	0.02	0
	-								
Cations									
Si	1.92	1.93	1.933	1.932	1.947	1.944	1.971	1.959	0
Ti	0.009	0.009	0.007	0.007	0.001	0.001	0.001	0	0.858
Al	0.171	0.157	0.144	0.148	0.08	0.086	0.087	0.063	0.001
Cr	0.001	0	0	0.003	0	0.001	0.001	0	0.001
Fe3+	0	0	0	0	0	0	0	0	0.28
Fe2+	0.293	0.291	0.277	0.277	0.727	0.741	0.675	0.728	0.827
Mn	0.01	0.008	0.009	0.011	0.018	0.021	0.019	0.02	0.004
Mg	0.688	0.692	0.714	0.692	1.223	1.208	1.215	1.228	0.03
Ca	0.858	0.856	0.867	0.863	0.017	0.012	0.016	0.013	0
Na	0.073	0.076	0.076	0.108	0	0	0.001	0	0
K	0	0	0	0	0	0	0	0	0
End members									
En	37	38	38	38	62	62	64	62	
Fs	16	16	15	15	37	38	35	37	
Wo	47	46	47	47	1	1	1	1	

Table 3.4b   Chemical analysis of plagioclase and hornblende from sample S-50.

Mineral	plagioclase				hornblende			
	core	core	rim	rim	core	core	rim	rim
SiO2	61.6	63.3	60.85	61.74	42.67	42.8	42.7	42.67
TiO2	0.02	0.03	0.02	0.01	2.04	2.16	1.96	2.05
Al2O3	25.47	26.18	25.54	25.67	12.7	12.83	12.61	12.97
Cr2O3	0	0.01	0.03	0	0.09	0.06	0	0
FeO	0.03	0.05	0.24	0.28	13.7	14.17	14.03	14.54
MnO	0.01	0.03	0	0.02	0.17	0.17	0.11	0.13
MgO	0.01	0	0.01	0.02	11.92	11.82	11.87	11.88
CaO	6.85	6.54	7.09	7.13	11.92	11.63	11.91	11.94
Na2O	7.18	6.48	7.25	7.2	1.59	1.63	1.56	1.59
K2O	0.38	0.41	0.45	0.5	2.17	2.08	2.08	2.14
P2O5	0.02	0	0	0.01	0.02	0	0	0.03
Cations								
Si	2.695	2.714	2.674	2.683	6.563	6.56	6.579	6.521
Ti	0.001	0.001	0.001	0	0.236	0.249	0.227	0.236
Al	1.314	1.323	1.323	1.315	2.303	2.318	2.291	2.337
Cr	0	0.001	0.001	0	0.011	0.007	0	0
Fe3+	0	0	0	0	0	0	0	0
Fe2+	0.001	0.002	0.009	0.01	1.762	1.816	1.808	1.858
Mn	0	0.001	0	0.001	0.002	0.022	0.014	0.017
Mg	0.001	0	0.001	0.001	2.732	2.7	2.732	2.706
Ca	0.321	0.3	0.334	0.332	1.964	1.91	1.966	1.955
Na	0.609	0.539	0.618	0.607	0.474	0.484	0.466	0.471
K	0.021	0.025	0.025	0.028	0.426	0.407	0.409	0.417
End members								
An	34	35	34	34				
Ab	64	63	63	0.63				
Or	2	3	3	3				

Table 3.5a   Chemical analysis of clinpyroxene and orthopyroxene from sample S-51

Mineral	clinopyroxene				orthopyroxene			
	core	core	rim	rim	core	core	rim	rim
SiO2	52.88	52.9	53.83	53.22	52.63	53.2	52.62	53.77
TiO2	0.21	0.23	0.14	0.14	0.2	0	0.21	0.04
Al2O3	2.8	2.87	1.67	2.82	2.84	1.29	2.76	1.17
Cr2O3	0.1	0.09	0.06	0.13	0.06	0.06	0.11	0.07
FeO	9.55	9.88	8.11	9.5	12.33	23.7	10.54	23.11
MnO	0.3	0.31	0.28	0.3	0.36	0.69	0.34	0.71
MgO	12.62	12.46	14.14	12.54	13.06	21.63	12.77	22.61
CaO	21.47	21.49	22.52	21.66	19.15	0.41	19.81	0.38
Na2O	1.29	1.26	0.82	1.29	1.13	0.01	1.23	0.02
K2O	0	0	0	0	0	0	0	0
P2O5	0.01	0	0	0.03	0	0	0	0.01
Cations								
Si	1.953	1.953	1.97	1.953	1.953	1.972	1.953	1.97
Ti	0.006	0.006	0.004	0.006	0.006	0.006	0.006	0.001
Al	0.122	0.126	0.072	0.126	0.126	0.056	0.126	0.051
Cr	0.003	0.004	0.002	0.004	0.004	0.002	0.004	0.002
Fe3+	0	0	0	0	0	0	0	0
Fe2+	0.295	0.294	0.248	0.294	0.294	0.735	0.294	0.708
Mn	0.009	0.007	0.009	0.007	0.007	0.022	0.007	0.022
Mg	0.695	0.682	0.771	0.682	0.682	1.195	0.682	1.234
Ca	0.85	0.856	0.883	0.856	0.856	0.016	0.856	0.015
Na	0.092	0.097	0.058	0.097	0.097	0.001	0.097	0.001
K	0	0	0	0	0	0	0	0
End members								
En	38	37	41	37	39	61	39	63
Fs	16	16	13	16	21	38	18	36
Wo	46	47	46	47	41	1	43	1

Table 3.5b Chemical analysis of plagioclase and ilmenite from sample S-51

Minerals	plagioclase				ilmenite
	core	core	rim	rim	
SiO2	65.12	64.42	64.7	64.65	0.02
TiO2	0	0	0.01	0.01	25.44
Al2O3	24.39	24.44	24.11	24.57	0.1
Cr2O3	0.02	0	0	0	0.45
FeO	0.06	0.13	0.07	0.09	70.5
MnO	0.03	0	0.01	0.01	0.1
MgO	0	0.01	0	0	0.34
CaO	5.23	5.62	5.15	5.74	0.01
Na2O	8.24	7.92	8.17	7.97	0.01
K2O	0.4	0.44	0.41	0.52	0
P2O5	0	0	0	0	0.02
Si	2.781	2.768	2.786	2.765	0
Ti	0	0	0	0	0.483
Al	1.228	1.238	1.224	1.239	0.002
Cr	0.001	0	0	0	0.009
Fe3+	0	0	0	0	1.023
Fe2+	0.003	0.003	0.003	0.003	0.465
Mn	0.001	0	0	0	0.002
Mg	0	0.001	0	0	0.012
Ca	0.239	0.259	0.238	0.263	0
Na	0.682	0.66	0.682	0.682	0.001
K	0.022	0.024	0.023	0.028	0
End members					
An	25	27	25	28	
Ab	72	70	72	69	
Or	2	3	2	3	

contents are very low. Fe, Al, Ti and Na generally decrease towards the margin of the grains. Ca and Mg show an increasing trend towards margin. Thus, during metamorphism clinopyroxene solid solution has changed by diffusion process towards diopside rich composition. In charnockite sample core to rim variation is very less or absent.

3.4.2 Orthopyroxenes

Irrespective of the location, orthopyroxene crystals do not show zoning. The orthopyroxene crystals are extremely homogeneous. Based on the enstatite content two groups of orthopyroxenes can be identified. In one group, enstatite content is ranging from 61-64 mol% while in the other it ranges from 52-54 mol%. Orthopyroxenes in the charnockite sample come in the former group. Ferrosilite content is consistent with this grouping. Ferrosilite content ranges from 35-38mol% in the former group while in the latter it ranges from 45-47mol%.

Al does not show any significant variation from core to rim of individual orthopyroxene crystals. Location wise also there is not much variation in the Al content. The Al content of orthpyroxenes is similar to the Al content of Nilgiri and Shevaroy Hills. Ca, Mn, Ti and Cr are low and they do not show any significant variation from core to rim. Thus orthopyroxenes also have homogeneous composition.

The composition of clinopyroxenes and orthopyroxenes are plotted in the pyroxene triangle (after Poldervaart and Hess, 1951) (Fig. 3.7). Clinopyroxenes of S-7, S-9 and P-50 are similar in composition and they fall in the salite field. In the case of P-45 and P-51, the clinopyroxenes fall in the augite and salite fields.

3.4.3 Garnet

It is observed in sample P-45 only. The garnet of this rock is essentially solid solution of the end members almandine, grossular, pyrope and spessartine. Generally almandine content shows a slight increasing trend
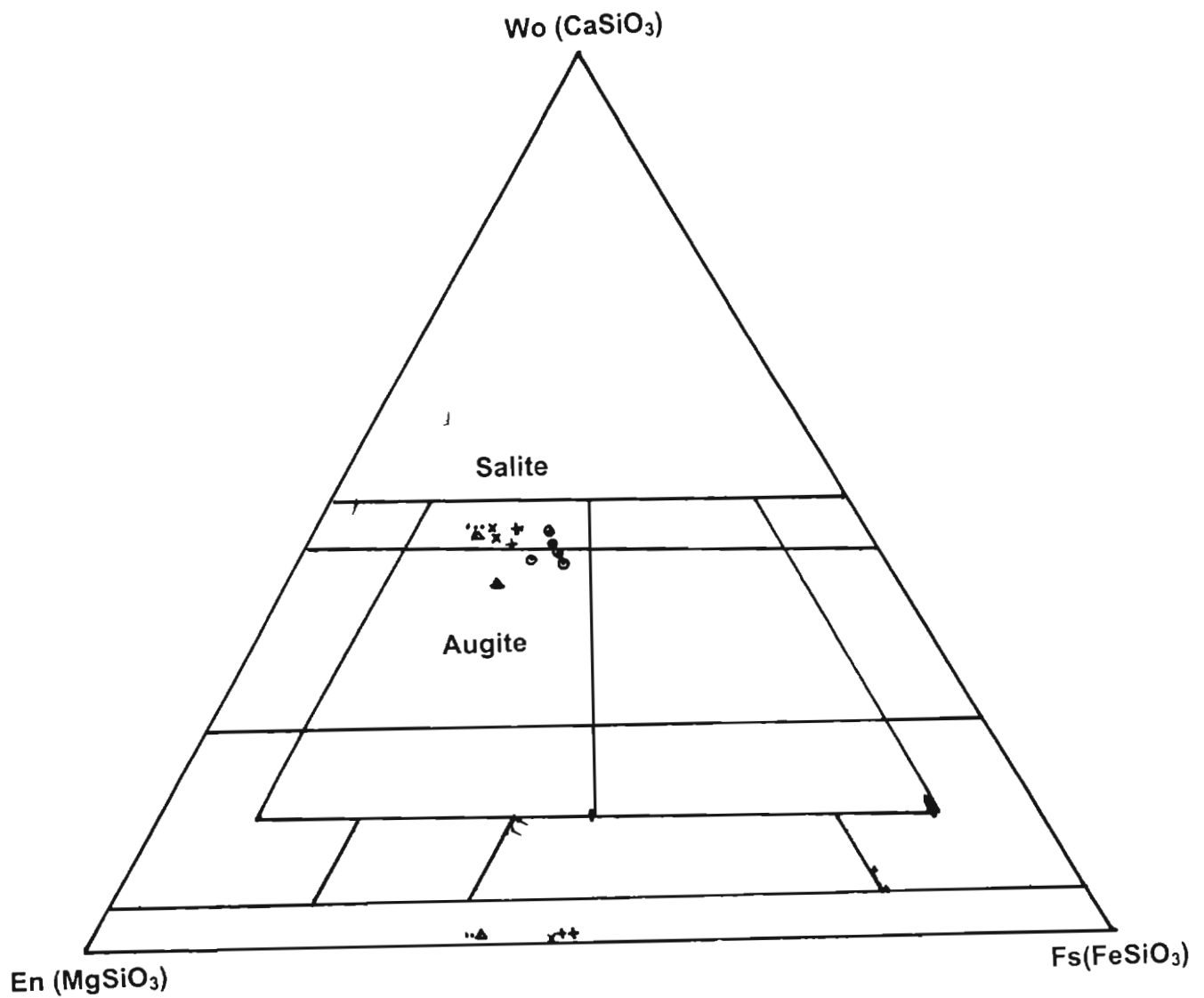
Fig. 3.7   Plot of clinopyroxenes and orthopyroxenes of the rocks of northern granulite province in the pyroxene triangle (after Poldervaart and Hess, 1951). Symbols: solid squares- S-7, plus- S-9, circle- P-45, dot- P-50 and triangle- P-51.

towards rim. Sometimes grossular also shows an increasing trend. Pyrope shows a decreasing trend from core to rim. Spessertine does not show core to rim variation. Almandine is the most dominant end member and it varies from 63-68 mol%. Grossular ranges from 18-21mol%. Pyrope ranges from 10-16 mol%. Spessertine is in the range of 2-3mol%. In this sample no orthopyroxene is present. In all other samples garnet is absent and orthopyroxene is present and this reflects change in bulk chemistry.

3.4.4 Plagioclase

Plagioclase shows wide variation in composition. Generally they are all of oligoclase-andesine range. In sample P-45, it shows small degree of zoning. An content increases from core to rim while Ab content decreases from core to rim. Orthoclase content remains same. In all other samples no zoning is observed and they are all of albitic in composition. Maximum albitic content is seen in the sample P-51 which is a charnockite. The lowest content of Ab (59mol%) is seen in the sample S-7, a mafic granulite.

The An content in the analysed samples varies from An_{25} to An_{39}. An content and bulk rock chemistry or the mineral assemblage has got some relation. High An content (ie., in the range An_{34} to An_{39}) is shown by the assemblage cpx-opx-hbl-plag. The range An_{25} to An_{27} is shown by the assemblage cpx-opx-plag. An content of plagioclase in the charnockite sample is 26mol%.

3.4.5 Hornblende

Hornblende is found in the samples S-7, S-9 and P-50. In all these rocks same assemblage is obtained (ie., cpx-opx-hbl-plag.). Hornblende in all these samples are similar in its composition. Core to rim variation in composition is also very much insignificant. Mg and Ca shows an increasing trend from core to rim. Na content is decreasing from core to rim.

3.4.6 Ilmenite

This mineral is present in all the analysed samples. Two groups of ilmenite is observed. In one group, Ti content is higher than Fe^{3+} while in the other Ti content is less than or almost equal to Fe^{3+} Ilmenite of the former group is present in the samples P-45, P-50 and P-51. Fe^{3+} content in ilmenite is more in samples in which magnetite is present. In other samples in which Ti is less than Fe^{3+}, magnetite is absent. In all the ilmenites small amount of Mg, Mn and Cr are present as impurities.

3.4.7 Magnetite

Magnetite is present in samples S-7 and S-9. Magnetite is almost pure. Very small amount of Mg, Mn and Cr are present as impurities.

3.5 Geothermobarometry

During the last few years, two methods are commonly used for the evaluation of temperatures and pressures of metamorphism. Comparison of observed mineral assemblages with those predicted from the experimentally determined positions of P-T reaction curves forms one method. The second method is the geothermobarometry based on the partitioning of elements or isotopes between coexisting phases. In this case single reactions written to relate a small group of mineral end members and calibrated by direct experimental investigations were used. Further refinements of this approach have resulted in the use of all available experimental information on thermodynamics in the evaluation of P-T locations of chosen reactions (Hansen,1983).

With more than one thermometer and barometer for a particular mineral assemblage, the system becomes over determined and some method is required for finding the best P-T. Powell (1985) applied a least-squares method for averaging the calculated pressures for an independent set of reactions for a rock representing all the available equilibria. Later he incorporated the

uncertainties and correlations of the calculated pressures. This method is called average P-T method (Powell and Holland, 1994). In this method an independent set of reactions representing all the equilibria are used. Earlier methods involve many equilibria to find the P-T of formation of a rock. In finding a P-T of formation, there is an implied displacement of the equilibria to coincide with this P-T. These displacements are mainly made by varying the activities of the end-members of the mineral in proportion to their uncertainties. As a consequence, the equilibria are constrained to move in a more or less highly correlated way because the equilibria involve overlapping subsets of the end-members. These essential correlation should be included in any thermobarometry calculations. Of the three thermobarometry approaches in use, the TWEEQU approach of Berman (1991), the individual species approach of Gordon (1992) and average P-T approach of Powell and Holland (1994), only the last two are optimal on this basis. In addition in the average P-T , uncertainties and a range of diagnostics for outlier identification can be calculated in a computationally straightforward way.

For this work, average P-T method of Powell and Holland (1994) is used for the evaluation of P-T of formation of the metamorphic rocks. In all the calculations XH_2O is assumed as 0.2. With this method considerable reliability can be claimed for the P-T values. Minerals attain equilibrium at the peak of metamorphism and this equilibrium is sometimes reset by later retrogression. Petrographically this may be evaluated by secondary mineral paragenesis replacing the peak metamorphic assemblage. The differences in compositions between the core and rim areas of coexisting phases and P-T estimates calculated for core and rim data separately may give quantification of the changes in P and T. Therefore, the interpretation of P-T estimates should take into account the late metamorphic history of the rocks.

3.5.1 Results of geothermobarometry

Average P-T method has been applied to estimate P and T of metamorphism by making use of the core and rim compositions of co-existing minerals of the assemblage. Retrogression to hydrous phases at lowered temperature is noticed in almost all the thin sections studied. Thus rim composition is important in the evaluation of re-equilibration conditions. P-T estimates from core compositions represent the conditions near the peak of granulite facies metamorphism. The validity of a regional metamorphic study rests on the assumption that the selected samples characterize the metamorphism of the given area. Samples from northern granulite province have two types of assemblages and of these pyroxene granulite samples show textural evidence of retrogression while charnockite does not show. P-T estimates of both core and rim were determined and thus peak and incipient retrogression phases of metamorphism can be assessed. Location of the samples and the estimated pressures and temperatures are given in figures 3.8 and 3.9.

3.5.1.1 Northern granulite province

For the geothermobarometric studies of this province, 5 samples viz., S-7, S-9, P-45, P-50 and P-51 were analyzed and a brief description is given below:

S-7: Mafic granulite from a location 1 km. south of Peringom (Location No. S7). Mineral assemblage is cpx-opx-plg-ilm-mt.

S-9: Mafic granulite from 50m south of the location S7.
Mineral assemblage is cpx-opx-hbl-plg-ilm-mt.

P-45: Mafic granulite from a location ½ km west of Kuttupuzha (Location No. P45). Mineral assemblage is cpx-hbl-gt-plg-ilm.
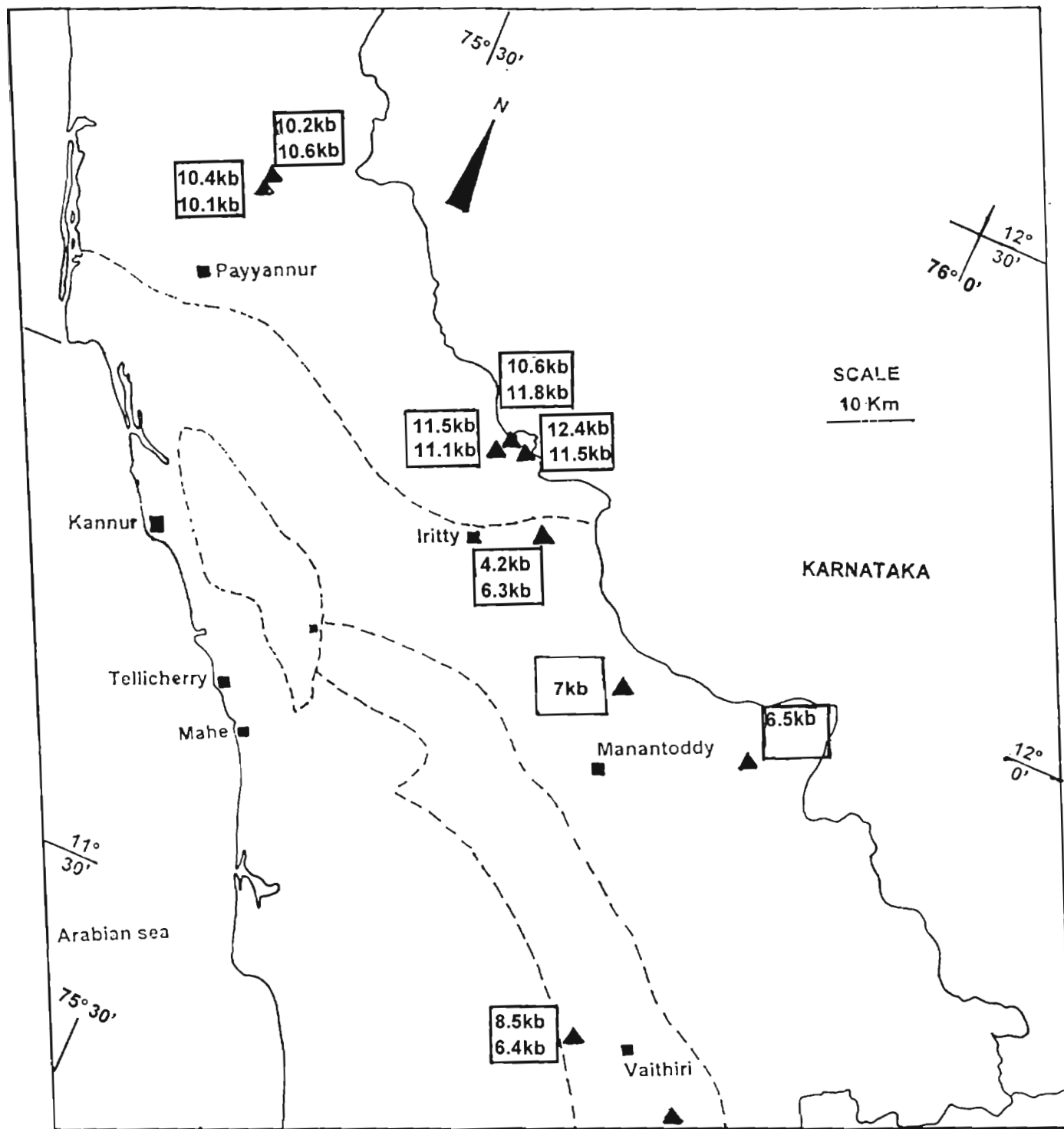
Fig. 3.8 Map of northern Kerala showing the location of the samples (solid triangles) and corresponding pressures calculated for core and rim compositions. The pressure values are given in boxes with core pressure in the upper half and rim pressure in the lower half.
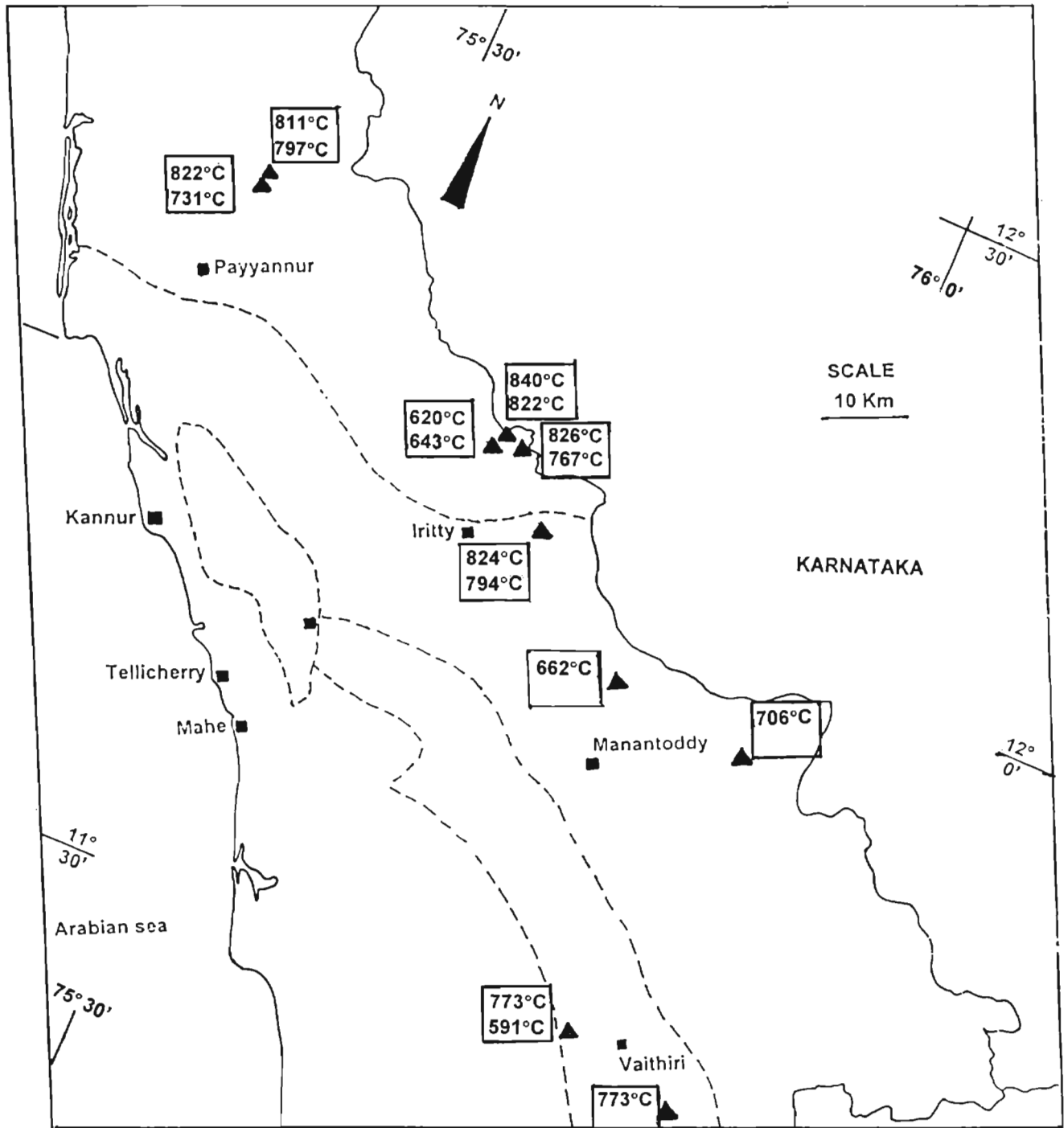
Fig. 3.9 Map of northern Kerala showing the location of the samples (solid triangles) and corresponding temperatures calculated for core and rim compositions. The temperature values are given in boxes with core temperature in the upper half and rim temperature in the lower half.

P-50: Mafic granulite from a location 100m east of Mattara junction (Location No. P50). Mineral assemblage is cpx-opx-hbl-plg-ilm.

P-51: Charnockite from a location 300m SW of Mattara (Location No. P51). Mineral assemblage is cpx-opx-plg-ilm.

The results of estimations of temperature and pressure are presented in table 3.6.

It is found that temperatures estimated from core composition of samples of the northern granulite province are very high (>800°C) with a narrow range among samples (811 to 840°C). This temperature indicates the peak temperature of the granulite facies metamorphism. The sample P-51 shows the lowest values of temperature for both core and rim compositions. Temperature values from rim compositions are slightly lower than the core temperature and it varies from 731°C to 822°C. Rim temperatures indicate that the marginal parts of the mineral grains were re-equilibrated at slightly lower temperatures. The difference between the temperatures calculated from core and rim compositions indicates that there was a resetting event associated with minor retrogression.

Pressure values estimated from core as well as rim compositions are very high(>10 kb). For sample S-7 and S-9, the difference between core and rim pressure is less and so an isobaric cooling event can be attributed. Except P-50, all the other samples show higher pressures in core. This feature and almost uniform high pressure indicate that lower crustal segments of the northern granulite province remained for considerably long period under the peak metamorphism at crustal depth of around 35km and have been uniformly exhumed. The pressure values are generally high towards SE end of this province and thus a tilt towards NW can be inferred. From the high pressure values it can also be concluded that the northern granulite province represents lower part of a thick Proterozoic crust.

Table 3.6   Results of geothermobarometry

Sample No.	assemblage	Temperature		Pressure	
		core	rim	core	rim
S-7	cpx-opx-hbl-plg-ilm-mt	811	797	10.2	10.6
S-9	cpx-opx-hbl-plg-ilm-mt	822	731	10.4	10.1
P-45	cpx-hbl-gt-plg-ilm	826	767	12.4	11.5
P-50	cpx-opx-hbl-plg-ilm	840	822	10.6	11.8
P-51	cpx-opx-p;g-ilm	620	643	11.5	11.1
I-4	gt-plg-bio	824	794	4.2	6.3
M-11	gt-opx-plg	706		6.5	
341	gt-plg-bio	662		7.0	
140	cpx-opx	773			
158	cpx-opx-gt	773	591	8.5	6.4

From the pressure estimates, approximate thickness of the crust during Precambrian time can be calculated by the method of Raith et al. (1983) who calculated the thickness of the Late Archaean crust of Nilgiri region under the assumption that no significant addition to the lower crust has occurred since that time. Load pressure increases with depth at a rate of about 250-350 bars/km (Winkler, 1988). The thickness of the present-day crust in Peninsular India is 30-40km (Kaila et al., 1979). Moreover, the depth at the time of metamorphism varies from 34km to 38km from NE to SW. From these values, thickness of the Proterozoic crust can be calculated assuming that there was no later addition to the lower crust. Thus the probable thickness of the Precambrian crust is found to be varying from approximately 69-73km. However, these values seem enormous, and thus the role of later addition to the crust by underplating may be one of the factors involved in the crustal evolution of this province. The felsic nature of the charnockites are also not in favour of extreme high thickness during Precambrian. Such lower crusts are generally more basic and depleted in K, Rb etc. than what is recorded for this area.

Geothermal gradient during the metamorphic peak can be assessed from the average temperature of this province(excluding the temperature estimates from P-51 in which very low temperature is obtained). The geothermal gradient is determined to be ~22°C /km. This is close to the normal geothermal gradient.

3.5.1.2 Wynad schist belt

For this province, miocroprobe data from previous works pertaining to three samples viz., I-4, M11and 341 are utilized. Samples I-4 and M11 are taken from Krishnaraj et al. (1994) and sample 341 is taken from Ravindra Kumar and Srikantappa (1987). Sample details are given below:

(1) I-4- Garnet-sillimanite-biotite gneiss from Angadikkadavu near Iritty (lat. 12° 2'and long. 75° 45').
Mineral assemblage: gt-plg-bio

(2) M-11 – Garnet-orthopyroxene-clinopyroxene-plagiloclase granulite from Kattikulam, Panavalli road, east of Mananthavady, 1Km SSW of Panavalli(lat. 11° 53'and long. 76° 2').

Mineral assemblage: gt-opx-plg

(3) 341 - meta pelite (lat. 11° 55' and long. 75° 52').

Mineral assemblage: gt-plg-bio

For M-11 and 341 temperature is low while for I-4 temperature is as high as northern granulilte province. Due to the lack of enough data, for M-11 and 341 only core temperature and pressure were determined. Pressures estimated from core compositions of these samples is very low compared to northern province. The pressure ranges from 6.3 to 7 kb. Pressure from rim composition of I-4 gives still lesser value of 4.2 kb.

Temperature values for this province is low for samples M-11 and 341 while I-4 has higher temperature. This higher value may be due to its proximity to the Karikkottakkari diorite intrusion. Pressure values are lesser in all the samples and is almost uniform. Thus an average temperature of 700°C and an average pressure of 6.5 kb can be assigned to this province. From this pressure, the average depth at the time of metamorphism is calculated to be 20 km and so in this province, relatively upper part of the crust is exposed.

3.5.1.3 Southern Charnockite province

Mineral chemistry data on two rocks of this province are taken from Nambiar et al. (1989) for P-T calculations of this province. A brief description of these two samples are given below:

140 - intermediate charnockite (latitude: 11° 45' 05" and longitude: 76° 03' 15")

Mineral assemblage: cpx-opx-plg-qtz

158 – basic granulite (latitude: 11° 07' 10" and longitude: 76° 10' 05").
Mineral assemblage: cpx-opx-gt-plg-qtz

Core temperatures calculated from these two samples are exactly same(773°C). This temperature is low compared to northern granulite province. For sample 140, the data is insufficient and hence only core temperature was calculated using this sample. Sample 158 gives a low temperature from rim compositions (591°C). Pressure estimated from 158 is higher than that of the Wynad schists and gneiss province and lesser than that of the northern granulite province. The pressure from rim composition is almost equal to the rim pressure of sample I-4. Harris et al., (1982) gave pressure estimates for north of Nilgiri area as 8.3±1.0 kb using the barometer of Perkins and Newton (1981). This is equal to the pressure estimated in this work. Temperature is also same in both cases.

Temperature estimated from the core composition of sample 158 is equal to the temperature estimated from sample 140. Rim temperature of the sample 158 is very low and this is manifested by the complete retrogression in this province. Core pressure is lesser than the pressure estimates of northern granulite province and greater than that of the schists and gneiss province. Rim pressure is low and it indicates an uplift event. The exposed crustal level was at a depth of around 25 km at the time of granulite facies metamorphism.

3.5.1.4 Province 4
Major rock type of this province is biotite-hornblende gneiss which is considered as product of retrogression of charnockites as relict enclaves of the latter are observed in them. No mineral chemistry data are available for this province and so P-T conditions of southern Indian charnockites (various workers) can be assumed for the province 4. Thus a temperature range of 600-700°C and a pressure range of 6-8 kb is assigned. The approximate depth at the time of metamorphism was calculated to be 23km.

3.5.1.4 Vengad basin

For this province, the pressure and temperature were determined qualitatively using the mineral assemblage. The mineralogy of biotite and muscovite of the schist suggest that the rocks have undergone metamorphism equivalent to that of the quartz-albite-epidote-biotite sub-facies of greenschist or lower amphibolite facies (Nair et al., 1980). The Vengad basin is the equivalent of Dharwar of Karnataka and geothermobarometric studies on Dharwar schists gave a temperature of 500°C and a pressure of 4-5 kb (Raase et al. 1986). Thus a temperature range of 450-500°C and a pressure range of 4-5 kb can be assigned to the Vengad group and its mineral assemblage supports this. Thus, in the Vengad basin, the crustal depth at the time of metamorphism is calculated to be approximately 15km.

The depth at the time of peak metamorphism calculated for all these provinces are given in figure 3.10. The P-T fields obtained for these provinces can be compared with the P-T fields of the adjoining areas calculated by earlier workers. These P-T fields are shown in the figure 3.11. Thus it is seen that P-T condition of the northern granulite province is higher than that of the Nilgiri uplands (N) and northern slopes of Nilgiri hills (Nm), Biligirirangan hills (BR hills), Kodaikkanal massifs, Palghat gap, and Madras granulites

3.6 Discussion and conclusion

The above detailed P-T data and their petrographic information regarding the metamorphic rocks of the northern part of Kerala reveal that the P-T conditions of metamorphism vary from province to province and thus had different tectonometamorphic history. The provinces 3 and 4 forms the western portion of the Nilgiri granulites and the 1st province is an isolated patch of granulites, separated from the Biligirirangan Hills by the intervening Sargur and Wynad schist belts. A continuity was established between Bililgirirangan hills and the Dharwar craton by Hansen et al. (1984) but a discontinuity was suggested between the Nilgiri granulites and the Dharwar craton (Raith et al.
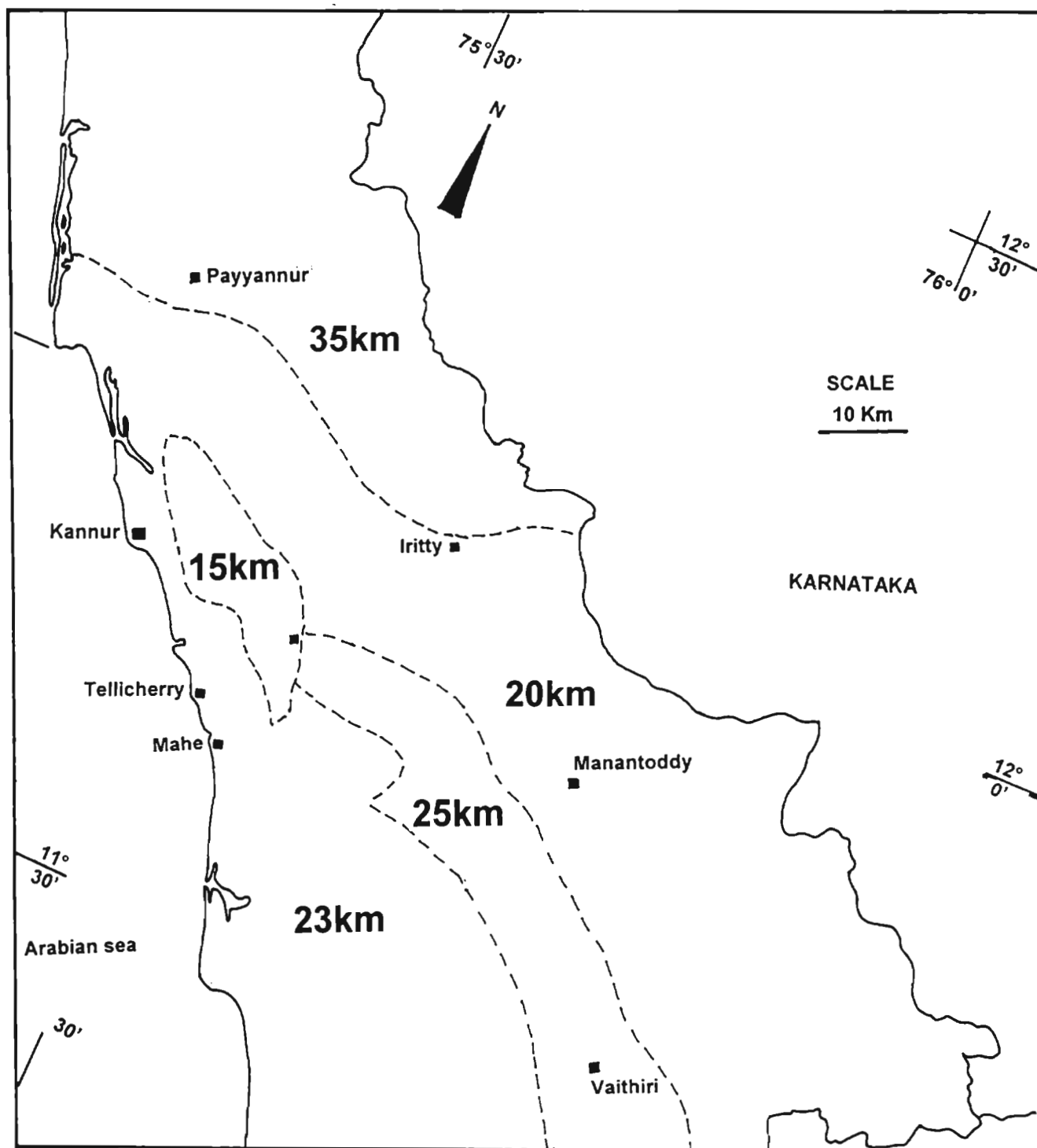
Fig. 3.10   Map of northern Kerala showing the inferred depths at the time of peak metamorphism for the different metamorphic provinces.
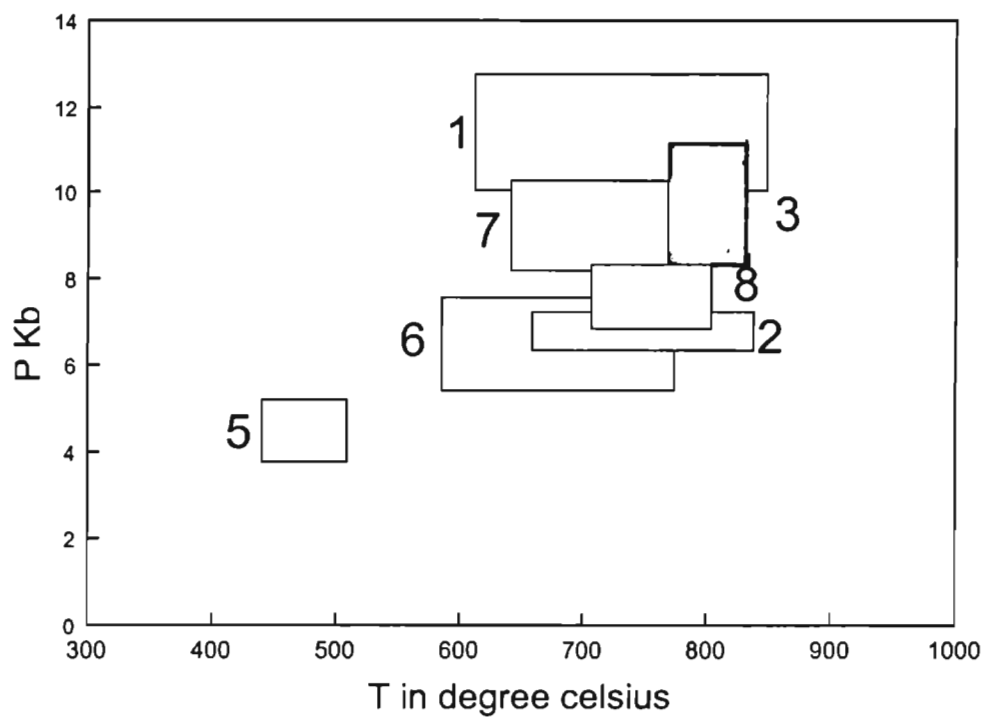
Fig. 3.11 Comparison of P-T fields of different metamorphic provinces of Northern Kerala (1 to 5). Province 4 falls within the field of province 3. Nilgiri massif- (6), Northern margin of Nilgiri massif- (7) and Biligiri rangan hills- (8).

1990 and Janardhan, 1989). The two granulite blocks of the region viz., Nilgiri granuliltes and Biligirirangan Hills were evolved in different geodynamic environments but witnessed a common granulite facies event at 2.51 Ga. (Janardhan et al., 1994). According to Janardhan et al. (1994), the Moyar shear zone represents the line of suture along which the Nilgiri terrain which evolved in an island arc like environment accreted onto the Biligirirangan hills terrain which forms the deformed marginal crust of the Dharwar craton and this happened at c.2600 Ma. It is suggested that during Archaean, plate tectonics was in operation (Bickle, 1978; Abbott and Hoffmann, 1984; Campbell and Jarvis, 1984; Martin, 1986) and so a model involving modern subduction zone like environment accompanied by collision and crustal thickening may be suggested for granulite terrains towards north and south of the Wynad schist belt where the line of suture is represented by the Bavali shear.

The provinces on either side of the Bavali shear zone (ie., province 1 and provinces 3 and 4) are showing two pressure levels. The pressure level is high in the northern province and this indicates that the northern block has been uplifted with respect to the southern crustal segment along the Bavali shear zone or alternatively it represents lower parts of a relatively more thickened crust. Structural studies as discussed in the previous chapter support that the northern block has moved relatively up along the Bavali shear. Interpretation of a preliminary Bouger gravity anomaly map of Southern India south of the 16th parallel (Krishna Brahmam, 1993) revealed the presence of a gravity high trending almost E-W with its peak at about 35 km north of the 12th parallel and it extends into Arabian sea. On land the axis of this gravity high has a length of about 195 km with its eastern end about 20km east of Mysore. Krishna Brahmam (1993) suggested that the source of a major part of this anomaly is certainly within the crust and could be ultrabasic rocks. Interpretation of a very recent gravity survey in Northern Kerala (Nambiar et al., 1999) revealed the presence of a thick and high density mafic body extending approximately in E-W direction under the block north of Bavali shear zone. This interpretation is based

49

on the gravity high observed towards the north of Bavali shear. At the same time, a gravity low is observed towards the south of the Bavali shear zone. These geophysical interpretations reveal contrasting subsurface nature of the crustal blocks north and south of Bavali shear. From all these it could be concluded that the granulite block to the north of Bavali shear zone (the block into which the Perinthatta anorthosite was emplaced) has been uplifted more with respect to the southern block.

• • •

Chapter IV
FIELD RELATIONSHIPS AND PETROGRAPHY

4.1 Introduction

The Perinthatta anorthosite has an area of exposure of about 60km^2 and it is located about 15km NE of Payyannur town in Kannur district. As discussed in the previous chapter, the anorthosite pluton is seen intruded in the granulite terrain. The exposures studied include working quarries, abandoned quarries, stream side exposures and well and road cuttings.

4.2 Field relationships

Western margin of the pluton is covered by coastal sedimentaries. Laterite cover also masks the pluton in various parts. Thus there is uncertainty regarding the aerial extent of the pluton. Fresh exposures of anorthosite are very scarce due to thick laterite and sedimentary cover. A few exposures are seen along stream courses, working/abandoned quarries, well and road cuttings etc. However, a large number of quarries (including abandoned ones) are present in the area and these provide a lot of information on the nature of the fresh rocks, their characteristics and their field relations. The places where more number of quarries are located are Perinthatta, Porakkunnu, Kuttur, Mathamangalam, Perul, Peruvamba, Peringom, Olayampadi, Kozhumal and Eramam (These and other important locations are shown in figure 4.1 and the sample locations are listed in Appendix-I).

In all the locations anorthosite shows alteration to laterite or sometimes to a clayey soil. In some cases only topsoil occurs as overburden and in other cases very thick cover of laterite is seen as overburden. Sometimes topsoil is observed above the laterite. Soil cover reaches a maximum thickness of 3m. Thickness of laterite zone is varying from 2 to 10m (Fig. 4.2). On weathering, feldspar which is originally grey becomes light grey in colour and in extreme case of weathering clay-rich soil is seen developed as a layer. Sometimes, the

Scale
2 km

N

PERINGOM

Chattiyol

PERINTHATTA

Aravamchal

Tavidisseri

Porakunnu

Mathamangalam

ERAMAM

ALAPPADAMBA

Ettukuduka

ALAKKAD

KOVUMMAL

PERALAM

75° 20'   75° 15'   75° 12'

14°

12°

12°
10'

12°
7'

75° 20'   75° 15'   75° 12'
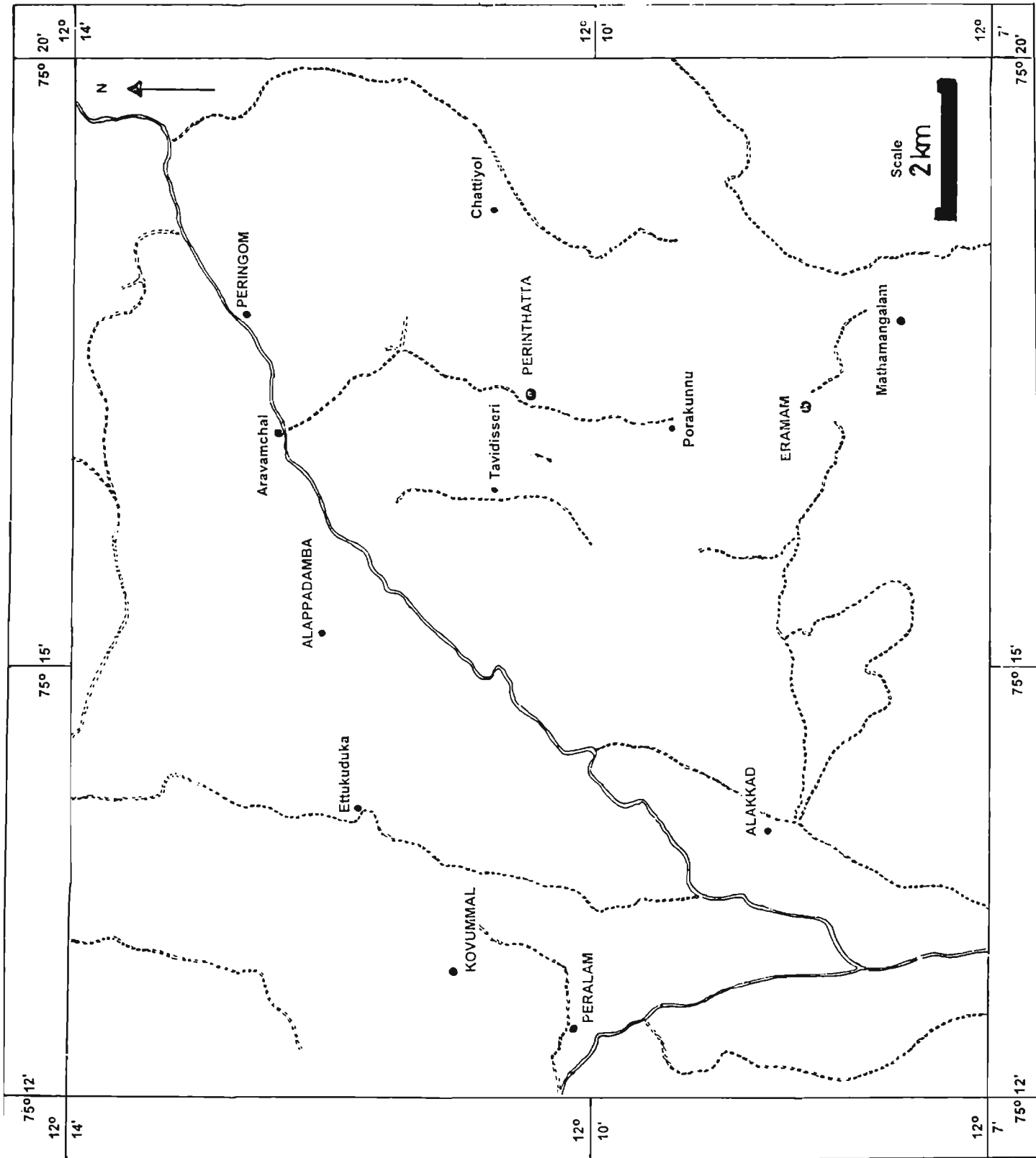
weathered surface of anorthosite shows a light yellowish colour. At Porakkunnu, this feature is clearly seen (Fig.4.3). The yellowish colour is developed when the mafic minerals in the anorthosite disintegrate at the surface. The weathering and lateritisation is seen going into the fresh rock along fractures or joints which are vertical or nearly so. At certain locations, on weathered outcrops of Perinthatta pluton, numerous pits are seen with diameter ranging from 0.2mm to 3cm. These pits were developed due to the removal in solution of pyroxene crystals. The diameter of the pits increases in accordance with the increase in the grain size of the pluton. The largest such pits are seen in Perinthatta area where the rock is very coarse-grained (Fig. 4.4).

In the field anorthositic rocks show variation in many aspects including structure, petrography, colour and texture. Variation in grain size is the most conspicuous one while the variation in others is not so discernible.

Generally, the Perinthatta pluton is composed of a coarse to very coarse grained rock and the rock is dark grey in colour with a slight variation in the shade (Fig. 4.5). The dark grey colour is essentially due to the dark grey colour of the plagioclase feldspar which is the dominant mineral phase. Even though the rock is dark grey coloured, feldspar crystals can easily be identified due to their cleavage and subvitreous lustre. These features are very clear in larger crystals as those seen in quarries near Perinthatta. In only one location, pluton shows a very light colour. The exposure of this bleached rock is limited to a road side outcrop at Alakkad. In an outcrop in a small stream very near to this also this lighter coloured rock is seen.

The coarsest type of anorthosite which is almost pegmatitic is restricted to Perinthatta region where the plagioclase crystals are about 10cm long and 1.5cm wide. Megacrysts of pyroxenes are also seen in them (Fig. 4.6). Next size grade of plagioclase feldspar is approximately 2cm. This very coarse grained type anorthosite is seen around Perinthatta, Porakkunnu and Vattappara. In this

region most of the crystals are large but smaller feldspars of size approximately 0.2cm were also observed in them. For bigger feldspar crystals, the maximum width observed is 1cm. These rocks are grouped as very coarse-grained type.

Grain size of anorthosite decreases towards west and it becomes medium to coarse grained in the western portion of the pluton. In these areas maximum size of plagioclase crystals is 0.7cm. Minimum size observed is 0.3cm. Very rarely one or two large plagioclase crystals assume a length of about 2cm. In all the locations pyroxenes crystals are slightly smaller than plagioclase crystals. These features are very well observed in quarries at Peralam and Kozhumal areas.

Shape of the plagioclase crystals are also showing a variation. In some areas most of the plagioclase crystals occur as long prisms (1 to 2cm long and 0.2 to 0.5cm wide). This feature is best observed in a quarry at Vattappara near Perinthatta. In other areas where the rock is medium grained long prisms of plagioclase crystals are not observed.

In some locations near Eramam (south) three size grades of anorthosite were observed in the same quarry. Coarse-grained type, medium-grained type and fine-grained type. The contacts between these three are gradational. Very fine grained type is seen as thin irregular veins. The same material was also observed in charnockites of Kanayi area.

Mafic content of the plagioclase in the anorthositic rocks also show variation and that has got no correlation with grain size of the rocks. Very coarse grained anorthositic rock can be grouped into two types based on their mafic content. In one type, mafic content is high and in the other the mafic content is very less. Very coarse-grained type anorthositic rock with very high content of mafic minerals is observed in location S1 and it is located at Porakkunnu. The minimum mafic mineral content is observed at quarries near Perinthatta. To be

53

precise, the locations S3 and S4 are coming in this area. The mafic content is intermediate towards the western side of the anorthosite pluton. Colour of the pluton does not change much in accordance with the variation in the mafic mineral content. This is because of the dark colour of the plagioclase which is the major component of all these rocks.

Since the Perinthatta pluton is massive and typical metamorphic minerals like garnet and hornblende are absent, it appears to be unmetamorphosed in hand-specimens and quarry exposures. It does not show any penetrative structural features. However, some minor brittle shear planes and pseudotachylite veins are observed in the pluton (Fig. 4.7). Pseudotachylite veins are seen in quarries at Aalakkad. Near Perinthatta where anorthosite is very coarse grained, plagioclase laths show a preferred orientation. This feature is very well observed in Vattappara quarry (Fig. 4.8). These plagioclase crystals trend N110° in Perinthatta and N93° at Vattappara quarry. The mineral lineation seems to be primary and it might have been developed due to magma flow. Coexisting pyroxenes do not show any preferred orientation. The feldspars which show preferred orientation are long prisms (upto 2 to 3cm long near Perinthatta). Along with these, equant crystals of plagioclase are also observed and most of them do not show preferred orientation. In Vattappara quarry, length of plagioclase crystals showing preferred orientation is in the range of 1cm. In Vattappara quarry, large plagioclase crystals form clusters of various sizes. The largest cluster is 30cm long and 15cm wide. Pyroxnene crystals also occur in small clusters.

The country rocks surrounding the anorthosite include charnockite and mafic granulite. Felsic granulite and gneisses are also seen in locations very close to Perinthatta anorthositic pluton. Majority of the exposures around the pluton are charnockite. Mafic granulite is restricted to the northeastern border of the pluton. The mafic granulite is seen in quarries at Peringom and Thandanat.

Charnockite is massive in almost all the locations, but at places it shows foliation. This foliation is developed due to the closely spaced thin bands of quartzo-feldspathic material. This feature is seen clearly in a quarry at Pullupara near Kanayi. The foliation here is vertical and it strikes N253° Compared to charnockite, mafic granulite is very less in its occurrence. Mafic granulite shows a crude gneissosity at some places which are defined by the linear arrangements of garnet grains. Gneissosity in mafic granulite strikes N167° and dips 80° due SW at Peingom. At some locations thin quartzo-feldspathic veins are observed parallel to the gneissosity in mafic granulite. This feature is clearly seen in quarries near Peringom. Highly mafic patches are seen as enclaves in mafic granulites. Very rarely only gneiss is seen in contact with the Perinthatta pluton. A gneissic exposure is observed in a quarry near to Kuvappa (S15). It is a grey gneiss and it shows a fine grained texture. Pseudotachylite veinlets were seen in them.

In the felsic granulites, quartz ribbons are often noticed. Strings of blue quartz is also observed in them. The occurrence of felsic granulites is mainly restricted to bands and some times they occur as patches. Patches of incipient charnockitization can be seen in the felsic granulite. The incipient charnockite is greenish grey in colour. These patches range in size from 10 to 45cm and they are seen along fractures only. The incipient charnockitization is very much prominent in quarries at Peruvamba. In some other quarries near Peruvamba, mafic granulite is seen as patches in charnockite and felsic granulite.

In the country rock of Perinthatta pluton, some brittle shear planes are noted with vertically oriented slikensides. The shear planes strike N65° and dip 79° due SE. Cordierite is observed along the shear planes and that might have been developed due to the lowering of pressure. Foliation in felsic granulite shows slight variation in strike from N285° to N330°.

A major dolerite dyke trending NNW-SSE is cutting the Perinthatta anorthositic rocks. The cross cutting relationship between this dyke and the anorthositic rocks is very well observed in a quarry at Perul. This dyke is fine grained and rich in plagioclase laths. Pyroxenes are also present and the rock shows a subophitic texture. Some plagioclase feldspar laths are about 0.5cm long. Large xenoliths of charnockite are observed in this dolerite dyke. Along the boundary of the xenolith, felsic granulite band of 1m width is noted. Chilled margin is seen surrounding the xenolith. The contact plane trends N125° and dips 74° due NE. Pegmatite veins with biotite are seen cutting across the dyke.

Very fine grained anorthositic rock is observed as a band of 45cm thickness cutting the charnockite. The band is horizontal. Numerous conjugate fractures are seen in it.   This feature is seen in quarries at Pullupara near Kanayi.   At some other locations anorthosite veins cutting the charnockite xenoliths are observed. The thickness of these veins is approximately 2cm. This feature is well observed in a quarry near at Eramam. These features are in favour of an intrusive relationship of anorthosite with the country rock.

Sharp contacts between anorthosite and the country rock is seen in some locations near to the border zones.   At a quarry in Eramam, this feature is very well observed (Fig.   4.9 a & b).   In the same location chilled margin of the contact between the anorthosite and the country rock is observed (Fig. 4.10).

Xenoliths of charnockite are observed in many locations. Numerous such xenoliths of various sizes and shapes are observed at Eramam and Peralam areas (Fig. 4.11). The biggest xenolith observed is 3m long and 24cm wide. This xenoliths is observed in a quarry near Malapp.

4.3 Rock Nomenclature

Megascopically the anorthosite and its mafic variants do not show much difference. All the samples are dark grey coloured and massive. Though the mafic variants associated with anorthosite are commonly considered as grading to gabbro (Buddington, 1975) the term dioritic is preferred for the variants here, because of the higher alkali content of the rocks and the low An% of the plagioclases of the rocks (see section 5.6.4 for alkalinity and 5.7.1 for An%). Based on modal composition of these rocks, the mafic percentage in particular, the Perinthatta pluton can be grouped into three main types, namely anorthosite, dioritic anrothosite and anorthositic diorite. For anorthosite, the mafic mineral content is less than 10%, for dioritic anorthosite, the mafic mineral percentage is between 10 and 22.5% and for anorthositic diorite, it is greater 22.5%.

The wide variation in the mafic content of the rocks is reflected in the range in their density. The density of selected samples of Perinthatta pluton is given below:

S-1/A	3.0135 g/cc
S-1/B	2.7317 g/cc
S-2/A	2.7501 g/cc
S-3/3	2.6997 g/cc
S-4/A	2.6858 g/cc
S-11/C	2.78 g/cc
S-12/T	2.7218 g/cc
S-21/1	2.7137 g/cc

Density variation can be attributed mainly to the variation in mafic mineral content and thus minimum density is shown by anorthosite samples and maximum density is shown by anorthositic diorite samples. However, the density is further controlled by the opaque minerals present in them (which varies from <1 to >10%) and so density alone cannot be used for a classification of the mafic variants associated with the Perinthatta anorthosite.

The relative abundance of the three rock types in the pluton could not be precisely estimated because of the lack of sufficient exposures especially along the interior portions of the pluton and for the difficulty in grouping the rocks in field. A rough estimate based on the available data can be made as ~50% dioritic anorthosite, ~45% anorthosite and ~5% anorthositic diorite.

4.4 Megascopic Petrography

The petrographic description is given separately for the three rock types of the anorthositic pluton below.

4.4.1 Anorthosite

The rock is very coarse grained and dark grey coloured. All the samples of this rock is massive. Plagioclase feldspar is the most dominant mineral phase and the grains of which are of different sizes. More than 90% of the rock is composed of plagioclase feldspar. Some of the plagioclase crystals are extremely long and some of them are approximately 2cm long. These long crystals are showing a rough parallelism among them. Equant crystals of plagioclase feldspar are also observed.

Pyroxenes are very less and they are sparsely distributed. They are of different sizes and very rarely they are as large as feldspar crystals. Some opaque minerals are observed.

4.4.2 Dioritic anorthosite

This rock is also dark grey coloured but they are heavier than anorthosite. This is because of the presence of more mafic minerals in this rock. Dioritic anorthosite also very coarse grained rock in which the plagioclase grains are sometimes 1.5 cm long and 0.5 cm wide. Samples S-21/1 and S-22 are medium grained while all others are coarse grained.

The sample S-12/L is the only one which shows a lighter colour.   The sample S-2/A shows a cumulus texture in which large subhedral plagioclase crystals are surrounded by a matrix containing anhedral pyroxene and opaque minerals.   In all other samples mafic mineral content is the more than the anorthosite samples but a cumulus texture is absent.   This rock also contains plagioclase as the most dominant mineral. The sample S-21/1 is showing equigranular texture.

Pyroxene crystals are of different sizes and some of them have a diameter of about 0.4cm.   In association with these pyroxenes opaque minerals can be seen.

4.4.3   Anorthositic diorite
The samples of this rock are most dark coloured varieties. At location S1 only these rock types are observed. Their dark colour is due to the presence of good amount of mafic minerals. Texturally these samples are very different from anorthosites and dioritic anorthosite. When grain size is concerned   this rock is very coarse grained.   The sample S-1/A shows very conspicous   cumulus texture.   In all these samples plagioclase is the dominant mineral and in the coarse grained variety plagioclase feldspar are approximately 1.5cm in length and 0.7cm in width.   All the plagioclase crystals are dark coloured due to the presence minute inclusions of Fe-Ti oxide. In the sample S1/A the feldspar show very rough preferred orientation.   In this sample pyroxene crystals are smaller than plagioclase crystals. Here the pyroxene and opaque minerals surround the larger plagioclase crystals. The opaque minerals could also be noticed owing to their metallic lustre.

4.5 Microscopic petrography
4.5.1 Anorthosite
In all the samples grouped as anorthosites, plagioclase is the dominant mineral phase and its modal content ranges from 91-94%.   Here plagioclase
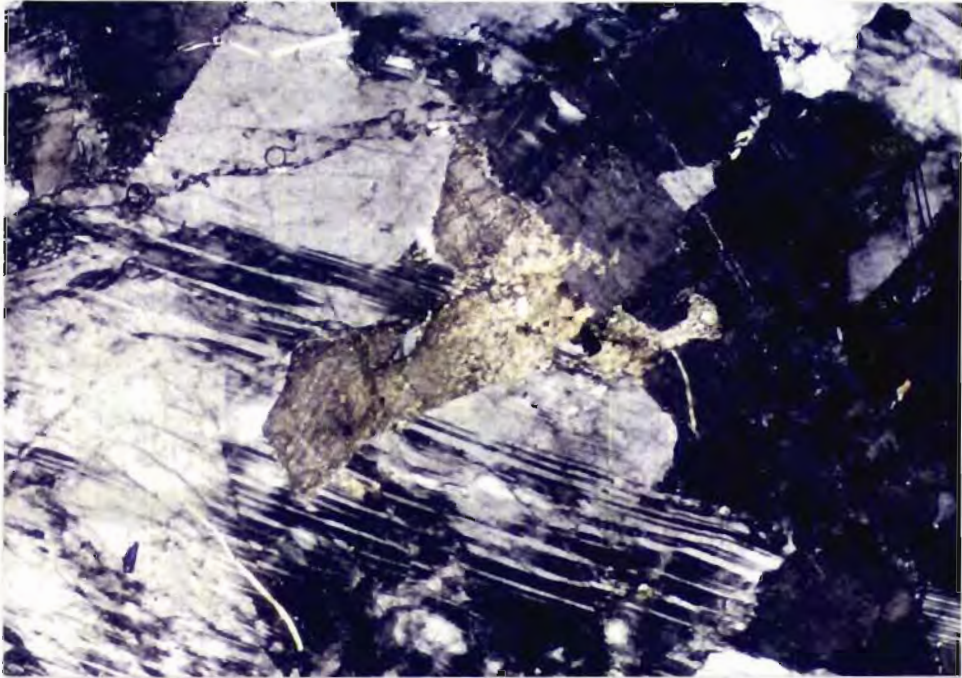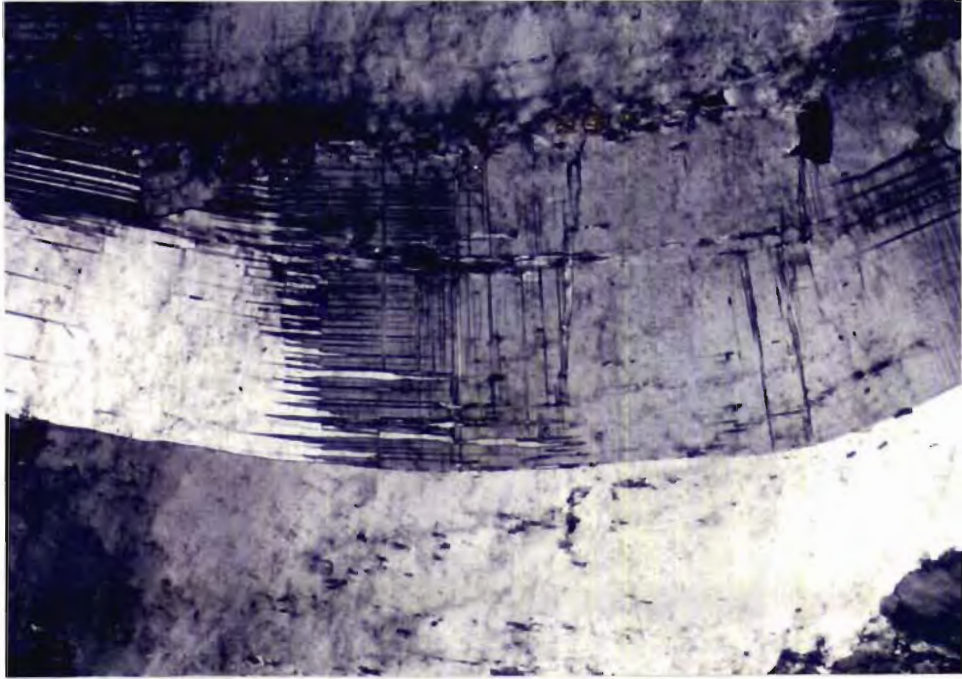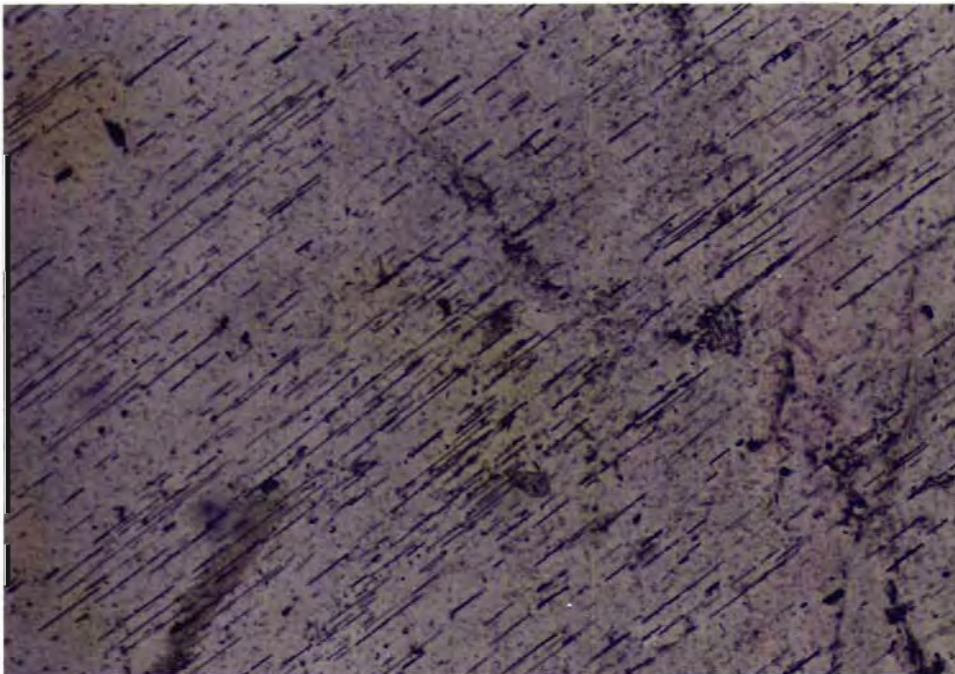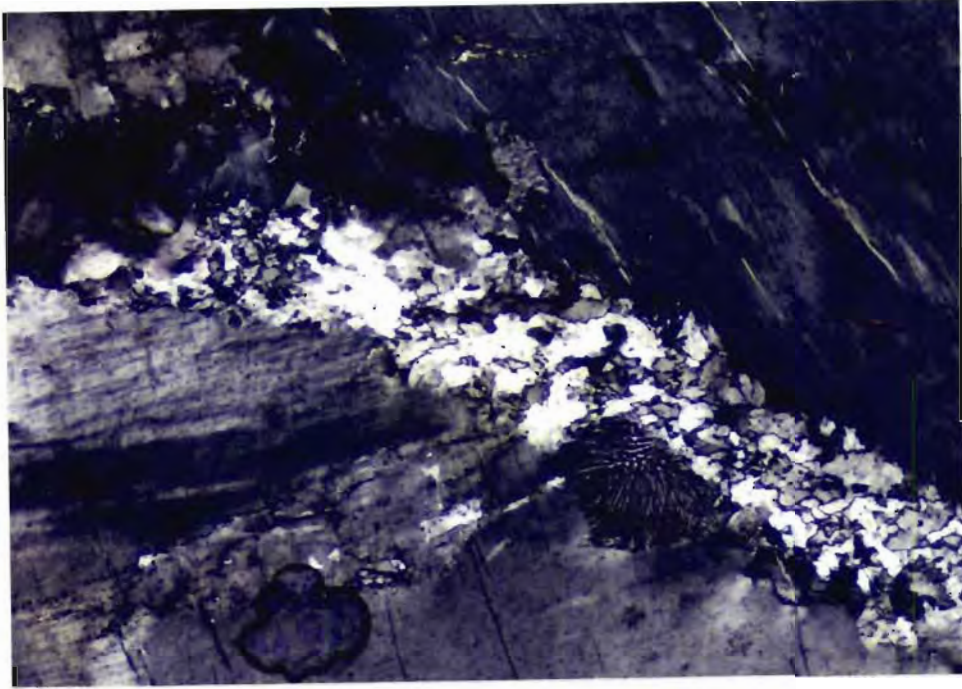
shows polysynthetic twinning and twin lamellae are alternatively thick and thin. In some crystals the twin lamellae are of uniform thickness and they are fine and closely spaced. Sometimes, twin lamellae show dislocations due to minor faulting. In addition to this albite twinning, plagioclase shows both pericline and Carlsbad twinning. Combination of these twins on the same grain was also noted (Fig. 4.12). Very few crystals are devoid of any twinning. Extinction angle of most of the plagioclase crystals of anorthosite samples is in the range of 15-22°.

Plagioclase crystals are devoid of antiperthitic exsolution lamellae in most of the anorthosite samples. Plagioclase crystals have amoeboid type grain boundaries between them. With pyroxene they show irregular grain boundaries and some of the pyroxenes embay into plagioclase crystals and that gives a remote subophitic texture (Fig. 4.13). Apatite and rarely zircon are present as inclusions in plagioclase. In some cases, adjacent plagioclase grains show effect of granulation along their grain boundaries (Fig. 4.14). In a thin section of the sample from location S3, some plagioclase crystals cut other plagioclase crystal at high angles. This is the location from where a preferred orientation of plagioclase crystals is noted. In another sample from the same location, minute fragments of plagioclase arranged randomly occur in groups between larger crystals

In most of the plagioclase crystals, very thin and needle like inclusions are seen in good amounts. These inclusions are opaques and they may be iron oxides and they are of different lengths. Their distribution is very much controlled by some crystallographic planes indicated by their perfect parallelism (Fig. 4.15).

Pyroxene is the major mafic mineral present in this rock. They occur interstitially to the plagioclase crystals and they impart a remote subophitic texture. Their modal content ranges from 2 to 5%. In the samples S-3/3 and S-4/A only orthopyroxene is present while in the sample S-3/A only clinopyroxene

is present. Always the pyroxene is seen associated with opaque minerals. The clinopyroxenes are greenish brown to dark brown in colour and they are non-plelchroic. Their interference colour varies from yellowish brown to orange. The extinction angle of clinopyroxene range from 20-36°. The pyroxene grains have anhedral shape, because they were crystallized after the plagioclase crystals and so they occur available spaces between the feldspar crystals. Some pyroxene grains show very minute rod shaped inclusions (opaque) arranged in a parallel fashion. Some clinopyroxene crystals show thin exsolution lamellae of orthopyroxene (Fig. 4.16).

Grain boundary of orthopyroxene and clinopyroxene is highly irregular. The pyroxene occur as sparsely distributed grains. Orthopyroxene crystals show faint pleochroism. They show inclusions of plagioclase. In this rock apatite is not seen as inclusions in pyroxenes.

In all the cases pyroxenes show alteration to biotite. In some cases biotite is seen along the contact between pyroxenes and opaque minerals. Good amount of opaques are seen in association with pyroxenes. In S-4/A clinopyroxene is found as an inclusion in biotite.

In the sample S-4/A, minute brittle shear bands are seen on a microscopic scale and they are manifested by bands of recrystallized minerals and these bands are seen cutting the plagioclase crystal. In this sample small amount of microcline crystals are observed near to the shear bands (Fig. 4.17). Presence of microcline indicates alkali metasomatism and the the shear planes might have acted as conduits for solutions. Moreover mafic minerals show alteration to chlorite also indicating hydrothermal alteration.

The samples S-3/3 and S-3/A can be considered as mesocumulates as per the original definition of cumulate terminology. The plagioclase crystals represent the primocrysts. To call a rock mesocumulate, the post cumulus
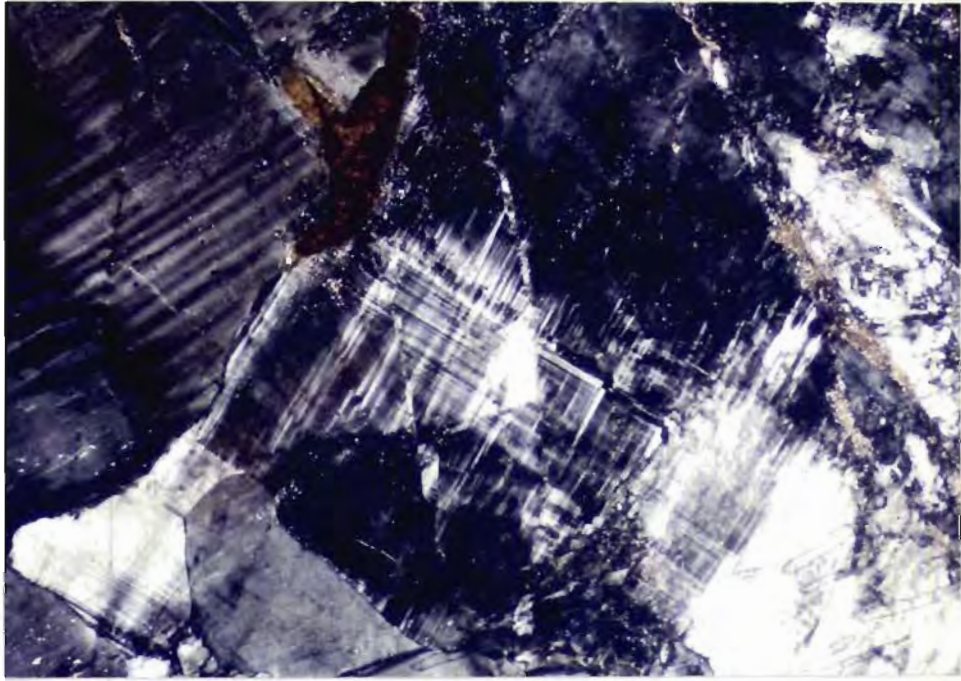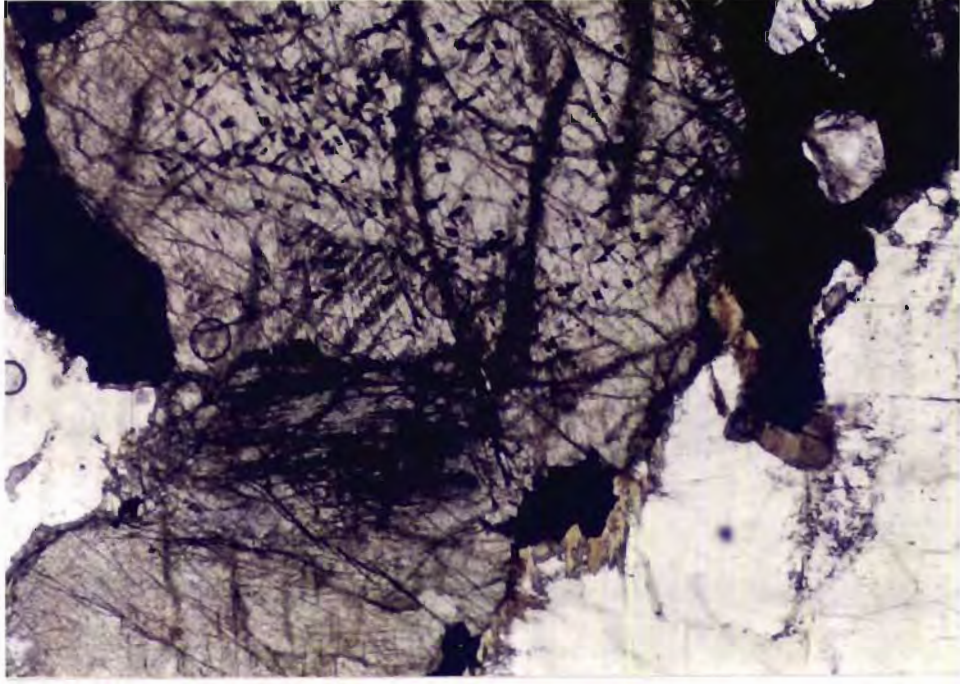
matrerial filling the porosity of the cumulus crystals should lie between 7% and 25% (Wager et al., 1960). For an adcumulus rock the volume of the postcumulus material should be less than 7%. The anorthosite samples AN-2, AN-3/B, AN-3/A, AN-4/A, S-4/A and AN-7/A also show adcumulus texture.

4.5.2 Dioritic anorthosite

In these rocks an inequigranular texture is observed. In S-2/A a very remote cumulus texture is observed and the intercumulus liquid is represented by pyroxenes, opques and apatite (Fig. 4.18). Here plagioclase crystals are of equal size. Highly irregular grain boudary is exhibited by plagioclase crystals. Exsolution texture is shown by plagioclase crystals in samples collected from location S2 and S12. These antiperthitic exsolution lamellae are of different nature. In some cases they occur as patches of different sizes and shapes (Fig.4.19). in some other cases the antiperthitic exsolution lamellae are in the form of undulating veins (Fig. 4.20). In the sample S-21/1, such antiperthitic texture is not observed.

In this rock, plagioclase crystals which do not show polysynthetic twinning are observed. Very rarely Carlsbad and Pericline twinning is observed in plagioclase grains of the sample S-2/A. The extinction angle shown by plagioclase is low and it averages about 20°. In all the samples of this rock, marginal granulation of plagioclase is observed and they form bands. In some cases the these sheared bands show recrystallized quartz grains (Fig. 4.21). In the sample S-12/T, antiperthitic fragments were noted in these sheared bands. Opaque inclusions are observed in plagioclase and they occur as rod shaped and sometimes as irregular patches.

The major mafic mineral is clinopyroxene and it occurs interstitial to plagiocalse crystals. They have a maximum size of 1mm. In most of the samples they show exsolution lamellae which are of uniform width and in a few cases very tiny opaque inclusions are noted in pyroxene as observed in the case
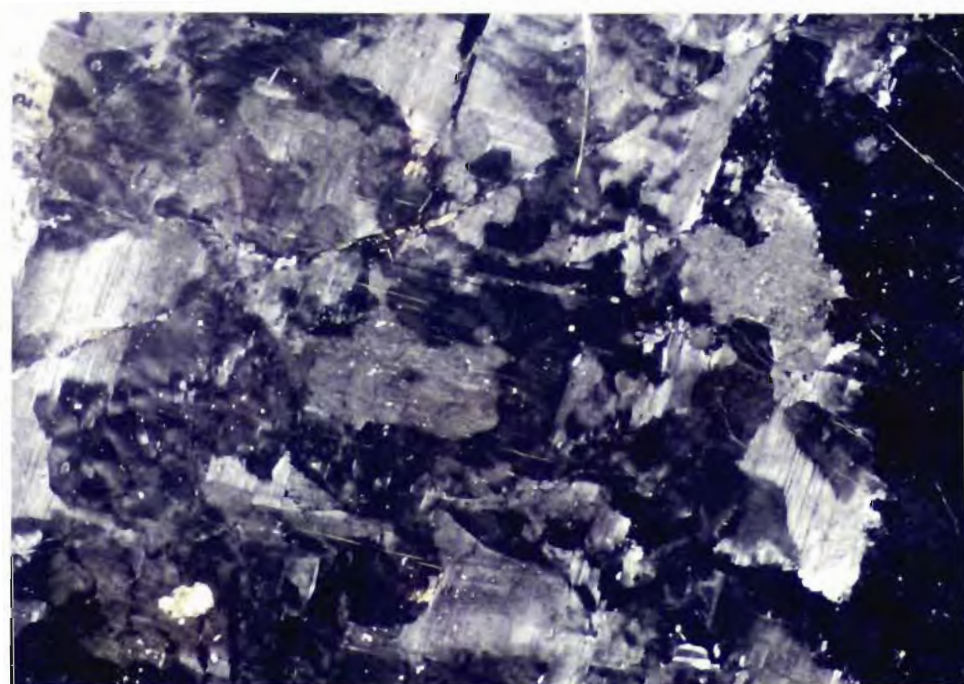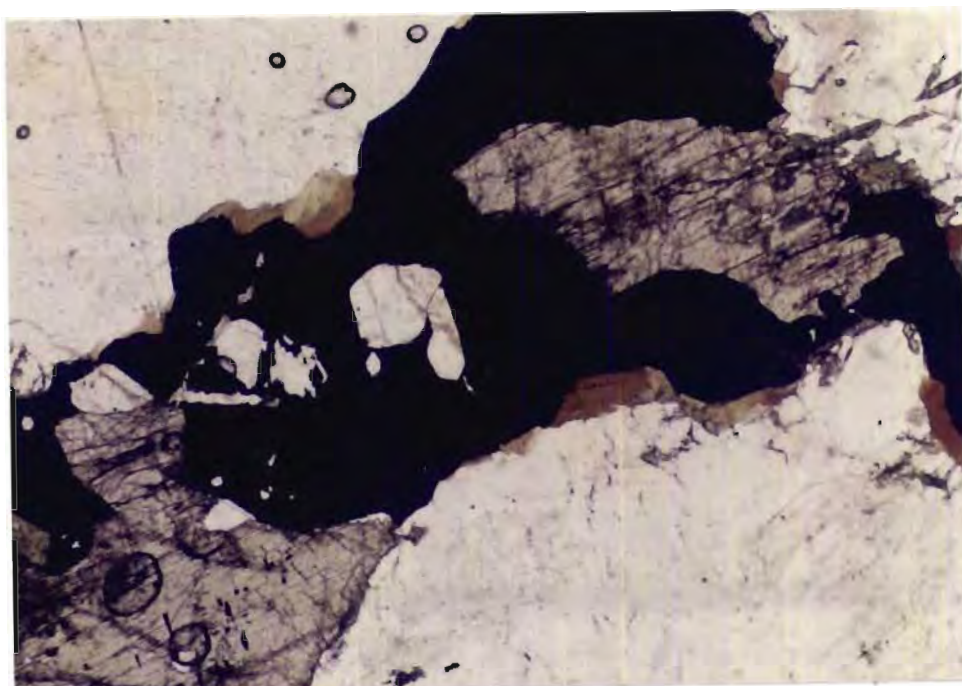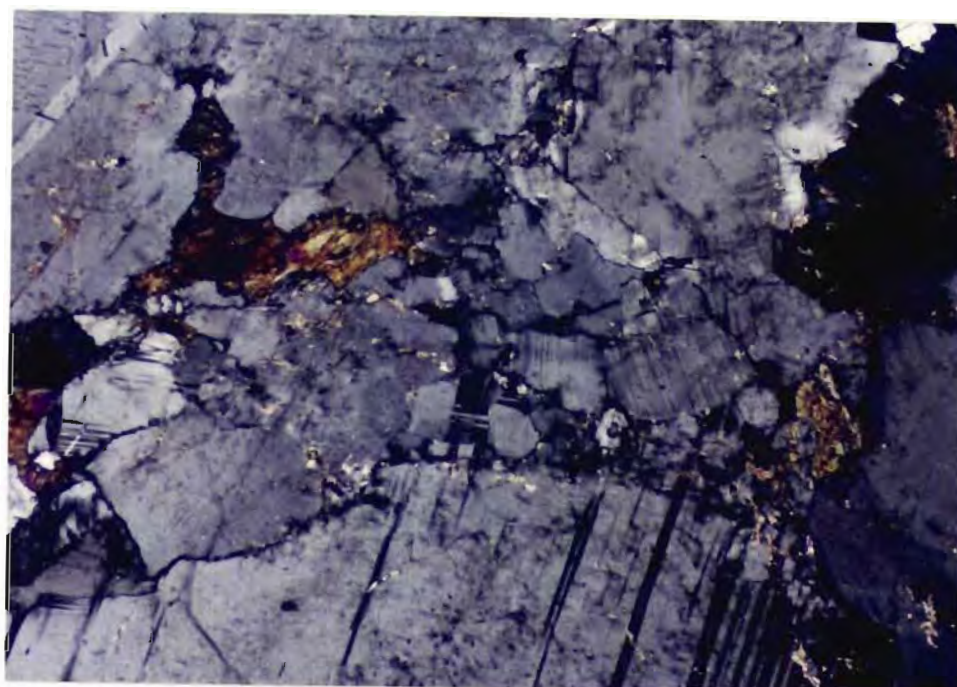
of some pyroxenes in the anorthosite samples. Very rarely the exsolution lamellae show cross hatching. Apatite inclusions are present in clinopyroxene crystals. Colour of clinopyroxenes shows wide variation from almost colourless to yellowish brown and greenish brown. They are non-pleochroic. The interference colours of clinopyroxenes include yellowish orange, light violet and reddish orange. The extinction angle of clinopyroxenes of this rock varies from 20-28°.

Orthopyroxene is present in samples S-12/C and S-12/T. Orthopyroxene occurs as isolated grains and they are pleochroic. Orthopyroxene shows alteration to biotite. In the sample S-12/C, biotite is more dominant than pyroxene. The biotite is the alteration product of the mafic minerals. This is evident from their occurrence along the grain boundary of pyroxene. Biotite crystals have irregular grain boundary. Opaque minerals are also seen in association with biotite. Some orthopyroxene show exsolution textures. Apatite inclusions are seen in most of the orthopyroxene grains.

In the sample S-22, two grains of olivine are observed and they are seen in association with pyroxene (Fig. 4.22). These olivine grains show very irregular grain boundary.

Apatite is the most important accessory mineral present in this rock. They are euhedral and occur in various sizes. Their approximate size is 0.2mm.

All the dioritic anorthosite samples show cumulate texture and can be classed as mesocumulates.

4.5.3 Anorthositic diorite.

The thin sections of these rock show typical cumulus texture (Fig. 4.23). From the figure, it can be seen that plagioclase crystals form the cumulus phase and the intercumulus liquid filling the space between cumulus feldspars in

cumulus plagioclase

mafic-rich interstitial

plagioclase

pyroxene

opaques

biotite

apatite

1 cm

1 mm
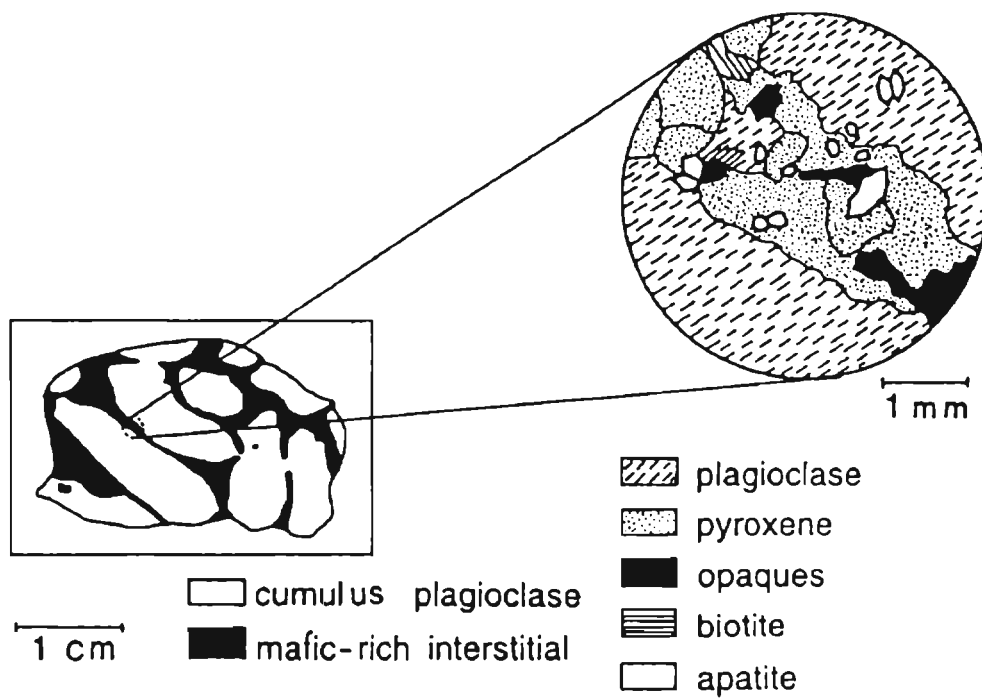
Fig. 4.23 Micrograph of anorthositic diorite (sample S-1/A) showing cumulus texture.
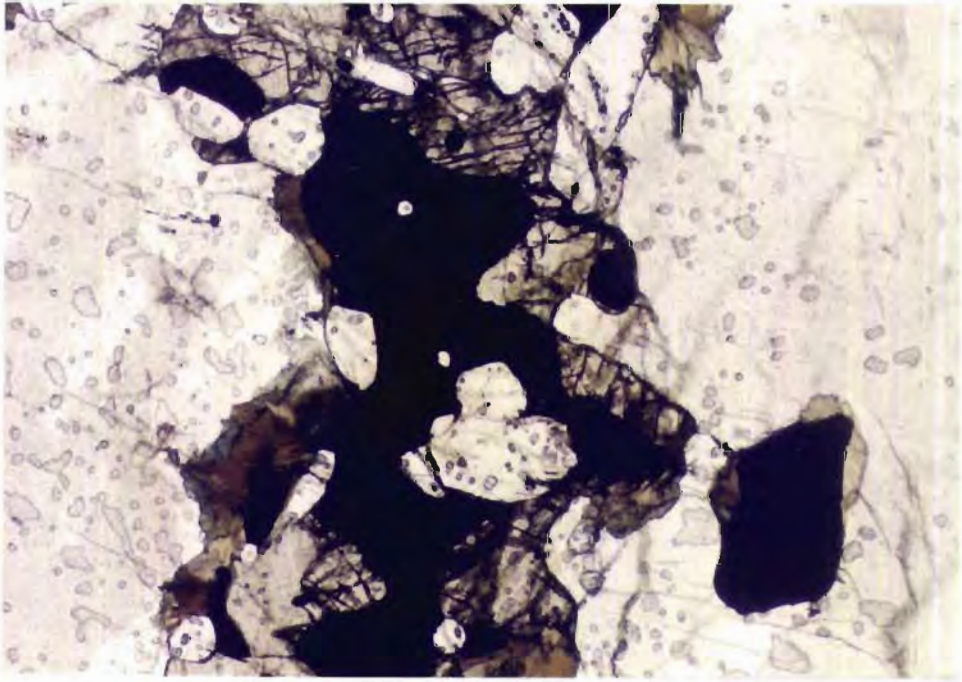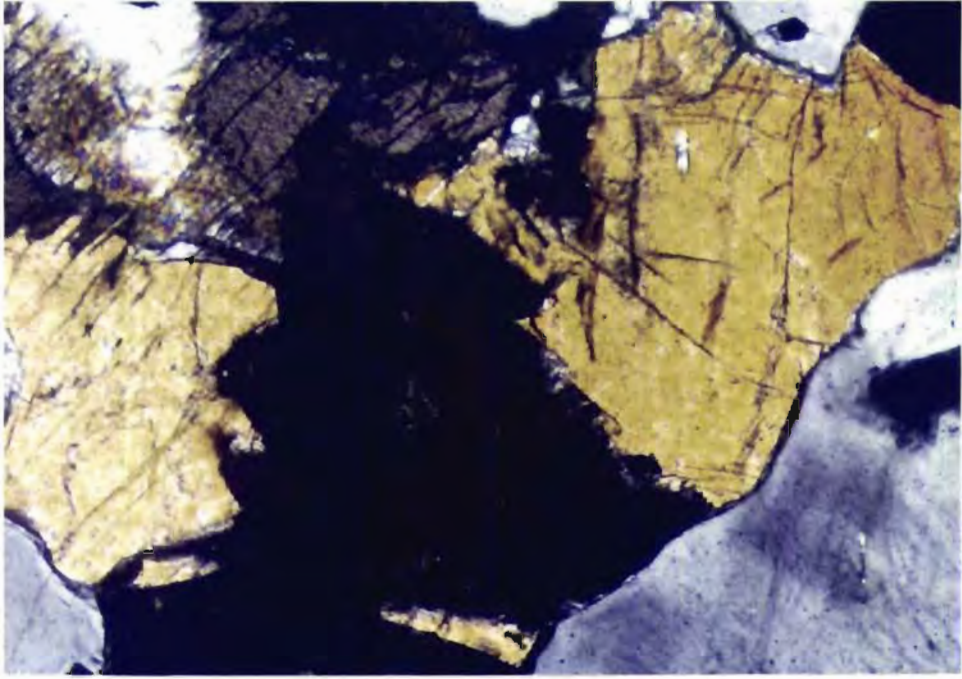
represented by pyroxenes, opaques, rarely olivine and apatite. These minerals also represents the liquid with which the plagioclase grains were in equilibrium during crystallization. A portion of the intercumulus material is shown in the figure 4.24. Plagioclase is the most dominant mineral phase in this rock and the modal content ranges from 60 to 68%. In these samples the plagioclase feldspar crystals are having an average length of 0.7cm. Some plagioclase crystals are 1cm long and 0.5cm wide. Majority of the plagioclase crystals in this rock are almost uniform in size. Only a very few crystals are smaller and they are seen included in the pyroxene grains. All the plagioclase crystals are devoid of polysynthetic twinning. Plagioclase crystals show both irregular and amoeboid type grain boundaries and sometimes tripple junctions can also be seen. All the plagioclase crystals are of equal size. Nevertheless, very small amount of tiny plagioclase crystals can be seen in the intercumulus material. Grain boundary between plagioclase and pyroxenes are often irregular. Very rarely only smooth boundary exist between them. The pyroxene crystals embay into plagioclase crystals. In most of the samples, some plagioclase crystals show antiperthitic exsolution lamellae. The exsolution lamellae are in the form of irregular veins of random distribution (Fig. 4.25). In some cases the exsolution lamellae are in the form very minute spindles arranged in a parallel fashion (Fig. 4.26). In a few samples, plagioclase crystals show effect of granulation along their grain boundaries. Apatite inclusions are common in all the samples. Needle like opaque inclusions in plagioclase is also a common feature. These inclusions occur as minute spindles and their distribution is controlled by crystallographic planes. The dark colour of the plagioclase crystals in hand specimens may be attributed to these opaque inclusions. In anorthositic diorite also, the extinction angle of plagioclase is low and it varies from 18-23°.

In most of the samples both clinopyroxene and orthopyroxene are present. In all the samples, clinopyroxene is the dominant mafic mineral phase and secondary biotite is also observed. The clinopyroxenes are non-pleochroic and they show light brown colour under open nicols. Interference colours shown by
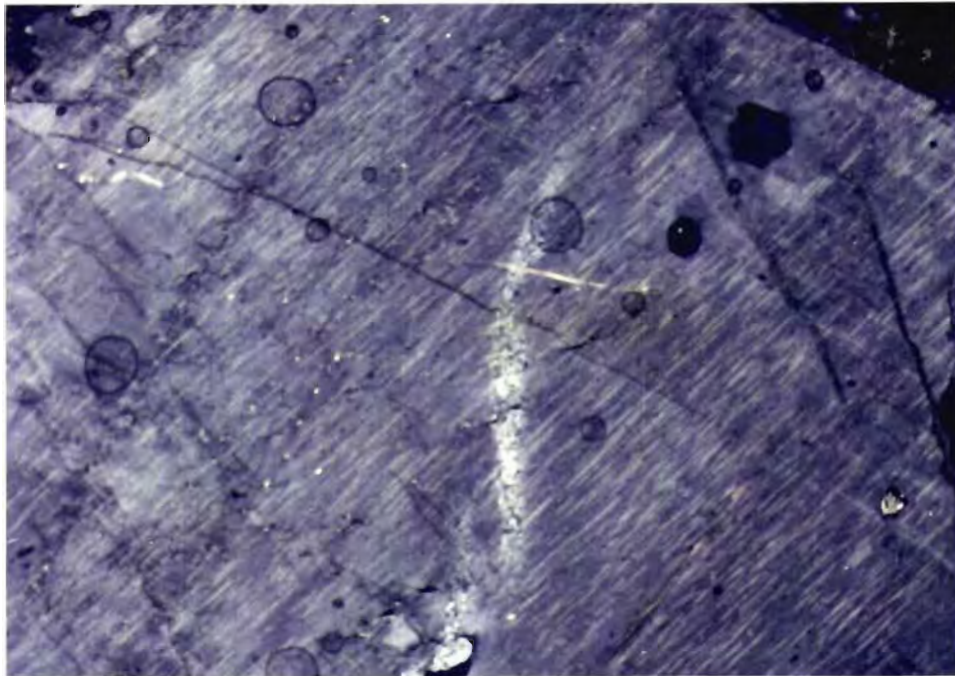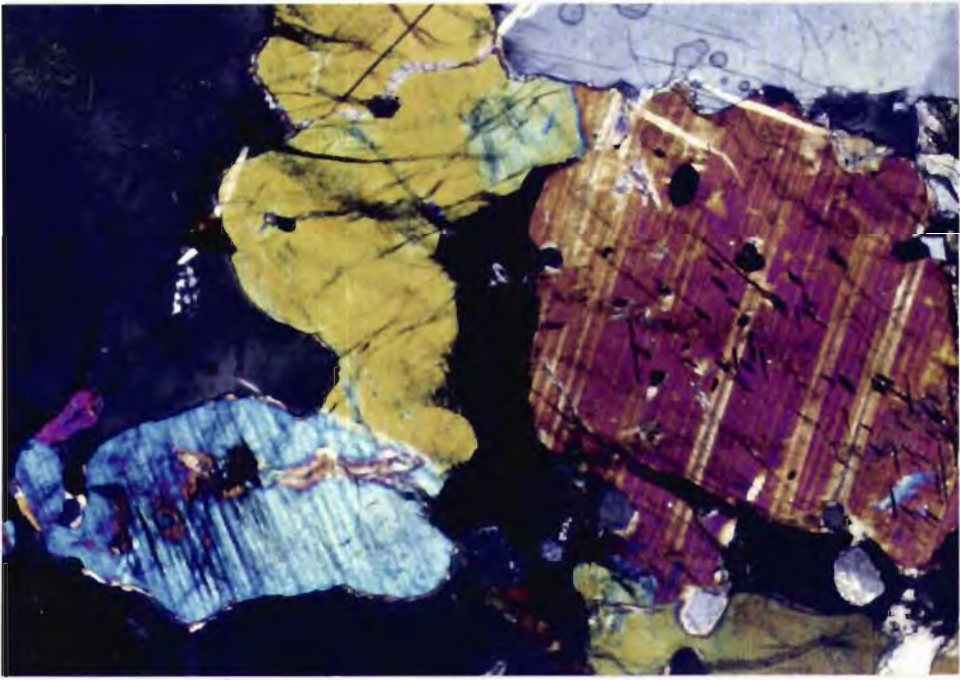
clinopyroxene include yellowish brown, yellowish green and greenish blue. Extinction angle of clinopyroxenes in anorthositic diorite samples range from 28-38°.

These mafic minerals occur interstitially to the plagioclase grains. Amoeboid type grain boundary is shown by these mafic minerals. The clinopyroxene crystals embay into orthopyroxene crystals. The orthopyroxene shows faint pleochroism. Good amount of opaque minerals are seen associated with them. Many clinopyroxene crystals show exsolution texture and the exsolution lamellae occur as parallel bands (Fig. 4.27). The exsolution lamellae are of orthopyroxene composition. The exsolution lamellae are at right angles to the cleavage traces. The distribution of opaque minerals occurring as inclusions is controlled by cleavage planes. Larger crystals of opaques can be seen associated with pyroxenes. Small amount of biotite can be seen around opaque minerals. They are the alteration product of opaques.

One crystal of olivine is observed in the sample S-1/A (Fig. 4.27). As observed in the sample S-22, this olivine grain is also seen in association with pyroxene and opaques.

Good amount of apatite inclusions can also be seen in all the pyroxene crystals. They are euhedral and occur in various sizes. They occur only as inclusions. Larger crystals of apatite seen as included or closely associated with pyroxene and opaques. Apatite occur as small inclusions in both plagioclase and pyroxenes.

The anorthositic diorite rocks can be classed as orthocumulates as the percentages of the postcumulus material in these rocks are 32 to 40%.

4.6 Discussion
Study of field relationship of Perinthatta anorthosite pluton revealed the intrusive nature of the rocks. The evidences include sharp contact with the

country rocks, presene of xenolliths of country rocks in the borders of the Perinthattta anorthosite pluton, presence of anorthositic veins in country rocks etc. Eventhough the rock is uniformly dark grey in all the locations, it shows variation in grain size and density. The central portion of the pluton is entirely composed of very coarse grained anorthosite. The grain size decreases towards west and it grades into dioritic anorthosite. Anorthositic diorite variety is restricted to southeast portion of the pluton. Preferred orientation plagioclase crystals in anorthosite is indicative of flow of magma at the time of crystallization.

Mineralogy of the Perinthattta anorthositic rocks suggests that it is an unmetamorphosed pluton. The pluton shows no penetrative sturctures but it shows some pseudotachylite veins at some locations.

Petrographic studies revealed the cumulate nature of the pluton. Pyroxenes and opques are occupying the intergranular spaces of plagioclase grains and it indicates that pyroxenes were crystallized from the intercumulus liquid. Later crystallization of pyroxenes is supported by the crosscutting relationship existing between clinopyroxene and plagioclases. In some locations, plagioclase crystals occurring in clusters can be identified in the field and it also supports a cumulate nature.

• • •

Chapter V
GEOCHEMISTRY AND PETROGENESIS

5.1 Introduction

Petrogenetic studies of intrusive rocks, which include the identification of the nature, source and generation of parental magma and understanding the various processes involved in its differentiation and solidification are most effectively done by analyzing the chemistry of rocks (in terms of major, trace and REE) and their interpretations. Further constraints on the evolution of the rocks could be arrived at by estimating the physical variables of crystallization like pressure and temperature based on mineral chemistry and from isotope data regarding age and source characteristics.

Fresh samples of anorthositic rocks were collected from both working and abandoned quarries. A total of eighteen representative samples of Perinthatta pluton were analysed for their major element composition by rapid methods of silicate analysis. For a few samples, the analysis was repeated by XRF at National Geophysical Research Laboratory (NGRI), Hyderabad. The results of the two analyses were found coinciding. Eleven samples were analysed for trace and rare earth elements. Trace and rare earth element analysis were done by ICP-MS at NGRI, Hyderabad following the procedure described in Balaram (1991). Geological map of Perinthatta anorthosite is given in figure 5.1 with the locations of the analyzed samples.

5.2 Rock types

As discussed in the previous chapter (section 4.3, chapter 4) the modal composition was used for the nomenclature of the samples of Perinthatta pluton. Thus the Perinthatta pluton is constituted by three rocks viz., anorthosite, dioritic anorthosite and anorthositic diorite.
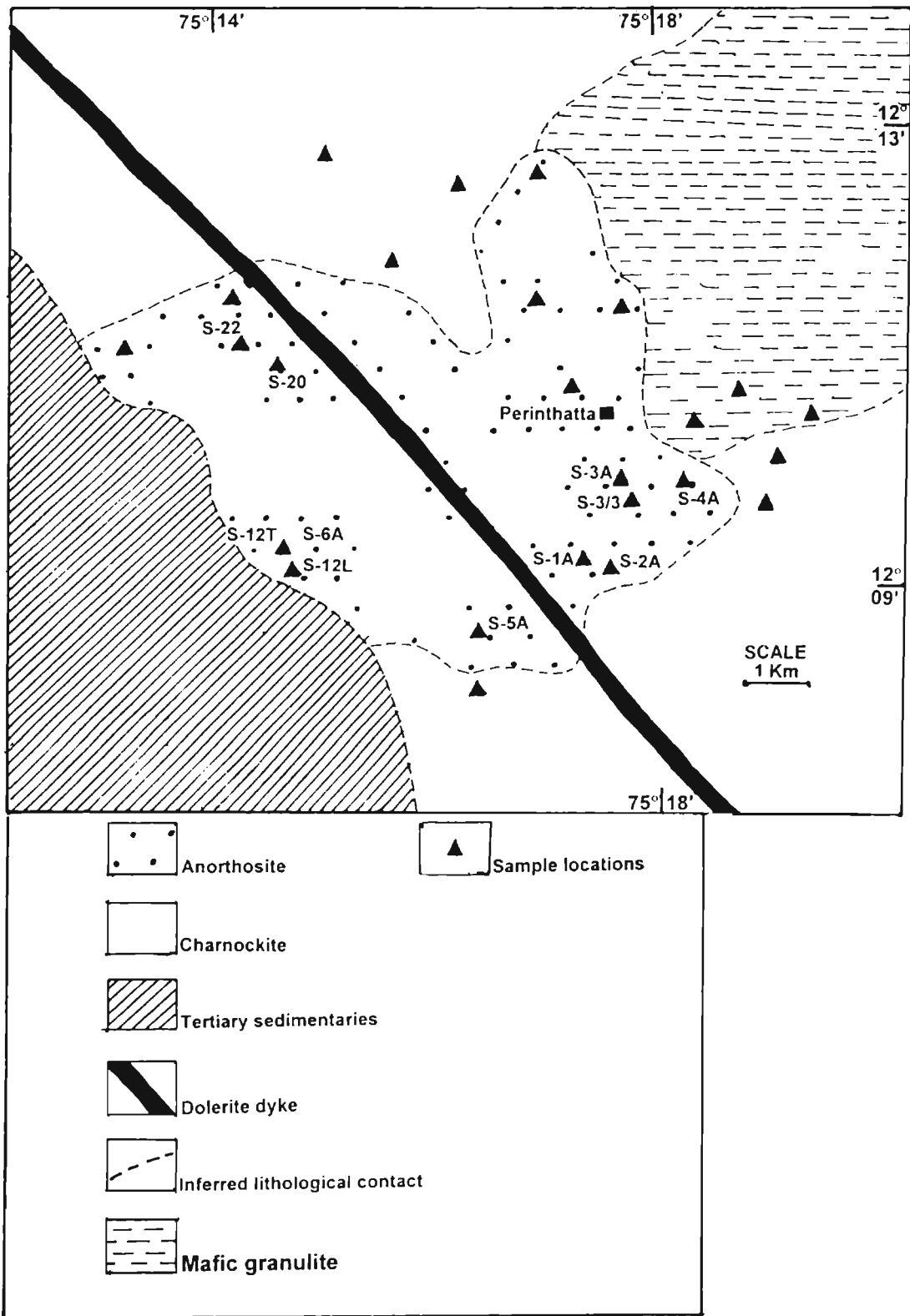
Fig. 5.1 Geological map of Perinthatta anorthosite with the locations of the analyzed samples.

Results of the analysis for the major elements and their calculated C.I.P.W norms are given in tables 5.1 (a & b), 5.2 (a & b) and 5.3 (a &b). Modal compositions of the samples of Peinthatta pluton are given in table 5.4 (a, b &c).

5.3 Major elements

Detailed description of geochemistry of the three rock types are given below, followed by a discussion of the variation of major element chemistry among them.

5.3.1 Anorthosite

SiO_2 content of anorthosite samples ranges from 47.55% to 58.93%. Al_2O_3 content shows a wide variation among the anorthosite samples. It ranges from 19.14 to 32.44%. Generally there is a decrease in the Al_2O_3 content with an increase in SiO_2 content. SiO_2 content of Perinthatta anorthosite samples is almost similar to that of the other massif type anorthosite {eg., Marcy massif (Buddington, 1939), Morin massif (Papizek, 1965)}. Eventhough Al_2O_3 content shows wide variation, its average (25%) is almost within the range of Al_2O_3 content of other massif type anorthosites. In the case of Fe_2O_3 and FeO contents also Perinthatta anorthosite samples are similar to other massif anorthosites. Fe_2O_3 ranges from 0.23 to 1.03% and FeO content ranges from 0.82 to 1.8%. MgO content is less but slightly higher than the Fe_2O_3 and FeO. In only one anorthosite sample (S-3/A), MgO content is as high as 6.04%. In other anorthosite samples MgO content ranges from 0.63 to 1%. MnO is very less in all the samples. In most of the anorthosite samples, CaO is relatively high compared to mafic variants and it ranges from 9.8 to 16.8%. The content of CaO is also comparable to that of other massif anorthosites. Na_2O is less than CaO but greater than K_2O. The content of Na_2O ranges from 4.37 to 5.81%. This is higher compared to massif type anorthosites in general. K_2O ranges from 0.45 to 0.75% and these values are close to the value of other massif-type anorthosites. TiO_2 content ranges from 0.16 to 0.4%. P_2O_5 content is lesser than TiO_2 and it ranges from 0.03 to 0.25% and these values are also close to

Table 5.1 (a) Major element analyses (wt%) of anorthosite samples

Sample No.	S-3/3	S-3/A	S-4/A	AN-3/A	AN-3/B	AN-4/A
SiO2	58.93	55.65	55.19	48.15	47.55	49.35
Al2O3	20.23	19.65	19.14	32.30	32.44	31.38
FeO	1.08	1.80	1.08	1.05	1.10	0.82
Fe2O3	1.03	0.23	0.59	0.49	0.50	0.37
MnO	0.08	0.10	0.06	0.03	0.02	0.02
MgO	1.00	6.04	1.00	0.63	0.69	0.63
CaO	11.20	9.80	16.80	10.94	11.17	10.74
Na2O	5.72	5.81	5.81	4.37	4.48	4.73
K2O	0.67	0.75	0.45	0.70	0.65	0.64
TiO2	0.27	0.27	0.27	0.40	0.27	0.16
P2O5	0.04	0.05	0.03	0.25	0.19	0.23

Table 5.1 (b) Calculated C.I.P.W norms of anorthosite samples

Sample No.	S-3/3	S-3/A	S-4/A	AN-3/A	AN-3/3	AN-4/A
Q	3.5	0.0	0.0	0.0	0.0	0.0
Or	3.9	4.5	2.8	3.9	3.9	3.9
Ab	48.0	39.3	36.7	30.6	26.5	32.4
An	27.5	25.3	25.0	52.3	54.5	5.1
Le	0.0	0.0	0.0	0.0	0.0	0.0
Ne	0.0	5.4	6.5	3.3	6.2	4.0
Ac	0.0	0.0	0.0	0.0	0.0	0.0
Ns	0.0	0.0	0.0	0.0	0.0	0.0
Di	7 1	18.5	7.6	0.0	0.0	0.0
Wo	7.8	0.0	20.4	0.0	0.0	0.0
Hy	0.0	0.0	0.0	0.0	0.0	0.0
Ol	0.0	7.7	0.0	1.8	2.1	1.8
Mt	1.7	0.3	1.1	0.7	0.7	0.5
Ht	0.0	0.0	0.0	0.0	0.0	0.0
Il	0.6	0.5	0.5	0.8	0.5	0.3
Ap	1.0	0.1	1.0	0.6	0.3	0.6

Table 5.2 (a) Major element analyses (wt%) of dioritic anorthositic samples

Sample No.	S-2/A	S-12/L	S-12/T	S-22	S-11/D	S-12/C	S-21/1	AN-11/D	AN-12/F	AN-22
SiO2	54.28	56.07	65.43	49.61	52.15	60.28	42.85	59.92	65.85	63.84
Al2O3	14.11	15.67	17.63	18.13	16.11	12.42	21.16	16.82	15.41	17.41
FeO	4.68	2.88	2.52	2.16	5.76	3.24	3.60	4.23	2.84	2.61
Fe2O3	1.72	0.04	0.14	1.85	1.41	0.00	1.25	1.94	1.30	1.20
MnO	0.08	0.06	0.10	0.03	0.07	0.07	0.03	0.16	0.08	0.08
MgO	10.10	13.08	1.51	10.06	10.56	10.06	12.08	0.67	1.07	0.37
CaO	5.60	2.80	3.55	2.80	4.90	3.50	5.60	3.71	3.75	1.97
Na2O	6.74	6.48	6.40	6.65	5.89	6.84	6.65	5.81	5.11	5.21
K2O	3.08	4.81	4.14	5.64	2.33	4.06	5.19	3.26	2.10	5.11
TiO2	1.09	0.65	0.54	1.44	0.95	1.49	1.44	1.07	0.50	0.51
P2O5	0.03	0.03	0.02	1.47	0.04	0.03	1.47	0.60	0.20	0.16

Table 5.2 (b) Calculated C.I.P.W norms of dioritic anorthositic samples

Sample No.	S-2/A	S-12/L	S-12/T	S-22	S-11/D	S-12/C	S-21/1	AN-11/D	AN-12/F	AN-22
Q	0.0	0.0	3.3	0.0	0.0	0.0	0.0	4.9	18.6	8.4
Or	18.3	28.4	24.5	33.4	13.9	23.9	0.0	19.5	12.2	30.0
Ab	24.1	21.5	54.0	12.1	28.3	41.4	0.0	49.3	42.9	44.0
An	0.0	0.0	7.2	2.8	10.5	0.0	12.5	10.0	13.1	8.9
Le	0.0	0.0	0.0	0.0	0.0	0.0	23.9	0.0		0.0
Ne	16.8	17.6	0.0	23.9	11.5	0.0	30.4	0.0		0.0
Ac	1.8	0.4	0.0	0.0	0.0	0.0	0.0	0.0		0.0
Ns	0.0	0.3	0.0	0.0	0.0	5.0	0.0	0.0		0.0
Di	21.8	10.7	8.3	7.5	10.9	13.6	4.1	4.0	3.9	0.0
Wo	0.0	0.0	0.0	0.0	0.0	0.0	0.0	0.0	0.0	0.0
Hy	0.0	0.0	3.4	0.0	0.0	2.0	0.0	4.4	4.2	3.9
Ol	14.9	22.6	0.0	18.0	23.1	14.5	22.6	0.0	0.0	0.0
Mt	1.9	0.0	0.3	0.9	2.5	0.0	2.3	2.8	1.9	1.9
Ht	0.0	0.0	0.0	0.0	0.0	0.0	0.0	0.0	0.0	0.0
Il	2.1	1.2	1.1	2.7	1.8	2.9	2.7	1.9	0.9	0.9
Ap	1.0	1.0	0.0	3.4	0.3	0.1	3.4	1.2	0.3	0.3

Table 5.3 Major element analysis (wt%) and calculated
C.I.P.W norms of anorthositic diorite samples

Sample No.	S-1/A	S-1/B	Norm	S-1/A	S-1/B
SiO2	38.01	47.81	Q	0.0	13.2
Al2O3	16.11	15.22	Or	10.0	10.0
FeO	3.24	11.96	Ab	3.1	14.1
Fe2O3	15.37	5.50	An	19.7	28.9
MnO	0.08	0.50	Le	0.0	0.0
MgO	10.10	0.29	Ne	17.9	0.0
CaO	7.70	8.50	Ac	0.0	0.0
Na2O	4.29	1.69	Ns	0.0	0.0
K2O	1.65	1.65	Di	13.6	0.2
TiO2	3.53	3.87	Wo	0.0	0.0
P2O5	2.04	2.04	Hy	0.0	12.6
			Ol	13.3	0.0
			Mt	0.6	7.9
			Ht	15.0	0.0
			Il	6.7	7.3
			Ap	4.8	4.3

Table 5.4 (a) Modal compositions of anorthosite samples

Sample No.	S-3/3	S-3/A	S-4/A	AN-3/A	AN-3/3	AN-4/A	Mean
plagioclase	92	91	94	93	95	93	93.0
microcline	0	0	0	2	0	0	0.3
orthopyroxene	5	0	2	0	0	0	1.2
clinopyroxene	0	4	0	4	2	2	2.0
biotite	1	1	1	1	1	0	0.8
apatite	0	0	0	0	0	1	0.2
zircon	0	0	0	0	0	0	0.0
opaques	2	4	3	4	2	4	3.2

Table 5.4 (b) Modal compositions of dioritic anorthosite samples (tr- in traces)

Sample No.	S-2/A	S-12/L	S-12/T	S-22	S-11/D	S-12/C	S-21/1	AN-11/D	AN-12/F	AN-22	Mean
ol							tr			-	-
plagioclase	89	88	89	88	87	89	88	86	87	89	88
microcline	0	1	0	0	0	0	0	0	0	0	0.1
orthopyroxene	0	3	0	2	1	0	2	0	0	1	0.9
clinopyroxene	7	0	3	8	11	4	8	9	1	5	5.6
biotite	1	7	6	0	0	5	0	0	12	1	3.2
apatite	1	1	1	1	0	2	0	1	0	1	0.8
zircon	0	0	0	0	0	0	0	0	0	0	0
opaques	2	0	1	1	1	0	2	4	0	3	1.4

Table 5.4 (c) Modal compositions of anorthositic
diorite samples (tr- in traces)

Sample No.	S-1/A	S-1/B	Mean
ol	tr		
plagioclase	68	59	63.5
microcline	0	0	0
orthopyroxene	8	0	4
clinopyroxene	13	31	22
biotite	0	0	0
apatite	4	5	4.5
zircon	0	0	0
opaques	7	5	6

the other massif anorthosites. Except for their slightly higher Na_2O content, major element composition of Perinthatta anorthosite samples are thus showing striking similarity to other massif-type anorthosites.

Among the six samples of anorthosite, only one sample (S-3/3) is quartz normative and four other samples are olivine normative. In most of the anorthosite samples, Ab is more than An and this reflects the higher sodium content (cf. Mineral chemistry of plagioclase in section 5.7.1).

5.3.2 Dioritic anorthosite

SiO_2 content of dioritic anorthosite samples ranges from 49.61 to 65.85%. Al_2O_3 content is lesser than that of anorthosite samples and it ranges from 12.42 to 21.16%. Generally there is a decrease in the Al_2O_3 content with an increase in SiO_2 content up to 55% of SiO_2. After 55% of SiO_2, a slight increasing trend is observed. Fe_2O_3 and FeO content of dioritic anorthosite samples are slightly lesser than that of anorthosite samples. Fe_2O_3 ranges from 0.04 to 1.94%. The FeO content ranges from 2.16 to 4.68%. MgO content is showing a wide range of variation among the samples of dioritic anorthosite. MgO content ranges from 0.37 to 13.08% with an average of 7%. CaO content of the rock is slightly less than that in anorthosite samples and it ranges from 1.97 to 5.6%. MnO is very less in all the samples. Na_2O content is higher than that of CaO. Moreover Na_2O content in dioritic anorthosite is higher than that of anorthosite samples. The content of Na_2O ranges from 5.11 to 6.84%. K_2O content is less than both CaO and Na_2O. K_2O content in dioritic anorthosite samples is slightly higher than that in anorthosite samples. K_2O content ranges from 2.1 to 5.64%. TiO_2 content ranges from 0.5 to 1.44% and this is slightly higher than that of anorthosite samples. P_2O_5 content is lesser than TiO_2 and it ranges from 0.02 to 1.47 wt%.

5.3.3 Anorthositic diorite

The samples which are grouped as anorthositic diorite are S-1/A and S-1/B. These samples are taken from the location S1 near Porakkunnu. SiO_2 content is higher for S-1/B. Al_2O_3 is higher in S-1/A and thus the modal plagioclase is more in S-1/A. MgO content shows great difference between the two samples. For S-1/A it is 10% and for S-1/B it is 0.29%. CaO content is slightly more in S-1/A. Na_2O is also slightly high in S-1/A. K_2O is exactly same in both the samples. TiO_2 and P_2O_5 contents are also same in both the samples. The total iron content is in both the samples is very high and the average value is 17%.

5.3.4 Variation in major element chemistry

The variation in chemistry of the anorthositic rocks within and among the three groups is analyzed with the help of oxides vs Mg number (Mg#) plots and the AFM diagram. Major element variations in relation to Mg# $\{(Mg\# = 100Mg/(Fe^{+2}+Mg)\}$ are presented in figure 5.2. All the anorthosite samples form small cluster because of the very limited range of Mg#. At the same time, dioritic anorthosite and anorthositic diorite samples show very wide range of Mg#.

Al_2O_3 does not show any trend. Three samples of anorthosite show higher Al_2O_3 content. CaO content also shows no trend. In the case of MgO, anorthosite samples form a cluster except one sample. In the dioritic anorthositic samples, MgO shows an increasing trend. Na_2O content of dioritic anorthosite samples shows a steady increasing trend. Anorthosite samples, though form a cluster, show a slight increasing trend. K_2O plots of dioritic anorthosite samples are highly dispersed. Dioritic anorthosite shows slight decreasing trend upto the anorthosite cluster and then an increasing trend in the case of Fe_2O_3. TiO_2 shows a decreasing trend upto anorthosite cluster and then an increasing trend. P_2O_5 shows a decreasing trend.
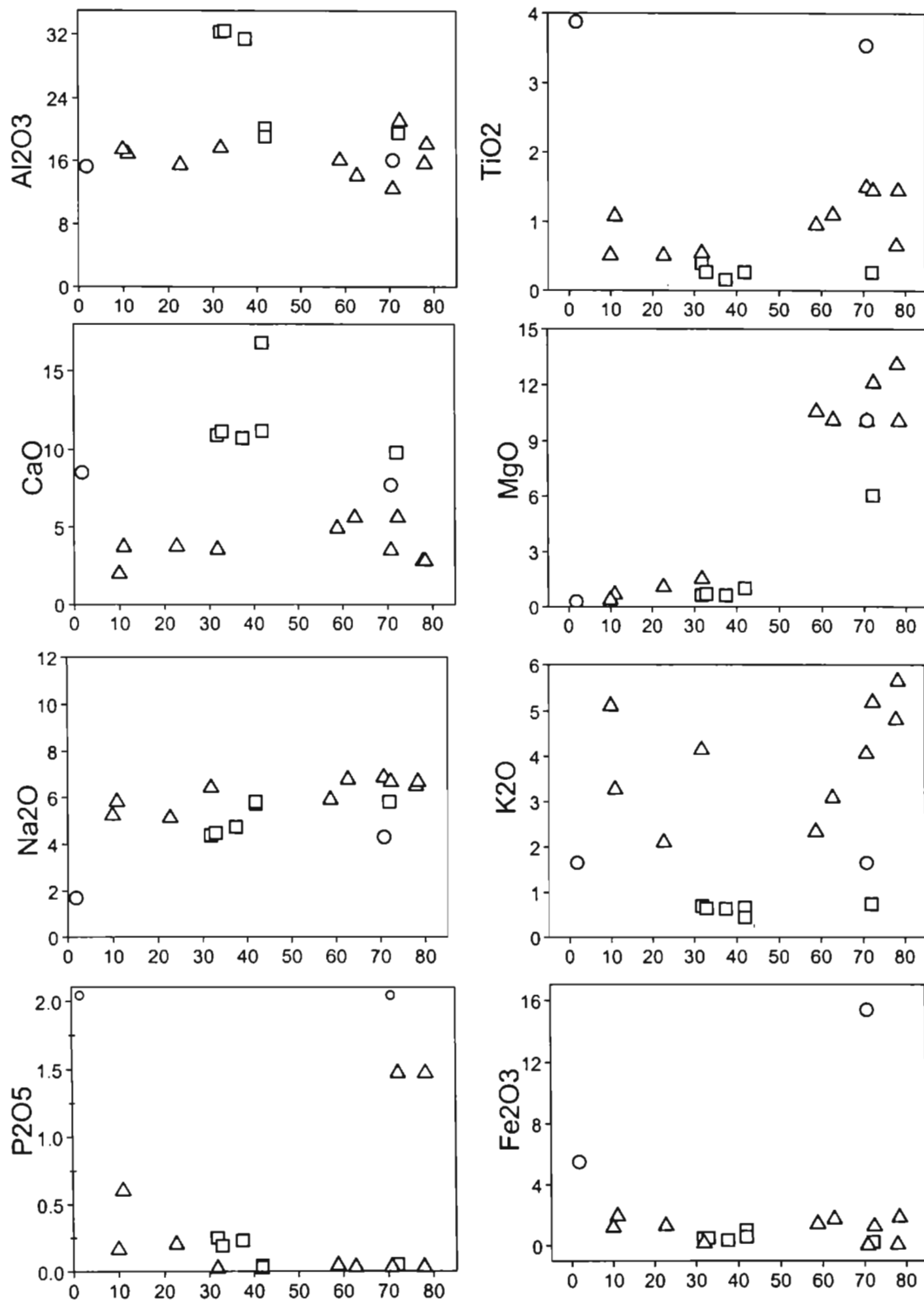
Fig. 5.2 Variation of major elements (wt%) with Mg number in Perinthatta anorthositic rocks. Symbols: square-anorthosite, triangle-dioritic anorthosite and circle-anorthositic diorite.

AFM {A= Na_2O+K_2O; F=FeO(t); M=MgO} diagram of these is presented in figure 5.3. There is considerable spread of the points. The two anorhositic diorite samples fall in the tholeiitic field because of their very high iron content. These are the rock samples which show orthocumulus texture. Majority of the anorthosite samples fall close to the Na_2O+K_2O corner while most of the dioritic anorthosites form a cluster with very low F content and almost equal amounts of A and M. Anorthosite and dioritic anorthosite samples show a remote calc-alkaline trend. The use of AFM diagram for cumulate rocks like anorthosites, gabbro and anorthositic gabbro and ultramafites is questionable (Leelanandam & Narsimha Reddy, 1985). However, this diagram is used in this work to study the variation in chemistry among the rock groups than to discriminate between tholeiitic and calc-alkaline trends.

In terms of major element chemistry, the most noteworthy feature of the Perinthatta anorthositic rocks is their high alkali content, especially the abundances of Na_2O. The alkaline chemistry of these rocks are further manifested by their normative mineralogy characterized by appreciable amounts of nepheline, acmite and rarely sodium metasilicate and low normative anorthite contents. However, these rocks cannot be treated as truly alkaline because of the absence of modal alkali mafic minerals in them. Many massif-type anorthosites like Adirondacks (Silver, 1968), Michikaman (Emsile, 1970), South Greenland (Upton, 1974) and Sept Isles, Quebec (Philpotts, 1990) are seen in close association with alkaline or peralkaline rocks. Thus the alkaline tendency of Perinthatta anorthositic rocks in terms of bulk chemistry is significant (This aspect is further discussed in section 5.6.2).

5.4 Trace elements

Three representative samples of anorthosite, seven samples of dioritic anorthosite and one sample of anorthositic diorite were analyzed for their trace element contents (Table 5.5). In anorthosite, Ba content ranges from 280 to 350 ppm. Sr in this rock samples ranges from 1150 to 1177 ppm and it is the most

71

Table 5.5 Trace element concentrations (ppm) of anorthositic rocks.

	anorthosites			dioritic anorthosites							anorthositic diorite
	S-3/3	S-3/A	S-4/A	S-2/A	S-12/L	S-12/T	S-22	S-11/D	S-12/C	S-21/1	S-1/A
V	14	20	14	18	19	8	26	26.8	10.6	10.9	49.49
Cr	16	62	54	48	34	64	35	51	48	36.99	27.16
Co	5	5	3	6	2	2	2.3	5.8	3.3	2.5	19.6
Ni	11	24	16	14	9	18	7.9	14.2	12.5	9.1	10.1
Cu	6	12	3	11	5.6	7	11	12.8	14.2	14.3	33.8
Zn	32	37	35	157	130	129	248	158	166	257	273
Ga	22	21	23	29	31	30	22	28	28.8	26	24.2
Rb	3	3.6	2.6	12.8	67	56	38	14	40	37	5
Sr	1177	1156	1150	501	290	297	254	548	337	281	311
Y	3	4.8	3.6	18.9	14.4	13.3	12.8	22	27.7	7.85	52
Zr	6	13	14	20	16	26	49	42	47	39	47
Nb	1.5	3.5	0.87	10.5	19	13.4	12	21.5	23	8.7	23
Cs	0.09	0.03	0.06	0.28	0.08	0.02	0	0.36	0.36	0.05	0.09
Ba	281	300	351	1198	995	1039	2511	1140	1275	2282	645
Hf	0.22	0.19	0.3	0.37	0.54	0.55	0.89	0.9	1.21	0.76	1
Ta	0.09	0.26	0.12	0.43	1.15	0.57	0.47	0.99	1.26	0.54	1
Pb	1.97	2.6	1.82	2.12	9.67	10.89	10.33	1.75	4.15	3.98	0.58
Th	0.11	0.6	0.09	0.08	0.6	0.31	0.12	0.25	1.32	0.16	0.22
U	0	0.08	0.01	0.05	0.37	0.09	0.02	0.08	0.43	0	0.12
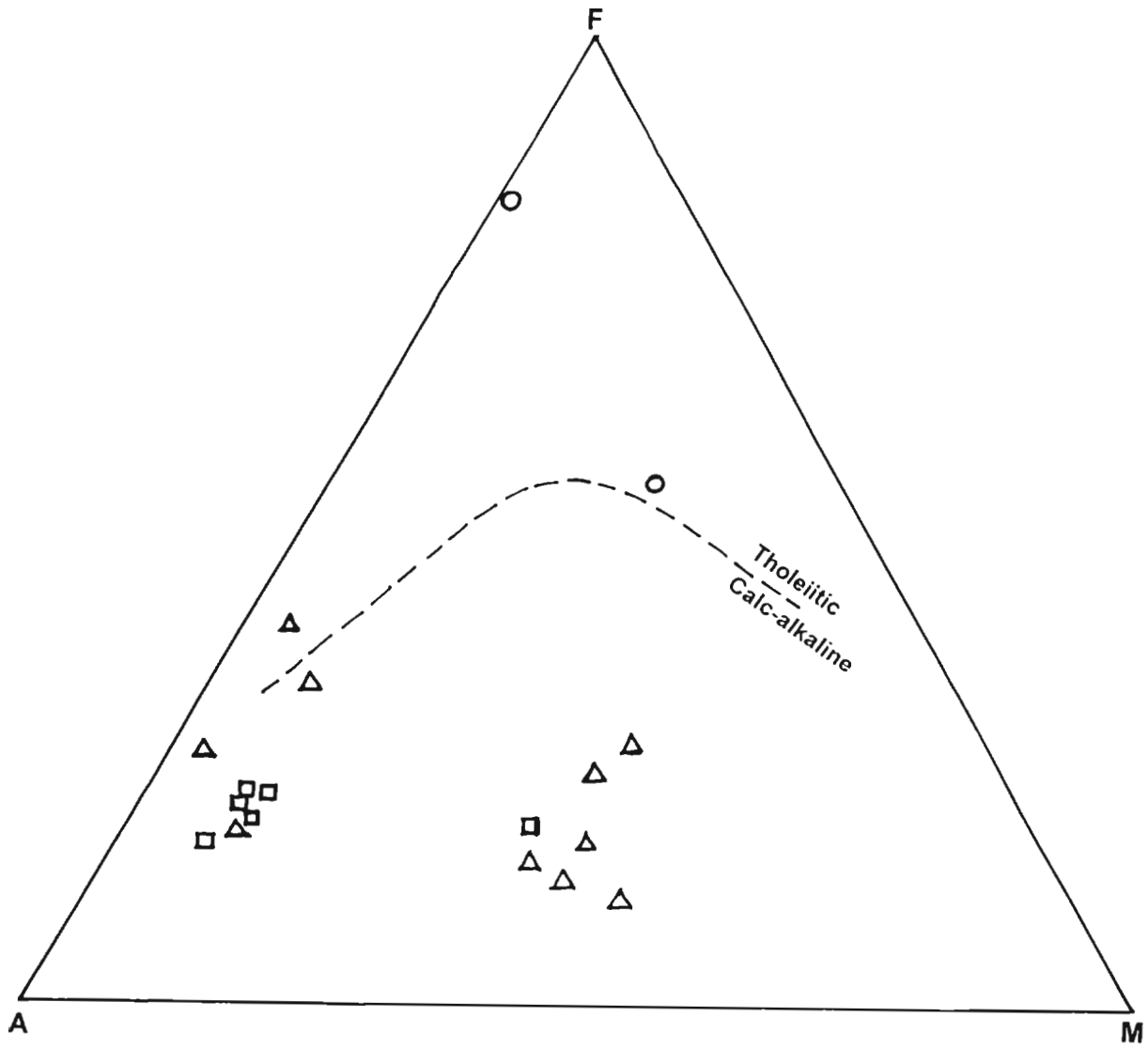
Fig. 5.3   AFM diagram for Perinthatta anorthositic samples (symbols as in figure 5.2).

abundant trace element in anorthosite. Rb content is very less compared to Ba and Sr and Rb ranges from 2.6 to 3ppm. Th content is very less and it ranges from 0.06 to 0.11ppm. U content is lesser than that of Th and it is absent in sample S-3/3 and the average content is 0.045ppm.

In dioritic anorthosite, Ba content is more than that in anorthosite samples. Ba is the most dominant trace element in dioritic anorthosite samples and it ranges from 995 to 2511ppm. Sr content is lesser than that in anorthosite samples and it ranges from 280 to 548ppm. Rb content is greater than that in anorthosite samples and it ranges from 12 to 67ppm Both Th and U contents are more than those in anorthosite samples. They range from 0.08 to 1.32ppm and 0.02 to 0.43ppm respectively.

In anorthositic diorite Ba content is 645ppm and Sr content is 311ppm. Rb content of anorthositic diorite is about 5ppm. Th and U contents are very less and their content is 0.22 and 0.12ppm respectively.

In figure 5.4, the concentrations of Rb and Sr were plotted to compare Perinthatta anorthositic rocks with some other anorthositic rocks of Nain Plutonic suite. Sr is very high in Perinthatta anorthosite samples compared to the rocks of Nain Plutonic suites. Extraordinarily high Sr content is common in massifs containing andesine anorthosites viz., Labrieville (upto 2600ppm) and Saint-Urban (upto 1400ppm) (Gromet and Dymek, 1982; Emslie, 1985). High Sr and low Rb is characteristic of the Nain anorthosites, as well as other massif anorthosites (Xue and Morse, 1993).

5.4.1 Trace element variations

Various variation diagrams were prepared for trace elements (Fig. 5.5). In the case of anorthosite, Ba shows a slight increasing trend when plotted against K. Dioritic anorthosite samples show a well defined increasing trend. When Ba is plotted against Ca+K, the anorthosite samples show a slight

72
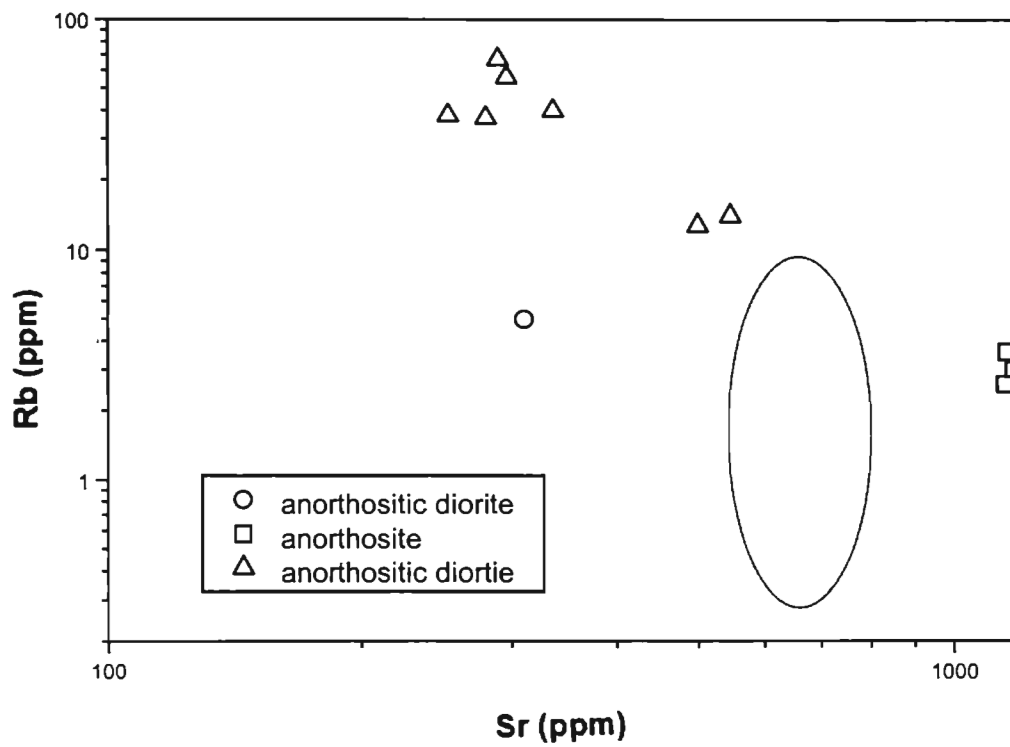
Fig. 5.4 Sr vs Rb diagram for Perinthatta anorthositic rocks. The oval
represents the field of Bird Lake massif, Susie Brook Slab, Kikkertavak
`area of in the Nain plutonic suite, Labrador (from Suizhou and Morse, 1993).
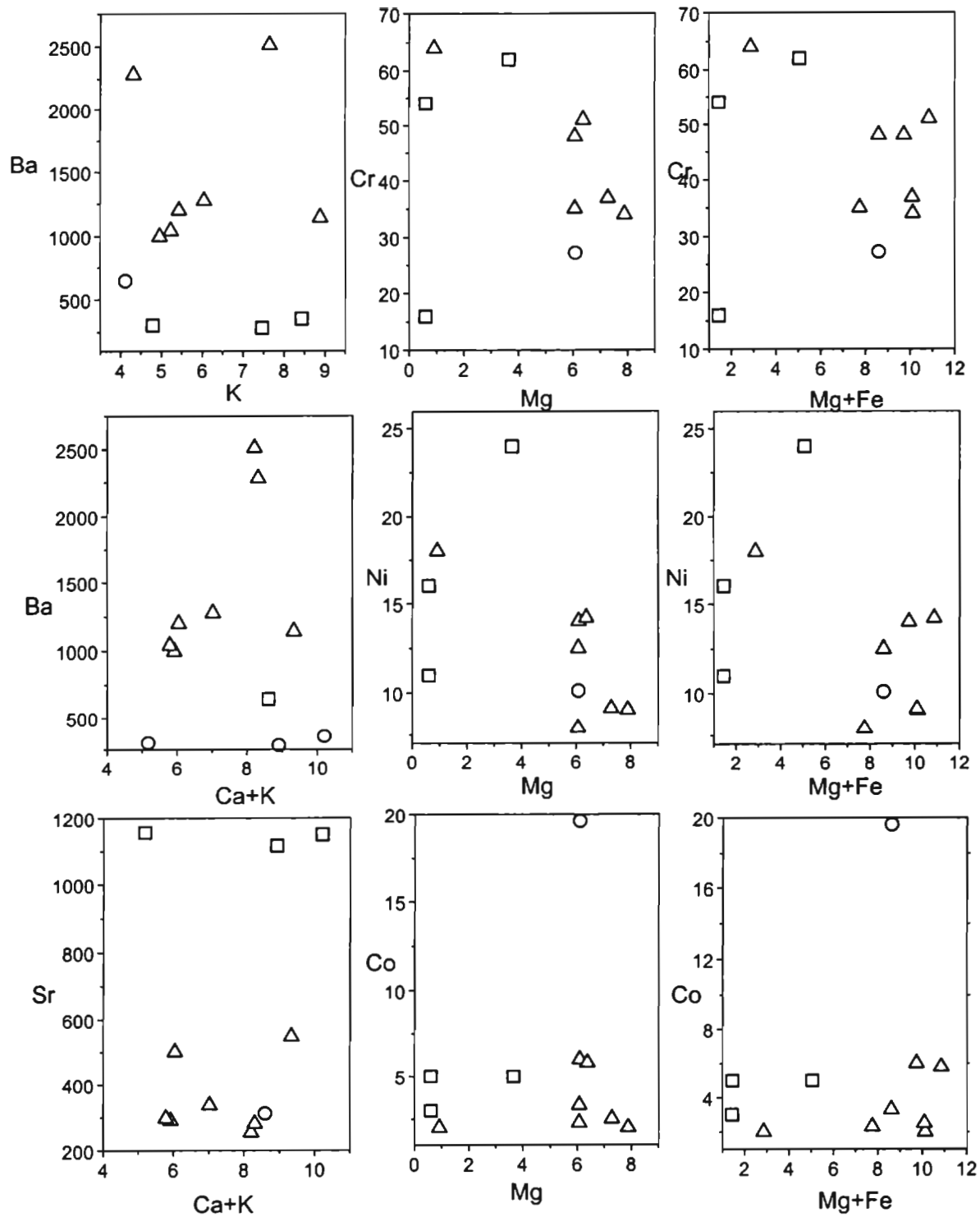
Fig. 5.5 Variation of trace elements(ppm) with K(ppm), Ca+K(ppm), mg+Fe(ppm) and Mg(ppm). Symbols as in figure 5.2.

increasing trend. A more pronounced increasing trend is given by dioritic anorthositic samples. In the Sr vs Ca+K diagram for anorthosite, no trend is observed indicating the absence of considerable change in Sr content with respect to Ca+K. In the same diagram, dioritic anorthositic samples show a decreasing trend. In Cr vs Mg diagram, anorthositic samples do not show any definite trend, while the dioritic anorthositic samples show a decreasing trend. In Cr vs Mg+Fe diagram, no definite trends are seen in both anorthositic and dioritic anorthosite samples. In Ni vs Mg plot, an increasing trend is observed for anorthositic samples while a decreasing trend is observed for dioritic anorthosite. In Ni vs Mg+Fe diagram, increasing trend can be seen for both anorthosite and dioritic anorthosite.

The Zr/Hf ratio ranges from 27 to 47. For dioritic anorthosite, it ranges from 29 to 55. Zr/Hf ratio S-1/A is 47. Ba/Sr ratio of anorthosite samples is very less compared to that of dioritic anorthosite. For anothosite, this ratio ranges from 0.24 to 0.31. For dioritic anorthosite, it ranges from 2.08 to 9.89. Average U/Th raito of anorthosite samples is 0.72 while this ratio for dioritic anorthosite ranges from 0.17 to 0.63.

Primitive mantle normalized trace element patterns of Perinthtta anorthositic rocks are given in figure 5.6. The patterns are very much similar for all the three rock types. Positive anomaly is shown by Ba and K while negative anomaly is shown by Th, U, Hf and Zr.

5.5   Rare earth elements

Rare earth element concentrations are presented in table 5.6. In anorthosite samples, concentration of La ranges from 6.15 to 8.97 ppm. Ce concentration in anorthosite ranges from 10 to 16 ppm. and this element is the most abundant of all the rare earth elements. Nd ranges in concentration from 5 to 9 ppm. The rest of the light rare earth elements (LREE) viz., Pr and Sm are very less and their average concentrations are 1.5ppm. and 1.4 ppm.

73

Table 5.6 Rare earth element concentrations (ppm) in anorthositic rocks

	anorthosites			dioritic anorthosite							anorthositic diorite
	S-3/3	S-3/A	S-4/A	S-2/A	S-12/L	S-12/T	S-22	S-11/D	S-12/C	S-21/1	S-1/A
La	6.15	8.97	6.6	26.13	22.26	19.95	21.11	28.6	36.18	11.19	54.1
Ce	10.09	16.09	11.66	52.9	38.57	34.26	35.23	58.07	72.35	17.27	123.43
Pr	1.15	1.91	1.33	6.36	4.31	3.86	4.14	7 18	9	2.13	17.36
Nd	5.42	8.81	6.41	27.95	16.79	15.86	17	35.21	36.44	9.39	83.1
Sm	1.09	1.81	1.32	5.22	3.93	3.58	3.51	7.39	8.03	1.89	18.92
Eu	1.32	1.58	1.99	5.27	4.61	4.55	7 13	6.06	5.15	6.83	5.49
Gd	1.03	1.61	1.11	5.94	4.27	3.67	4.13	6.72	7.9	2.25	17.54
Tb	0.13	0.24	0.16	0.83	0.44	0.43	0.51	0.88	0.99	0.28	2.24
Dy	0.52	1.11	0.65	3.6	2.66	2.29	2.47	4.07	4.82	1.28	10.62
Ho	0.08	0.17	0.15	0.69	0.49	0.43	0.42	0.73	0.88	0.28	1.81
Er	0.23	0.39	0.31	1.62	1.19	1.05	1.04	1.93	2.1	0.63	4.5
Tm	0.02	0.05	0.03	0.22	0.18	0.16	0.14	0.23	0.26	0.06	0.53
Yb	0.1	0.38	0.18	1.56	1.35	0.85	1.13	1.6	1.77	0.6	3.65
Lu	0.02	0.06	0.02	0.25	0.18	0.17	0.17	0.27	0.22	0.14	0.51
REE	86.3	134.1	106.86	437.9	329	300.7	349	501.8	563.9	227.8	1095.7
Eu*	4.5	7.6	5.1	25	18	16.2	16.5	30	39	9	80
(Eu/Eu*)	3.9	2.83	5.31	2.87	3.41	3.82	5.88	2.75	1.79	10.32	1.83
(La/Sm)	3.54	3.11	3.13	3.15	3.55	3.5	3.78	2.44	2.83	3.72	1.79
(Gd/Yb)	8.14	3.44	5	3.05	2.54	3.46	0.72	3.36	3.59	3	3.87
(La/Yb)	41.34	10.06	24.77	11.24	11.05	15.71	12.61	11.99	13.73	12.45	9.97
(LREE)	56.3	88.4	64.1	275.3	202.9	183.2	191.9	319.7	381.9	100.4	705.1
(HREE)	30	45.7	42.76	162.6	127	117.5	157.1	182.1	182	127.4	390.6
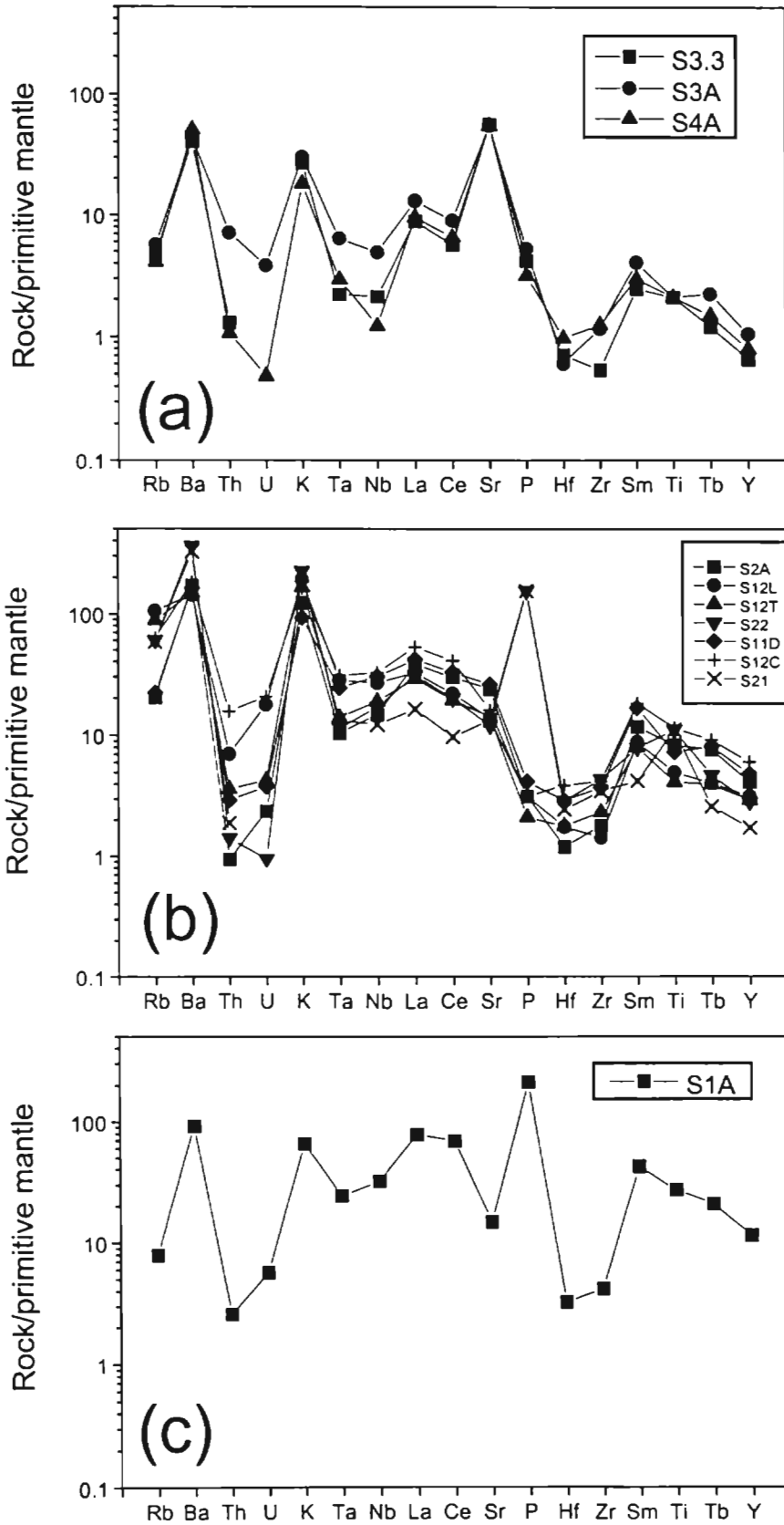
Fig. 5.6. Primitive mantle-normalized trace element patterns of (a) anorthosite (b) dioritic anorthosite and (c) anorthositic diorite.

respectively. Average concentrations of Eu and Gd are 1.6 ppm. and 1.3ppm. respectively. Compared to LREE, heavy rare earth elements (HREE) are very less in their concentrations. Tb ranges in concentration from0.13 to 0.24ppm. Dy is the most abundant of all the HREE and it ranges from 0.52 to 1.11ppm. Average concentrations of Ho, Er, Tm, Yb and Lu are 0.1 ppm, 0.3ppm,0.03 ppm, 0.2ppm and 0.03ppm respectively.

In dioritic anorthosite, concentrations of both LREE and HREE are more than those in anorthosite samples. In dioritic anorthosite samples, concentration of La ranges from 11ppm to 36ppm. As in the case of anorthosite samples, Ce is the most abundant REE and it ranges from 17 to 72ppm. Concentration of Pr ranges from 2 to 7ppm. Concentration of Nd is also showing some variation and it ranges from 9 to 36ppm. Sm ranges in concentration from 2 to 8ppm. Concentration of Eu is not varying much and its average concentration is 6ppm. Average concentration of Gd is 5ppm. The dioritic anorthosite samples also are depleted in HREE compared to LREE. Among HREE, Dy is the most abundant element and it ranges from 1 to 5 ppm. Tb ranges in its concentration from 0.3 to 1ppm. Concentration of Er ranges from 0.6 to 2ppm. Abundance of all other HREE like Ho, Tm, Yb and Lu are very less and their average concentrations are 0.6 ppm, 0.2ppm, 1ppm and 0.2ppm respectively.

Concentrations of REE in the anorthositic diorite sample (S-1/A) are more than those in the anorthosite and dioritic anorthosite samples. This can be attributed to the higher content of modal apatite and mafic content of this sample.

In table 5.6, some important rare earth elemental ratios and parameters are also given. These ratios are $(Eu/Eu^*)_N$, $(La/Sm)_N$, $(Gd/Yb)_N$ and $(La/Yb)_N$. Thus it can be seen that anorthosites show low concentrations of REE and Σ $(REE)_N$ ranges from 86 to 107. Σ $(REE)_N$ values of dioritic anorthosite samples are three to five times that of anorthosite samples. Σ $(REE)_N$ values of dioritic anorthosite samples range from 228 to 564. Among the dioritic anorthosite

samples, the sample S-21/1 is having bulk REE concentration almost similar to that of anorthosite samples. All the samples of Perinthatta pluton have higher LREE than HREE contents.

The chondrite normalized REE patterns of these three rock units are given in figure 5.7. The chondrite values used for normalization were those recommended by Brynton (1984). The chondrite normalized pattern of all the rock samples show that they are moderately fractionated. Degree of fractionation is slightly more in anorthosite samples than that in dioritic anorthosite samples. This is indicated by the $(La/Yb)_N$ ratio which is ranging from 16 to 41 for anorthosite samples and from 11 to 15 for dioritic anorthosite samples. When the fractionation among the LREE is considered, it is almost same for all the analysed samples of the anothosite and the dioritic anorthosite. The average value of this ratio for anorthosite samples is 3.26 and that of dioritic anorthosite samples is 3.28. The anorthositic dioritic sample shows a value of 1.79 and it indicates the less evolved nature of the sample S-1/A. Considerable difference in the degree of fractionation among the HREE can be seen between the samples of anorthosite and dioritic anorthosite. This is indicated by the ratio $(Gd/Yb)_N$ and the average values of this ratio for anorthosite and dioritic anorthosite are 6 and 3 respectively. Value of this ratio for anorthositic diorite sample is 4.

All the samples of Perinthatta pluton show pronounced positive europium anomaly. The values of $(Eu/Eu^*)_N$ ratio of anorthosite samples range from 3 to 5. For dioritic anorthosite samples, this ratio ranges from 2 to 6. For the sample S-21/1, the value for this ratio is abnormally high ($\sim$ 10). The bulk REE and the chondrite normalized REE pattern of these rocks are analogous to the anorthosites and associated mafic derivatives of Adirondacks (Ashwal and Seifert, 1980).
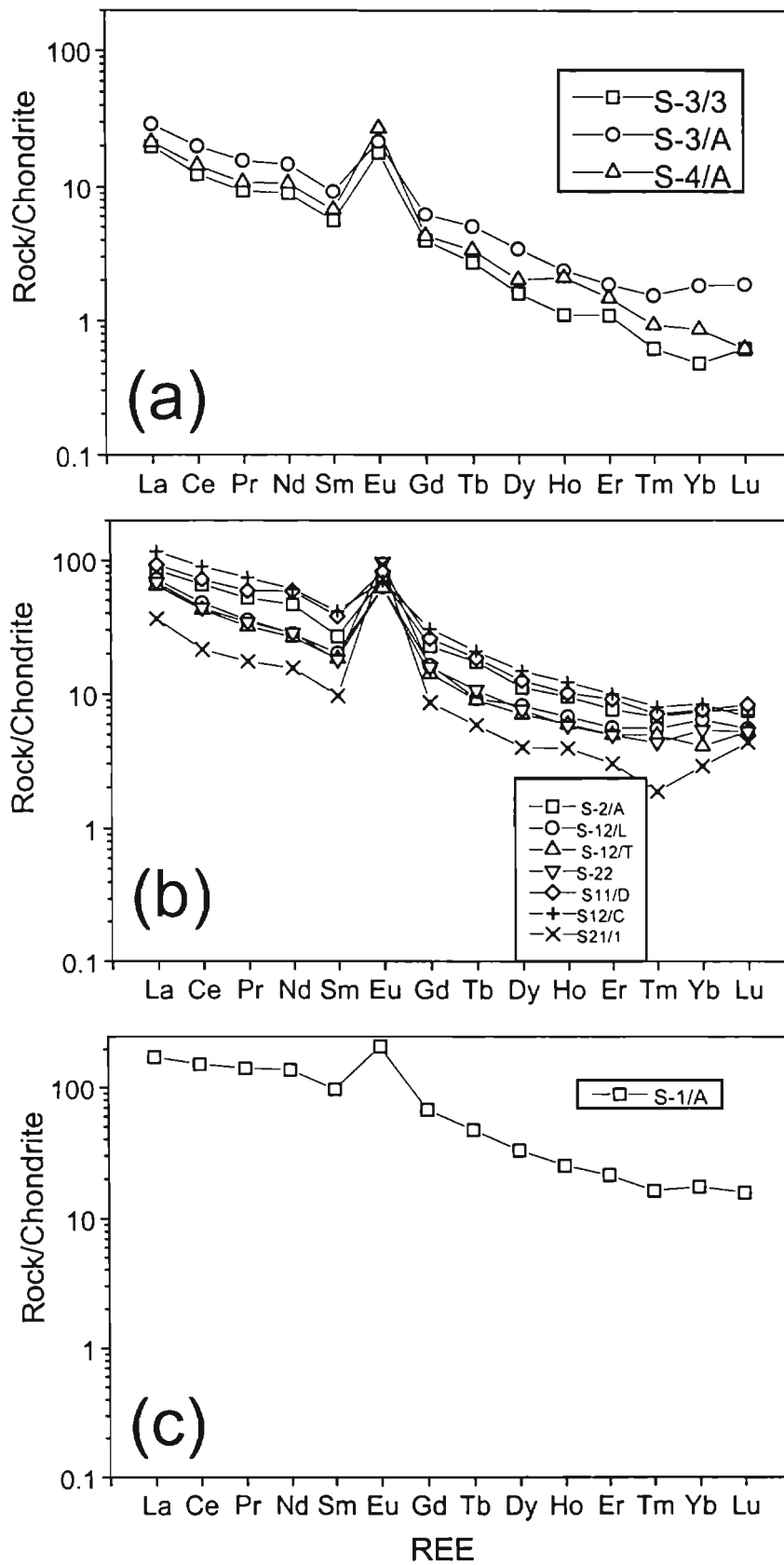
Fig. 5.7 Chondrite-normalized REE pattern of the Perinthatta anorthositic rocks: (a) anorthosite (b) dioritic anorthosite and (c) anorthositic diorite {Chondrite values are from Brynton (1984)}

5.6   Petrogenesis

5.6.1 Petrogenesis of massif-type anorthosites

A general and brief account of the different approaches towards the problem of petrogenesis of massif anorthosites are discussed below as summarized by Ashwal (1993).

Some early workers influenced by the Neptunist thought believed that the anorthosites are sedimentary rocks and some interpreted the anorthsoites as igneous rocks. The modern thinking about anorthosite problem was a result of N.L. Bowen's experimental work. In 1917, Bowen emphasized the gravitational accumulation of plagioclase crystals as an important process in anorthosite petrogenesis. Thus the debate over the composition of the parental melt or magma and whether plagioclase sank of floated began.

Some, as early as 1940s, considered a metasomatic origin for anorthosites and therefore 'anorthositization' was introduced. Gresens (1978) proposed that massif anorthosites were formed by metasomatism of evaporites and pelites.

Anorthsoites were considered as crystalline residue left behind after melt removal during deep crustal anatexis by some other workers. This was also not generally accepted as a viable explanation of anorthosite petrogenesis, because it failed to explain coarse grained igneous texture and isotopic characteristics.

Many workers considered that anorthosites and associated granitoids in some areas are consanginous suites and interpreted that granitoid suites represent later stage differentiates from a common parental magma. Thus different magma composition have been proposed including basalt, diorite, granodiorite (de Warrd and Whealer, 1971), monzodiorite or jotunite (de Waard et al., 1974).

76

Most of the petrologists favour simple crystal fractionation as a mechanism of differentiation, whereas Philpotts (1981) proposed liquid immiscibility as a mechanism. Regarding the origin of magmas, intracrustal melting was favoured by some workers while others favoured assimilation of large volumes of crustal materials by mantle-derived melts (Philpotts, 1968). However, consanguinity of anorthosite was questioned by several workers on the basis of geochemistry especially REE data of granitoids which do not show the complimentary negative Eu anomaly indicating the fractionation of plagioclase.

Some workers proposed that anorthosites crystallized from metls of anorthositic composition. Eventhough the existence of anorthositic melts remains a possibility, it is questionable due to the amount of melts required for large massifs to crystallize.

As early as 1910s, many considered basalt as the most satisfactory choice of parental melts of massif anorthosites. Many evidences including the mineralogic composition and An relations indicate that basaltic magma could indeed produce the plagioclase composition found in Nain Anorthosites (Morse, 1982). Composition of mafic silicate minerals of massif type anorthosites resemble those of layered intrusion for which a basaltic parentage is almost confirmed.

The evidence against a basaltic parentage is the absence of sufficient volume of complementary mafic or ultramafic material left after the removal of plagioclase crystals to form the anorthosite. Gravity surveys over many anorthosites denied the presence of such mafic bodies beneath anorthosites. Eventhen, a magmatic detachment process may be invoked for the absence such a mafic body.

If an anorthosite formed as cumulate, it is questionable whether the plagioclase sank or floated. Anorthosite massifs giving evidence for a sinking or floating of plagioclase is very rare. Some experiments conducted by Kushiro and Fujii (1977) and Kushiro (1980) concluded that basaltic melts are more compressible than crystals above 6 kb such that any plagioclase more sodic than An_{90} will have a tendency to float. So in deep crust, floating of cumulate plagioclase can be expected.

In a plausible model of anorthosite petrogenesis as proposed by Ashwal, 1993 involves ponding and fractional crystallization of basaltic melts in deep crust. During crystallization, the early crystallizing mafic silicates will sink and when the plagioclase crystallizes it forms floatation cumulates. These will ascend through the crust as buoyant anorthositic mushes. In the upper crust, these plagioclase-rich diapirs coalesce to form massif-type anorthosites.

5.6.2 Petrogenesis of Perinthatta anorthositic rocks

The major, trace and rare earth elements were used to arrive at various constriants on the petrogenesis of Perinthatta anorthositic rocks. Any valid model for the evolution of the anorthositic rocks of Perinthatta should account for the following field, petrographic and geochemical characteristics.

1. Field relations favouring their intrusive nature.
2. Dark grey colour essentially due to the presence of minute oriented iron-oxide inclusions in the plagioclase.
3. Plagioclase-rich mineralogy of all the rocks.
4. Unzoned and low-calcium nature of the plagioclases (see section 5.7.1 on mineral chemistry).
5. Anhydrous nature of the mafic minerals in the rocks with the presence of co-existing orthopyroxene and clinopyroxene.
6. Cumulus texture of the rocks with varying amounts of intercumulus matter rich in opaques, mafics and apatite.

7. Major element chemistry indicating an alkaline affinity with high (Na_2O+K_2O) but lower Al_2O_3 and CaO.

8. Fractionated chondrite normalized REE patterns with pronounced positive europium anomalies.

9. Overall consistency of the REE abundances with modal mineral contents.

10. Concentrations and ratios of certain key trace elements like extremely high Sr in anorthosites, very low Rb, Cs and Pb in all the rocks, almost constant Zr/Hf and Co/Fe ratios.

The magmatic nature of the Perinthatta anorthosite body can be ascertained from the following features. Field relationship including the sharp contact with the host rocks, presence of xenoliths of country rock in the pluton, limited variation in their mineralogy and the presence of iron-oxide inclusions in plagioclase. Clinopyroxene and orthopyroxene are present in all the samples of the pluton and these mafic assemblage is of uniform nature. This feature and the occurrence of this pluton in high grade metamorphic rocks are indicating a deep seated emplacement. Very coarse grained to coarse grained nature of the rocks also favours this. The anhydrous nature of the mafics indicates a low activity of H_2O during crystallization.

All the samples of Perinthatta anorthositic rock show cumulus texture with varying percentage of postcumulus material. Thus these rocks of the area can be grouped into orthocumulate, mesocumulate and adcumulate. The cumulus nature of the rocks was identified by the textural features. Currently emerging view is that textural criteria alone cannot be used to call a rock 'cumulate' and in the absence of other evidences it can be misleading to refer to it in terms of the cumulate nomenclature (McBirney and Hunter, 1995).

Following the original definition of cumulus terminology (Wager et. al, 1960), the best examples of orthocumulates are from Lower Zone A of Skaergaard Layered Series, East Greenland (Wager, 1963). When the texture of

this rock is compared with the texture of the orthocumulate samples of Perinthatta anorthositic rock (samples S-1/A and S-1/B), some major differences are noticed. In the S-1/A and S-1/B samples plgioclase feldspar crystals (representing 'primocrysts') are uniformly large. This is not the case of Skaergaard sample (McBirney and Hunter, 1995). In the samples S-1/A and S-1/B, poikilitic textural relationship is not observed between pyroxene and plagioclase crystals. In the case of Skaergaard sample, the poikilitic texture is very clear and the plagioclase inclusions in the central portions of pyroxene oikocrysts are smaller while those towards the margin are larger. Therefore, McBirney and Hunter (1995) precluded the earlier observation that the plgaioclase crystals grew to large dimensions before settling to the floor. In the case of Perinthatta anorthositic samples, pyroxene crystals embay into plagioclase crystals. Thus the uniform size of plagioclase crystals and later crystallization of pyroxene crystals indicate that the samples S-1/A and S-1/B can be considered representing the orthocumulate according to the present view also.

Some of the mesocumulate samples from the western portion of the Perinthatta anorthositic rock shows a granoblastic texture which indicates recrystallization to some extent. Eventhough there is no evidence for metamorphism or widespread metasomatic repalcement in the field, the geochemistry of these samples is in favour of alkali metasomatism. So all the mesocumulate rocks from the western portion of the Perinthatta anorthositic rock samples cannot be considered as mesocumulate in the McBirney and Hunter's (1995) point of view. The alkali metasomatism might have destroyed the original texture of these samples.

The Perinthatta anorthositic rocks show adcumulus texture also in some locations. Majority of these samples are anorthosites. These samples have textures that meet almost all the criteria of adcumulate. The textral features typical for an adcumulate rock are absence of zoning, uniform large size of

80

plagioclase crystals, scarcity of other minerals etc. These textures are reported from the samples of Skaergaard intrusion but for these samples field relations indicated a postcumulus metasomatic replacement (McBirney and Hunter, 1995). Thus for the samples of Skaergaard intrusion, field relations does not favour a magmatic origin for their textural features. In the case of Perinthatta anorthosite samples, the field evidence support a magmatic origin for their textural features.

Near Perinthatta, the anorthosite rock shows preferred orientation of plagiclase crystals. This is only a linear fabric and that may be attributed to the flow of magma. Since the postcumulus material does not show any preferred orientation it can be argued that the plagioclase crystals attained the preferred orientation before postcumulus material started crystallizing. The preferred orientation indicates the existence of an anisotropic stress field in the Perinthatta area at the time of crystallization of cumulus plagioclase. The preferred orientation is not shown by all the plagioclase crystals. Only the long prismatic crystals show this feature while majority of the stubby crystals do not show any preferred orientation. Thus two generation of feldspars can be seen in this area and the long prismatic crystals showing preferred orientation are the older ones.

All the samples of the pluton shows very pronounced Eu anomaly. All the plagioclase feldspars are unzonned. Thus, a major process involving plagioclase accumulation from a melt can be envisaged for the formation of Perinthatta pluton. There is a general consistency between the modal mineralogy and REE geochemistry. This supports their derivation by crystal fractionation from a common or similar parental magma. Samples S-1/A and S-1/B collected from location S1 gives a dioritic composition. These samples have high content of opaque minerals. This implies the generation of a ferrodioritic residual liquid. Association of massif anorthosite and ferrodioritic rocks is significant as ferrodioritic rocks represent the residual liquid left after the process of anorthosite formation (Emslie, 1994).

The elemental ratios like Zr/Hf and Co/Fe ratios are almost constant. This indicates a comagmatic nature of the anorthosite, dioritic anorthosite and anorthositic diorite. No considerable Hf enrichment is noticed in these rock samples.

From the major element chemistry of all the samples of Perinthatta pluton, it is evident that the rocks in general are alkalline in nature. In the AFM diagram, the rocks fall in the calc-alkaline field. In the Na_2O-K_2O-CaO diagram (Fig. 5.8), the rocks define a differentiation trend with cumulates represented by anorthosites falling towards CaO corner while the mafic variants away from it. Though there are evidences of local shearing and introduction of alkaline fluids, the consistent alkaline nature of the rocks can be atributed to alkaline metasomatism or any process of post-crystallisation introduction of alkaline fluids. Trace element geochemistry also supports a primary non-potassic nature. Trace elements like Rb, Cs and Pb are very low in all the samples of Perinthatta pluton. Since these are diadochic with potassium, the low content these elements indicates a primary non-potassic nature.

Alkaline nature of the Perinthatta pluton can be further discussed by using the tri-linear diagram of Ca-Al-(Na+K) after Currie, 1989 (Fig. 5.9). This diagram can give a better picture of the attainment of alkalinity of these rocks. The solid triangle marked 'B' and the solid circle marked 'G' represent average tholeiitic basalt and average granodiorite respectively. The basaltic and granodioritic rocks affected by alkali metasomatism will proceed along the arrows. The shaded region in the diagram represents the field of peralkaline rocks. The plots of the rock samples fall roughly along a line parallel to the basalt- granodiorite line. This clearly define a fractionation-related enrichment trend. Since they are away from the common basalt-granodiorite line, it can be inferred that the attainment of alkalinity was prior to evolution of anorthositic rocks. Influx of alkaline fluids at the time of generation of the melt or immediately after it or assimilation of alkali-rich crustal material prior to crystallization.
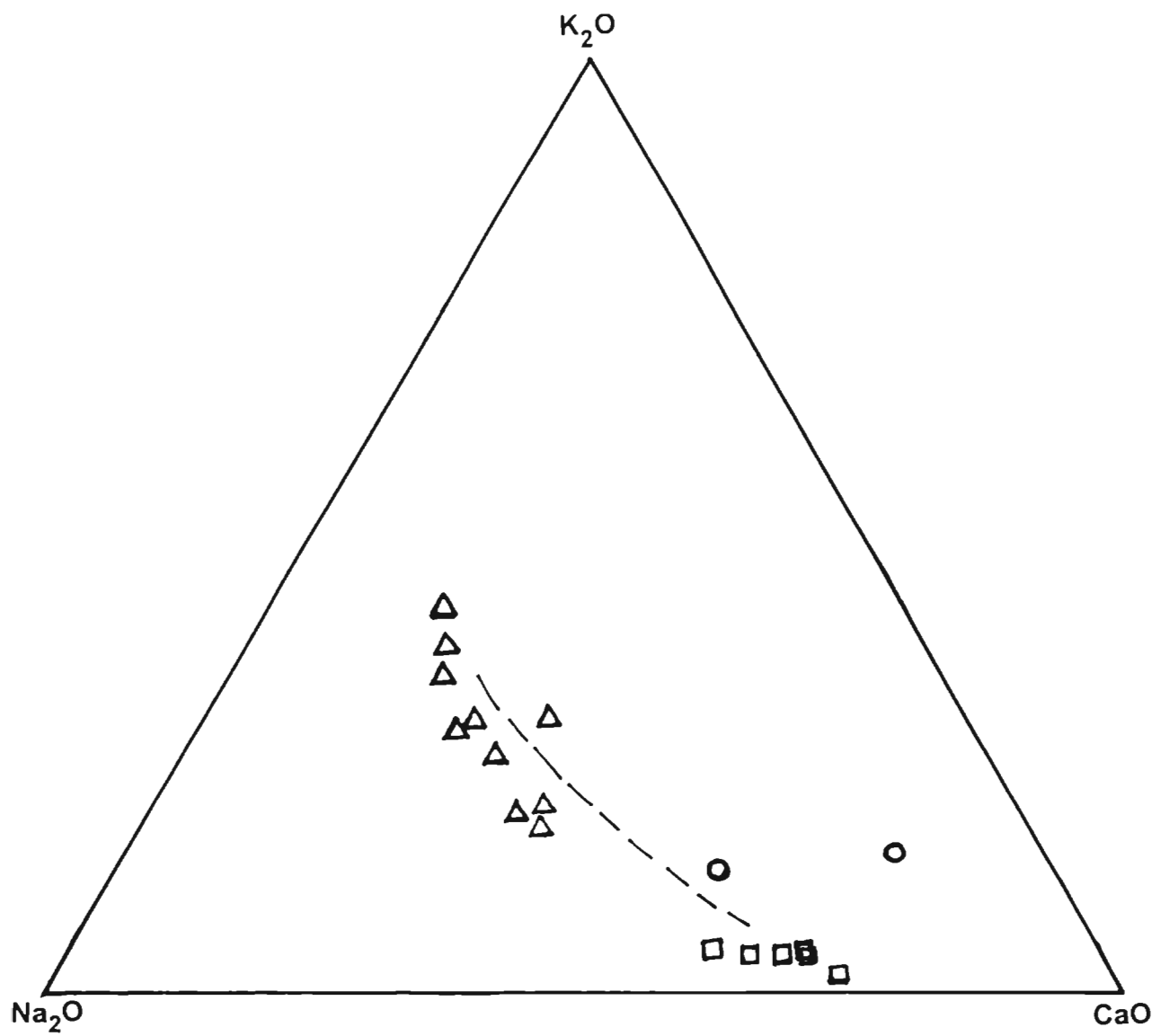
Fig. 5.9 Na$_2$O-K$_2$O-CaO diagram for the rocks of Perinthatta anorthositic rocks (symbols as in figure 5.2).
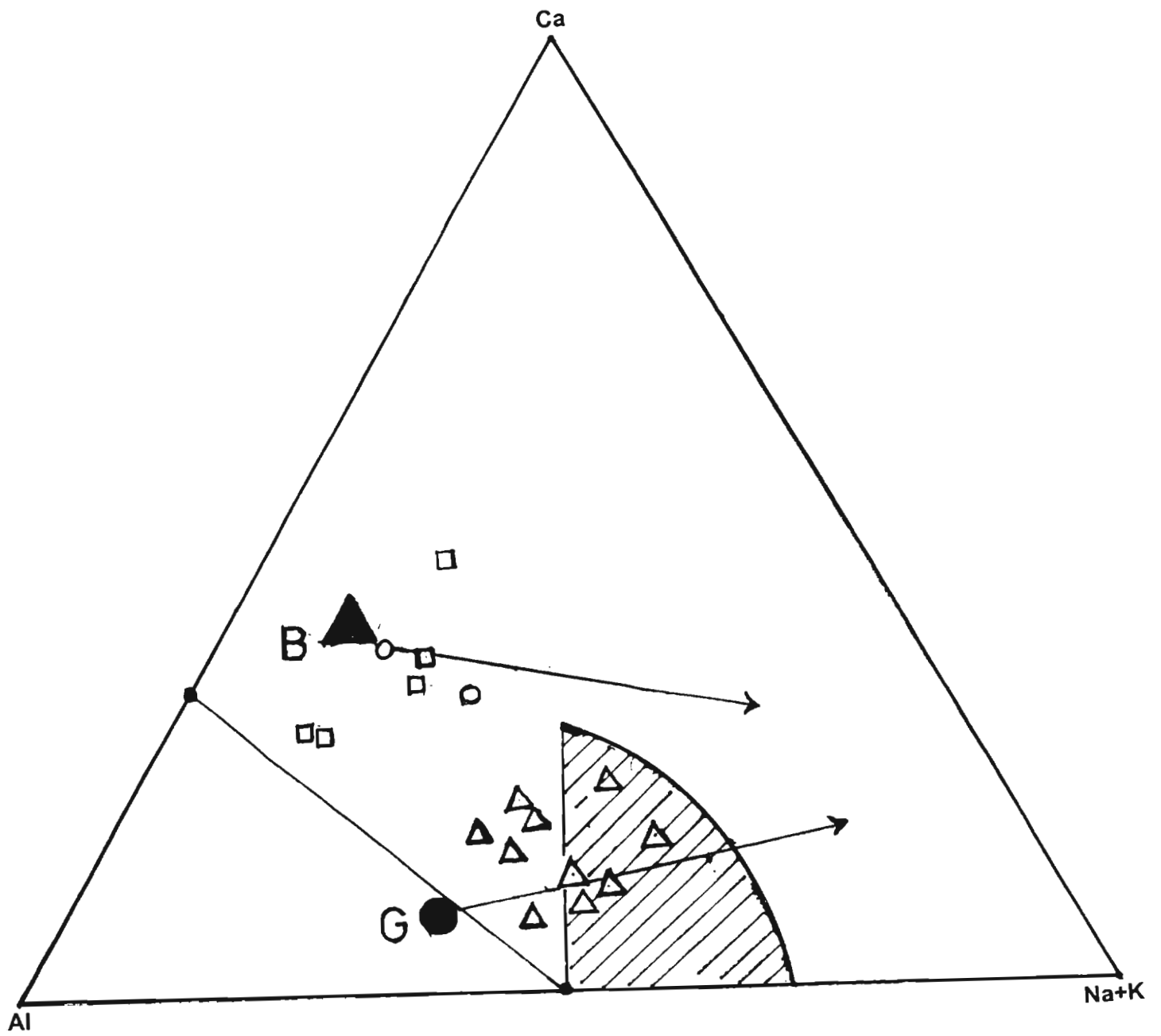
Fig. 5.10 Ca-Al-(Na+K) triangular diagram (after Currie, 1989) for Perinthatta anorthositic rocks for testing the factors of alkalinity. Symbols used for the anorthositic rocks are same as in figure 5.2. The solid triangle marked B represents average tholeiite basalt and the solid circle marked G represents average granodiorite.

The dioritic anorthosites associated with the anorthosites have lower Ca contents and no appreciable enrichment of Ni, Co and Cr and also no higher $MgO/FeO+Fe_2O_3$. Thus the dioritic anorthosites cannot be considered as closer to parental melt. The anorthositic dioritic samples show a ferrodioritic nature because of their higher opaque mineral content. This indicates that they have higher concentration of residual melt which contributed to the higher mafic content.

5.6.3 Rare earth element based modelling of parental melt

For modelling the parental melt of Perinthatta anorthosite, it is assumed that the anorthosites are essentially cumulates from a melt of intermediate composition. The modelling is based on the REE using their partition coefficients. The modelling can help to arrive at more constriants on the nature and evolution of parental magma.

Two basic equations describe the extremes of behaviour of trace elements during crystallization.

1. $C_l/C_o = F^{(D_\alpha - 1)}$

for perfect (or Rayleigh) fractional crystallization

2. $C_l/C_o = 1/(F+D_\alpha (1-F))$

for equilibrium crystallization

where C_o = concentration of element α in the original melt.

C_l = concentration of element α in the residual melt.

F = weight fraction of melt remaining.

D_α = bulk distribution coefficient for element α

($D_\alpha = \Sigma K_\alpha X_i$ where K_α = distribution coefficient for element α

in phase I, X_i = weight fraction of phase I)

In carrying out the modelling only the results based on the Rayleigh fractionation equation are reported since surface equilibrium is likely to be a better assumption than total equilibrium. An estimate of the phases involved can be derived from modal mineral contents.

In the present work three anorthosite samples (S-3/3, S-3/A and S-4/A) are selected for modelling the parent magma. The samples represent the cumulate solid. By modelling, concentration of REE in the parental magma, denoted by C_o, is calculated assuming a cumulate to residual liquid ratio of 1:9

i.e., $C_o = 0.9 \ C_l + 0.1 \ C_s$

To find out the C_o, Rayleigh's fractionation equation for the distribution of trace elements in mineral-melt systems, $C_l/C_o = F^{(D_\alpha \ -1)}$ can be used. To use this equation to find out the C_o (concentration in the parental melt), C_l (concentration in the residual liquid) has to be calculated. C_l can be found out by following Rayleigh's fractionation principle for the distribution of trace elements in mineral-melt systems, $D_\alpha = C_s \ / \ C_l$, where D is mineral/melt distribution coefficient for an element α and C_s is the concentration of elements in the solid. The solid here represents the anorthosite samples. The different phases which are included in the calculation are plagioclase, clinopyroxene, orthopyroxene and opaques. The distribution coefficients of the REE used for the calculation are after Arth (1976), Phinney and Morrison (1990) and Wilson (1989). These values are presented in table 5.7.

The concentration of REE in the modelled parent magma and residual melt are given in the table 5.8. The values given are chondrite-normalized and the pattern is given in figure 5.10. In the figure, average of the chondrite-normalized pattern of anorthosites and chondrite-normalized pattern of modelled parent magma are compared. The calculated parent has about hundred times chondritic REE abundance than the average anorthosite of Perinthatta. There is

Table 5.7 Distribution coefficients of REE used in the calculation

Element	plagioclase	orthopyroxene	clinopyroxnene	opaques
Ce	0.120	0.024	0.150	0.090
Sm	0.067	0.054	0.500	0.150
Eu	0.340	0.054	0.510	0.200
Yb	0.067	0.091	0.620	0.300

Table 5.8 Chondrite normalized REE abundance in the modelled
parent magma and residual liquid of anorthosite

	S-3/3	S-3/A	S-4/A
Ce	100	153	107
Sm	75	97	90
Eu	52	59	77
Yb	6	17	11
Chondrite normalized values in the residual liquid			
	S-3/3	S-3/A	S-4/A
Ce	110	168	117
Sm	83	107	99
Eu	56	64	83
Yb	7	19	12
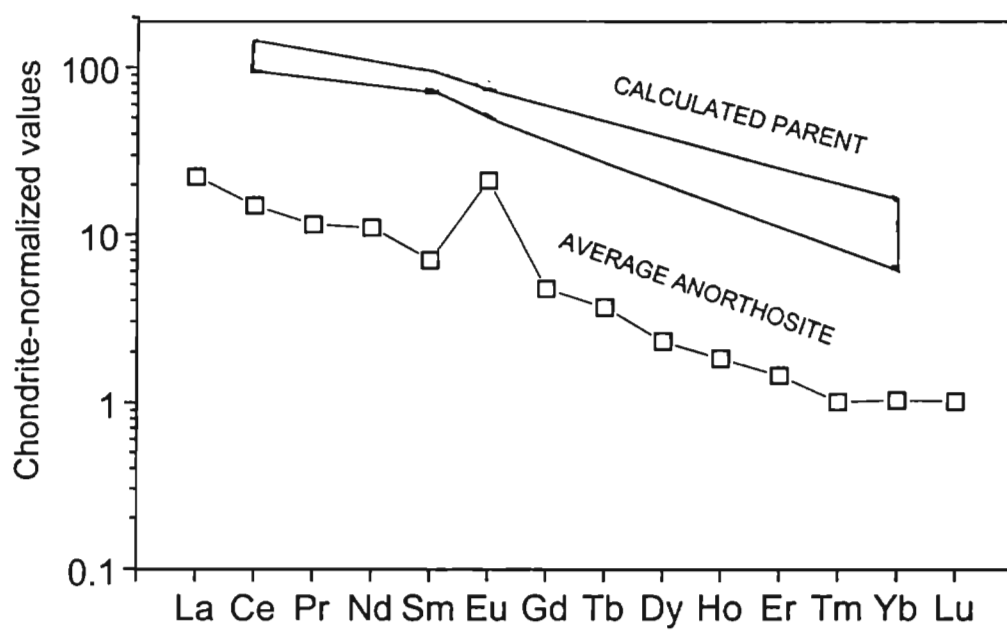
Fig. 5.10 Chondrite-normalized REE patterns of calculated parent magma of Perinthatta anorthosite. Chondrite normalized REE pattern of average anorthosite is also given for comparison.

no Eu anomaly in the calcuated parent and the pattern is slightly fractionated with the average value of $(Ce/Yb)_N$ ratio being 12.5. The slightly fractionated pattern and the absence of Eu anomaly in the parent magma points to the presence of HREE-retaining phases like clinopyroxene, garnet, etc. in the residue during their generation. This indicates a granulitic or eclogitic source. Thus it can be concluded that the anorthosite pluton was formed from a soda-rich magma of intermediate nature in a dehydrating environment.

Among the three rock units, anorthosite show the most evolved nature and the process of plagioclase cumulation progressed enough to produce the anorthositic composition. In the other two rock units, the plgioclase accumulation was not enough to produce anorthosite instead they became dioritic anorthosite and anorthositic diorite. So these three rock units represent different stages in the gradual process of generation of anorthosite

5.7 Mineral chemistry

The samples S-1/B and S-21/1 were selected for EPMA analysis. The results of the analysis are given in table 5.9.

5.7.1 Plagioclase

In S-1/B, large plagioclase crystals free of perthite spindles as well as feldspars with abundant microperthite spindles were analyzed. In S-1/B, five different plagiocalse crystals were analyzed (No. 1 – 5) in which three crystals (1-3) are free of perthitic spindles. In the three crystals free of antiperthitic exsolution lamellae, the average composition of the feldspar is found to be An_{12} Ab_{87}. Moreover, the composition is almost same for all the three grains. In feldspar crystals with antiperthitic spindles, orthoclase content is very high. In the crystals showing exsolution texture (No. 4 and 5), the compositions are An_8 Ab_{61} Or_{31} and An_6 Ab_{51} Or_{43}. In sample S-21/1, two feldspar grains with exsolution lamellae were analyzed and their orthoclase content is high. In this case, the composition is An_6 Ab_{52} Or_{42} and An_6 Ab_{65} Or_{29}.

Table 5.9 EPMA analysis of plagioclase crystals free of antiperthitic spindles (1-3) and plagioclase showing antiperthitic spindles in sample S-1/B (analysis 4 and 5), analysis of a plagioclase across the grain in sample S-21/1 (6-11) and antiperthitic exsolution lamellae (12 and 13).

(wt%)	Plag S-1/B					S-21/1							
	1	2	3	4	5	6	7	8	9	10	11	12	13
SiO2	63.24	64.84	63.95	64.36	65.36	61.15	61.99	60.08	59.22	58.7	58.85	61.4	62.81
TiO2	0.03	0.03	0.03			0.17	0.03		0.16		0.08	0.11	0.08
Al2O3	21.53	21.73	21.88	20.73	20.73	25.42	25.15	24.78	24.87	25.14	24.47	20.91	21.63
FeO	0.05	0.06	0.01	0.14	0.14	0.19	0.15	0.08	0.25	0.06	0.06	0.1	0.03
MnO			0.06	0.03	0.03								
MgO								0.22	0.09			0.02	
CaO	2.64	2.44	2.76	1.67	1.67	3.52	3.25	3.64	3.33	3.34	3.22	1.27	1.4
Na2O	10.67	10.53	10.84	7.18	7.18	10.54	10.56	10.55	10.21	11.03	10.55	6.04	7.94
K2O	0.12	0.13	0.13	5.58	5.58	0.32	0.31	0.26	0.28	0.28	0.27	7.39	5.37
Cr2O3		0.03				0.2				0.04			
NiO	0.04	0.06	0.02	0.04	0.04	0.05				0.02	0.12	0.02	0.04
Total	98.32	99.85	99.68	99.73	99.73	101.56	101.44	99.61	98.41	98.61	97.62	97.26	99.3
An	12	11	12	8	6	15	14	16	15	14	14	6	6
Ab	87	88	87	61	51	83	84	83	83	84	84	52	65
Or	1	1	1	31	43	2	2	1	2	2	2	42	29

One of the plagioclase feldspar grain of S-21/1 was analyzed across the grain at 20microns interval. In this case the chemistry of the plagioclase does not change across the grain. The composition was found to be same in all the locations of the grain (An_{16} Ab_{83} Or_1). This indicates absence of zoning. Compositional homogenity over large distance is characteristic of anorthositic plagioclase (Ashwal, 1993). From the mineral chemistry it is evident that the plagioclase feldspars in Perinthatta anorthosite are more sodic in composition. Massif type anorthosite generally have more sodic plagioclase (Ashwal, 1993). An content of Perinthatta anorthosite is very less compared to the range of Nain complex of Labrador. The total range for Nain is An_{34-90} (Ashwal, 1993). The An content in plagioclase of Perinthatta anorthosite is very less compared to the Rogaland complex, the composition of plagioclase of which is around An_{45} (Duchesne and Demaiffe, 1978).

Composition of the feldspars are plotted in the feldspar solid solution triangle (Fig. 5.11). The composition of the individual grains fall in the oligoclase field and exsolution lamellae fall in the anorthoclase and sanidine fields.

K-contents in antiperthitic plagioclase in Perinthatta anorthosite is abnormally higher than that reported elsewhere. In Labrieville, Quebec the orthoclase content ranges from 4-25 (Herz and Force, 1984) and this high content of orthoclase is characteristic of alkali anorthosite.

5.7.2 XRD analysis of plagioclase

Powdered plagioclase from two anorthosite samples S-3/A and S-4/A and one each from dioritic anorthosite (S-21/1) and anorthositic diorite (S-1/B) were subjected to X-ray powder diffraction and the patterns are given in figure 5.12. Peaks of maximum intensity are observed at 2θ values of 27.76 { Reference: Joint Committee on Powder Defraction Standard (JCPDS – files. Vol-1 & 2)}. Thus the plagioclase is identified to be andesine.
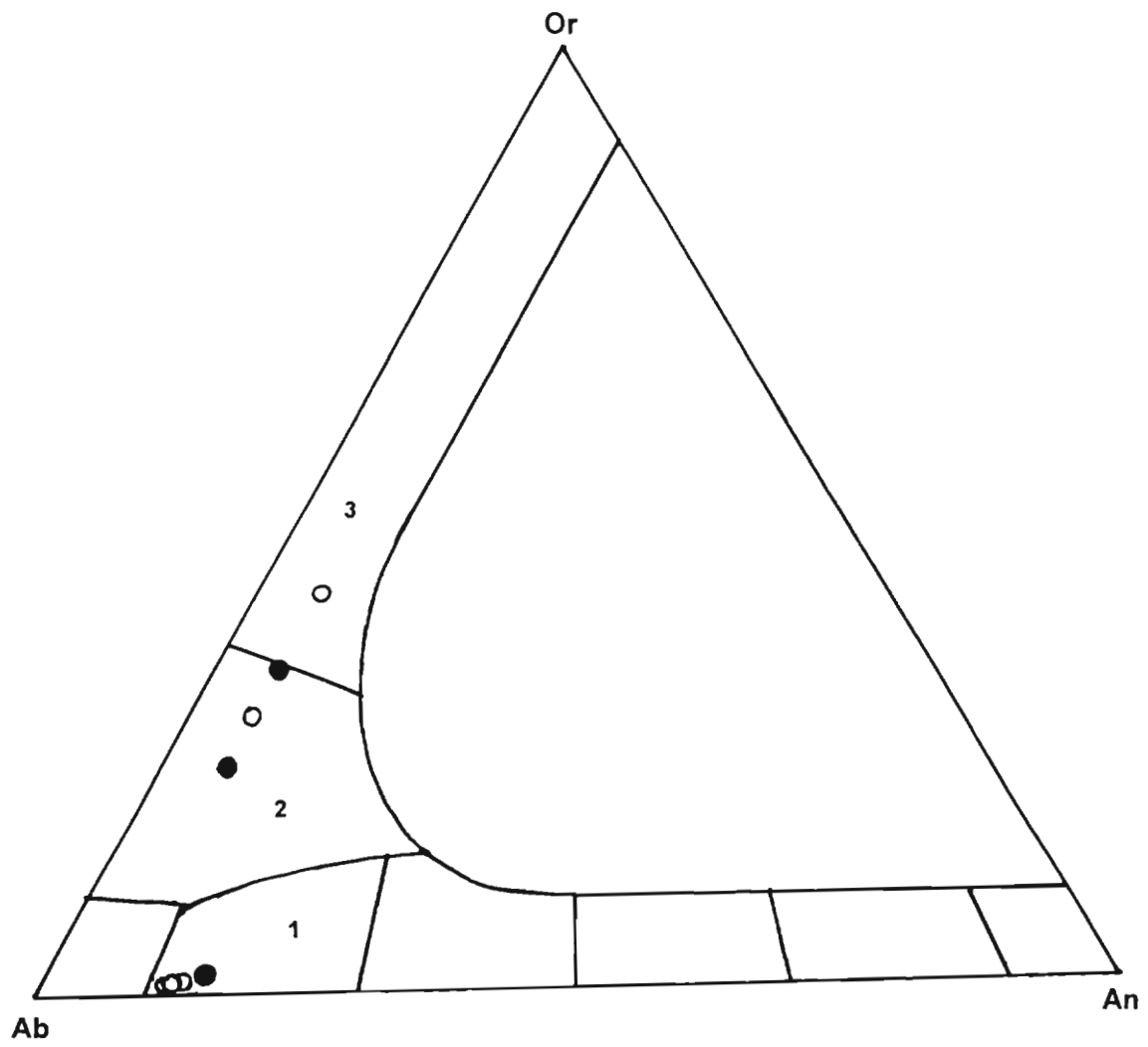
Fig. 5.11 Triangular diagram of the feldspar solid solution series showing the composition of feldspars in Perinthatta anorthositic rocks. The different fields are 1. oligoclase, 2. anorthoclase and 3. sanidine. Symbols: open circle- sample S-1/B and solid circle- sample S-21/1.
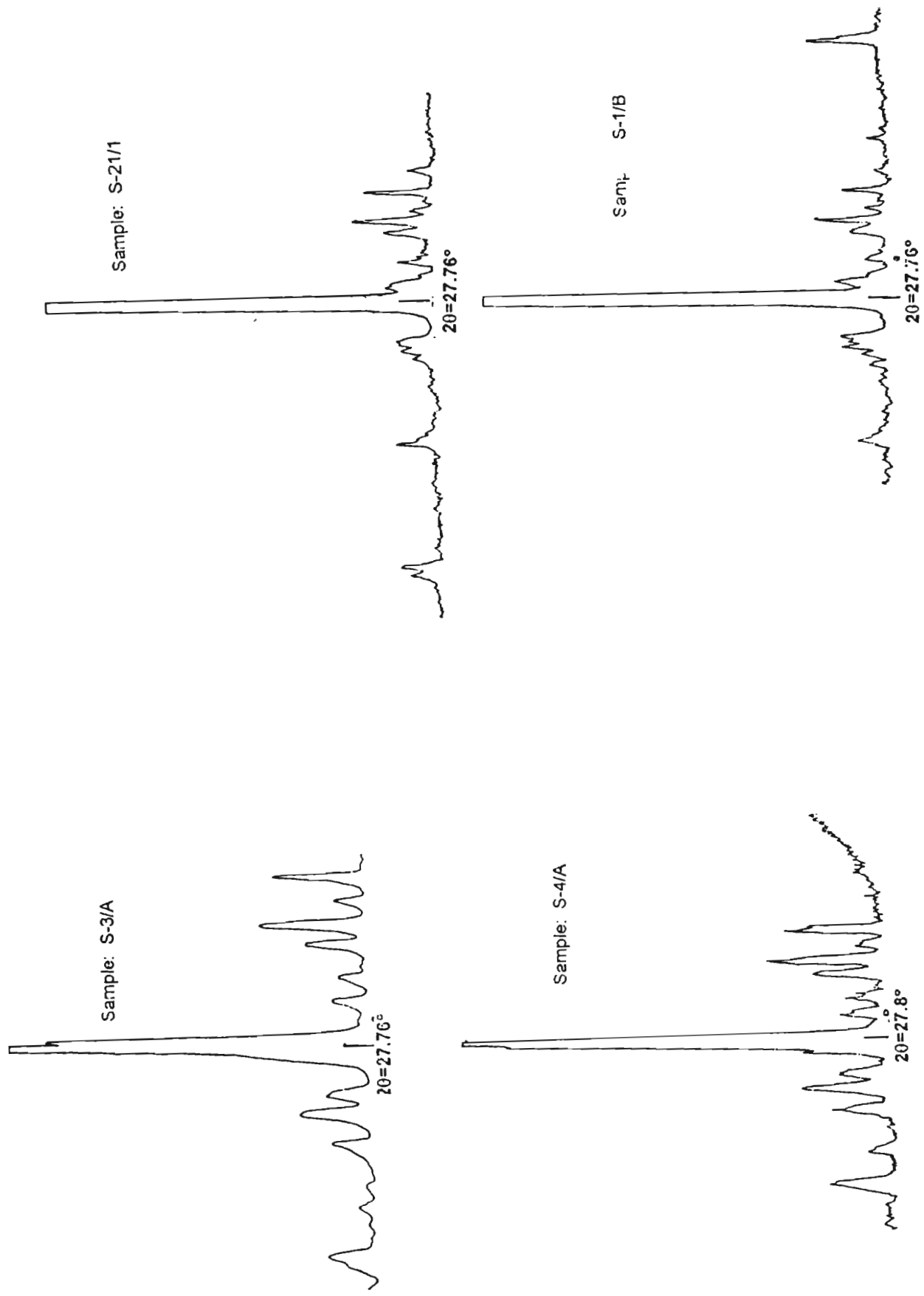
Fig. 5.12   XRD patterns four samples of Perinthatta anorthositc rock.

5.7.3 Pyroxenes

The EPMA data of pyroxenes are given in table 5.10. Coexisting clinopyroxene and orthopyroxene crystals were analyzed. Some pyroxene grains show exsolution lamellae and thus exsolved orthopyroxene lamellae in clinopyroxene and the host clinopyroxene grain were also analyzed.

In S-1/B, composition of clinopyroxene grains (No. 3 and 4 in table 5.10) showing exsolution lamellae of orthopyroxene is Fs_{32} En_{30} Wo_{38}. Another clinopyroxene coexisting with the orthopyroxene, but without exsolution lamellae (No. 6) shows a composition of Fe_{29} En_{32} Wo_{39}. Thus it is clear that all the clinopyroxenes are of same composition irrespective of whether they show exsolution texture or not. Free clinopyroxene grains have more enstatite content and less ferosilite content.

Orthopyroxene occurs in two different forms: (a) it occurs as exsolution lamellae in clinopyroxenes and (b) it occurs as individual grains coexisting with clinopyroxene. The orthopyroxene occurring as exsolution lamellae (No. 1 & 2) in clinopyroxenes show a composition of Fs_{63} En_{35} Wo_2. Composition of coexisting orthopyroxene and augite commonly reflect subsolidus equilibration, even in unmetamorphosed massifs {eg., Harplake (Emslie, 1980)}. The orthopyroxene (No. 5) coexisting with clinopyroxene grain shows a composition of Fs_{58} En_{35} Wo_7. Individual orthopyroxene grains are having lesser ferrosilite content than those occurring as exsolution in clinopyroxene. Enstatite content is same in both cases. The orthopyroxenes occurring as individual grains are slightly more calcic also.

In sample S-21/1, variation in composition between rim and core of clinopyroxene was also tested. Core of clinopyroxene is more calcic. Rim is more ferric. Enstatite content is almost same. This is true in all the cases.

Table 5.10 EPMA analysis of pyroxene grains in sample S-1/B and S-21/1. Analysis 1 and 2 represent exsolved orthopyroxene in clinopyroxene analysis 3 and 4 represent the host clinopyroxene, analysis 5 and 6 represent coexisting orthopyroxene and clinpyroxene respectively and analysis 7 represents magnetite. For the sample S-21/1, 8 and 9 represent core and rim composition for a clinopyroxene.
Analysis 8 and 9 represent core and rim of another clinopyroxene grain. Analysis 10 and 11represent core and rim of a clinopyroxene and analysis 12-14 represent ilmenite and magnetite

(wt%)	S-1/B							S-21/1						
	1	2	3	4	5	6	7	8	9	10	11	12	13	14
SiO_2	48.81	49.38	52.38	51.84	50.35	51.63	0.64	45.31	45.9	48.47	48.34	0.04	0.07	0.2
TiO_2	0.17	0.14	0.23	0.2	0.13	0.18	0.42	0.48	0.26	0.42	0.29	50.6	0.32	0.3
Al_2O_3	0.34	0.21	1.04	1.12	0.39	0.84	0.32	1	0.76	1.06	0.91		0.54	0.49
FeO	35.59	35.05	18.08	17.48	32.6	16.6	90.28	22.01	27.06	22.39	26.43	46.77	90.72	90.76
MnO	2.3	2.25	1.07	1.13	2.42	1.07		1.06	1.42	1.25	1.27	1.65		0.06
MgO	11.25	11.08	9.46	9.11	10.92	10.31		8.83	8.94	7.05	7.56	0.19		
CaO	0.76	0.65	17.25	17.13	3.01	17.33	0.03	20.86	16.43	18.44	15.96	0.05		0.01
Na_2O	0.09		0.56	0.34	0.13	0.47	0.05	0.36	0.38	0.37	0.02			
K_2O	0.03	0.03	0.03	0.04	0.03	0.02	0.13	0.1	0.09	0.06	0.14	0.08	0.12	0.11
Cr_2O_3	0.1			0.05	0.12	0.07	0.05							0.08
NiO	0.06	0.04	0.09		0.1		0.07		0.09					
Total	99.5	99.83	100.19	98.44	100.17	98.52	91.99	100.01	101.33	99.51	100.92	99.38	91.77	92.01
Fs	63	63	32	31	58	29		34	42	38	44			
En	35	35	30	29	35	32		25	25	22	22			
Wo	2	2	38	40	7	39		41	33	40	34			

Pyroxene compositions were plotted in the triangular diagram for nomenclature of clinopyroxenes in the system $CaMgSi_2O_6$ – $CaFeSi_2O_6$ – $Mg_2Si_2O_6$ – $Fe_2Si_2O_6$ (Fig. 5.13) {after Poldervaart & Hess (1951)}. Clinopyroxene without exsolution lamellae in the sample S-1/B falls in the augite field but close to the boundary of ferroaugite field. Orthopyroxene occurring as individual grain falls close to the boundary between intermediate pigeonite and ferriferrous pigeonite fields. Orthopyroxenes occurring as exsolution lamellae in clinopyroxene fall in the orthopyroxene field. The host clinopyroxene of this exsolution lamellae falls in the ferroaugite field but close to the augite field. Core and rim composition of clinopyroxene in S-21/1 falls in the frerroaugite field and that shows the absence of zoning in pyroxenes. Thus there is an iron enrichment for these pyroxenes. This is an important characteristic of anorthositic pyroxene. This has often been cited as evidence for crystallization of the anorthosites from fractionated magma or melts (Emslie, 1985).

5.7.4 Fe-Ti oxides.

The EPMA data of these are also given in table 5.10. Magnetite and ilmenite are almost pure with extremely low impurities. Magnetite in S-1/B has the impurities Si (0.03 mol%), Al (0.02 mol%), Na (0.01 mol%), Ti (0.02 mol%). Si is very less or absent in magnetites of S-21/1. Other impurities include Ti (0.01 mol%), K (0.01 to 0.03 mol%) and Al (0.03 mol%).

Ilmenite is more pure compared to magnetite. The impurities present in the ilmenite of S-21/1 are Mn (0.04 mol%) and Mg (0.01 mol%).

5.8 Geothermobarometry of anorthosites

5.8.1 Barometry

The barometer used in the present work is a reaction between clinopyroxene and plagioclase, viz.,
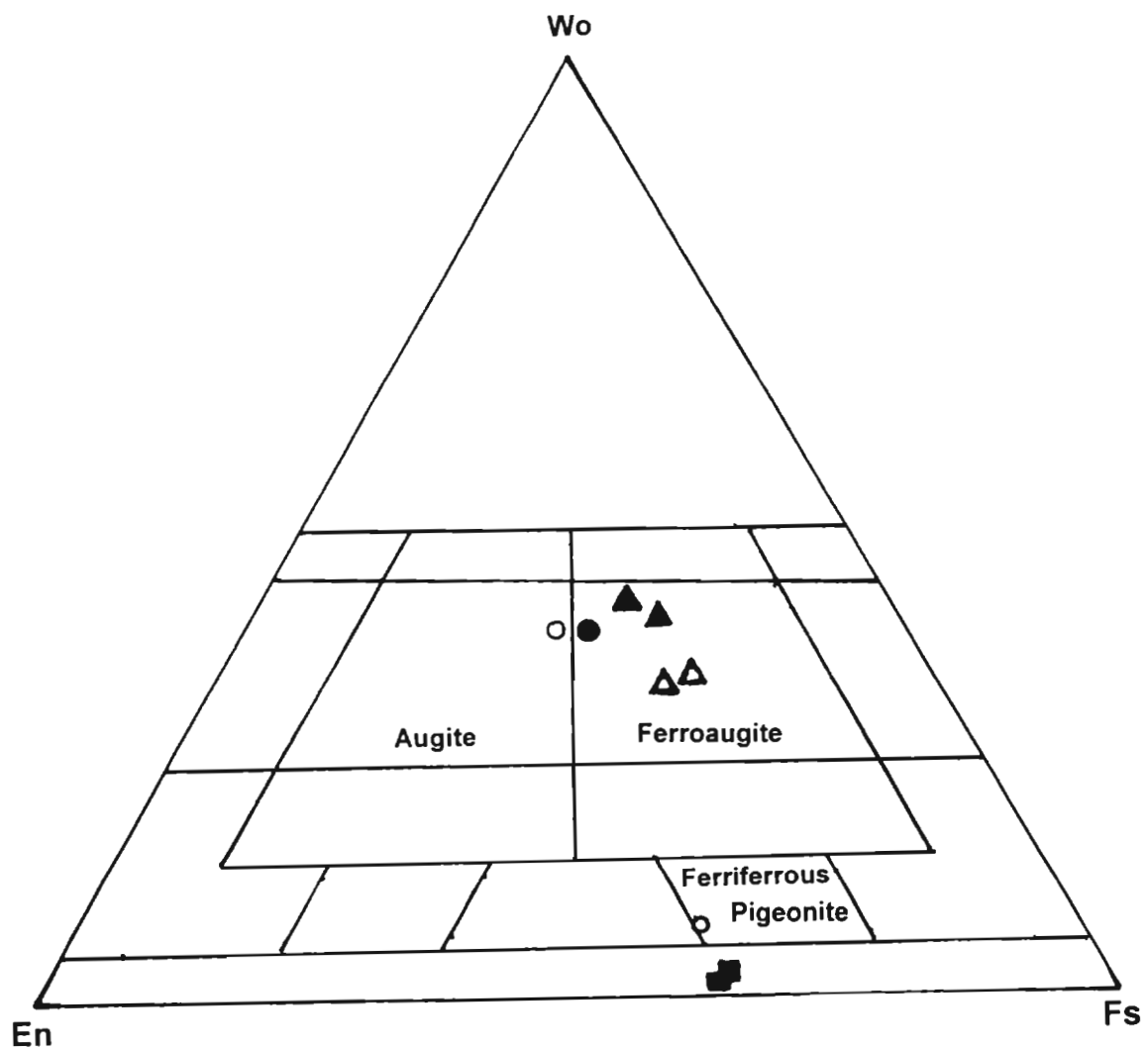
Fig. 5.13 Plot of clinopyroxenes and orthopyroxenes of the Perinthatta anorthositic rocks in pyroxene triangle (after Poldervaart and Hess, 1951). Symbols: open circle- individual grains of clinopyroxene and orthopyroxene in the sample S-1/B, solid square- exsolved orthopyroxene lamellae in clinopyroxene, solid circle- host clinopyroxene of exsolved orthopyroxene , open triangle- rim composition of clinopyroxene in sample S-21/1 and solid triangle-core composition of clinopyroxene in S-21/1.

$$Ca\ Al_2\ Si_2\ O_8\ ==\ Ca\ Al_2\ SiO_6\ +\ SiO_2$$

plg   cpx   qz
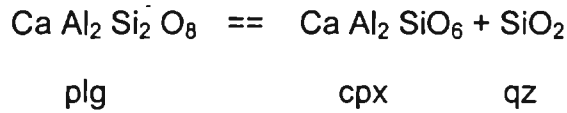
This reaction controls the concentration of Ca-Tschermak component in the clinopyroxene in the assemblage with plagioclase and quartz provides a potential geobarometer (Wood, 1974). The calculation was done based on the expression given by Raith et al. (1983), which is a modified form of the calibration by Ellis (1980). The expression is given below:

$$P(b) = (5360 + 2.9876T + 1.9872T\ lnK) / 0.349$$

$$= \{12864X_{CaTs}(1 - X_{CaTs}) - 26885\ [\ X_{CaTs}(1 - X_{CaTs})]^2\} / 0.349$$

$$= (1 - X_{An}^{Plg})^2\ (2075 + 9318X_{An}^{Plg}) / 0.349 \quad \pm 1kb$$

where X_{CaTs} = Al-Na-K-2Ti / 2 as per the calculation scheme of Cawthorn and Collerson (1974).

The pressure obtained from this calculation is 7±1kb. This is slightly less than the pressure estimate for granulites and charnockites of the northern charnockite province (~ 10 kb) into which the anorthosite has intruded.

5.8.2 Thermometry

Two thermometric calculations were done for anorthosite. One of them is a two pyroxene thermometry in which co-existing clinopyroxene and orthopyroxene are used. This method is adopted from Wells(1977). The equation used for the thermometric calculation is given below:

$$T\ in\ K = 7341/(3.355 + 2.44X_{Fe/opx} - ln\ K)$$

where $X_{Fe/opx}$ = $Fe^{2+}/(\ Fe^{2+} + Mg^{2+})$.

Three such co-existing pairs of pyroxenes were used in the calculation. In one of them coexisting clinopyroxene and orthopyroxene grains were used. This can give the magmatic crystallizatioin temperature because they were not

metamorphosed. In the other two exsolved orthopyrxene lamellae and their host clinopyroxene were used. The temperature obtained for the first calculation gave a temperature of 1213°C. Temperatures obtained for the exsolution are 1169°C and 1163°C.

Two feldspar thermometry was also applied for Perinthatta anorthosite. In two feldspar thermometry co-existing plagioclase and orthoclase grains are used (Stormer,1975, Haselton et al., 1983). In Perinthatta anorthosite orthoclase is very rare and so here exsolved orthoclase phases and their host plagioclase phases were used. So the temperature thus obtained will be representing the temperature at which the exsolution ocurred. The equation used for the calculation is taken from Haselton et al.(1983) which is given below:

$$T \text{ in} K = \frac{(X_{Or/AF})^2 (18810 + 17030 \, X_{Ab/AF} + 0.364 P) - (X_{An/Pl})^2 (28230 - 39520 \, X_{Ab/Pl})}{10.3(X_{Or/AF})^2 + 8.3143 \, \ln \left\{ (X_{Ab/Pl})^2 (2 - X_{Ab/Pl}) / X_{Or/AF} \right\}}$$

where the mole fractions refer to the ternary system and P is in bars. The value of P used in the calculation is the value obtained in the above pressure estimate (i.e., 7 kb). For this pressure the temperature of exsolution obtained for anorthosite is as follows:

sample S-1B: 525°C and 518°C

sample S-21/1: 835°C

5.9 Isotope analysis

Two samples from Perinthatta anorthositic pluton were subjected to a preliminary dating by Sm-Nd system. The samples S-3/3 and S-12/C were used for the dating in which S-3/3 is anorthosite while S-12/C is dioritic anorthosite. From the coarsely powdered samples (S-3/3 and S-12/C), pyroxene and plagioclase feldspar were separated by handpicking. These separated minerals were then fine powdered using an agate mortar. Thus a for a

single sample, a whole rock sample was also analyzed for dating in addition to mineral separates.

From the analysis, two different ages are obtained. The sample S-3/3 sample gave an age of 559±64 Ma with Nd_I = 0.51174±6. The sample S-12/C gave an age of 705±77 Ma with Nd_I = 0.51144±6. This difference can be seen from the difference in the slope of the isochrons for these two samples (Fig. 5.14). In the figure, the ratio Sm^{147}/Nd^{143} is taken along X-axis and the ratio Nd^{143}/Nd^{144} is taken along Y-axis.

The Pb isotopic studies were done on the several subsamples of the anorthosite sample S-3/3 and the data are given in table 5.11. The data has been corrected for mass fractionation and the procedural blank during the analysis were less than 300 pg. The Pb isotopic composition of the subsamples are somewhat primitive, implying low U abundances in the subsamples. They have low calculated μ_1 values of close to 7. This indicates that the Pb incorporated into the anorthosite at the time of its formation was derived from sources that were slightly depleted in U compared to bulk earth. The Pb in this anorthosite is unlikely to be of older continental crustal origin.

5.10 Discussion

The salient aspects of the petrogenesis of the anorthositic rocks of Perinthatta has already been discussed in section 5.6. Further constraints on the evolution of these rocks based on mineral chemistry, thermobarometry and isotope analysis are given in the following paragraphs.

Certain significant information from the chemistry of minerals (like iron enrichment of pyroxenes, unzoned nature of plagioclase as well as pyroxenes and exsolution in pyroxenes) indicate high temperature magmatic crystallization and support the deductions on petrogenesis inferred from major, trace and REE geochemistry.
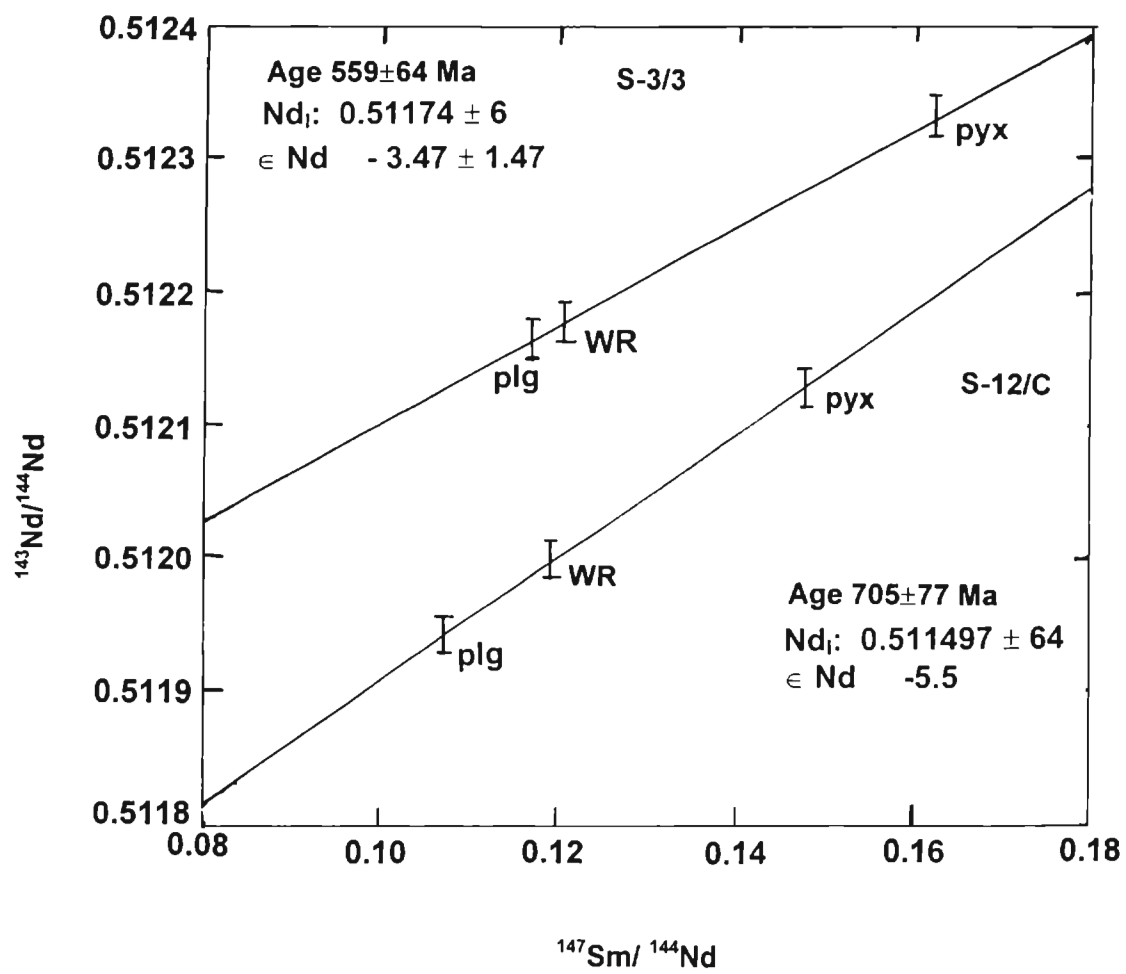
Fig. 5.14   Graph showing the Sm-Nd isochrons of the Perinthatta anorthosite samples.

Table 5.11   Results of the Pb analyses on several sub samples from the Perinthatta anorthosite.

Sample ID	$^{206}Pb/^{204}Pb$	2 sigma	$^{207}Pb/^{204}Pb$	2 sigma	$^{208}Pb/^{204}Pb$	2 sigma
S 3/3-6	16.090	0.001	14.895	0.003	36.437	0.004
S 3/3-5	15.728	0.001	14.967	0.002	36.166	0.005
S 3/3-4	15.882	0.003	14.986	0.006	36.280	0.011
S 3/3-1	15.185	0.010	14.330	0.023	34.476	0.030

Geothermobarometric studies indicate that Perinthatta anorthositic pluton was emplaced at deeper crustal levels following the granulite facies metamorphism in the region. The different temperatures obtained for crystallization of pyroxenes (1213°C), exsolution in pyroxene (1163°C) and exsolution in plagioclase (518-835°C) indicate a high initial temperature of magma and prolonged cooling history. As there is a difference of 2kb in the estimated pressures for the peak metamorphism of the granulitic country rocks and for the crystallization of anorthosite, it can be deduced that anorthosite was emplaced after the exhumation of the granulite crust for about 7km.

The geochronologic data suggest two different ages for anorthositic samples and that may indicate two different pulses of magma and the composite nature of the pluton. Pb isotope studies indicate a mantle source for Perinthatta anorthosite and high Sr content also points to a mantle source.

• • •

Chapter VI
ASSOCIATED PLUTONS

6.1 Introduction

The Perinthatta anorthosite is spatially associated with a series of mafic and felsic plutons. Ezhimala gabbro-granophyre complex, Peralimala syenite, Adakkathod and Karikkottakkari diorites are the important among them (Fig. 6.1). These plutons are studied in terms of their field relations, petrography, geochemistry and petrogenesis to understand their genetic relationship, if any, with Perinthatta anorthosite.

6.2 Ezhimala gabbro-granophyre complex

The coastal hillocks situated 15km towards southwest of Payyannur known as 'Ezhimala' is lithologically composed of a variety of plutonic rocks. They are located towards the western end of the Bavali lineament and approximate area of exposure is ~18km^2 The country rock is granitic gneisses within which enclaves of sillimanite-kyanite bearing schists and quartzites as well as meta-ultramafites belonging to the Wynad schist complex are observed (Nair et al., 1976). Major part of the pluton is a granophyre which was reported earlier by Varadan and Venkataramana (1976) and the associated rocks include gabbro and granitic rocks. Towards the SE portion of the Ezhimala pluton, rapakivi granite is seen. An intrusive relationship is regarded between this granite and the gabbro which fringes the southern and eastern portions (Nair and Vidyadharan, 1982). The plutons of the area together are sometimes referred to as the Ezhimala Igneous Complex (EIC) (Santosh and Nair, 1983). Later it was grouped to be a gabbro-tonalite-trondhjemite granite suite (Sinha-Roy and Ravindra Kumar, 1986). Towards the northern end of the complex there exists a narrow zone with rafts and xenoliths of mylonite, well banded quartzite, quartz-mica schist and amphibolite. Geological map of the Ezhimala Igneous Complex is given in figure 6.2.
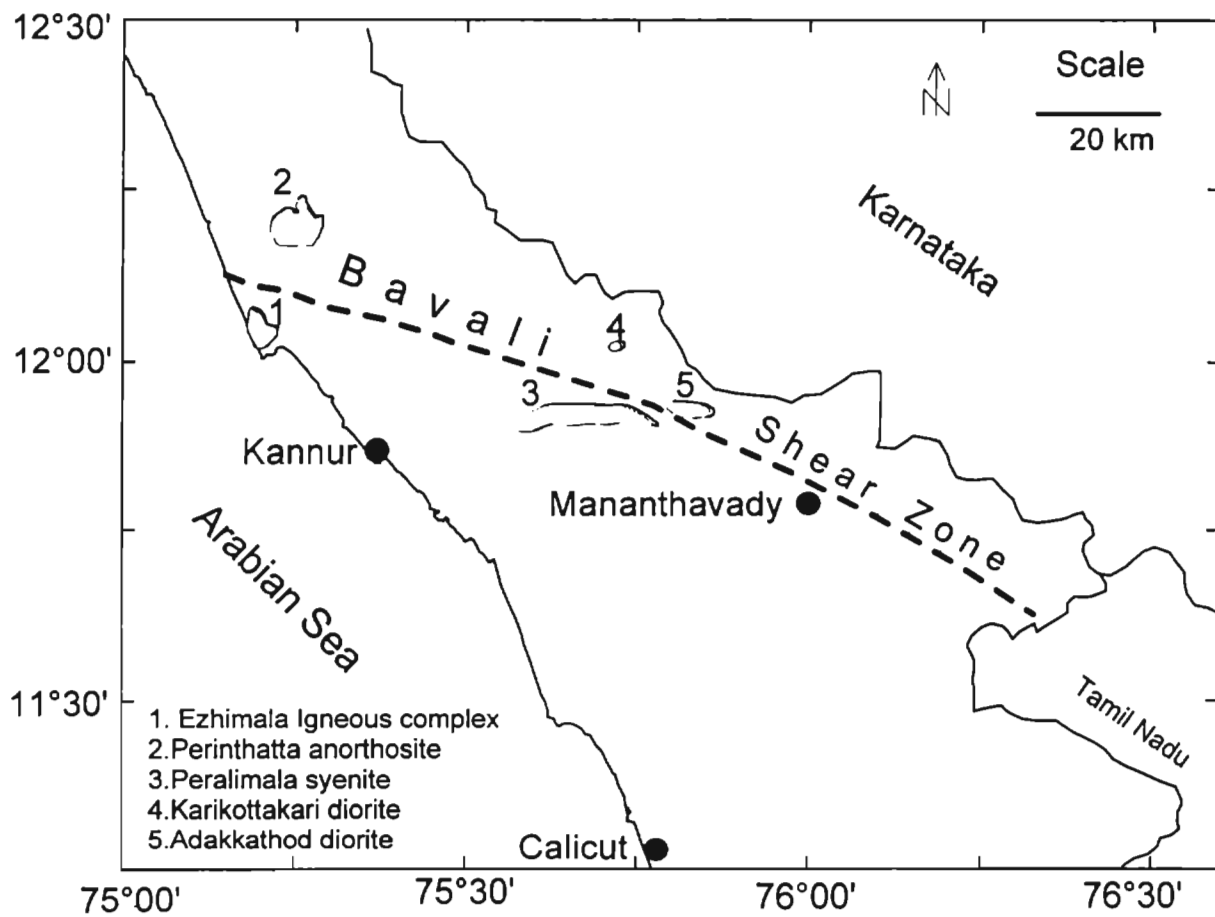
Fig.6.1: Schematic map of northern Kerala showing Perinthatta anorthosite and associated plutons and Bavali shear zone.
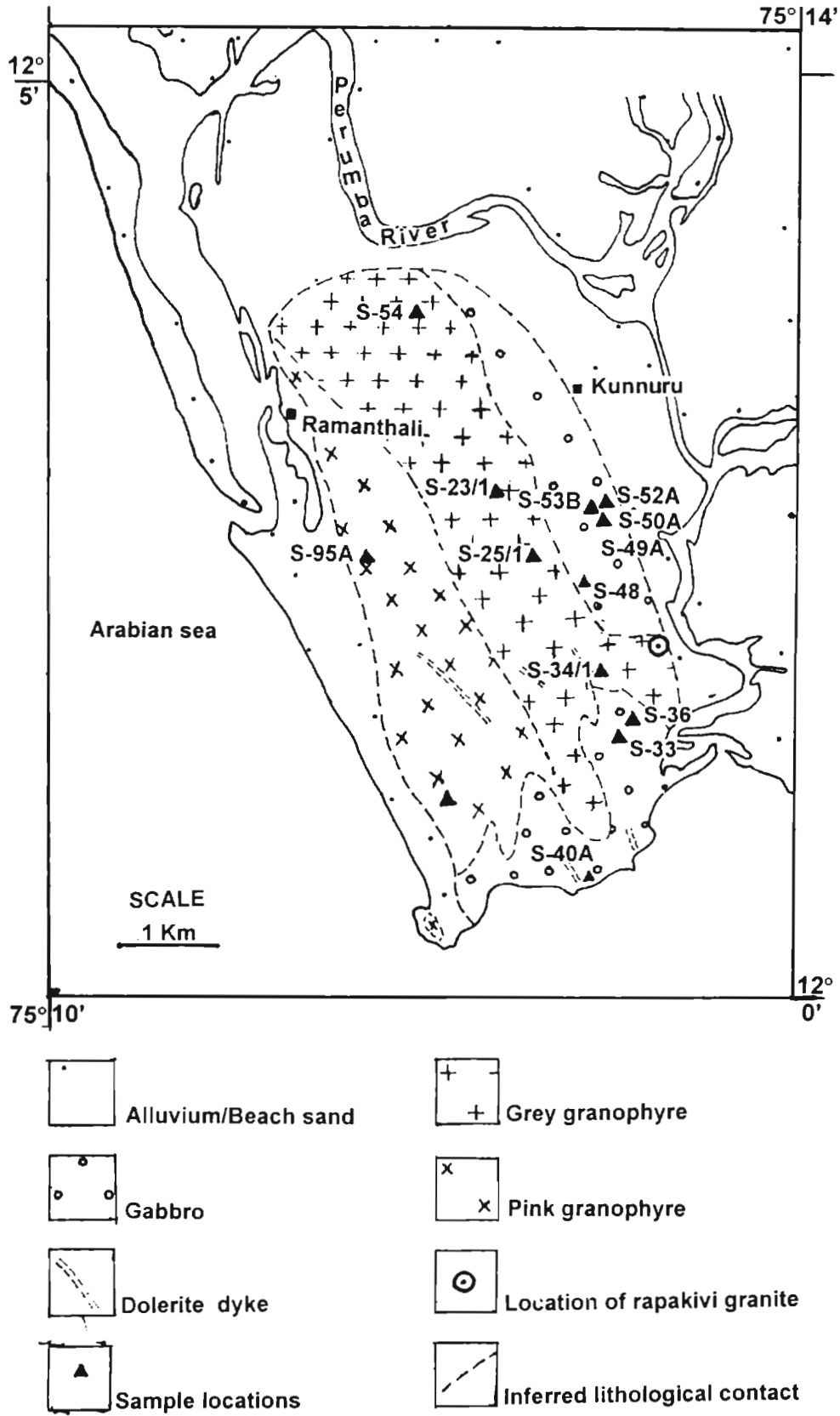
Fig. 6.2 Geological map of Ezhimala igneous complex with the location of the samples analyzed.

6.2.1 Ezhimala gabbro

The Ezhimala gabbro is seen fringing the Ezhimala granitoids along the eastern and southern margins (Fig. 6.2).

6.2.1.1 Field relationships

The rock is massive in all the locations and in some locations grain size becomes very large. The gabbro is dark coloured except the very coarse grained one. The very coarse grained gabbro is having white patches and these patches are feldspar. Pyroxenes appear as dark spots in the coarse grained type. Some big crystals of molybdenite are also noted in this rock. These very coarse grained variety are observed along the southern end of the gabbro body only. At location S36, this coarse grained rock is seen in a well section. At location S33, this rock occurs as viens of ½ m width. At location S38, the gabbro is seen fragmented into angular patches of different sizes and shapes by an intruding felsic magma. At locations (S49 and S51) the gabbro shows a spotted appearance due to the presence of pyroxene clots (6-7mm in diameter). At a location, gradational contact between gabbro and granophyre can be seen.

6.2.1.2 Megascopic petrography

Generally the Ezhimala gabbro is a coarse grained and dark coloured rock. Rarely a very coarse grained and lighter coloured (e.g., sample S-36) is seen. In this, the plagioclase feldspar crystals attain a maximum length of 2cm. Pyroxene crystals attain a size of about 1.5cm. Striations or partings revealing polysynthetic twinning in plagioclase feldspar can be seen in the hand specimens. The most finer grained sample is S-48/B. Mafic content of the rock varies to a small extent. The most mafic sample is S-48/B and the least mafic sample is S-33. As the rock becomes coarser, the mafic content decreases. In almost all the samples feldspar patches can be observed. Good amount of molybdenite crystals are observed in the sample S-36.

94

6.2.1.3 Microscopic petrography

Except for the sample S-36, which is the very coarse grained sample, all other samples show subophitic texture. Plagioclase is the most abundant mineral and they are euhedral which show Albite, Carlsbad and Pericline twinning. The albite twin lamellae are uniformly thick. Some plagioclase feldspar crystals show Carlsbad and Pericline twinning also. Some plagioclase crystals show zoning and plagioclase inclusions can be seen in plagioclase itself. Composition of plagioclase estimated by Michael Levy method is found to be labrodorite. Clinopyroxenes are the major mafic mineral and they occur as subhedral to anhedral crystals. In this, a remote cumulus texture is seen. Small amount of biotite is noted. In sample S-33, the pyroxene crystals show alteration to hornblende along the grain boundaries and alteration is not seen in any other samples. Pyroxene inclusions can be seen in some plagioclase crystals. Opaque minerals are observed in association with pyroxenes. Apatite which is seen as minute crystals is the most common accessory mineral and they are associated with pyroxenes and opaques. Some samples show very minute graphic intergrowth of quartz and feldspar (Fig. 6.3).

6.2.1.4 Major element geochemistry

Results of major element analysis and corresponding C.I.P.W norms of 11 samples are presented in table 6.1. When plotted in the diagram for nomenclature of normal igneous rocks (after Cox et al., 1979), they fall in the field of gabbro, diorite, quartz diorite and granodiorite (Fig. 6.4). SiO_2 content of the gabbro ranges from 41.25 to 52.38%. For the sample which falls in the diorite field, the SiO_2 content is 56.25%. In the granodiorite sample, average SiO_2 content is 64.25%. Al_2O_3 content of gabbro samples ranges from 15.36 to 20.2%. For diorite sample Al_2O_3 content is 15.65%. Average Al_2O_3 content of granodiorite sample is 12.39%. MgO content of gabbro samples is fairly high and it ranges from 5.3 to 9.18%. MgO content of diorite sample is 2.44%. Average MgO content of granodiorite samples is 1.27%. MnO is very less in all the samples (<1%). FeO is high and it ranges from 7.29 to 12%. For the diorite sample it is 9.12%. Average FeO content of granodiorite samples is 6.75%.

Table 6.1   Major element analysis (wt%) of Ezhimala gabbroic samples with calculated C.I.P.W norms

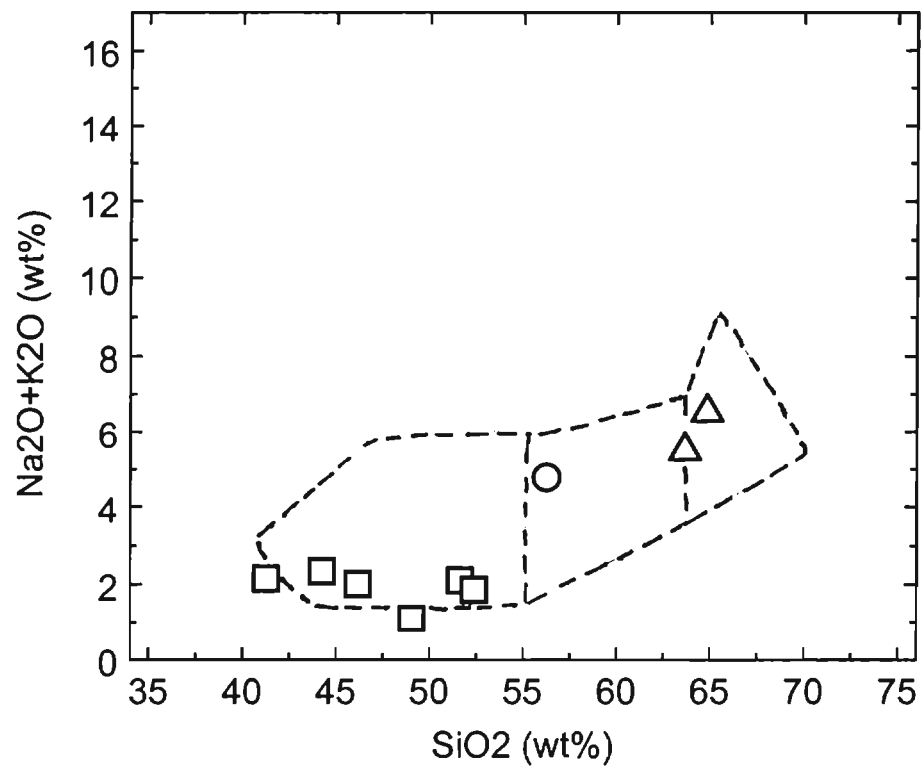| Sample No.	S-33	S-36	S-40/A	S-48/A	S-49/A	S-48/B	S-50/A	S-52/A	S-53/B
SiO2	52.38	51.63	64.85	63.65	49.03	56.25	46.15	41.25	44.24
Al2O3	16.82	15.36	13.97	10.81	17.55	15.65	18.81	20.20	19.17
FeO	8.60	8.57	4.43	6.34	7.21	7.26	5.81	7.24	7.56
Fe2O3	3.39	3.38	1.75	2.51	2.85	2.87	2.29	2.86	2.98
MnO	0.16	0.18	0.15	0.18	0.16	0.18	0.11	0.14	0.15
MgO	5.30	6.55	1.10	1.43	7.73	2.44	7.09	9.18	8.01
CaO	8.63	8.46	4.13	6.13	11.76	6.50	13.72	14.94	13.00
Na2O	1.51	1.35	4.09	3.95	0.92	3.06	1.81	2.02	2.15
K2O	0.36	0.76	2.43	1.54	0.18	1.72	0.20	0.13	0.19
TiO2	2.06	2.66	1.02	1.51	1.61	2.19	1.27	0.98	1.00
P2O5	0.36	0.64	0.41	0.63	0.34	0.62	0.04	0.03	0.17
Norm									
	S-33	S-36	S-40/A	S-48/A	S-49/A	S-48/B	S-50/A	S-52/A	S-53/B
Q	13	11.6	21.1	22	6	13.6	0	0	0
Ap	0.9	1.6	0.9	1.2	0.6	1.2	0	0	0.3
Ilm	4	5	2	2.9	3	4.1	2.4	1.8	2
Or	2.2	4.5	14.5	8.9	1.1	10	1.1	0	1.1
Al	12.6	11.5	34.6	33.5	7.9	25.7	0	0	12.7
An	38.1	33.6	12.5	7.2	43.1	23.9	42.5	45.6	42.8
Hy	22.3	24	5.8	2.6	22.6	11.9	10	0	0
Di	1.6	3	4.5	16.5	10.8	3.9	20.6	19.5	16.9
Wo	0	0	0	0	0	0	0	0	0
Mt	4.9	4.9	2.6	3.7	4.2	4.2	3.2	4.2	4.4
Ol	0	0	0	0	0	0	3.5	28.3	15.7
Le	0	0	0	0	0	0	0	0.4	0
Ne	0	0	0	0	0	0	0	9.4	3.1
Cal	0	0	0	0	0	0	0	2.8	0

Fig. 6.4   SiO2 vs Total alkali diagram for the Ezhimala gabbroic samples. (Symbols: square- gabbro; circle- diorite; triangle- quartz diorite)
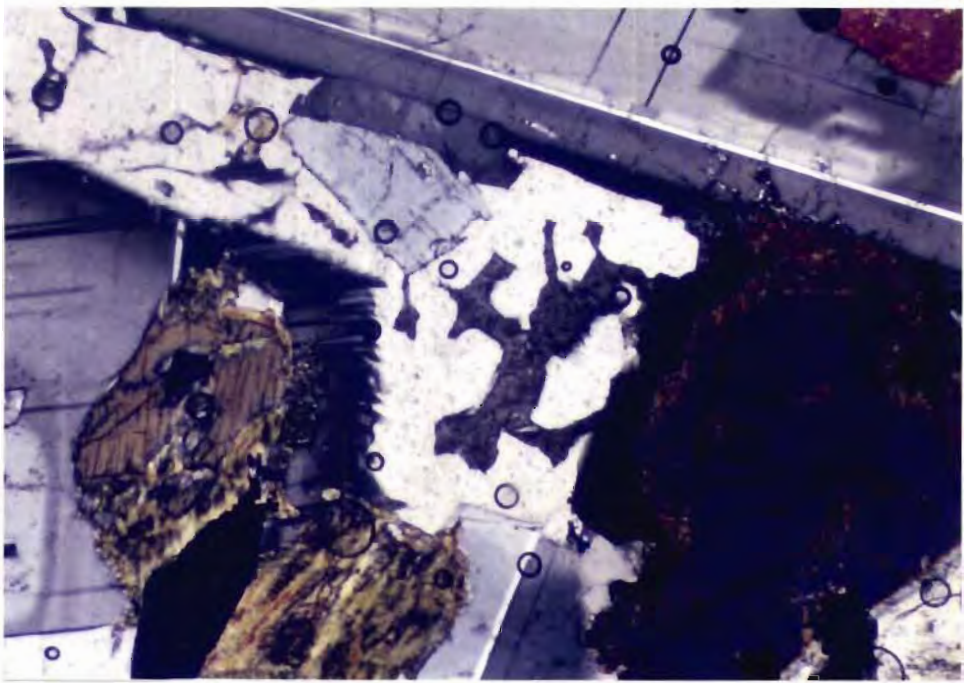
CaO content is high for gabbro samples and it ranges from 8.46 to 14.94%. CaO content of diorite sample is 6.5%. For granodiorite samples the average CaO content is 5.13%. Na_2O and K_2O content is less than CaO. Na_2O is more than K_2O. Na_2O content of gabbro samples ranges from 0.92 to 2.15%. Na_2O content of diorite sample is 3.06%. Average Na_2O of granodiorite is 4.02%. K_2O is very less compared to Na_2O. K_2O is less than 1% for gabbro samples (average=0.3%). For diorite and granodiorite samples it is slightly higher than that of gabbro. Average K_2O content of these two groups of rocks is 1.89%. P_2O_5 is very less and its content is less than 1% in all the samples. TiO_2 is slightly greater than P_2O_5. For gabbro samples it ranges from 0.98 to 2.06%. The diorite sample has a TiO_2 content of 2.19% and average TiO_2 content of ganodiorite sample is 1.2%.

The SiO_2 and total alkali (Na_2O+K_2O) contents of the gabbro samples are very close to the range of 45-52% and <5% respectively, suggesting their basaltic affinity according to the TAS scheme recommended by IUGS (Le Bas and Streckeisen, 1991). In the diagram of SiO_2 vs Na_2O, Ezhimala gabbro samples fall in the field of sub-alkali basalts (Fig.6.5). The other two groups fall in the alkalic basalts. Thus the Ezhimala gabbro samples show a subalkaline nature. Majority of the samples fall in the tholeiite field in Al_2O_3 vs Alkaline Index diagram (Fig. 6.6) and in the AFM diagram (Fig. 6.7). Ezhimala gabbro samples show a tholeiitic trend. In the $K_2O - TiO_2 - P_2O_5$ diagram (Fig. 6.8), the samples S-33, S-52, S-50/A, S-53/B and S-49/A fall in the oceanic tholeiitic field and the samples S-36, S-48/B, S-48/A and S-40 in the continental tholeiitic field.

6.2.1.5 Trace element geochemistry

Two samples viz., S-36 and S-49/A (gabbro samples) are analyzed for trace elements and the results are given in table 6.2. Petrographically these samples are different in their grain size. S-36 is very coarse grained and less mafic also.

Table 6.2 Trace element concentrations
(ppm) of Ezhimala gabbro samples

Sample No.	S-36	S-49/A
V	430.02	265.19
Cr	53.02	157.14
Co	52.79	40.92
Ni	40.11	78.10
Cu	77.70	76.54
Zn	160.78	67.66
Ga	26.90	21.51
Rb	9.62	2.68
Sr	249.90	269.38
Y	38.89	24.93
Zr	45.60	42.38
Nb	20.12	8.32
Cs	0.20	0.27
Ba	96.05	54.96
Hf	1.57	1.48
Ta	1.13	0.56
Pb	6.54	6.75
Th	1.59	0.46
U	0.24	0.16

Table 6.3 Rare earth element concentrations
(ppm) of Ezhimala gabbro samples

Sample No.	S-36	S-49/A
La	9.19	3.30
Ce	29.15	17.80
Pr	2.85	1.81
Nd	24.83	16.68
Sm	7.42	5.03
Eu	2.28	1.73
Gd	5.67	3.93
Tb	1.14	0.74
Dy	7.43	4.96
Ho	1.37	0.85
Er	3.36	2.08
Tm	0.40	0.25
Yb	3.03	1.89
Lu	0.41	0.26
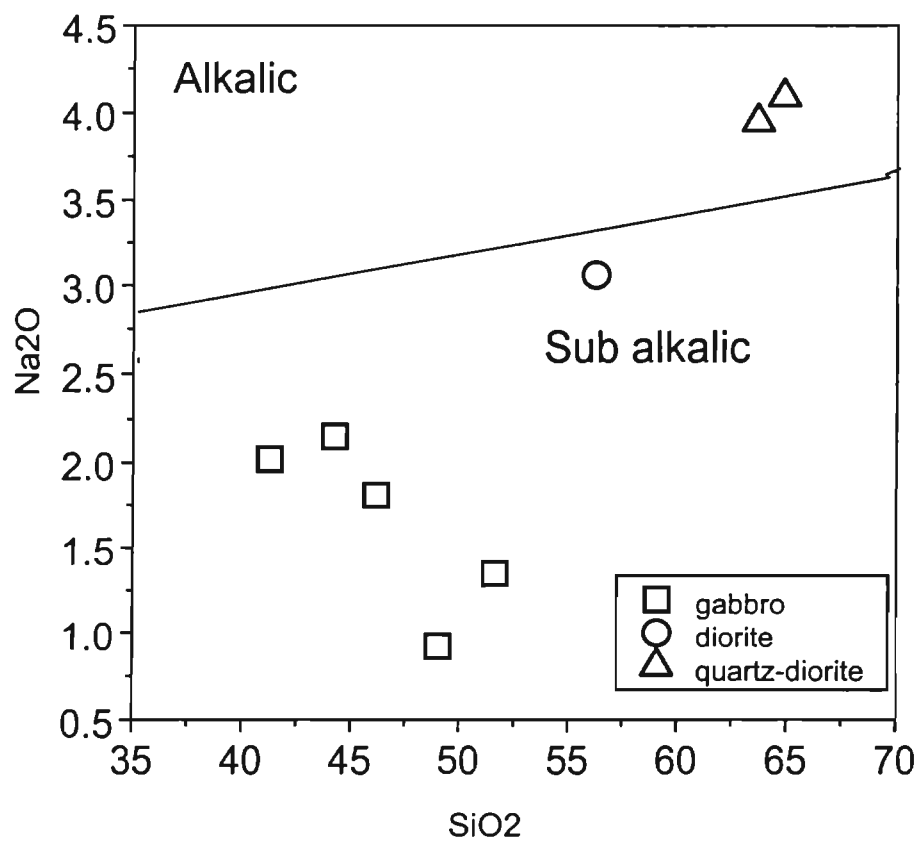
Fig. 6.5 SiO2(wt%) vs Na2O(wt%) diagram for the Ezhimala gabbòr samples. Field boundaries are after Middlemost (1975).
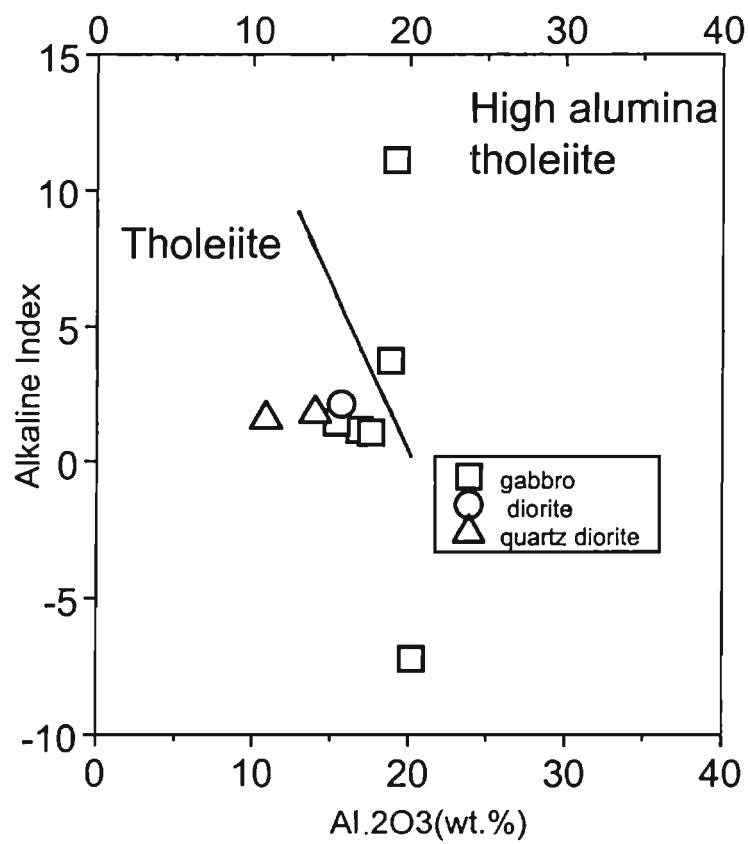
Fig. 6.6   Al2O3 vs Alkaline Index(A.I) plots for Ezhimala gabbroic samples.
Fields after Middlemost (1975). Alkaline Index= Na2O+K2O/(SiO2-43)*0.17
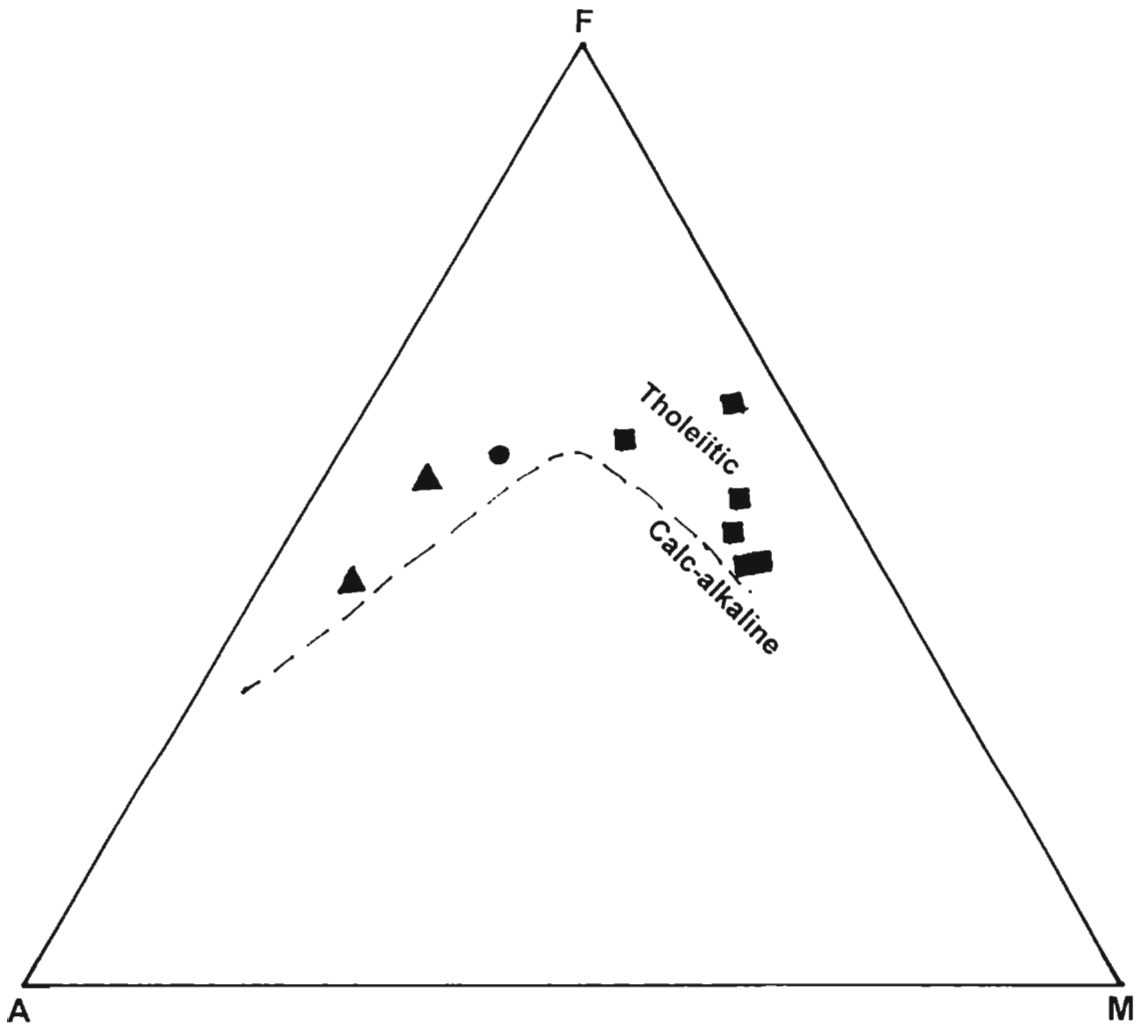
Fig. 6.7 AFM diagram showing tholeiitic trend of the Ezhimala gabbroic samples (symbols as in figure 6.4).
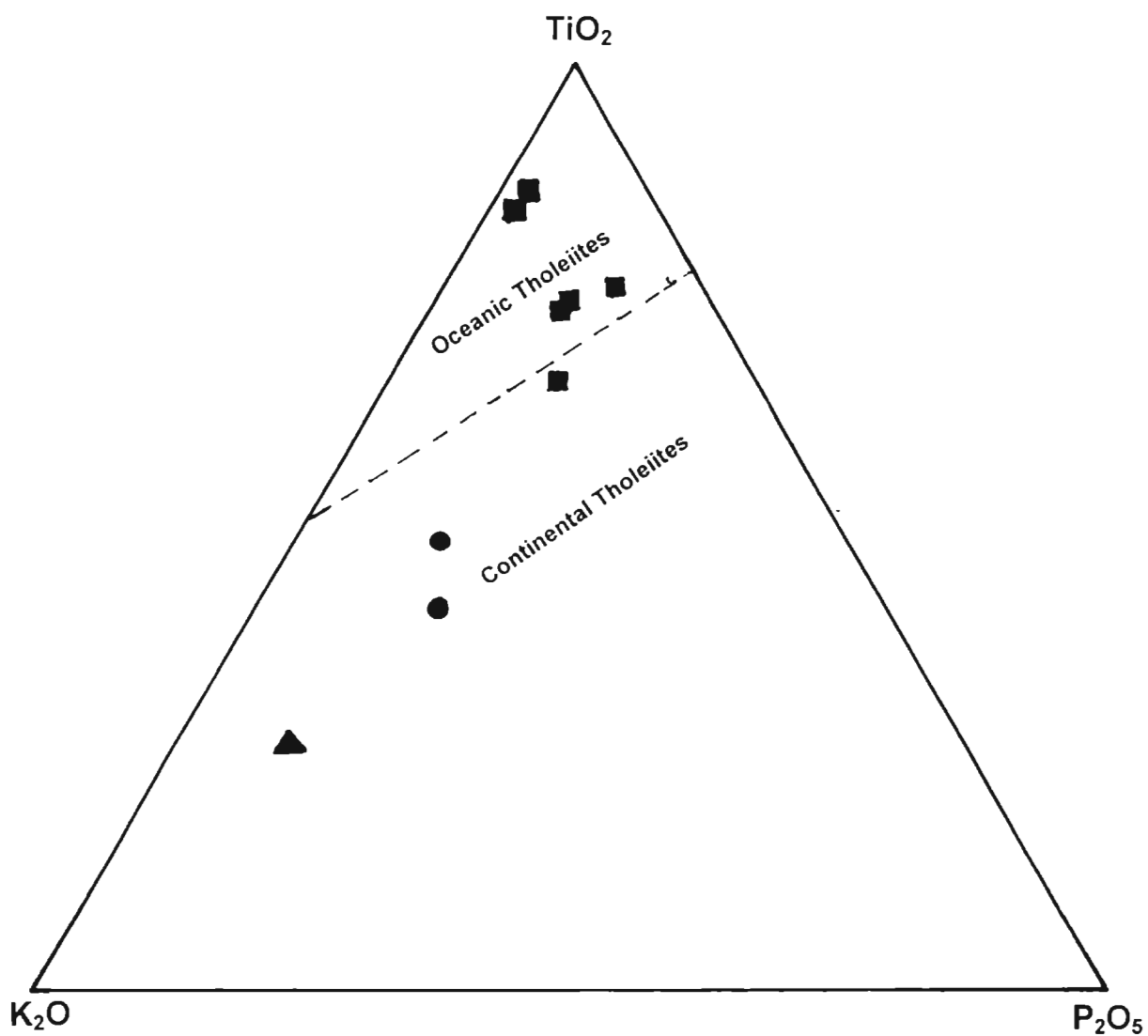
Fig. 6.8 TiO_2-K_2O-P_2O_5 diagram (after Pearce et al. 1975) showing plots for Ezhimala gabbroic rocks (symbols as in figure 6.4).

Ba content of the coarse grained sample is 96ppm and that of S-49/A it is 54ppm. This can be attributed to higher content of K_2O in the sample S-36. Ba decreases with decrease in SiO_2. Rb content is also more in the sample S-36 (Rb=9ppm) and this also can be attributed to the higher content of K_2O in this sample. Sr content in S-36 is 250ppm while the Sr content in S-49/A is 270ppm. Higher content of Sr can be attributed to the higher content of CaO in the sample S-49/A. Ba/Sr ratios of the these two samples are 0.384 (S-36) and 0.2 (S-49/A). K/Rb ratios are 559 (S-49/A) and 655 (S-36). Rb also shows a decrease with decrease in SiO_2. Among HFSE, Ta and Lu (HREE) are the less abundant ones. Ta is higher in the sample S-36. The rock is more enriched in LILE than HFSE. Zr/Hf ratio ranges from 28 to 49.

Ni content varies from 40 to 78ppm. Cr has a content of 53ppm in the sample S-36. Cr is very high in the sample S-49/A (157ppm). Cr increases with increase in MgO and decrease in $SiO_2$. Sc does not show much variation in the samples and it has an average value of 45ppm. U content is very less in both the samples (average value is 0.2ppm). Th content is also very less (average value is 1ppm). Th/U ratios are 1.62 and 4.97ppm. In both the samples Th content is higher than that of U. Ga concentrations in sample S-36 is 27ppm and that in S-49/A is 21ppm.

Sample S-36 is showing slightly higher content of REE (table 6.3). This difference may be attributed to: (1) the more differentiated nature of sample S-36 (as evidenced by the higher SiO_2 content and lower MgO content) and (2) the higher content of apatite in S-36 and this is supported by the higher content of P_2O_5 in that sample. The chondrite normalized REE patterns (Fig. 6.9) is not showing any Eu anomaly. Degree of fractionation is slightly more in sample S-36. This is indicated by the $(La/Yb)_N$ ratio. This ratio for S-36 is 2.04 and for S-49/A, 1.18. Average $(Ce/Yb)_N$ ratio is 2.4. Fractionation among LREE is almost same in both the samples and the ratio $(La/Sm)_N$ for these samples are 0.41 (S-
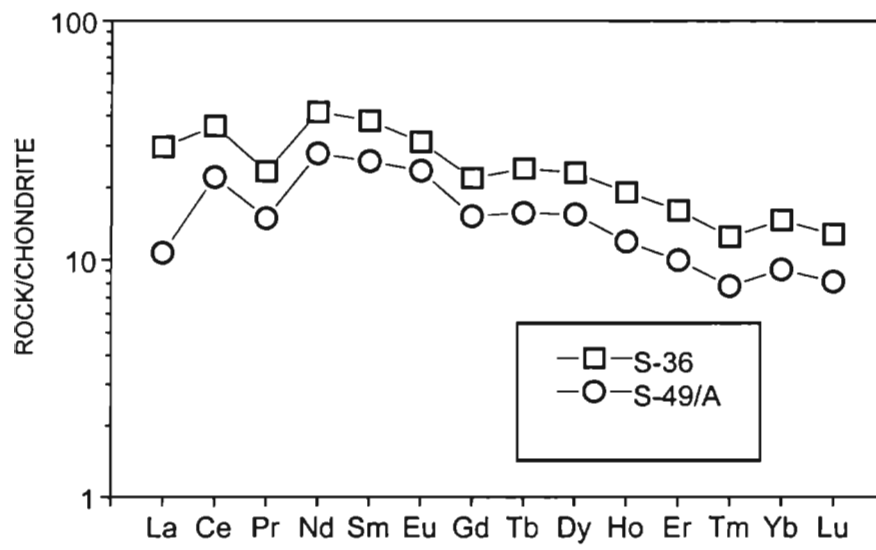
Fig. 6.9 Chondrite-normalized REE patterns of Ezhimala gabbro. Normalizing values are from Brynton (1984).

49/A) and 0.78 (S-36). Degree of fractionation among HREE is also not much different. The ratio $(Gd/Yb)_N$ for these samples are 1.2 (S-49/A) and 2 (S-36).

6.2.1.6 Tectonic discrimination

From the tectonic discrimination triangular diagram (Fig. 6.10) of Al_2O_3-MgO-FeO, it is found that the gabbro samples (S-49/A, S-50/A, S-52/A and S-53/B) fall in the orogenic basalt field. Another two gabbro samples (S-36 and S-33) fall in the continental basalt field but close to the orogenic basalt field. The diorite and granodiorite samples (S-40/A, S-48/A and S-48/B) fall in the intraplate spreading centre island basalts.

6.2.1.7 Petrogenesis

Major elements like TiO_2, K_2O, Na_2O, MgO, Al_2O_3 and CaO are plotted against SiO_2 to assess the differentiation trends (Fig. 6.11). Al_2O_3 , MgO, and CaO   show a decreasing trend with SiO_2 These decreasing trends are in favour of fractional crystallization.   Decreasing trend of MgO indicates that orthopyroxene does not form a major fractionation phase throughout the evolution. In the case of TiO_2 two separate trends are seen in which gabbro samples show an increasing trend and the diorite and granodiorite samples show a decreasing trend. The samples which show the decreasing trend are from the quarry where the gradational contact between Ezhimala gabbro and Ezhimala granophyre is seen.   In the gabbro samples showing an increasing trend is due to the crystallization of accessories bearing TiO_2 The decreasing trend in the other group can be due to the mixing with a felsic magma. In the gabbro samples Na_2O shows a decreasing trend while the diorite and granodiorite samples show an increasing trend. The decreasing trend in the first case is due to fractionation of early phases like plagioclase. Increasing trend shown by the other group may be due to the addition of Na_2O due to the crustal contamination or due to mixing with a felsic magma. In the case of K_2O also two groups can be noticed. The group of gabbro samples do not show any trend with SiO_2. K_2O remains a constant with increasing SiO_2. A slight increasing trend is noticed in
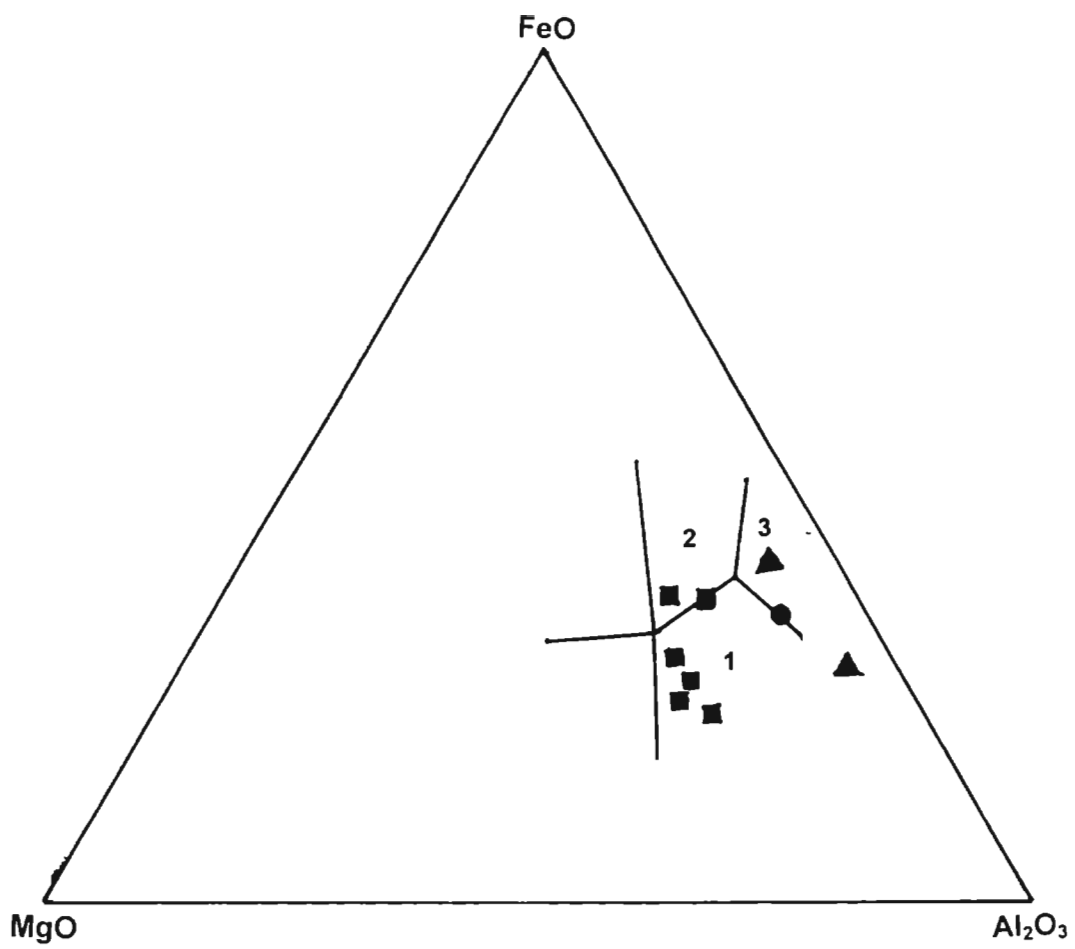
Fig. 6.10 Plot of Ezhimala gabbroic samples in the Al₂O₃-MgO-FeO diagram for the tectonic discrimination of basaltic rocks (symbols as in figure 6.4). The different fields are 1. Orogenic basalt field, 2. Continental basalt field and 3. Intraplate spreading center island basalt field.
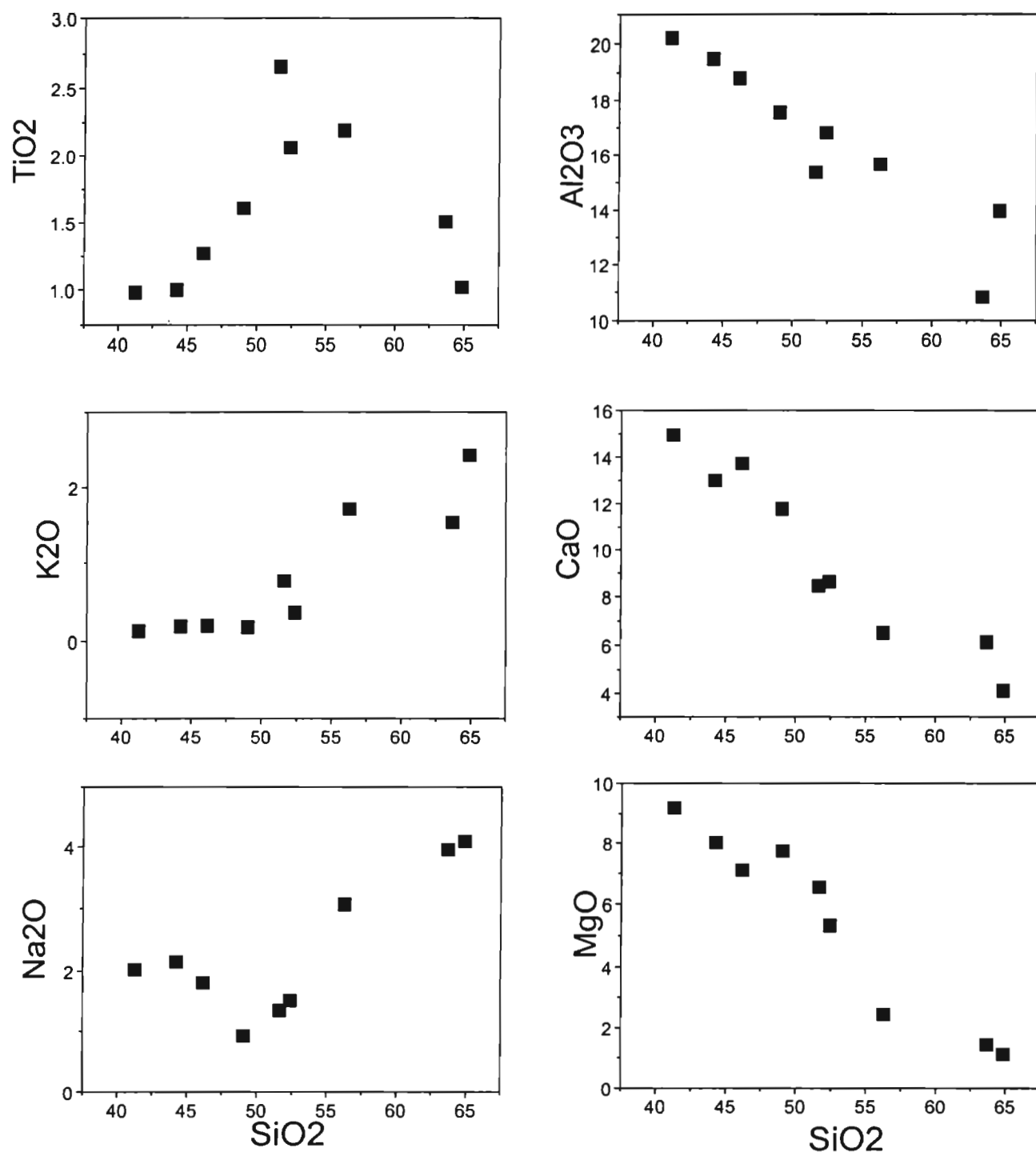
Fig. 6.11   Plots showing the variation of major element oxides with SiO2 in Ezhimala gabbroic samples.

the other group. This sudden increase may be due to the addition of K$_2$O through contamination or mixing with a felsic magma.

The major oxides were plotted against MgO also (Fig. 6.12) to identify the possible role of crystal fractionation. CaO shows an increasing trend with MgO indicating clinopyroxene-plagioclase fractionation. Trace elements like Rb, V, Cr, Ni, Co, Y, Sr and Ba were also plotted against MgO. Most of them do not show any clear cut trend while Sr, Cr and Ni are showing an increasing trend. Ba and V show a decreasing trend.

Heavy REE depletion indicates the presence of garnet in the source residue. No Eu anomaly is observed in REE pattern. This can be explained by a source which has no significant amount of residual plagioclase in it. Alternatively it rules out a plagioclase cumulation and removal event.

Ba/Sr ratio of gabbro samples do not vary much and that indicates consanguinity. Ba shows a decreasing trend with increasing MgO. This is consistent with the decreasing trend shown by K$_2$O against MgO.

In the AFM diagram (Fig. 6.7) the samples show a tholeiitic trend. Magma type and evolutionary path in mafic rocks can be identified from the FeO(t)/MgO vs FeO(t) diagram and FeO(t)/MgO vs TiO2 diagram (Fig. 6.13 a & b) of Miyashiro (1973). In both these diagrams iron enrichment trend typical of tholeiitic suites is shown by the gabbro samples. The diorite and granodiorite samples do not show any recognizable trend. These rocks behave differently in all the major element aspects. Thus either these rocks originated differently or they represent modified gabbroic melt.

Spider diagram of incompatible elements normalized by primitive mantle values (values from Sun and McDonough,1989) is shown in figure 6.14. Except for K, Th and Ti all others do not show any irregularity. The pattern does not

99
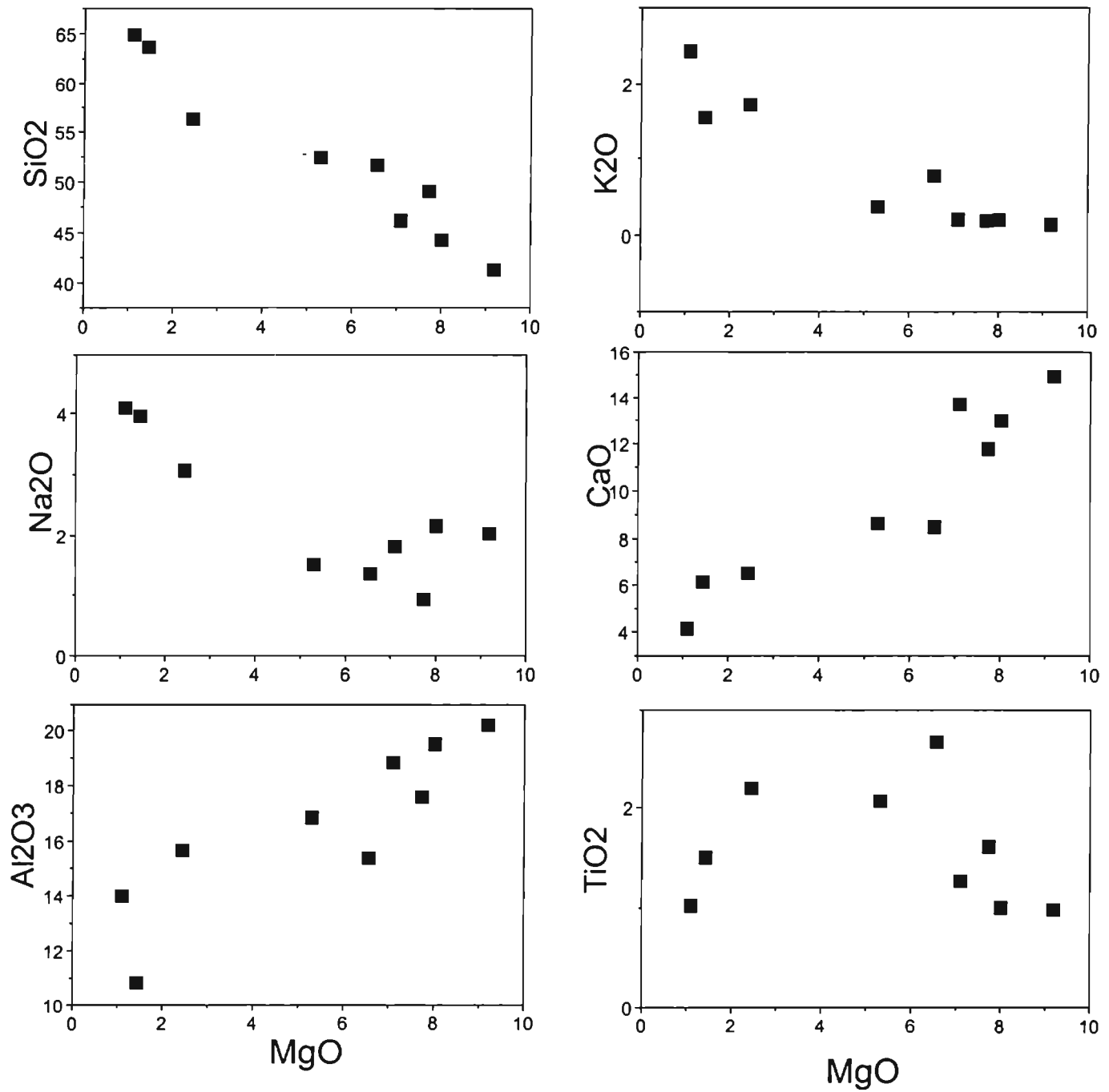
Fig. 6.12 Plots showing the variation of major element oxides with MgO (wt%) in Ezhimala gabbroic samples.
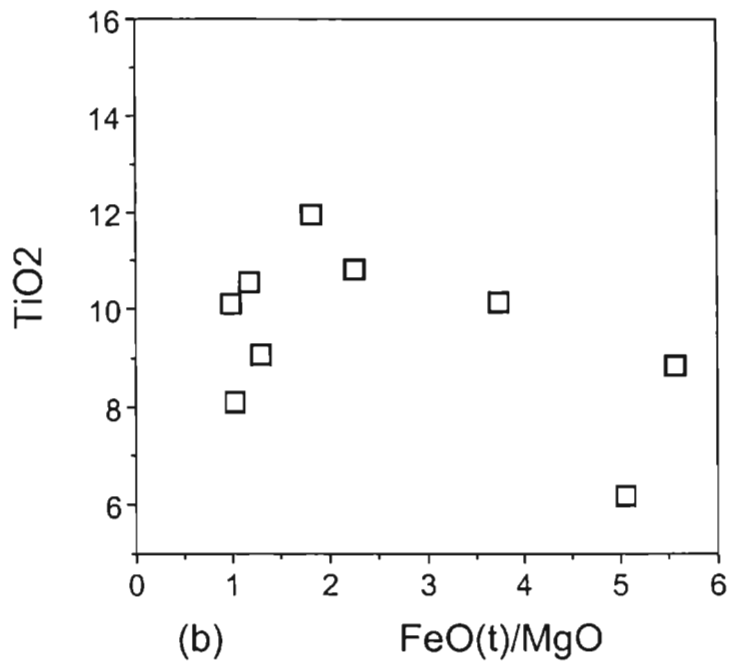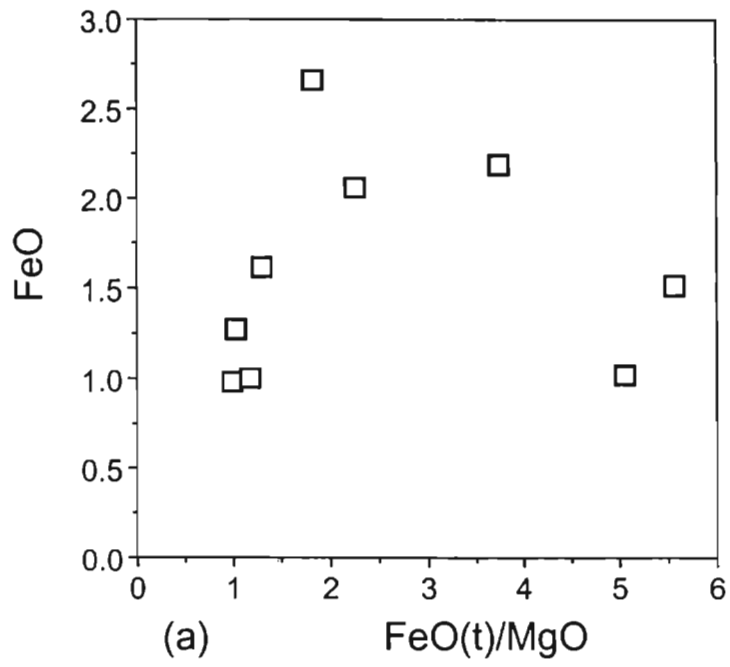
Fig. 6.13 FeO(t)/MgO versus FeO(t) and TiO2 diagram (after Miyashiro, 1973) showing the plots for Ezhimala gabbroic samples.
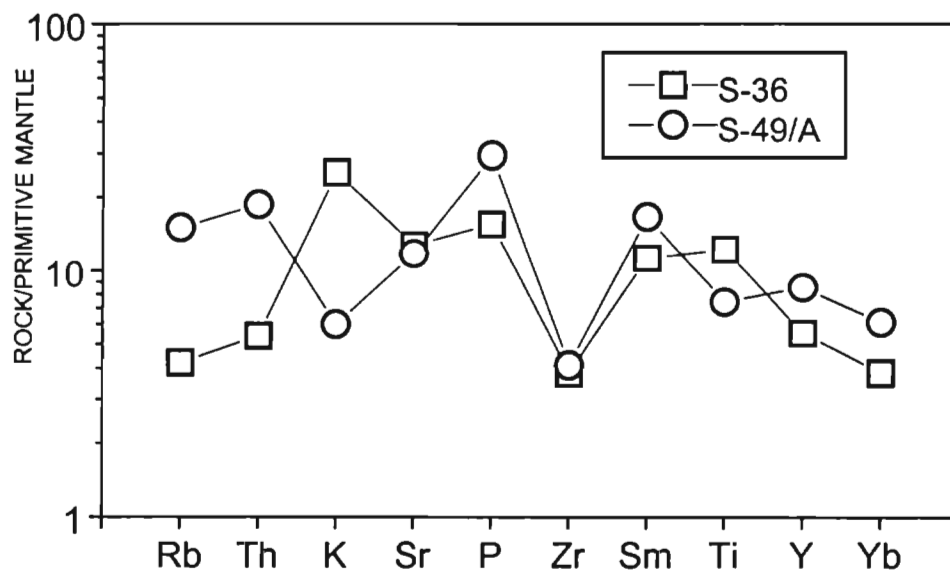
Fig. 6.14 Primitive mantle-normalized incompatible element patterns Ezhimala gabbro samples. The primitive mantle values are from Sun and McDonough (1989).

show any fractionation.   The pattern is almost similar to primordial mantle normalized incompatible element abundances of continental tholeiite (Holm, 1985).   Thus the mafic melt which crystallized as such or after crustal contamination has a tholeiitic nature.   It has a deep seated (as the inferred source had garnet but not plagioclase), possibly mantle origin.

6.2.2 Ezhimala granitoids
6.2.2.1 Field relationships
·The rock units encountered along the quarries and exposures of Ezhimala are grey granophyre, pink granophyre, rapakivi granite and gabbro. Along the eastern flank of the Ezhimala hill, grey granophyre is seen. Pink granophyre is seen along the western flank. Both grey granophyre and pink granophyre are medium to coarse grained. Within the same outcrop itself grain size varies. Mafic content of both grey and pink granophyres varies from one location to another. Contact between pink and grey granophyres is not observed due to thick vegetation and soil cover. At many locations of grey granophyre, xenolith patches are observed. They are of different sizes and shapes with a minimum diameter of 3cm. Gabbro veins are noted and their width is about 5 cm. Gabbro body fringing the granite-granophyre pluton along the eastern and southern side shows a gradational contact with grey granophyre at a location S48.

Along the southeastern portion of the granite, there is a small patch of granitoids showing rapakivi texture.   The feldspar phenocrysts show preferred orientation (N 307°) and these are rimmed by plagioclase feldspar. Maximum length of phenocrysts is 2.5 cm and width is 0.5 cm.   Quartz grains are also slightly elongated. Rapakivi texture changes merely to a porphyritic texture.

6.2.2.2 Megascopic petrography
Ezhimala granitoids have three varieties viz., pink granophyre, grey granophyre and rapakivi granite. The rocks range from very coarse grained to medium grained and all the samples are unfoliated. Pink granophyres are

coarser grained than grey granophyres. Sample S-90/A (pink granophyre) is the most coarse grained type. The most fine grained rock is a grey granophyre sample (S-34/1). Both pink and grey granophyres are equigranular while the rapakivi granite is porphyritic (samples S-45/A and S-45/B). In this rock mantled feldspar crystals can be seen. Mafic content of the rocks varies considerably. Grey granophyres are more mafic than pink granophyres. The most mafic sample is S-25/1. The common mafic mineral observed in these rocks is a dark brown coloured amphibole. Grey coloured samples have biotite also in them. In most cases the amphibole crystals are smaller than the alkali feldspar crystals. In sample S-90/A which is pink granophyre, the amphibole crystals and the feldspar are of same size. In some cases the feldspar crystals occur as long crystals.

6.2.2.3 Microscopic petrography
6.2.2.3.1 Grey granophyre

The grey granophyre samples show micrographic texture (Fig. 6.15). In this rock, alkali feldspar is the dominant mineral and they occur as anhedral to subhedral crystals. In the graphic texture, orthoclase occurs as intergrowth with quartz. In the graphic intergrowth, quartz patches are optically continuous. Orthoclase free of intergrowth are also observed. Some of the orthoclase crystals show Carlsbad twinning and zoned orthoclase are observed in some samples of grey granophyre. In some samples microcline also shows intergrowth relationship with quartz (S-25/1). Size of the grains showing intergrowth relationship is varying within the same thin section. Development of graphic texture is maximum in grey granophyre.

Small amount of plagioclase is present in some of all the granophyre sections. The polysynthetic twin lamellae are thin. Using the Michael Levy method, the composition of the plagioclase is found to be in the range of An_{56} to An_{64}. They show straight and curved grain boundaries. Some crystals show Carlsbad twinning. Different sizes of plagioclase crystals are present. Zoning is
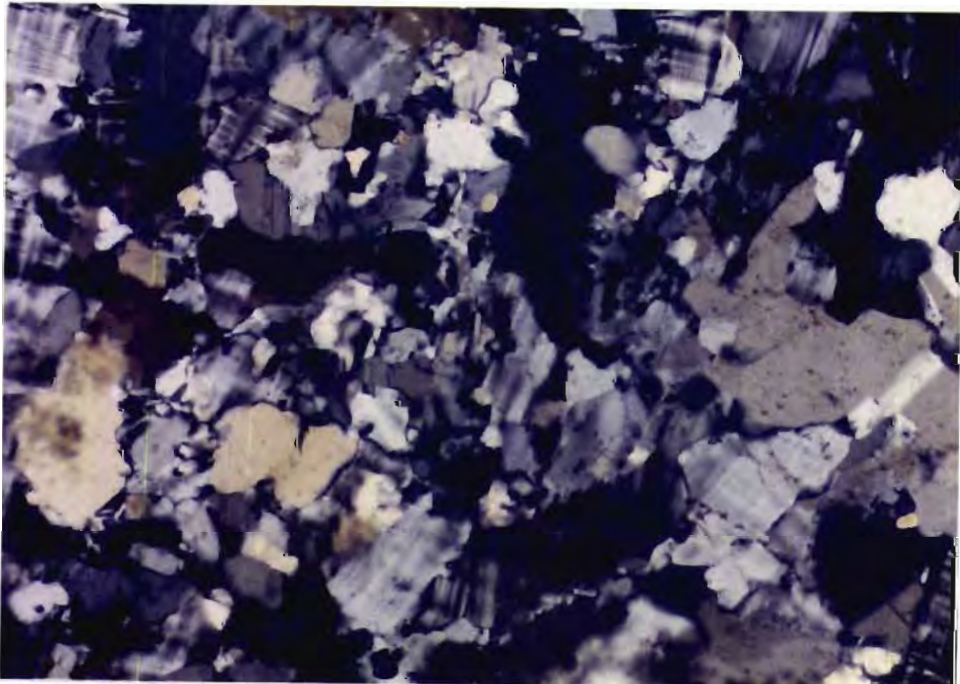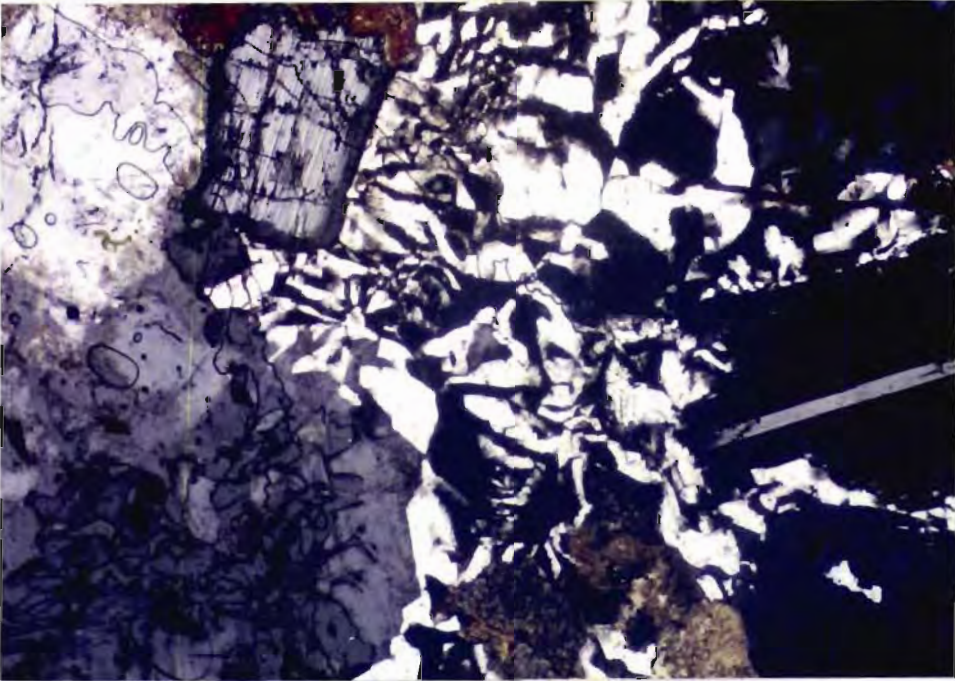
observed in some plagioclase crystals of sample S-34/1. Plagioclase crystals show intergrowth relationship with quartz and in some cases plagioclase crystals can be seen replaced by graphically intergrown mixture of quartz and feldspar along the grain boundaries (Fig. 6.16) representing a disequilibrium texture. In the sample S-34/1 quartz-orthoclase intergrowth cuts plagioclase crystals. Many of the feldspar crystals are sericitized.

Quartz mainly occurs as intergrowths with orthoclase/microcline or plagioclase. Mafic minerals include hornblende, biotite and sphene etc. Hornblende is the most dominant mafic mineral and others occur in very small amounts. In grey granophyre samples, some pyroxenes are also present and they show alteration to hornblende. Both clinopyroxene and orthopyroxenes were observed. Average mafic mineral content is 5%. Accessory minerals include epidote and apatite.

6.2.2.3.2 Pink granophyre

This rock also shows micrographic texture. Anhedral to subhedral alkali feldspar is the dominant mineral in these rocks. Orthoclase crystals with straight grain boundaries are present. Carlsbad twinning can be seen in some orthoclase crystals. Intergrowth of alkalifeldspar and quartz is common and they are of different sizes. Mostly the quartz patches are smaller than those seen in grey granophyre. In sample S-95/A, size of the crystals showing graphic texture is smaller compared to the sample S-90/A.

Small amount of plagioclase is present in a few pink granophyre samples. Modal percentage is less compared to that in grey granophyre samples. Albite twin lamellae are thin. In pink granophyres also hornblende is the most dominant mafic mineral. Very small amounts of opaques are present. Apatite and epidote are the accessory minerals present.

Samples S-54/C and S-54/D are not showing any intergrowth between quartz and feldspar. In these rocks also alkali feldspar is the dominant mineral and their crystals are subhedral to anhedral. Recrystallized quartz is present and they exhibit polygonal grain boundaries. Plagioclase is totally absent in these rocks. Hornblende is the dominant mafic mineral but the modal percentage is very less. Very small amounts of opaques are present in this rock.

6.2.2.4 Major element geochemistry

Nine samples of Ezhimala granitoids were analysed for major elements and that is presented along with corresponding C.I.P.W norm in table 6.4. Modal composition of selected samples are given in table 6.5. For the grey granophyre samples SiO_2 content ranges from 65.85 to 69.43%. Average SiO_2 content of the pink granophyre samples is 71.97%. Rapakivi samples have an average SiO_2 content of 74.72%. Al_2O_3 is almost a constant in all the samples. Average Al_2O_3 content is 14%. MgO and MnO contents are very low and in all the samples they are less than 1% except for the samples S-54/C and S-54/D in which MgO content is greater than 1%. FeO content is varying from 5.4 to 5.98% for grey granophyre samples. Average FeO content in pink granophyre samples is 3.5%. Rapakivi granite samples have an average FeO content of 1% while high FeO value (~6%) is shown by samples S-54/C and S-54/D. The average CaO content of grey granophyre samples (4%) is higher than that of pink variety (1.6%). Rapakivi granite samples have an average CaO content of 0.8%. For samples S-54/C and S-54/D, CaO content is having an average value of 4.5%. Na_2O is not showing much variation and it ranges from 2.84 to 4.16%. Average Na_2O content of pink granophyre is 4.3% and that of rapakivi granite is 4%. K_2O is slightly less than Na_2O in all the granophyre samples. Average K_2O content of grey granophyre is 2.2% and that of pink granophyre is 3.14%. K_2O is slightly high for the rapakivi granite sample (average=4.4%). P_2O_5 is less than 1% in all the samples irrespective of the petrographical differences. TiO_2 is slightly higher in grey granophyres than pink granophyre. In grey granophyre, it

Table 6.4 Major element analysis (wt%) of Ezhimala granitoid samples with
calculated C.I.P.W norms

Sample No.	S-23/1	S-25/1	S-34/1	S-45/A	S-45/B	S-54/C	S-54/D	S-90/A	S-95/A
SiO2	69.43	65.85	68.00	74.02	75.41	65.71	63.52	71.72	72.22
Al2O3	13.05	13.75	13.46	14.24	13.60	14.15	14.48	13.21	13.26
FeO	3.20	3.80	3.40	0.55	0.60	3.55	3.64	2.18	1.90
Fe2O3	2.40	2.81	2.54	0.40	0.45	2.63	2.70	1.61	1.40
MnO	0.16	0.17	0.16	0.04	0.04	0.15	0.16	0.11	0.09
MgO	0.17	0.70	0.27	0.31	0.25	1.04	1.27	0.44	0.37
CaO	3.69	3.62	4.39	0.79	0.93	4.10	4.74	1.58	1.64
Na2O	2.84	4.16	3.14	4.06	3.74	4.30	4.27	4.13	4.65
K2O	2.25	2.37	2.21	4.36	4.52	2.51	2.28	3.14	3.14
TiO2	1.15	1.07	1.11	0.11	0.14	1.12	1.15	0.62	0.72
P2O5	0.33	0.32	0.42	0.03	0.03	0.38	0.49	0.11	0.13
Norm									
	S-23/1	S-25/1	S-34/1	S-45/A	S-45/B	S-54/C	S-54/D	S-90/A	S-95/A
Q	35.9	24.2	31.9	31.6	33.9	22	19.4	31.2	29.4
Ap	0.6	0.6	2.6	0	0	0.9	0.9	0.3	0.3
Ilm	2.1	2	2.1	0.2	0.3	2.1	2.1	1.2	1.4
Or	13.3	13.9	13.3	25.6	26.7	15	13.3	18.4	18.3
Al	24.1	35.1	26.7	34.1	31.4	36.2	36.2	35.1	39.3
An	16.1	12	15.8	3.9	4.7	12	13.6	7	6.1
Hy	2.5	3.2	1.9	1.5	1.1	3.1	3.2	2.9	1.6
Di	0	3.5	3	0	0	4.6	6	0	0.9
Wo	0	0	0	0	0	0	0	0	0
Mt	3.5	4.2	3.7	0.7	0.7	3.7	3.9	2.3	2.1

Table 6.5 Modal composition of the selected samples of Ezhimala granitoid samples

	S-23/1	S-25/1	S-45/A	S-34/1	S-54/C	S-54/D	S-90/A	S-95/A
alkalifeldspar	60	67	75	45	75	72	63	40
microcline	0	3	0	0	0	0	0	0
plagioclase	20	3	0	5	0	20	0	10
quartz	17	20	2	35	20	0	36	45
mafics	1	3	5	10	3	5	0	5
sphene	0	0	0	0	0	0	0	0
opaques	2	4	0	5	2	3	1	0

Modal composition of the selected samples of
Ezhimala gabbro

	S-33	S-36	S-40/A	S-53/B
plagioclase	55	58	75	68
quartz	5	0	15	4
clinopyroxene	28	35	5	17
orthopyroxene	2	0	1	4
biotite	5		0	0
apatite	0	2	0	2
opaques	5	5	4	5

Modal composition of the selected samples of
Peralimala syenite

	S-19/1	S-58/A	S-74/A	S-75/A	S-83/A
orthoclase	65	75	43	44	78
quartz	0	5	46	45	5
plagioclase	1	6	6	6	7
hornblende	30	9	4	2	8
sphene	3	2	0	1	0
apatite	1	1	1	0	1
opaques	tr	2	0	2	1

ranges from 1.07 to 1.15%. Average TiO_2 content of pink granophyre samples is 0.67%. In rapakivi granite TiO_2 is very less (average= 0.13%).

6.2.2.5 Trace element geochemistry

Trace element concentrations in two samples (S-23/1 and S-34/1) of grey granophyre samples are given in table 6.6. In these samples Ba contents ranges are 498ppm and 500ppm. Average value of Rb is 46ppm. Ba/Sr ratio of these samples is almost a same(1.58 and 1.33). Rb also shows a decrease with increase in SiO_2. Higher content of Sr can be attributed to higher content of CaO. Ta is ranging from 2.14 to 2.5ppm. The rock is more enriched in LILE than HFSE. Zr/Hf ratio ranges from 22 to 31 with an average value of 27. Average Nb/Ta ratio is 19. These values are close to crustal values. Cr has an average value of 49ppm. Average content of Ni in these samples is 22ppm. Cr increases with increase in SiO_2. Ni content is showing an increasing trend with SiO_2. Sc does not show much variation (average is 19ppm). U content in Ezhimala granophyre samples are 1.84ppm and 2.25ppm. Average Th content is 10ppm. Th/U ratio is almost a constant and the average value is 5. In all the samples Th content is higher than that of U. Ga concentrations are almost same (average = 32ppm.). No significant correlation exists between Ga and Al.

The REE analysis is presented in table 6.7. REE abundances of grey granophyre samples S-23/1 and S-34/1 are very similar. The chondrite normalilzed REE patterns are given in figure 6.17. No Eu anomaly is shown by them. $(La/Yb)_N$ ratio for these samples is almost same and the average value is 7.14. This ratio indicates that the REE fractionation is very low for Ezhimala granite. $(La/Sm)_N$ ratios is almost same and is around indicating that the fractionation among LREE is not strong. $(Gd/Yb)_N$ ratio also is very less indicating a less degree of fractionation among HREE.

104

Table 6.6   Trace element concentrations
(ppm) of Ezhimala granophyre sampes

Sample No.	S-23/1	S-34/1
V	52.76	74.51
Cr	51.31	45.72
Co	5.98	7.13
Ni	22.33	21.52
Cu	20.12	20.36
Zn	195.65	176.87
Ga	31.27	33.42
Rb	48.65	43.97
Sr	315.11	375.62
Y	87.36	82.50
Zr	54.27	86.95
Nb	49.38	40.96
Cs	1.01	1.13
Ba	500.16	498.18
Hf	2.44	2.80
Ta	2.50	2.14
Pb	11.24	13.34
Th	9.37	10.64
U	1.84	2.25

Table 6.7   Rare earth element concentrations
(ppm) Ezhimala granophyre samples

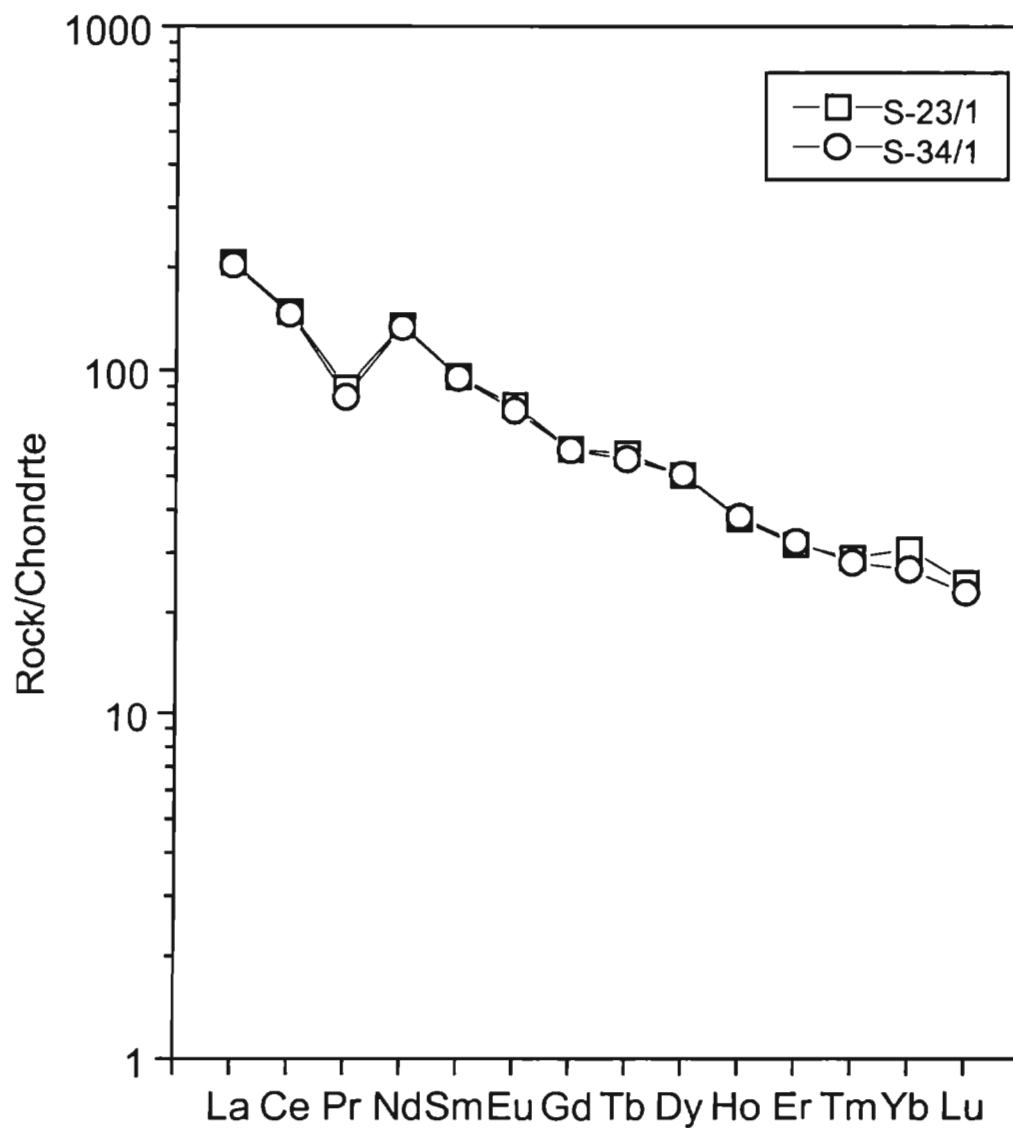| Sample No.	S-23/1	S-34/1
La	64.00	62.92
Ce	119.78	118.09
Pr	10.87	10.24
Nd	81.38	80.29
Sm	18.75	18.57
Eu	5.85	5.65
Gd	15.47	15.35
Tb	2.75	2.65
Dy	16.18	16.24
Ho	2.70	2.74
Er	6.66	6.79
Tm	0.94	0.91
Yb	6.42	5.61
Lu	0.79	0.74

Fig. 6.17 Chondrite-normalized REE patterns of Ezhimala granophyre samples.   Normalization values are from Brynton (1984).

6.2.2.6 Geochemical classification and Tectonic discrimination

CIPW norms calculated from major element analysis were plotted in QAP diagram with the fields after Streckeisen (1976) (Fig. 6.18). Majority of the samples of the Ezhimala granitoid pluton fall in the   granite field. Two of them fall in the alkali granite field. The grey granophyre samples and the samples S-54C and S-54D fall in the   granite field. The pink granophyre samples fall along the boundary of the alkali granite and   granite fields. The rapakivi samples fall in the alkali granite field. CIPW normative Ab, Or and An of the rocks were plotted in the O'Connor diagram (Barker, 1979) (Fig. 6.19). In this diagram, the pink granophyre samples fall in the trondhjemite field. Sample S-25/1, which is a grey granophyre falls in the trondhjemite field while the other two grey granophyre samples falls in the granodiorite field. The rapakivi samples fall in the granite field. The samples S-54/C and S-54/D fall in the trondhjemite field.

Major element chemistry can be effectively used for multivariate discriminant analysis as presented by Agrawal (1995) to successively distinguish late-orogenic (LO) form post-orogenic (PO) granites related to orogeny as well as the anorogenic granites in the anorthosite/rapakivi complexes (AR) and the alkaline ring complexes (RC). The Ezhimala granite samples were subjected to above analysis and it is found that all the samples were assigned to the group of orogenic granites. In orogenic variety, the Ezhimala granite samples were assigned to the group of late-orogenic (LO) group. Irrespective of all the differences in the petrography, all the samples show same tectonic setting.

Based on the tectonic discrimination diagrams (after Pierce et al., 1984) (Fig. 6.20) like SiO_2 vs Nb, SiO_2 vs Rb and Y vs Nb, the Ezhimala granitoid samples fall in the WPG+ORG, Syn-COLG and WPG fields respectively. A-type character of Ezhimala granitoid pluton is indicated by plots (after Whalen et al.,1987) like 10000*(Ga/Al) vs FeO/MgO, 10000*(Ga/Al) vs K_2O/MgO and 10000*(Ga/Al) vs K_2O+Na_2O (Fig.6.21).

105
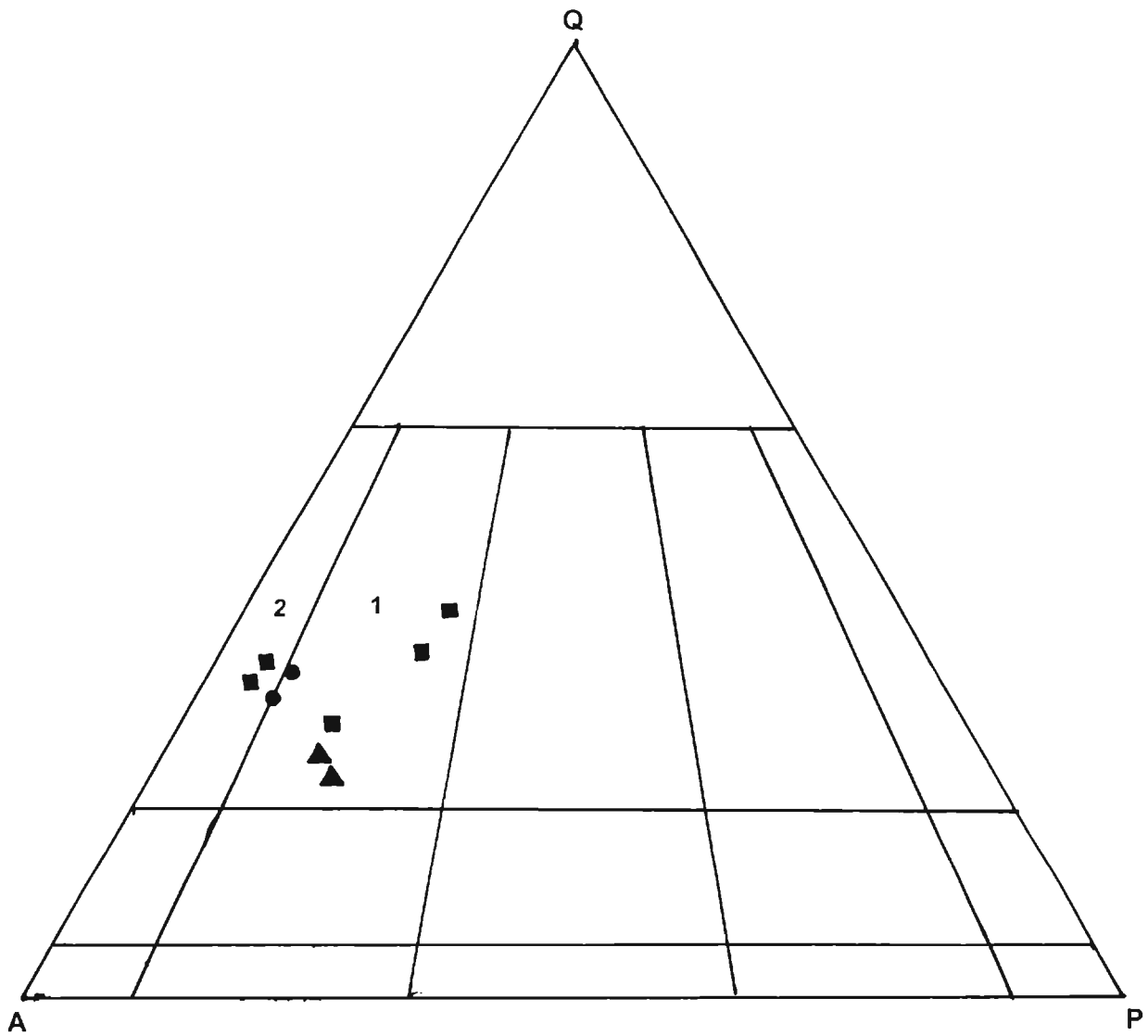
Fig. 6.18 Normative quartz(Q)-alkali feldspar(A)-plagioclase(P) diagram for Ezhimala granitoids (symbols: squares- grey granophyre, circles- pink granophyre and triangle-S 54/c & S 54/p). Fields: 1. Granite and 2. Alkali feldspar granite(after Streckiesen, 1976).
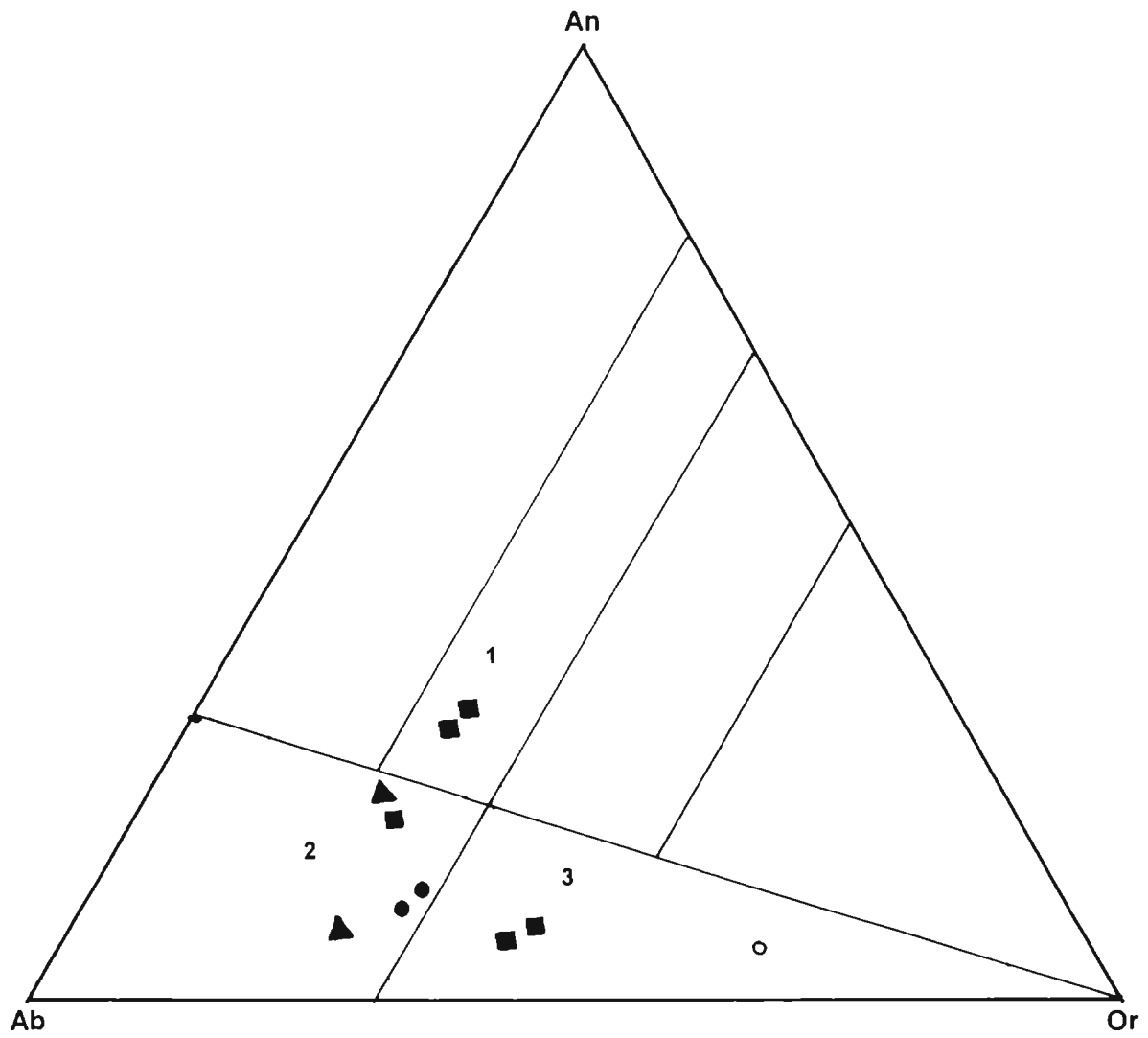
Fig. 6.19 Normative albite(Ab)-anorthite(An)-orthoclase(Or) diagram for Ezhimala granitoids (symbols as in figure 6.17). Fields: 1.Granodiorite, 2. Trondhjemite and 3. Granite (fields after O' Connor, 1965).
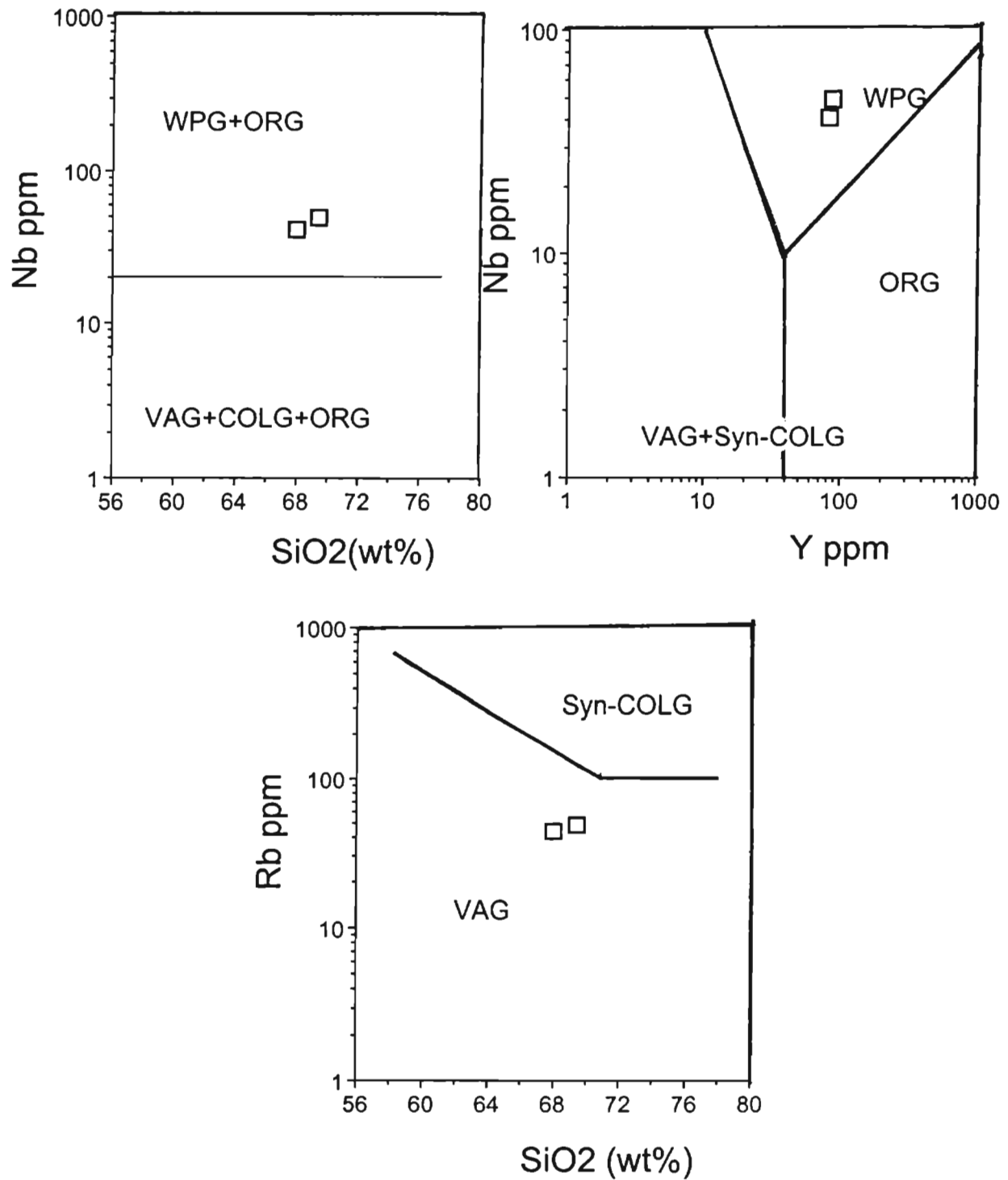
Fig. 6.20 Tectonic discrimination diagrams for Ezhimala granophyre samples (after Pearce et al.,1984).
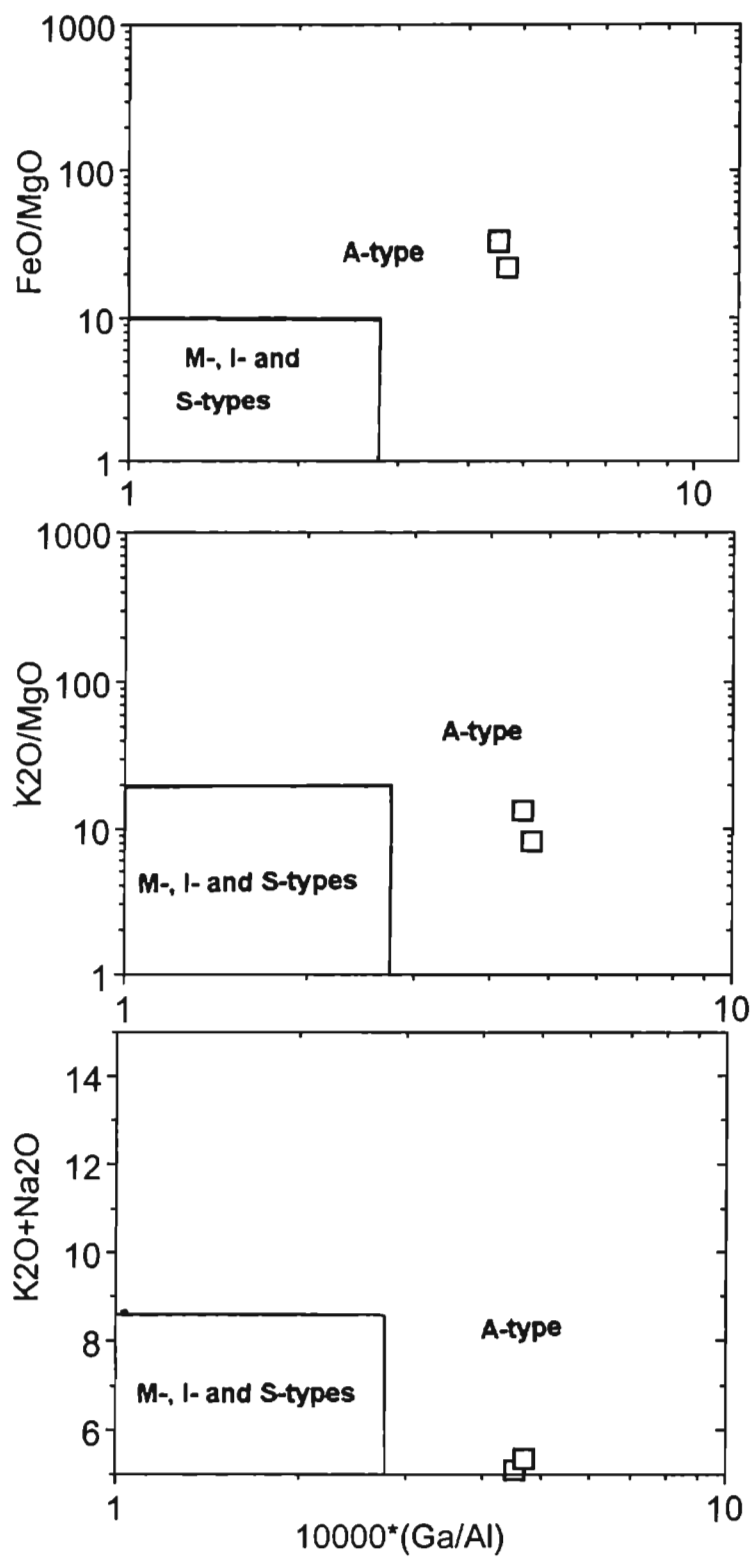
Fig. 6.21   Plots of Ezhimala granophyre samples in
10000*(Ga/Al)vs FeO/MgO, 10000*(Ga/Al) vs K2O/MgO
and 10000*(Ga/Al) vs K2O+Na2O diagrams.
Fields after Whalen et al. (1987).

In the SiO_2 vs total alkali diagram (after ~~Le Bas~~ et al., 1985) (Fig.6.22), the samples S-45/A, S-45/B, S-90/A and S-95/A fall in the granite field. The samples S-23/1, S-25/A and S-34/1 fall in the Gdiorik field. The sample S-54D falls in the Ediorite field.

6.2.2.7 Petrogenesis

Fractionation trends were studied by plotting major elements like TiO_2 K_2O, Na_2O, MgO, Al_2O_3 and CaO against SiO_2 and differentiation index (DI) (Fig. 6.23 and Fig.6.24 respectively). Two different trends are observed. One trend is defined by grey granophyre samples and the samples S-54/C and S-54/D. The second trend includes pink granophyre samples and rapakivi granite samples. These two groups fall on either side of 70% SiO_2. In both the groups Na_2O and MgO of both the groups show a sharp decreasing trend. Decreasing trend of Na_2O indicates that the feldspars involved in the late stages of differentiation were not of sodic composition. Decreasing trend of MgO indicates the early fractionation of pyroxenes of amphiboles. In the group of grey granophyre samples K_2O does not show any trend with SiO_2. In the group of pink granophyre and rapakivi samples, it shows an increasing trend with increasing SiO_2. Absence of any trend in the first case may be due to the development of quartz-feldspar intergrowth. K_2O increases in the pink granophyre group because of the fractionation of K-feldspar without the development of intergrowth.

CaO in the group of grey granophyre group does not show a clear cut decreasing trend indicating that plagioclase has not played any role in the fractionation. In the case of pink granophyre and rapakivi granite, CaO shows a decreasing trend. This is consistent with the early fractionation of plagioclase feldspar. Al_2O_3 in the first group shows a decreasing trend. No clear cut trend is seen in the other group.

106
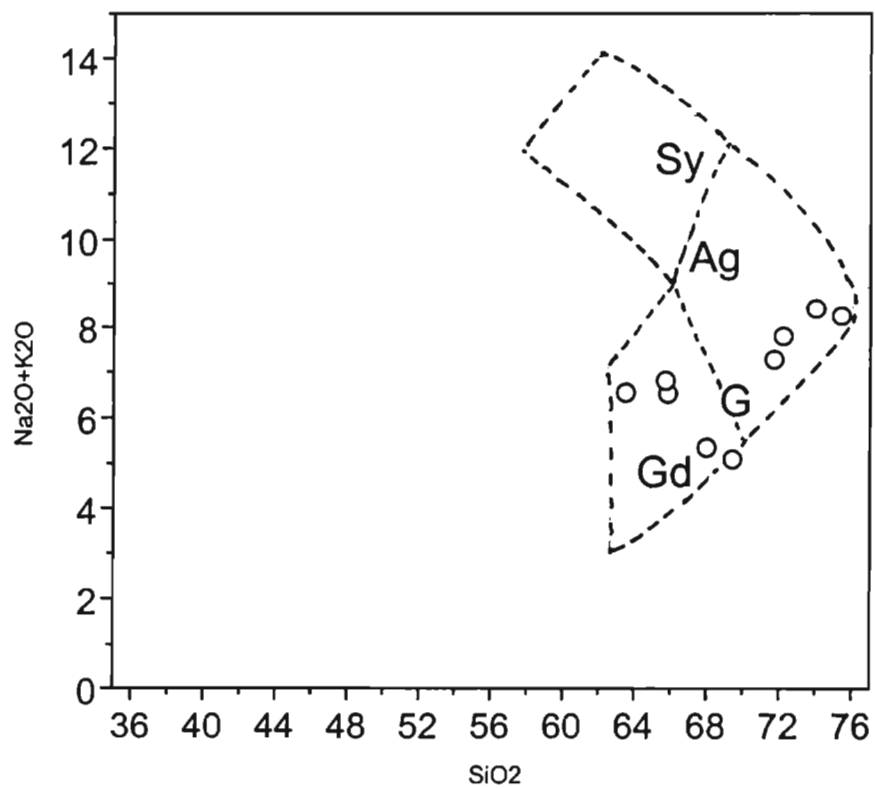
Fig. 6.22 SiO2(wt%) vs total alkali (wt%) diagram of Ezhimala grnophyre samples for nomenclature of igneous rocks (Cox et al., 1979).

Sy- syenite, Ag- alkali granite, G-granite, Gd- granodiorite or quartz diorite
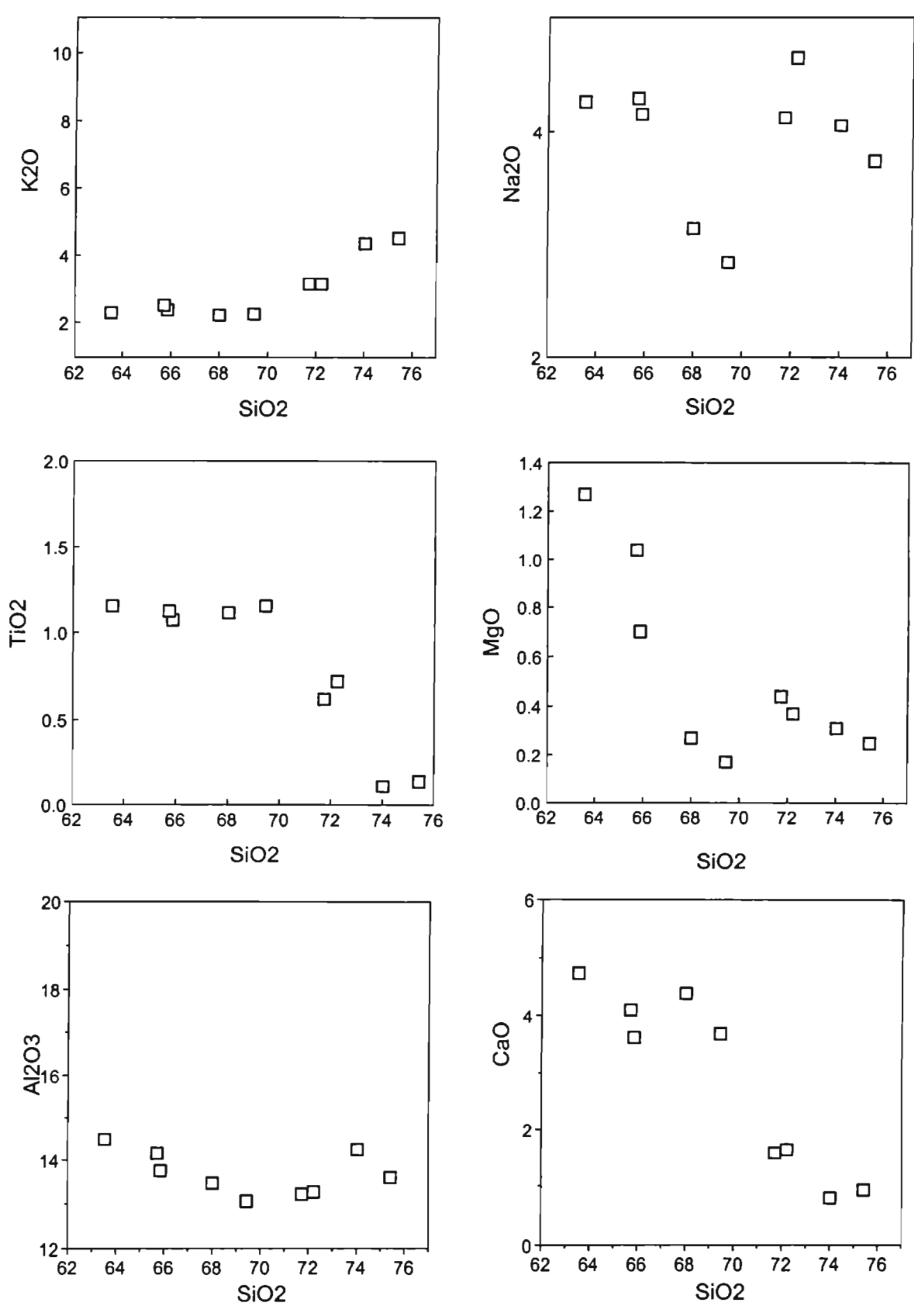
Fig. 6.23   Variation of major element oxides of Ezhimala granophyre samples with SiO2 (wt%).
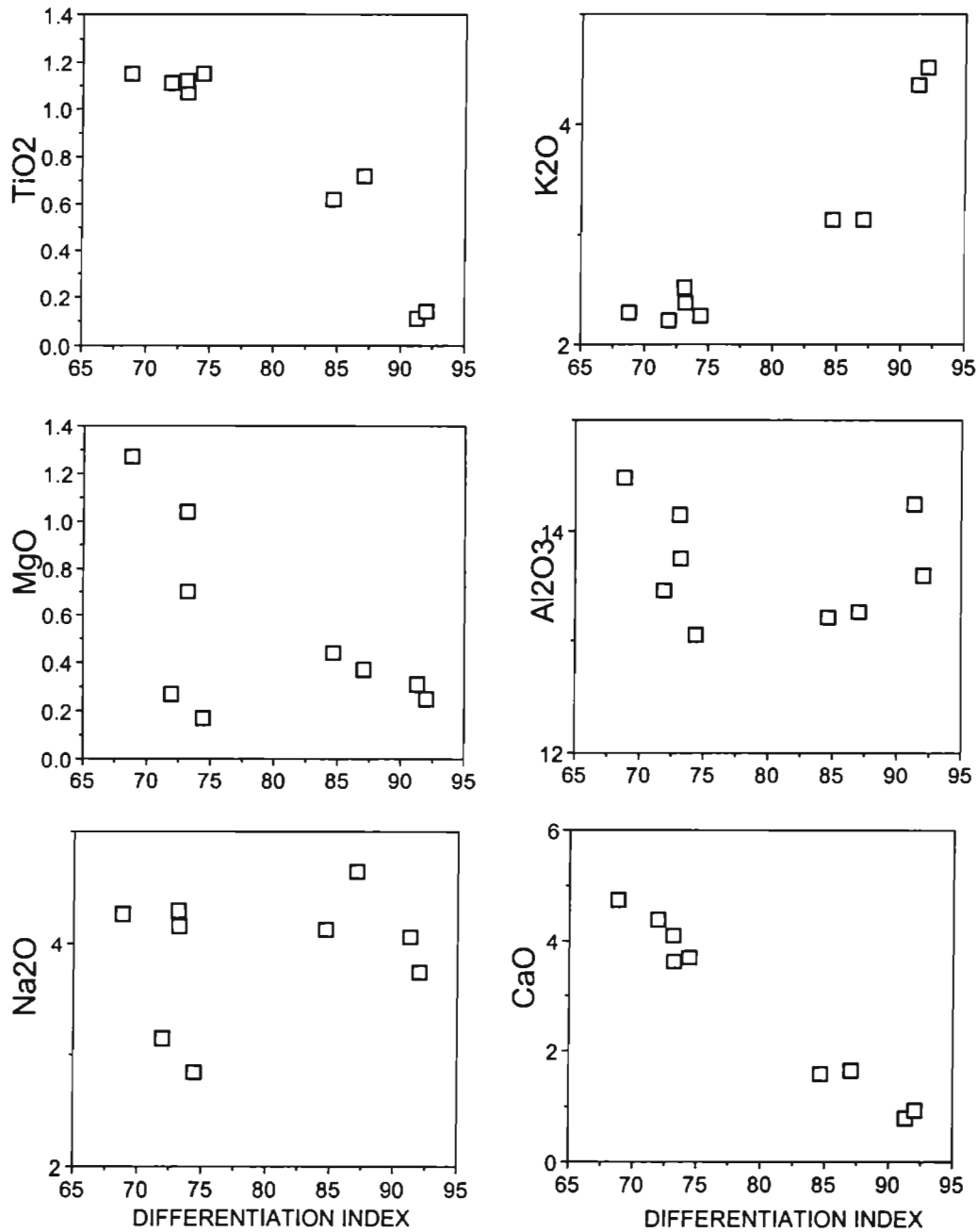
Fig. 6.24   Plots showing the variation of major element oxides (wt.%)of
Ezhimala granophyre samples with differentiation index (DI) of Thornton
and Tuttle (1960). DI= sum of normative quartz, orthoclase, albite and
nepheline, leucite, and Kaliophilite.
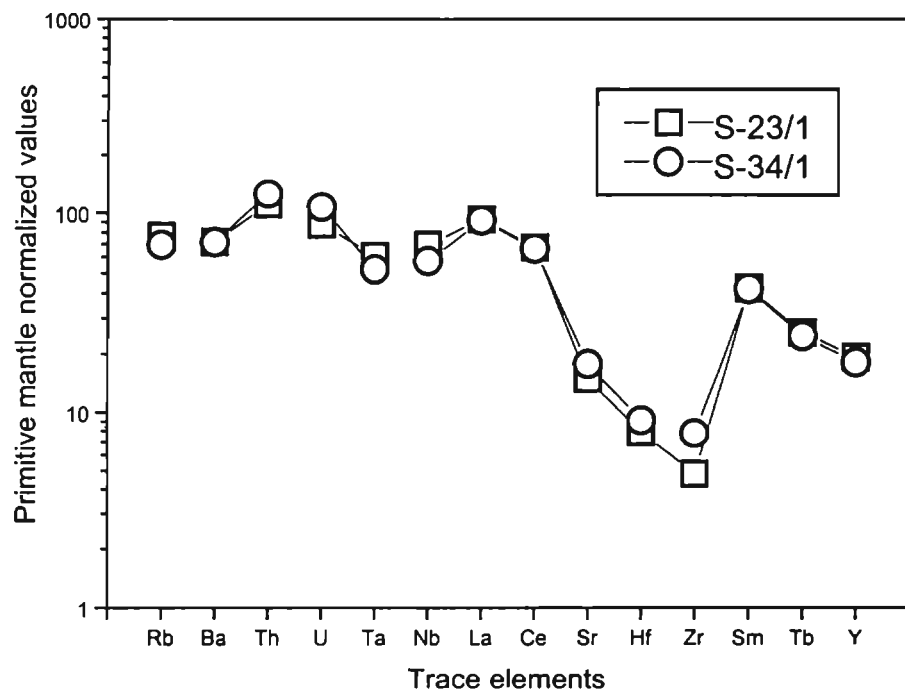
Fig. 6.25 Primitive mantle normalized trace element patterns of Ezhmala granophyre samples. Primitive mantle values are from Sun and McDonough (1989).

Ba/Sr ratio of grey granophyre samples do not vary much and that indicates consanguinity.   High   K/Rb values are exhibited by these samples. Rb, and Ba are almost same in both the samples and this is consistent with the almost same content of K_2O. Sr shows a decreasing trend with increasing SiO_2. This may be due to the early fractionation of Ca-bearing minerals like apatite and pyroxene.   All these variations indicate fractional crystallization as one of the processes involved in the petrogenesis of the Ezhimala   granitoids. However, the trace element characteristics do not support that the granitic melts are highly fractionated type.   McCarthy and Hasty (1976) had shown quite conclusively that fractionated granite melts have high Rb (appr. 700ppm) and very much lower Sr (appr. <10 ppm).   For Ezhimala samples Rb is very less and Sr is very high and thus it indicates a partial melting origin for the granitic melt. Similarly, the low Mg/Mg+Fe levels also preclude a fractional crystallization from a basic magma.

Spider diagrams (Fig. 6.25) of trace elements normalized by primitive mantle values produced similar pattern for two samples of grey granophyre for which data is available. The pattern is highly rugged and therefore single step evolution from mantle can be ruled out. LIL elements are about 100 times those of mantle and the refractory elements like Ta, Nb, Y and HREE are higher than that of mantle.   These features indicate a crustal source.

Chondrite normalized REE patterns (Fig. 6.17) show no Eu anomaly and thus it can be concluded that the residue of the source does not contain plagioclase. Thus it supports a source other than a plagioclase feldspar bearing rock. The adjacent Vengad basin which is essentially quartz + feldspar+ mica rock can be considered as the possible parent. The narrow zone of well banded quarzite, quartz-mica schist and amphibolite observed towards the north end of the Ezhimala granitoid may be the representing the source which had undergone partial melting to give rise to the felsic melt to form the Ezhimala granitoids.

Gabbroic intrusions can cause partial melting of metasedimentaries to give rise to high-silica melts and some hybrid rocks. In the model proposed by Huppert and Sparks (1988), mafic intrusions act as the "trigger" in the generation of large granitic plutons. The compositional similarity between the plagioclase (An_{56} to An_{64}) in the granophyres and the associated gabbro body indicates that plagioclase feldspars in the granite were originally from the gabbro. From the microscopic study it is clear that these plagioclase feldspar crystals from the gabbro body are disintegrated to graphic intergrowth of quartz and orthoclase. These evidences are in favour of a mixing of gabbro body and a granitic melt. Droplets of granophyric intergrowth is a disequilibrium texture indicating mingling and mixing of contrasting magmas (Sparks and Marshall, 1986; Hibbard, 1991). Here, the grey granophyre represents the mixed rock (granite+gabbro) while pink granophyre represents somewhat the pure granitic melt. Field observations also support this. The gabbro body is fringing the Ezhimala granitoids along the eastern and southern margins. Grey granophyre is also observed along the southern part of the pluton. Pink granophyre is seen along the western side and there is no gabbro along the western margin.

Thus it can easily be concluded that mixing is the exact mechanism which produced the granophyres. The mixing of granitic melt and gabbro would not have been possible if the granitic melt was generated by the fractional crystallization of that gabbroic melt because then the granitic melt would be too cool to interact with the early formed gabbro. This also supports different source and time of origin for the Ezhimala granitoid and the associated gabbro.

Based on the observations that grey granophyre is a mixture of granitic and gabbroic melts and that pink granophyre represents the original granitic melt, a mixing calculation using the major element chemistry has been done to assess the degree of mixing. From the calcualations it was found that 85% pink granite melt got mixed with 15% gabbro to produce the grey granophyre. From this result REE abundance in pink granophyre was calculated. Calculated REE

abundance of pink granophyre was not much different from the REE abundance of grey granophyre.

Depending on the proportions of basaltic-granitic magmas, the above mentioned process can be a mingling or mixing (Eklund et al., 1994). In the case of Ezhimala granitoids, the disequilibrium texture (large plagioclase crystals being partially replaced by graphic intergrowth) and field observations (close occurrence of the gabbro along the eastern flank of Ezhimala, gradational contact and presence of xenoliths in grey granophyre are the evidences for an interaction between the mafic and granitc magama. Some other evidences for a proper mixing include corroded K-feldspar megacrysts mantled with labrodorite, quartz ocelli (Eklund et al.,1994). These features are not observed in the present case and moreover the mixing calculations showed that only 15% mafic magma interacted with 85% granitic melt. So this process is just a mingling and not mixing.

As discussed earlier a few of the Ezhimala gabbroic samples (eg., S-33) also show a micrographic texture but very small and very less compared to Ezhimala granophyre. In such rocks, large laths of labrodorite plagoclase are being replaced by a quartz-alkalifeldspar intergrowth. The variation diagrams of the gabbroic samples are in favour of a late stage addition of a felsic magma. Thus in the Ezhimala gabbroic rocks also geochemistry and petrography indicate a process involving an interaction between gabbroic magma and felsic magma.

6.3 Peralimala syenite

The Peralimala pluton is an elongated body lying in an east-west direction and it is found towards the southern block of the Bavali lineament and it is located approximately 40km ESE of Perinthatta anorthosite. The pluton covers an area of about 60km^2. The country rocks include schists and hornblende gneiss. It has been termed by various authors as granite (Nair and Vidyadharan, 1982), alkali granite (Nair and Santosh, 1984) and syenite (Ravindrakumar and

Sinha-Roy,1985). It occupies the core portion of a tight, isoclinal antiformal fold (Anilkumar et al. 1992). Geological map of Peralimala syenite is given in figure 6.26.

6.3.1 Field relationships

The rock is composed of both massive and foliated varieties. In a location near Perumpunna, shear planes are noted and they dip 80° due N5°. Biotite patches with boudin shape can be seen along the shear planes. The biotite here is a product of shearing. Gneissocity is seen developed parallel to the shear planes indicating a simultaneous origin. Mafic enclaves are observed in many locations. Pegmatite veins are noted cutting the shear planes and they are of syenitic composition. They essentially contain pink feldspar and dark grey amphibole. At some locations, the pegmatite veins are parallel to the foliation and they contain minerals like galena and pyrite in addition to feldspars, quartz and minor mafics.

Foliation along the northern flank is generally dipping away from the pluton and that indicates an intrusive nature for the Peralimala pluton. Southern flank is almost free of foliations.

6.3.2 Megascopic petrography

The rock ranges from very coarse grained type to medium grained and both foliated and non-foliated varieties are noticed. Sample S-80/A is the most coarse grained type and in which feldspar crystals attain a maximum of 1.5cm length. The rock occurs in pink and grey colours, the latter being the dominant one. Most of the samples contain feldspar as the dominant mineral and quartz in less amounts. Mafic content of the rock varies considerably and the size of the mafic mineral crystals also changes drastically. The sample S-74/A is the most felsic sample and sample S-81/A is the most mafic sample. In S-74/A the mafic crystals are in the smallest size. All the samples show equigranular texture while in some samples (eg., S-83 /A and S-75/A) large crystals of feldspar can
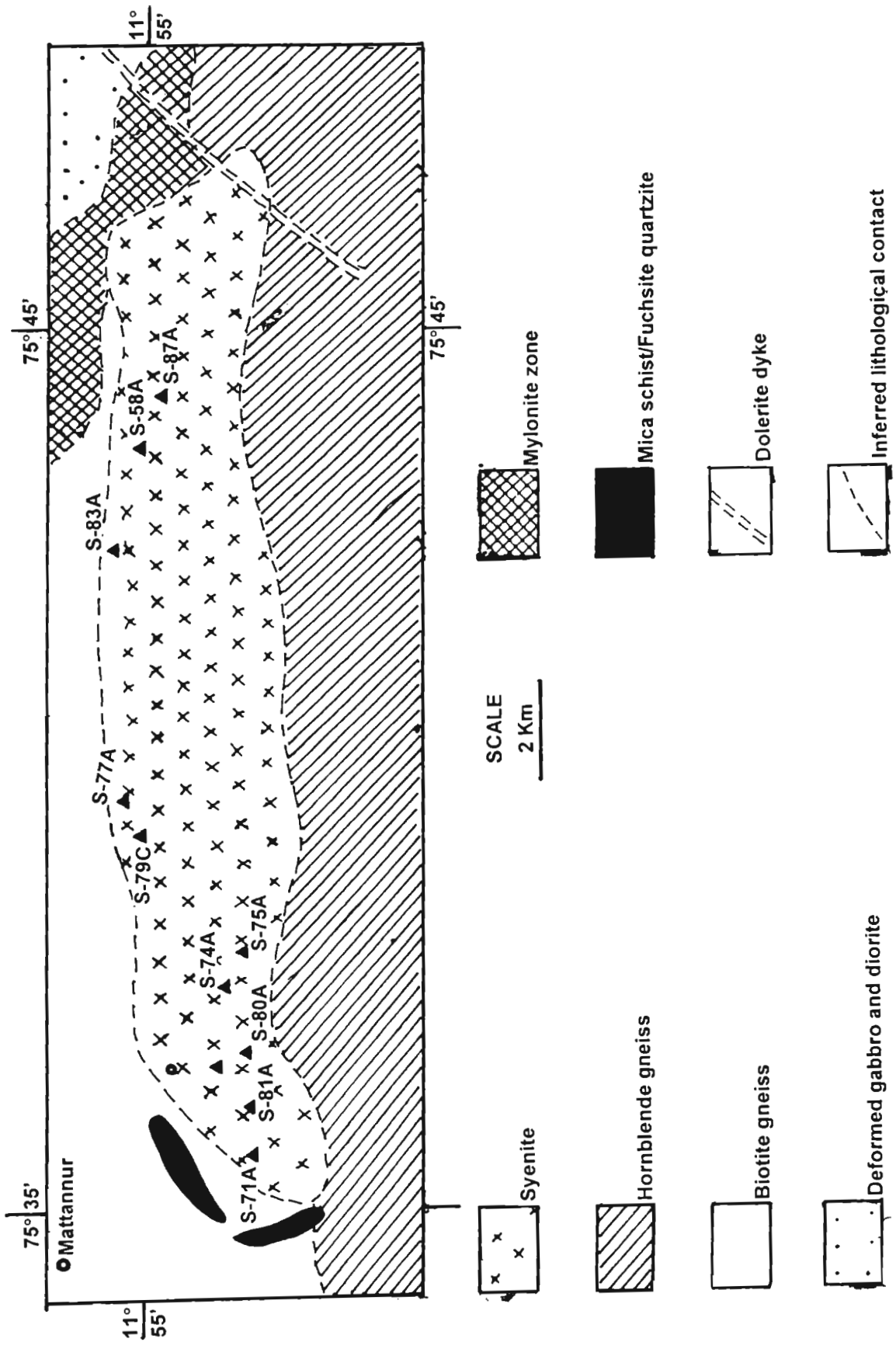
Fig. 6.26 Geological map of Peralimala syenite with the location of the
samples analyzed.

be seen (length varies from 0.5 to 0.8cm). In some samples mafic mineral clots are also noted (diameter is >1cm). The weak foliation observed in some samples is developed by the preferred orientation of prismatic crystals of mafic minerals.

6.3.3 Microscopic petrogrpahy

Most of the samples show equigranular texture. Orthoclase feldspar is the dominant mineral and they occur as anhedral to subhedral crystals. They show curved, straight and irregular grain boundaries. Some of the orthoclase crystals show perthitic texture and the exsolution lamellae are thin and spindle shaped. Small amount of plagioclase feldspar is observed and very small amount of microcline is also present. Grain boundaries of microcline are irregular and in some cases microcline shows wavy extinction. All the plagioclase crystals are small while some microcline crystals are as large as orthoclase crystals. Slightly bent twin lamellae is shown by plagioclase crystals. Some plagioclase occurs as small inclusions in orthoclase crystals. Quartz is present in very small amounts and occurs as small anhedral crystals. Quartz shows irregular grain boundaries. In samples S-19/1 and S-74/A, which are sheared rocks, recrystallized quartz can be seen and they are formed at the expense of feldspars (Fig.6.27). The recrystallized quartz crystals are euhedral and show tripple junctions of grain boundaries.

Mafic minerals include hornblende, biotite and sphene etc. Hornblende is the most abundant mafic mineral and others occur in very small amounts. Hornblende occurs as large crystals with highly irregular grain boundaries. Some of the hornblende crystals show very thin rim of epidote along their grain boundary and epidotization is probably due to shearing. Quartz and orthoclase inclusions can be seen in hornblende crystals.

A few calcite crystals are observed which are found interstitial to hornblende and orthoclase. Good amount of sphene crystals are found and they

111
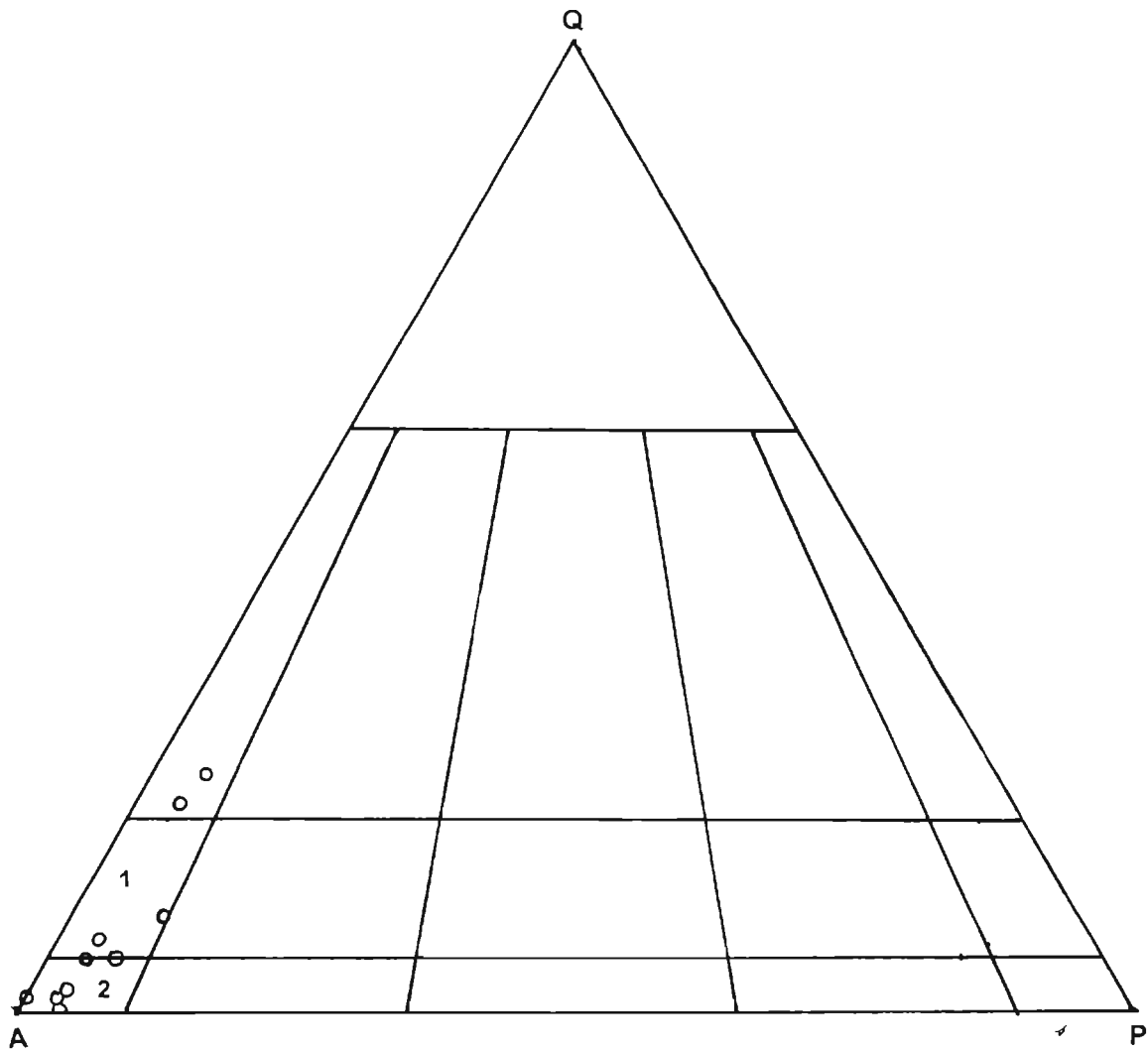
Fig. 6.28 Normative quartz(Q)-alkali feldspar(A)-plagioclase(P) diagram for Peralimala syenite. Fields: 1. Alkali feldspar-quartz-syenite, 2. Alkali feldspar-syenite, 3. Alkali feldspar granite and 4. granite(Streckiesen, 1976).

are euhedral. Sphene also occurs as inclusions in hornblende. Percentage and size of sphene varies widely. In sample S-83/A, sphene crystals are smaller and lesser in number than that in S-58/A. In S-83/A perthites are also less and exsolution lamellae are thin and faint. Apatite occurs as accessory mineral and it is found mostly as inclusion in mafic minerals and opaques. Biotite is found as an alteration product of hornblende. In some samples garnet is also found in minute quantities.

Shearing has caused textural and mineralogical changes in the rocks. S-19/1 and S-74/A are sheared rocks and in these samples large amount of recrystallized quartz is present. Their grain boundaries meet at tripple junctions. There are two generations of recrystallized quartz. These two differ in their grain size. Microcline and plagioclase are smaller than orthoclase crystals. Hornblende is seen in very small quantity and minute inclusions of apatite can be seen in hornblende crystals. Garnet is observed in those areas in thin sections where recrystallization has taken place. This indicates a reaction where hornblende is getting converted to garnet releasing quartz.

6.3.4 Major element geochemistry

Results of major element analysis and corresponding C.I.P.W norms of 11 samples of Peralimala syenite are presented in table 6.8. Their C.I.P.W normative QAP values are plotted in the triangular diagram for classification of plutonic rocks (Streckiesen, 1976) (Fig. 6.28). SiO$_2$ content of the rocks which fall in the syenite and quartz syenite field varies from 63.07 to 66.2% which corresponds to the average range of quartz in syenites. For two samples which fall in the rhyolite field in the total alkali vs silica diagram of Le Bas et al. (1986) (Fig. 6.29), the SiO$_2$ content is higher (average= 70.61%). Majority of the samples fall in the alkali feldspar syenite field. The samples fall in this field are S-74/A, S-77/A, S-80/A and S-81/A. S-75/A and S-83/A fall along the boundary between the fields of alkali feldspar syenite and quartz alkali feldspar

Table 6.8   Major element analysis (wt%) of Peralimala syenite samples with
calculated C.I.P.W norm

| Sample No.	S-58/A	S-71/A	S-74/A	S-75/A	S-77/A	S-79/C	S-80/A	S-81/A	S-83/A	S-87/A
SiO2	64.78	65.81	66.21	65.52	65.27	70.44	64.19	63.59	63.07	70.78
Al2O3	17.37	17.19	17.83	17.46	18.53	15.40	18.88	18.38	17.12	14.36
FeO	1.98	0.59	0.39	0.97	0.57	0.39	0.39	1.10	1.88	1.74
Fe2O3	1.47	0.44	0.28	0.72	0.43	0.28	0.29	0.81	1.39	1.28
MnO	0.08	0.03	0.02	0.04	0.03	0.02	0.02	0.05	0.08	0.04
MgO	0.12	0.18	0.14	0.24	0.13	0.11	0.24	0.36	0.01	0.28
CaO	2.02	0.86	0.55	1.34	0.78	0.78	0.63	1.36	2.48	0.91
Na2O	2.70	5.37	7.35	5.95	6.49	2.10	3.22	5.49	2.49	4.32
K2O	9.00	6.54	5.77	5.97	6.30	9.20	10.70	7.29	10.15	4.96
TiO2	0.25	0.10	0.05	0.13	0.06	0.04	0.18	0.16	0.29	0.26
P2O5	0.07	0.02	0.01	0.05	0.01	0.01	0.03	0.04	0.16	0.04
Norm										
	S-58/A	S-71/A	S-74/A	S-75/A	S-77/A	S-79/C	S-80/A	S-81/A	S-83/A	S-87/A
Q	9.2	7.1	1.6	5	1.5	20.9	2.7	0.2	5.3	23.3
Ap	0	0	0	0	0	0	0	0	0.3	0
Ilm	0.5	0.2	0.2	0.3	0.2	0.2	0.3	0.3	0.6	0.5
Or	53.4	38.9	33.9	35.6	37.3	54.5	63.4	43.4	60.1	29.5
Al	23.1	45.6	59.7	50.3	55	17.8	27.2	46.6	21	36.7
An	8.3	3.3	0	3.1	2.8	3.9	3.1	3.6	5.6	4.4
Hy	1.8	0.7	0	0	0.4	0.6	0.7	0.8	0	2.5
Di	1.5	0.7	1.4	3	0.9	0	0	2.6	3.5	0
Wo	0	0	0.5	0	0	0	0	0	0.8	0
Mt	2.1	0.7	0.5	1.2	0.7	0.5	0.5	1.2	2.1	1.9
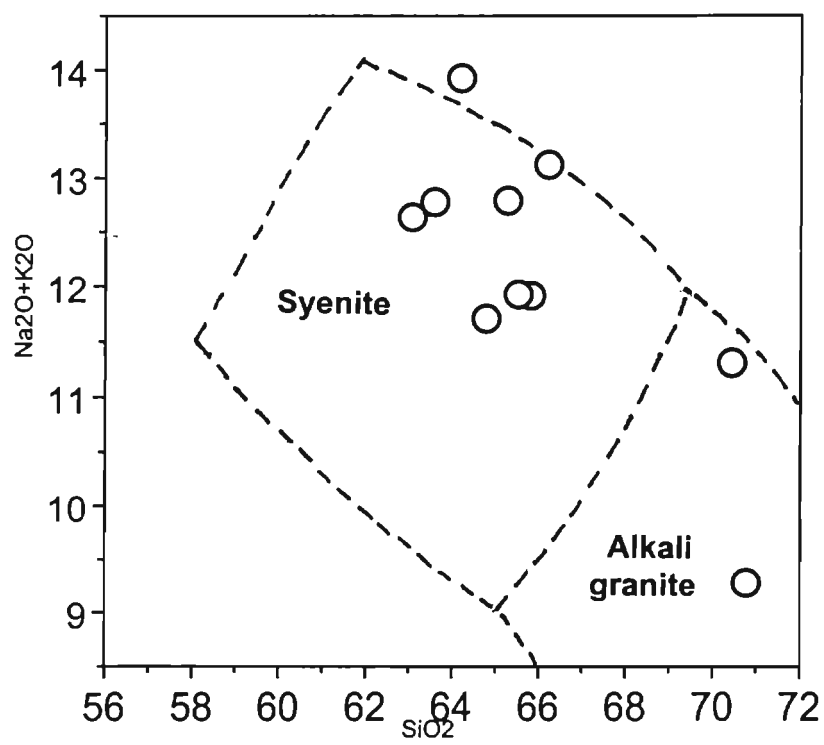
Fig. 6.29 SiO2 vs Na2O+K2O diagram of Peralimala syenite samples
for the nomenclature of igneous rocks(Cox et al.,1979).

syenite. S-19/1 and S-58/A fall in the quartz alkali feldspar syenite field. Samples S-79/C and S-87/A fall in the alkali granite field. From QAP diagram it is clear that the pluton has an overall syenitic chemistry. This is consistent with the mode of the rocks discussed earlier. Normative and modal content of plagioclase feldspar is very much lesser than that of alkali feldspar. CIPW normative values of An, Ab and Or are plotted in the An-Ab-Or modified O'Connor diagram (Barker, 1979) (Fig. 6.30).

Total alkali vs silica diagram of Le Bas et al. (1988) (Fig. 6.29) and QAP diagram (Fig. 6.28) can be compared. Samples plotted in the syenite field of QAP diagram fall in the syenite field of figure 6.28.. Samples plotted in the alkali feldspar granite field of QAP fall in the granite field. Thus the Peralimala pluton can be considered as a syenite body with minor granitic differentiates.

6.3.5 Trace element geochemistry

Trace element concentrations are given in table 6.9. Of the four samples analyzed for trace elements, samples S-19/1 and S-74/A show depletion in all trace elements relative to other two samples. Petrographically these samples are found to be sheared and the shearing might have caused majority of their trace elements to be moved out of the system. Average Ba content of unsheared samples is 4700ppm and the sheared samples have an average Ba content of 764ppm. This higer content of Ba can be attributed to high content of K_2O. Ba decreases with increase in SiO_2 and has a maximum value of 4997 ppm. Rb content is not varying much and a maximum value 103ppm is observed in sample S-83/A in which K_2O content is very high (10.15%). This may be due to the fact that Rb fractionates strongly into potash feldspars. Ba/Sr ratio of the unsheared samples is almost same (2.18 and 2.75) while that of sheared sample is having an average value of 0.707. Higher content of Sr can be attributed to higher content of CaO. Among HFSE, Ta is the least abundant element and it ranges from 0.29 to 1.27ppm. The rock is more enriched in LILE than HFSE. Zr/Hf ratio ranges from 37.5 to 56.7ppm with an average value of

113

Table 6.9 Trace element concentrations (ppm)
of Peralimala syenite samples

Samle No.	S-19/1	S-58/A	S-74/A	S-83/A
V	38.48	143.17	61.22	156.87
Cr	20.51	44.85	20.27	33.43
Co	1.07	6.05	0.98	4.78
Ni	7.99	25.28	12.50	19.88
Cu	18.69	58.03	1.70	14.00
Zn	56.37	324.79	32.75	371.48
Ga	22.36	15.03	29.91	14.49
Rb	160.86	97.69	92.84	103.48
Sr	1227.25	2012.99	736.29	1812.17
Y	5.36	20.02	4.49	25.75
Zr	47.05	24.00	42.05	58.41
Nb	5.77	12.39	11.83	19.24
Cs	1.39	0.33	0.82	0.51
Ba	1007.31	4402.91	521.21	4997.18
Hf	1.06	0.64	1.02	1.03
Ta	0.21	0.74	0.29	1.27
Pb	20.08	16.67	13.03	17.80
Th	1.90	2.37	1.94	3.48
U	1.03	0.53	1.20	1.08

Table 6.10 Rare earth element concentrations
(ppm) of Peralimala syenite samples

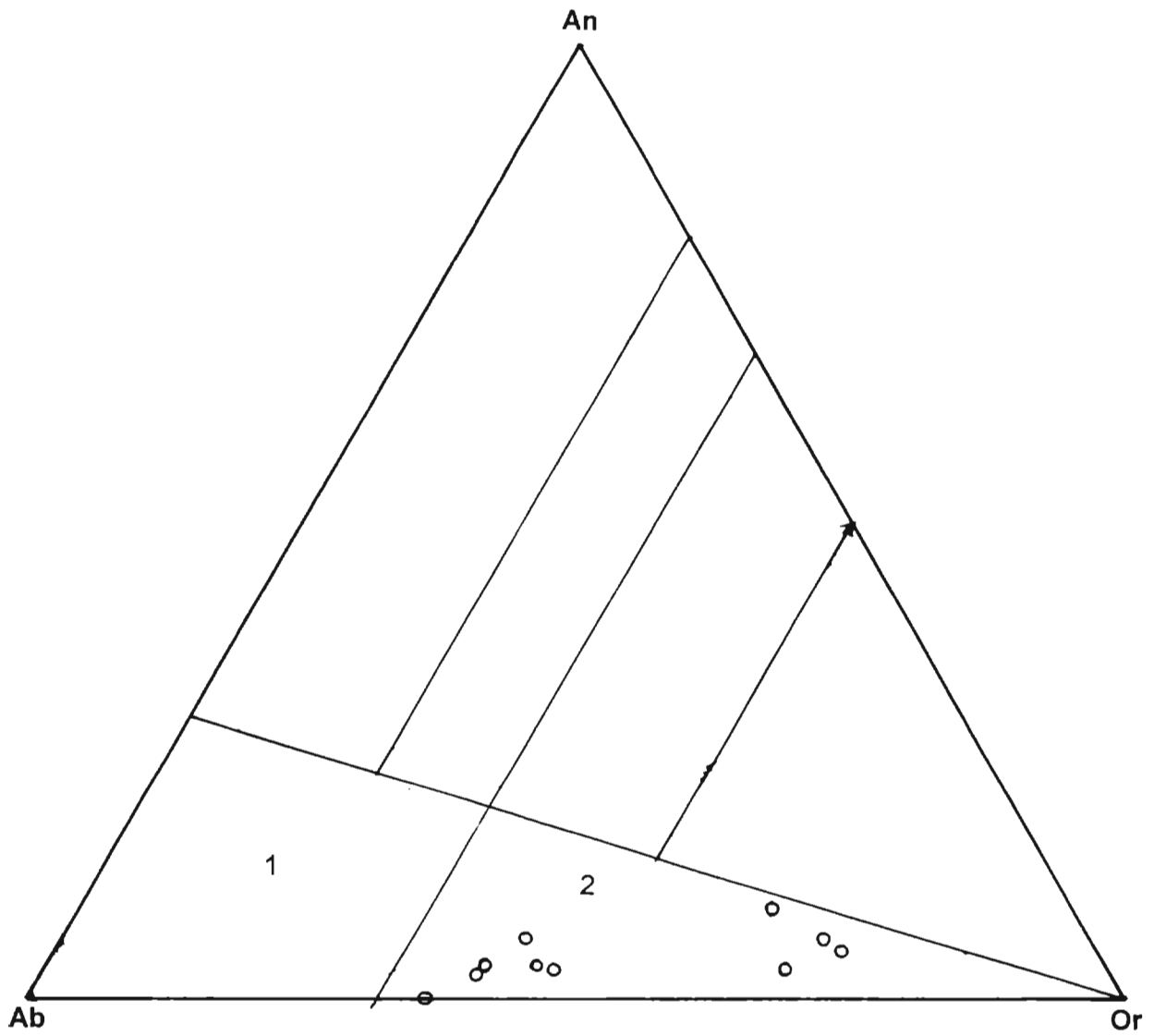| Sample No.	S-19/1	S-58/A	S-74/A	S-83/A
La	2.59	18.99	0.00	24.42
Ce	9.99	36.83	5.63	46.42
Pr	0.65	2.84	0.45	3.50
Nd	3.87	19.87	2.39	25.83
Sm	0.91	4.54	0.69	5.58
Eu	0.57	1.89	0.26	2.55
Gd	0.47	2.81	0.26	4.35
Tb	0.07	0.50	0.03	0.65
Dy	0.85	3.27	0.51	4.28
Ho	0.15	0.62	0.13	0.80
Er	0.51	1.57	0.41	2.01
Tm	0.05	0.31	0.06	0.31
Yb	0.64	1.54	0.61	2.13
Lu	0.08	0.23	0.08	0.31

Fig. 6.30 Normative albite(Ab)-anorthite(An)-orthoclase(Or) diagram for
Peralimala syenite. Fields: 1. Trondhjemite and 2. Granite (fields after O'
Connor, 1965).

45.14ppm. Ni content varies from 12 to 25ppm with an average value of 19ppm. Cr has a value of 33ppm. Cr increases with increase in MgO and decreases with increase in SiO_2. Sc does not show much variation in the samples S58/A and S-83/A and it has an average value of 5.87ppm. Th/U ratio ranges from 1.62 to 4.97ppm. In all the samples Th content is higher than that of U. Ga concentrations in the S-58/A and S-83/A are almost same and the average value is 14ppm. Average Ga concentration in S-19/1 and S-74/A is 26ppm. There is no significant Ga enrichment relative to Al.

REE concentrations are given in table 6.10. Peralimala syenite samples S-58/A and S-83/A have higher REE content. Compared to these two samples, S-19/1 and S-74/A show lesser content of REE. Sphene content is very less in these samples. It is well known that minerals like sphene and allanite can drastically concentrate the REE (Henderson, 1983). The chondrite normalized REE pattern (Fig. 6.31) is showing a positive Eu anomaly. $(La/Yb)_N$ value is almost same for samples S-58/A and S-83/A. Compared to these samples S-19/1and S-74/A have lower values of this ratio. $(La/Sm)_N$ and $(Gd/Yb)_N$ ratios also do not show any variation except for the samples S-19/1 and S-74/A for which the ratios are very less. Degree of fractionation is more pronounced in LREE.

6.3.6 Chemical grouping and tectonic discrimination

Based on the discriminant diagrams like 10^4 *(Ga/Al) vs FeO/MgO, 10^4 *(Ga/Al) vs K_2O/MgO and 10^4 *(Ga/Al) vs K_2O+Na_2O it is found that, the Peralimala syenite can be called as an A-type granitoid (fields of A-type and M-, I- and S-type granitoids are after Whalen et al. (1987) (Fig.6.32).

Tectonic discrimination diagrams like SiO_2 vs Nb, SiO_2 vs Rb and Y vs Nb were also prepared (Fig. 6.33). Peralimala samples fall in the volcanic arc granite(VAG)+collision granite(COLG)+ocean ridge granite(ORG) field of the SiO_2 vs Nb diagram. They fall in the VAG field of SiO_2 vs Rb diagram and
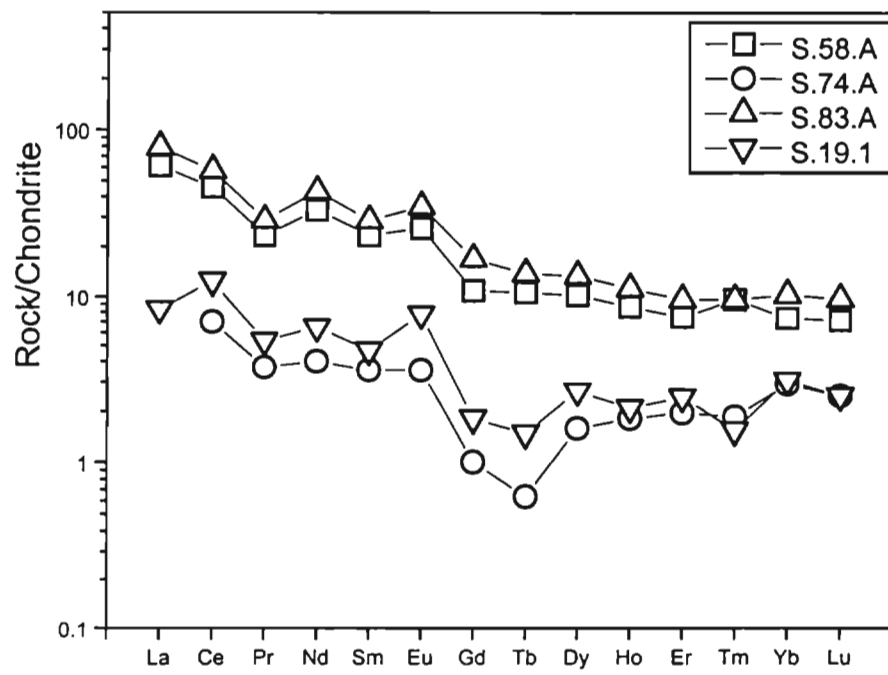
Fig. 6.31 Chondrite-normalized REE patterns of Peralimala syenite
samples. Normalization values are taken from Brynton (1984).

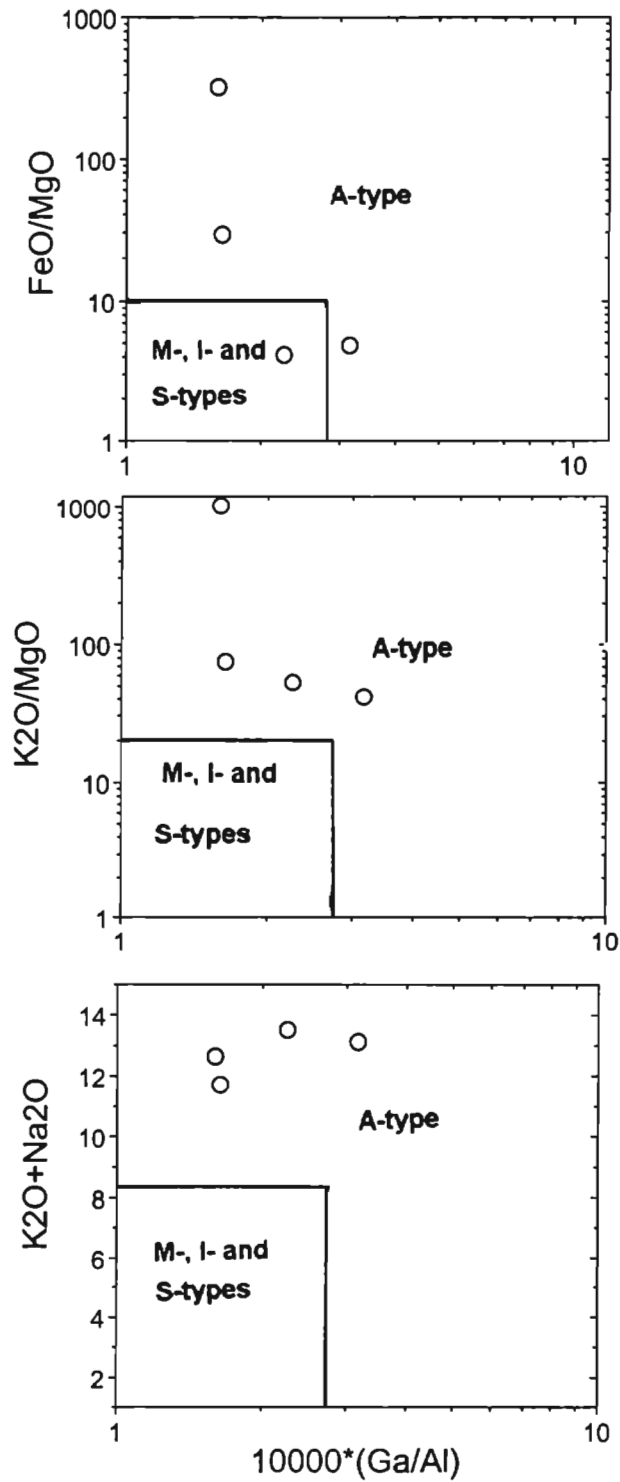Fig. 6.32 10000*(Ga/Al) vs FeO/MgO,   10000* (Ga/Al) vs K2O/MgO
and 10000*(Ga/Al) vs K2O+Na2O diagrams for Peralimala syenite.
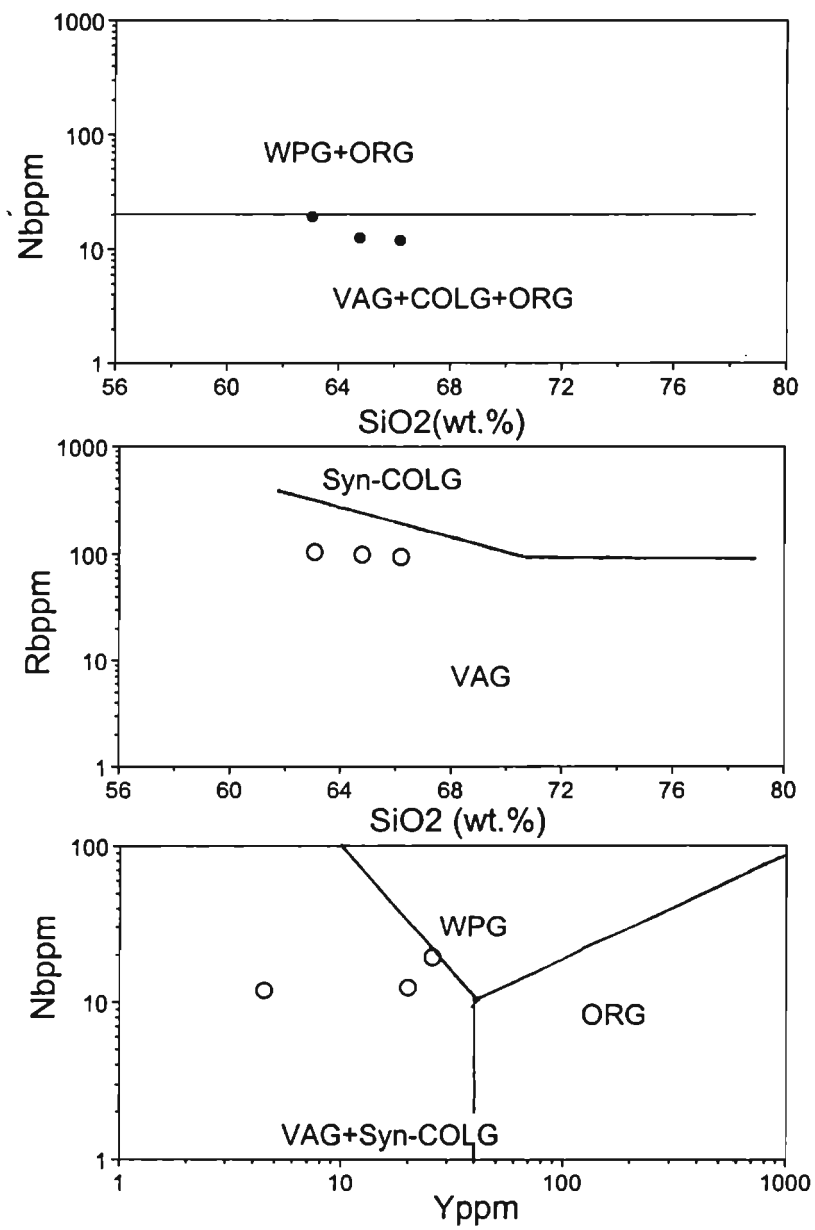Fields after Whalen et al. (1987).

Fig. 6.33 Tectonic discrimination diagrams for Peralimala syenite

Y+Nb vs Rb diagram. In the Y vs Nb diagram, they fall in the VAG+syncollision granite field.

Major element chemistry was used in multivariate discriminant analysis (Agrawal,1995) to successively distinguish late-orogenic (LO) form post-orogenic (PO) granites related to orogeny as well as the anorogenic granites in the anorthosite/rapakivi complexes (AR) and the alkaline ring complexes (RC). The Peralimala syenite samples were assigned to the group of anorogenic granites.

Thus from the chemical grouping it is seen that the Peralimala syenite is showing A-type character. From the tectonic discrimination, it is seen that this is anorogenic with a probable volcanic arc/collision setting.

6.3.7 Petrogenesis

Major elements like TiO_2 K_2O, Na_2O, MgO, Al_2O_3 and CaO are plotted against SiO_2 and differentiation index(DI) to assess the fractionation trends (Fig. 6.34 and 6.35). K_2O, TiO_2, CaO and P_2O_5 show a decreasing trend with both SiO_2 and DI. Decreasing trend of TiO_2 and P_2O_5 may be due to the early crystallization of accessory minerals. CaO is showing a decreasing trend and that may be due to the early fractionation of plagioclase feldspars. Decreasing trend of K_2O indicates that at the late stages of crystallization, K-feldspar was not a dominant phase. Increasing trend of Na_2O implies that the feldspar fractionated at the late stages were of more sodic in composition. MgO and Al_2O_3 show a decreasing trend with SiO_2 while an increasing trend is shown with DI. Na_2O shows an increasing trend with both SiO_2 and DI and thus K_2O and Na_2O are inversely related. So, the rocks of Peralimala syenite are related by fractional crystallization involving alkali feldspar, amphibole and quartz as dominant phases or by generation of felsic melt by partial melting.

Ba/Sr ratio of Peralimala samples do not vary much and that indicates consanguinity. Rb, Sr and Ba show a decreasing trend with increasing SiO_2.
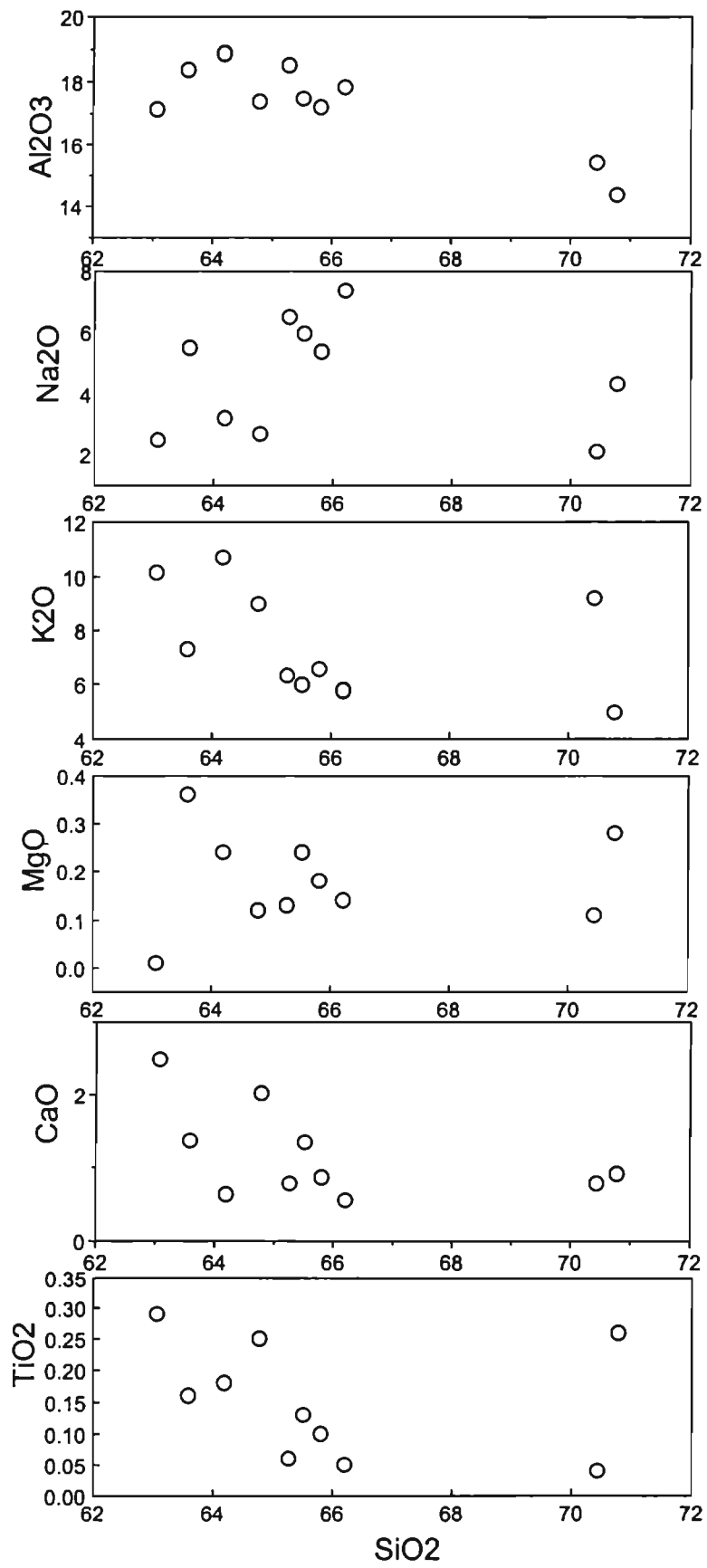
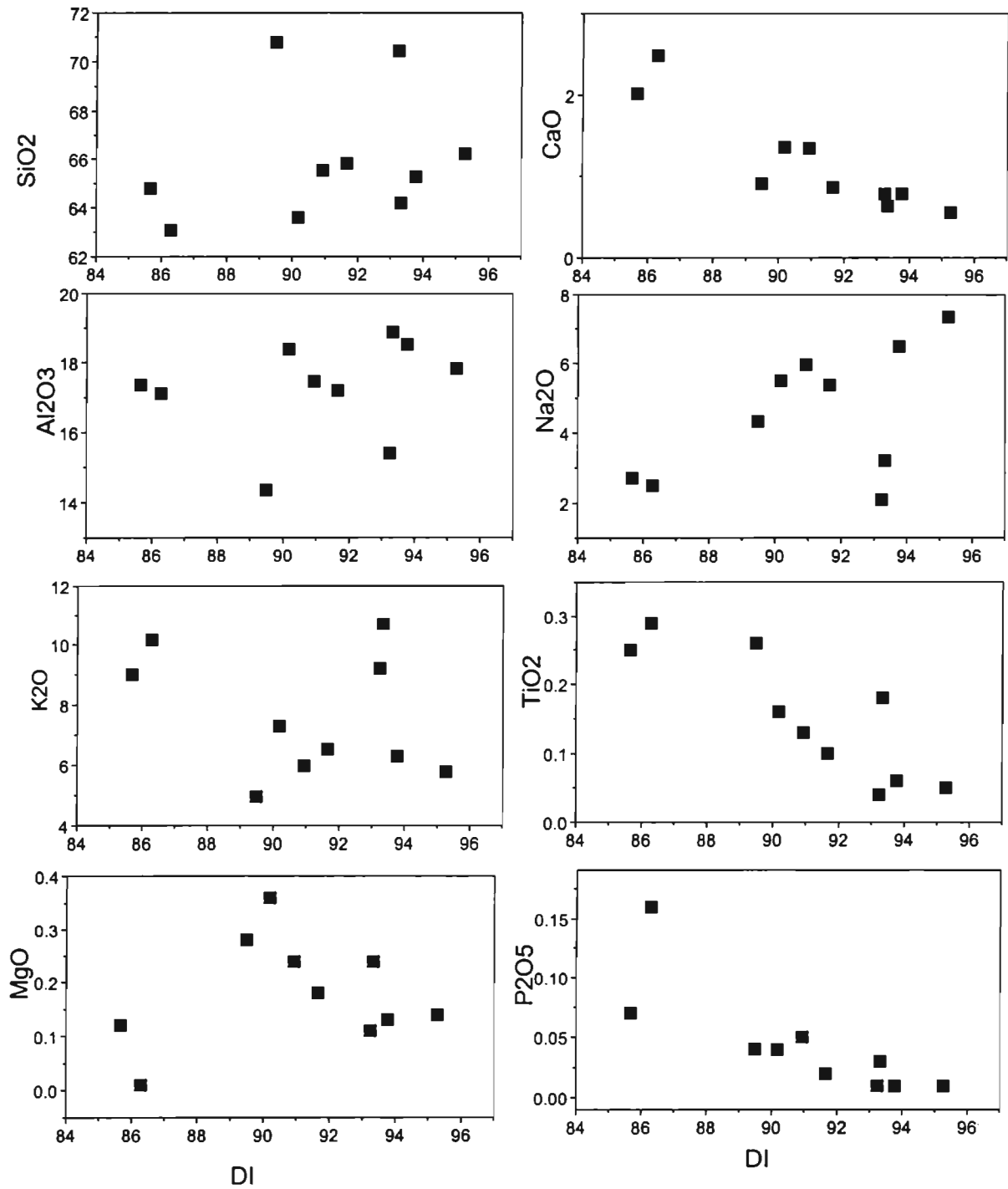Fig. 6.34   Variation of major element oxides of Peralimala syenite with SiO2.

Fig. 6.35 Diagrams showing the variation of major element oxides
of Peralimala syenite samples with differentiation index (DI) of Thornton
and Tuttle (1960). (DI= normative quartz+orthoclase+albite+nepheline+
Leucite+kaliophilite)

This is consistent with the decreasing trend shown by K_2O. Sr shows an increasing trend initially and then decreases at higher levels of SiO_2. This could be due to the early fractionation of Ca-bearing minerals like apatite and pyroxene.

Spider diagram (Fig.6.36) of trace elements normalized by primitive mantle values produced similar pattern for the samples S-58/A and S-83/A. The pattern is highly rugged and therefore single step evolution from mantle can be ruled out. LIL elements are about 100 times that of mantle and the refractory elements like Ta, Nb, Y and HREE are higher than that of mantle. These features also indicate a source other than mantle. Mg/Mg+Fe values are very less with an average value of 0.109 and it varies from 0.023 to 0.232. High content of Sr and low Mg/Mg+Fe levels precludes a fractional crystallization from a basic magma. Thus a partial melting of pre-existing crustal rocks or a residue left after an extensive fractional crystallization from mafic or intermediate magma can be assumed for Peralimala syenite.

6.4 Diorites

The diorites associated with Perinthatta anorthosite include Karikkottakkari diorite and Adakkathod diorite (Fig. 6.1). The geological map of Karikkottakkari diorite is given in figure 6.37 Adakkathod diorite was not mapped because of the lack of exposures. Karikkottakkari diorite is foliated (dipping 20° due NW) in almost all the locations while Adakkathod diorite is generally massive with a slight porphyritic texture. Numerous enclaves of mafic patches rich in biotite are seen in both of these diorites. Garnet is seen developed in folation planes of Karikkottakkari diorite at some locations.

6.4.1 Petrography

Karikkottakkari diorite is grey to dark grey in colour and Adakkathod diorite is light grey in colour. Both these rocks are coarse grained. Plagioclase is the most dominant felsic mineral and biotite is the most dominant mafic mineral in Karikkottakkari diorite. Small amount of hornblende is also observed in it. In the
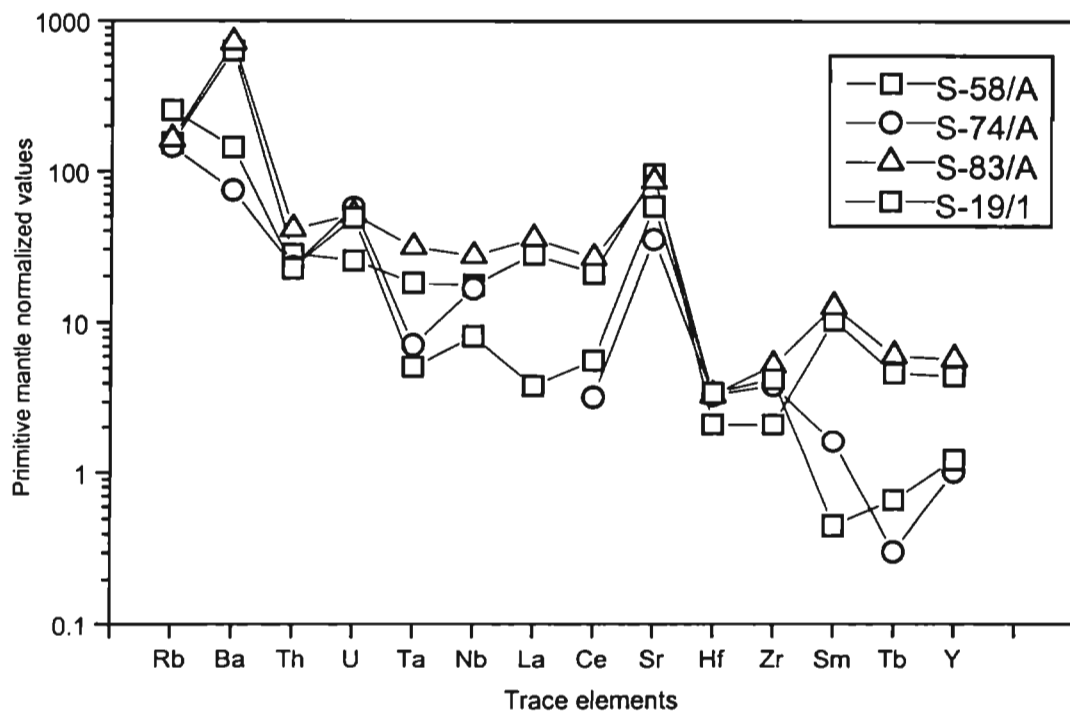
116

Fig. 6.36 Primitive mantle-normalized trace elelment pattern of Peralimala syenite samples. Normalization values are from Sun and McDonough, 1989.
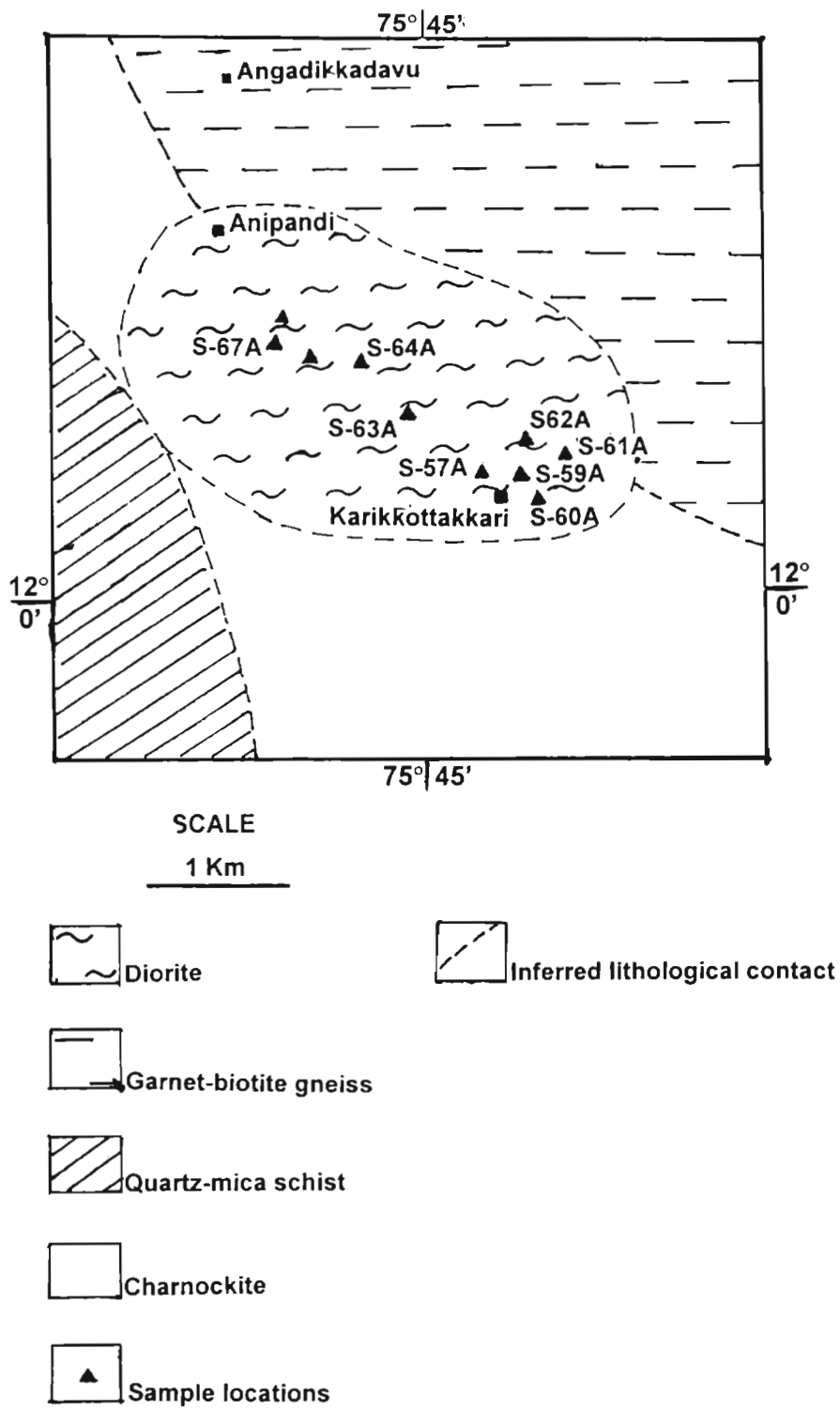
Fig. 6.37 Geological map of Karikkottakkari diorite with the locations of the samples analyzed.

case of Adakkathod diorite, alkali feldspar is also present in good amounts. Mafic minerals in Adakkathod diorite include biotite and hornblende.

Microscopically, all the samples of Karikkottakkari diorite exhibit equigranular texture. Biotite is the most dominant mafic mineral and foliation is developed by the preferred orientation of secondary biotite flakes after hornblende. Hornblende is present in all the samples in minor amounts. In Adakkathod diorite also, hornblende shows alteration to biotite. Plagioclase feldspar is the dominant felsic mineral in both Karikkottakkari and Adakkathod diorites. In these two diorites, composition of plgioclase is in oligoclase to labrodorite range. Alkali feldspar (both microcline and orthoclase) is present in both the diorites but it is slightly more in Adakkathod diorite. Perthites and small amount of quartz are seen in Karikkottakkari diorite.

6.4.2 Major element geochemistry

Eight samples of Karikkottakkari diorite and two samples of Adakkathod diorite were analyzed for major elements and the results along with the corresponding C.I.P.W norms are given in table 6.11. The Karikkottakkari diorite samples fall in the diorite field and Adakkathod rock samples fall in the quartz diorite/granodiorite field of diagram for nomenclature of normal igneous rocks (Fig. 6.38).

SiO$_2$ content of Karikkottakkari diorite ranges from 56.96% to 69.71% with an average of 64% while the average SiO$_2$ content of Adakkathod diorite is 70%. Al$_2$O$_3$ content of Karikkottakkari diorite ranges from 14.75 to 18.03% and the average Al$_2$O$_3$ content in Adakkathod diorite is 16%. FeO content is higher in Karikkottakkari diorite than Adakkathod diorite. Average MgO content of Karkkottakkari diorite and Adakkathod diorite is 1.3 and 1.6% respectively. MnO is very less and it is less than 1% for the rocks. CaO for Karikkottakkari diorite is varying from 3.45 to 6.34% while the average CaO content in Adakkathod diorite is 4%. In both the rocks P$_2$O$_5$ and TiO$_2$ content is less than unity.

Table 6.11 Major element analyses (wt%) of Karikkottakkari diorite and Adakkathod diorite
with calculated C.I.P.W norms.

| Sample No.	Karikkottakkari diorite								Adakkathod diorite	
	S-57/A	S-59/A	S-60/A	S-61/A	S-62/A	S-63/A	S-64/A	S-67/A	S-101/B	S-103/B
SiO2	68.19	64.24	60.94	67.41	57.85	69.71	67.52	56.96	68.07	71.28
Al2O3	16.20	16.53	15.41	16.49	18.03	15.60	15.27	14.75	16.18	15.79
FeO	2.66	3.18	5.21	2.97	3.14	1.75	2.50	6.59	2.00	1.26
Fe2O3	1.35	1.62	2.65	1.51	1.59	0.89	1.27	3.35	0.79	0.49
MnO	0.06	0.07	0.09	0.07	0.16	0.02	0.05	0.13	0.05	0.03
MgO	0.16	1.35	1.43	0.43	3.01	0.76	0.93	2.05	2.67	0.58
CaO	4.83	4.96	5.14	4.61	6.80	3.45	4.27	6.37	4.81	3.29
Na2O	2.46	3.88	3.69	2.56	3.11	3.62	3.74	3.43	3.09	3.12
K2O	1.90	2.25	1.81	1.94	1.73	2.89	2.13	2.12	1.53	2.28
TiO2	0.53	0.57	1.28	0.55	2.05	0.36	0.49	1.93	0.25	0.19
P2O5	0.26	0.24	0.36	0.28	0.77	0.12	0.21	0.74	0.26	0.04
Norm										
	S-57/A	S-59/A	S-60/A	S-61/A	S-62/A	S-63/A	S-64/A	S-67/A	S-101/B	S-103/B
Q	35.5	19.8	18.7	33.9	15.8	28.7	26.5	13	29.6	35.9
Ap	0.6	0.6	0.9	0.6	1.6	0.3	0.3	1.6	0.6	0
Ilm	1.1	1.1	2.4	1.1	4	0.8	0.9	3.6	0.5	0.3
Or	11.1	13.3	10.6	11.7	10	17.2	12.8	12.8	8.9	13.3
Al	21	33	31.4	21.5	26.2	30.4	31.4	28.8	26.2	26.2
An	22	20.9	20	20.9	29	16.4	18.6	18.6	22	16.4
Hy	3.4	6.3	7.7	4.5	8.8	3.6	4.5	8.1	9.5	3.2
Di	0	1.6	2.3	0	0	0	1.4	7	1.2	0
Wo	0	0	0	0	0	0	0	0	0	0
Mt	1.9	2.3	3.9	2.1	2.3	1.4	1.9	4.9	0	0.7
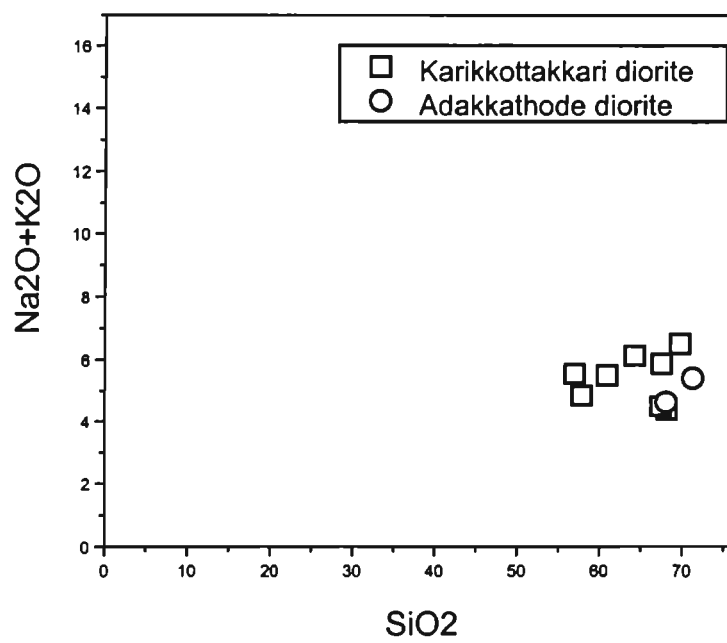
Fig. 6.38 SiO2 (wt%) vs Na2O+K2O (wt%) diagram (after Cox et al. 1979
for the nomenclature of igneous rocks showing the plots of Karikkottakkari
and Adakkathode.

6.4.3 Trace element geochemistry

Two samples each were analyzed for their trace element contents for Karikkottakkari diorite (S-57/A and S-61/A) and for Adakkathod diorite (S-101/B and S-103/B). The results are given in table 6.12. There is not much difference in the trace element abundance between the samples of the same pluton, but there exists certain differences between the two plutons.

Ba contents of Karkkottakkari diorite (average=660ppm) is less than those of Adakkathod diorie (average= 746ppm). Rb content is slightly higher in Karikkottakkari diorite. Sr content is very high (1030ppm) in one of the Adakkathod diorite sample (S-103/B) and this can be attributed to the high content of CaO in that sample. Average Ba/Sr ratio of Karikkottakkari diorite is 0.9 and that of Adakkathod diorite is 0.8. Among HFSE, Ta is the least abundant in both the rocks and they are more enriched in LILE than HFSE. Zr/Hf ratio is almost same for these two rocks. Average Th/U ratio of Karikkottakkari diorite is 36 and that of Adakkathod diorite is 9.

REE concentrations of the four analyzed samples are given in table 6.13 and their chondrite normalized patterns are given in figure 6.39. For Karikkottakkari diorite the chondrite normalized abundance is almost same in both the samples. This is the case of Adakkathod diorite also but its abundance is slightly less than that of Karikkottakkari diorite. Average $(La/Yb)_N$ ratio of Karikkottakkari diorite is 35 and that of Adakkathod diorite is 78. $(Ce/Yb)_N$ ratio ranges from 20 to 23. $(La/Sm)_N$ ratio of these rocks differ very much. This ratio is very high for adakkathod diorite (average 48) and this indicates the higher degree of fractionation among LREE. $(Gd/Yb)_N$ ratio is almost same for the all the rocks.

Table 6.12 Trace element concentrations (ppm)
Karikkottakkari and Adakkathod diorites

Sample No	Karikkottakkari diorite		Adakkathod diorite	
	S-57/A	S-61/A	S-101/B	S-103/B
V	66.22	72.03	64.38	60.02
Cr	94.56	76.08	76.02	119.07
Co	9.74	9.68	6.61	4.04
Ni	47.35	42.23	49.75	56.21
Cu	9.07	7.04	12.53	6.62
Zn	103.41	102.27	76.70	88.66
Ga	24.58	23.20	26.28	22.57
Rb	38.60	37.22	27.55	27.65
Sr	729.16	684.40	851.35	1030.13
Y	19.20	20.70	9.12	6.26
Zr	5.58	2.78	5.75	18.08
Nb	11.77	10.96	3.29	3.52
Cs	0.46	0.53	2.25	0.95
Ba	669.69	651.43	487.74	1005.22
Hf	0.24	0.07	0.16	0.56
Ta	0.49	0.42	0.13	0.27
Pb	12.20	11.68	19.29	21.72
Th	9.03	13.15	5.47	14.25
U	0.33	0.30	0.84	1.26

Table 6.13 Rare earth element concentrations (ppm) of
Karikkottakkari and Adakkathod diorite samples

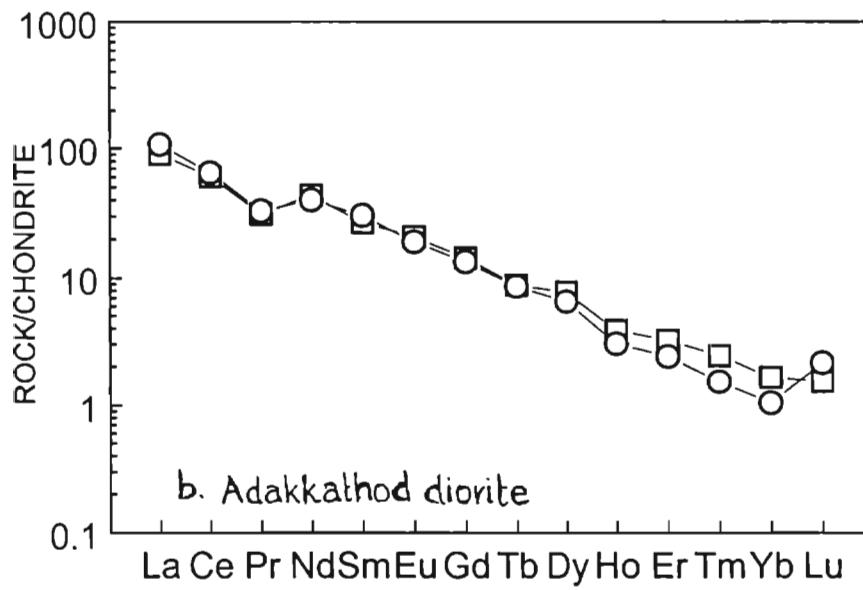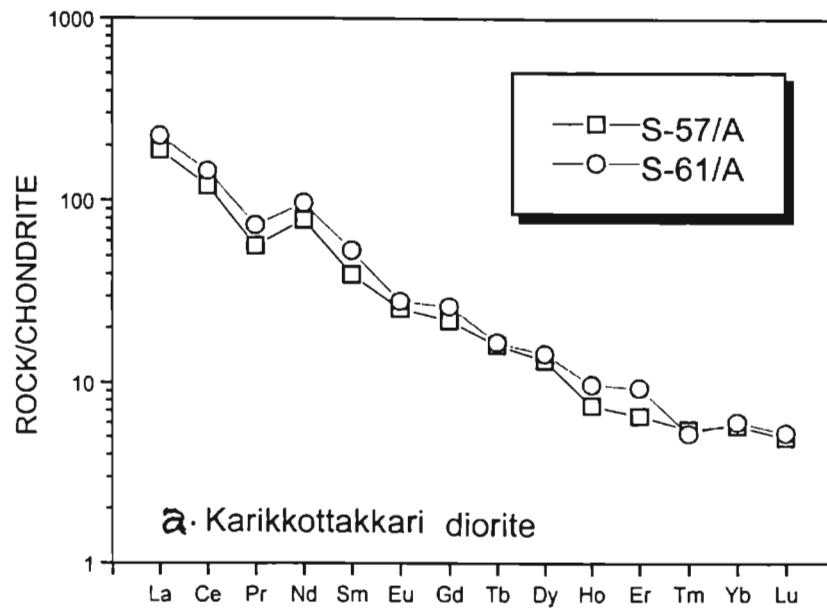|	S-57/A	S-61/A	S-101/B	S-103/B
La	58.72	69.93	28.18	33.30
Ce	97.15	117.23	49.17	52.48
Pr	6.92	8.97	3.82	4.04
Nd	47 19	58.22	26.06	23.99
Sm	7.73	10.41	5.26	5.93
Eu	1.88	2.07	1.53	1.10
Gd	5.69	6.82	3.70	3.47
Tb	0.76	0.79	0.42	0.41
Dy	4.26	4.63	2.52	2.13
Ho	0.54	0.70	0.28	0.22
Er	1.38	1.97	0.68	0.51
Tm	0.18	0.17	0.08	0.05
Yb	1.21	1.27	0.35	0.22
Lu	0.16	0.17	0.05	0.07

Fig. 6.39   Chondrite-normalized REE patterns of Karikkottakkari and Adakkathod diorites. Chondrite values are taken from Brynton,1984

6.4.4 Petrogenesis

Major elements like TiO_2 K_2O, Na_2O, MgO, Al_2O_3 and CaO of both the diorites are plotted against SiO_2 to assess the fractionation trends (Fig. 6.40). Samples of Karkkottakkari diorite show decreasing trend in the case of TiO_2, P_2O_5, CaO, and MgO with increase in SiO_2. For Adakkathod samples the trend is not clear as there are only two samples. Nevertheless, the two plots follow the trend of Karikkottakkari samples. The decreasing trend of TiO_2 and P_2O_5 may due to the early crystallization of accessory minerals with these oxides as major components. CaO is showing a decreasing trend and that may be indicating that plagioclase feldspar fractionation was a major process during early crystallization. The decreasing trend shown by MgO indicates early fractionation of mafic minerals. K_2O, Na_2O and Al_2O_3 do not show clear cut trends with change in SiO_2.

These major elements were plotted against MgO also (Fig. 6.41). SiO_2 and Al_2O_3 show a decreasing trend in both the rocks. This trend is consistent with early fractionation of mafic minerals. The increasing trends shown by TiO_2, P_2O_5 is consistent with decreasing trend shown when they were plotted against SiO_2. The increasing trend shown by CaO indicates the fractionation of plagioclase feldspars along with mafic minerals.

Magma type and evolutionary path in mafic rocks can be identified by the relations between FeO(t)/MgO versus FeO(t) and TiO_2 (Miyashiro, 1973) (Fig. 6.42 a & b). Except two samples all other samples show iron enrichment trend typical of tholeiitic suites.

Primitive mantle normalized patterns of incompatible elements of Karikkottakkari and Adakkathod diorites are almost similar (Fig. 6.43). The patterns are similar to those of continental tholeiite, though the values of Rb,Th, K, Sr and P are slightly higher than those in tholeiite. Among moderately incompatible elements Zr and Ti show negative anomalies. These features are

119
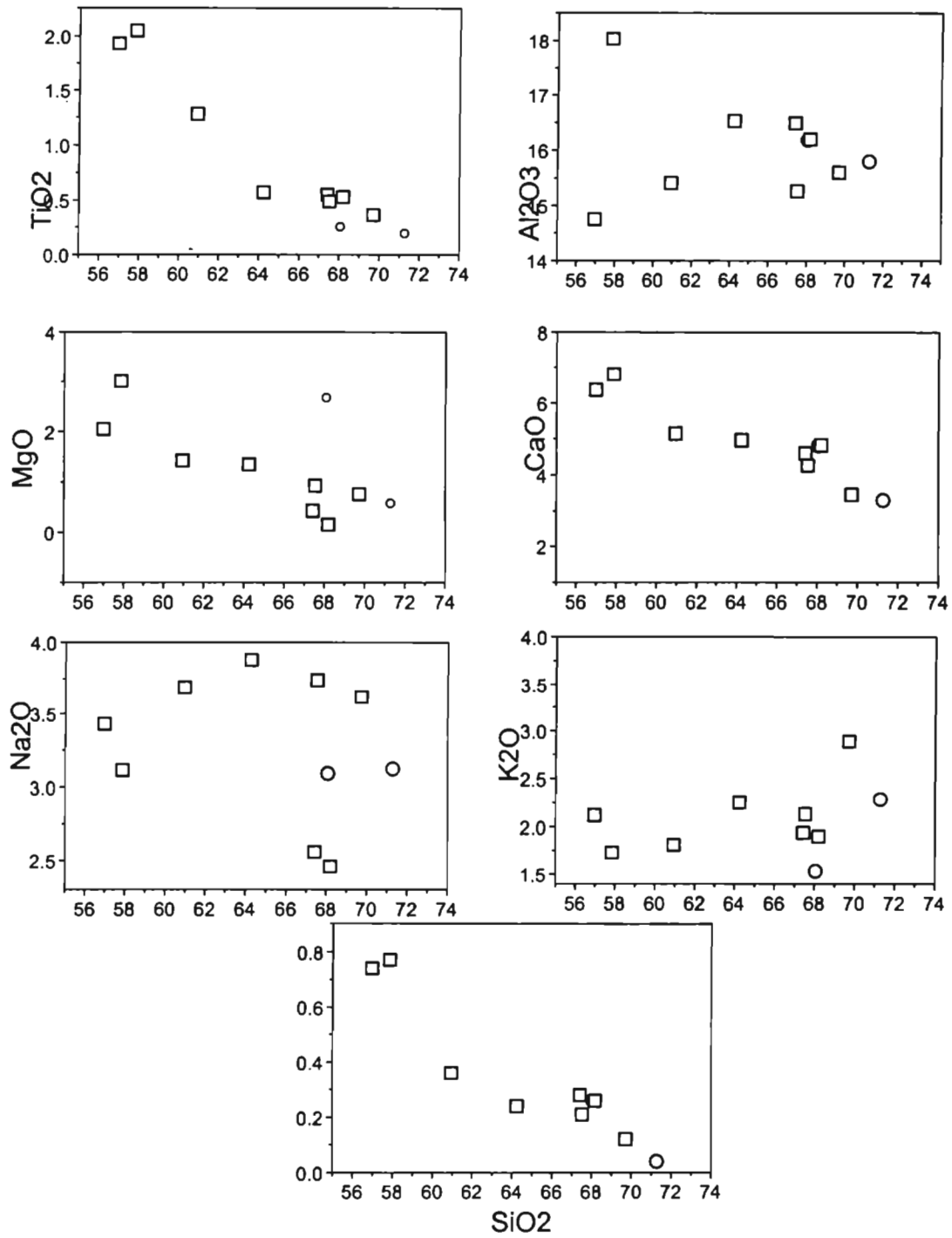
Fig. 6.40 Diagrams showing the variation of major elements with SiO2 in Karikkottakkari and Adakkathod diorites. Symbols as in figure 6.38.
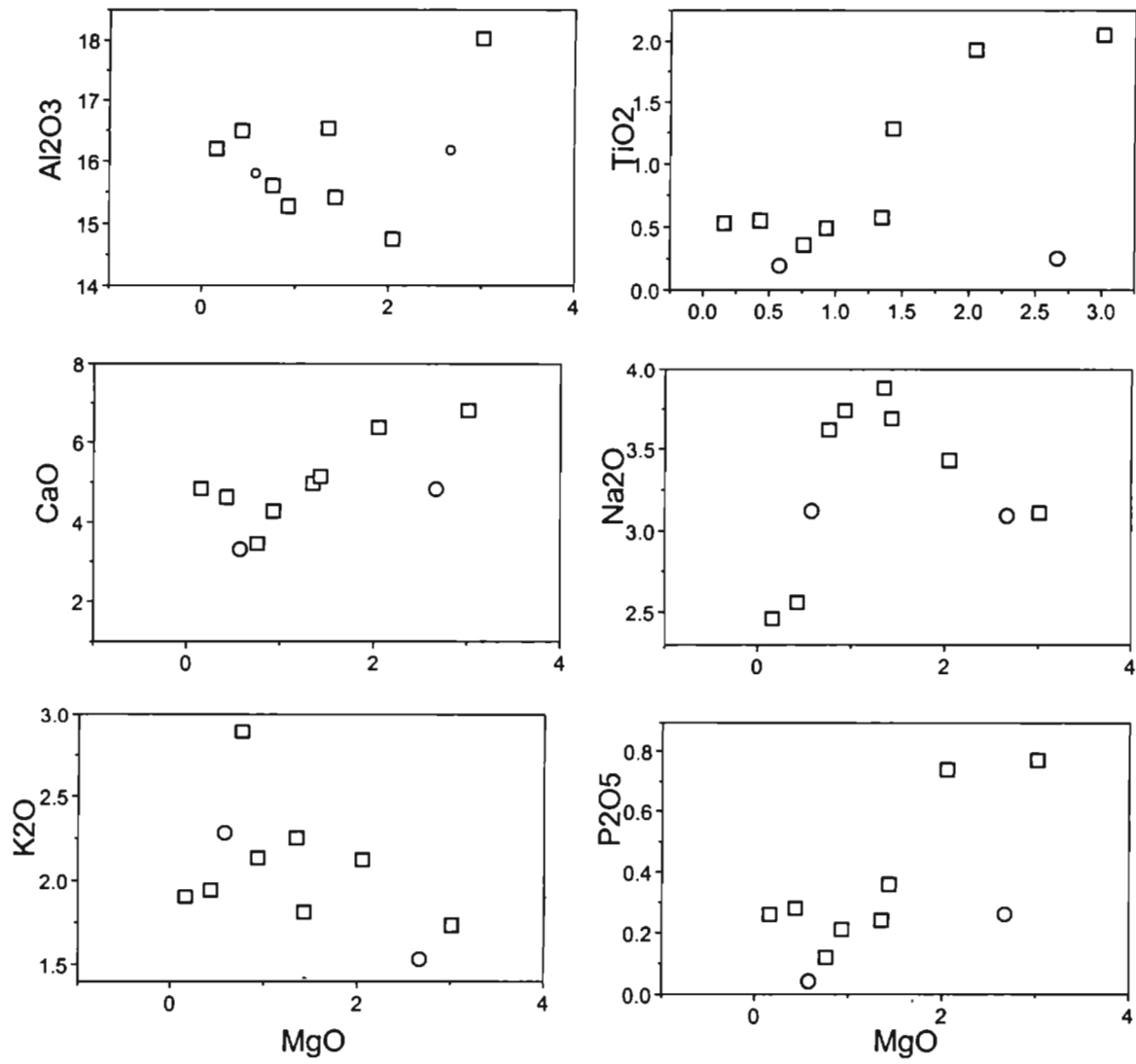
Fig. 6.41   Diagrams showing the variaition of major elements(wt%) of Karikkottakkari and Adakkathode diorites with MgO (wt%). Symbols as in figure 6. 38.
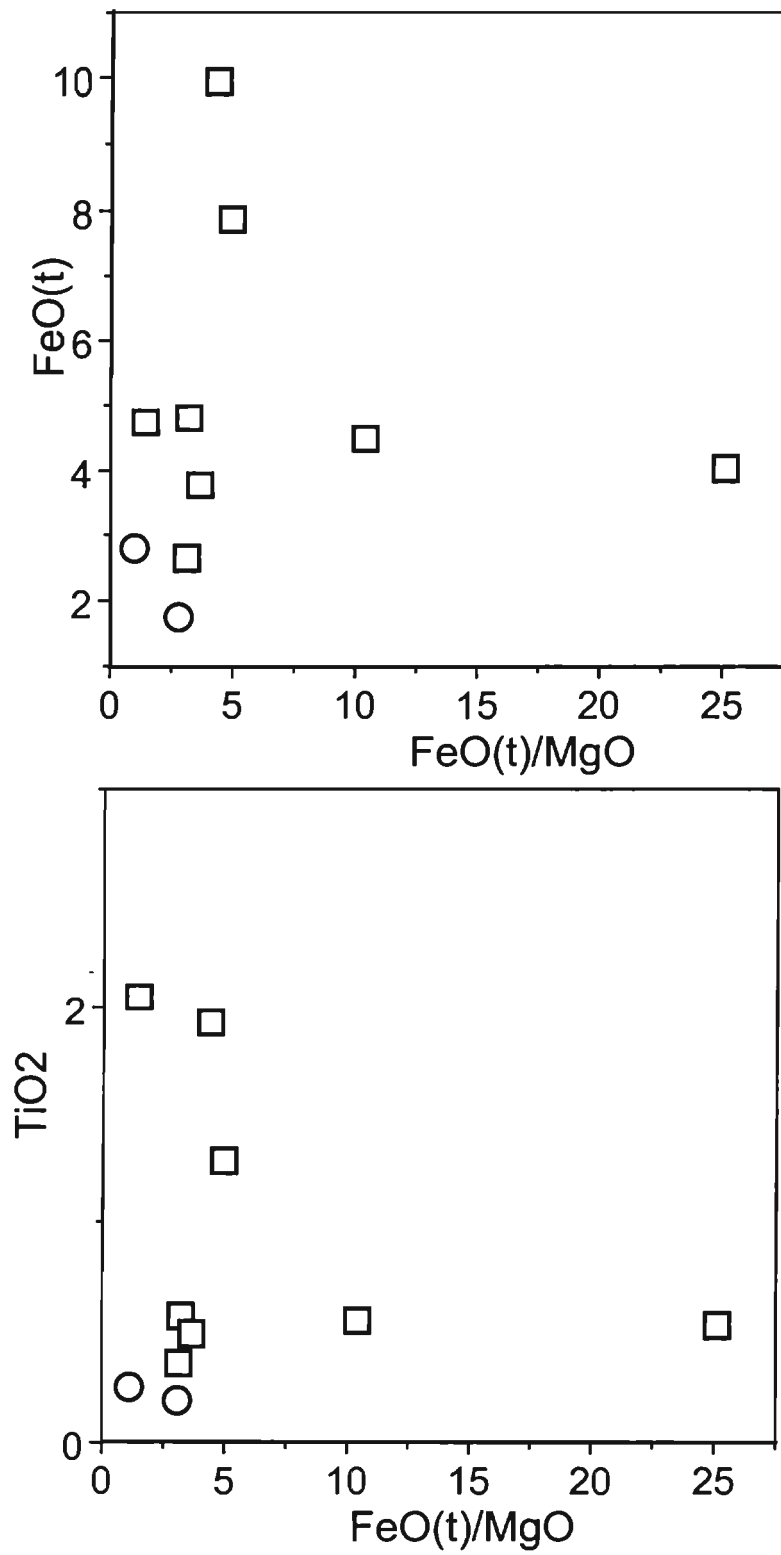
Fig. 6.42 FeO(t)/MgO vs FeO(t) and TiO2 diagrams (Miyashiro, 1973) showing the plots for Karikkottakkari and Adakkathod diorites.
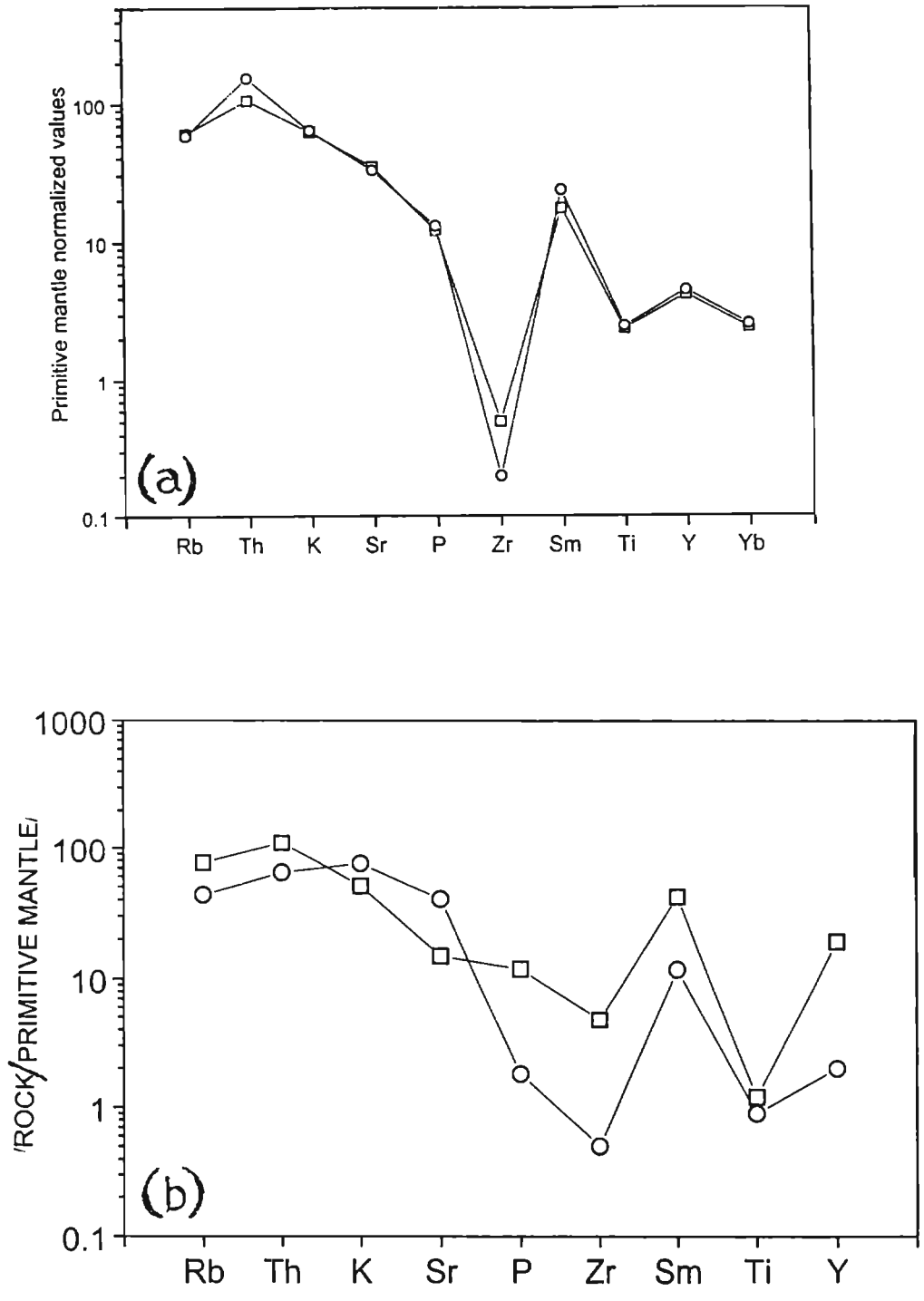
Fig. 6.43 Primitive mantle- normalized trace element patterns of trace elements of Karikkottakkari and Adakkathod diorites(a & b) Normalization values are from Sun and McDonough (1989).

commonly regarded as pointing to enriched mantle source (Amitab and Mallik,1995). Thus an enriched mantle source is assumed for both Karikkottakkari and Adakkathod diorites.

6.5 Discussion

The field, petrographic and geochemical data and their interpretations given in the preceeding sections on the plutons associated with the Perinthatta anorthosite provide some ideas regarding their petrological nature, magmatic affinities and tectonic setting. The purpose of this exercise in the present context is to examine whether these plutons are genetically related in anyway to the Perinthatta anorthosite.

The aspects worth discussing are:
1) having established the cumulate nature of the anorthositic rocks, can any of the associated plutons be regarded as the complimentary residual liquid ?
2) can any of the associated rocks represent the parental liquid which gave rise to the Perinthatta anorthosite on fractional crystallization and cumulate formation ?
3) Is there any general or common character among the plutons of the region indicating similar source characteristics or petrotectonic environment ?

The complimentary residual liquid derived after the separation of Perinthatta anorthosite as cumulate phase has been inferred to have a significant negative Eu anomaly. Further the ratio between the anorthosite and the complementary residual liquid will be of the order of 1:9. None of the above plutons are large enough to qualify this and none is having a significant negative Eu anomaly. Thus the associated rocks do not represent the residual liquid.

120

The parent melt inferred for the Perinthatta anorthosite (section 5.6, chapter 5) is an intermediate magma with ~100 times chondritic REE with a slightly fractionated pattern and no Eu anomaly. This melt yielded plagioclase (with oligoclase composition), clinopyroxene, orthopyroxene, apatite and opaques as the early crystallizing phases. None of the associated plutons is matching with these stipulations. The intermediate rocks seen in the nearby area are the diorites of Karikkottakkari and Adakkathod. Though their REE concentration is matching with the inferred parent, the mafic phases present in the diorites are hornblende and biotite while the mafics in the anorthosite are pyroxenes. Whether these contrasting mafic mineralogy is due to different X_{H2O} prevailed during the crystallization or as a result of different types of magma is not certain. Further, the plagioclase present in the anorthosite are less calcic than those in the diorites. In general, cumulates should have more An rich plagioclase than the parent. Thus the dioritic rocks of the area cannot be regarded as representing the parental magma for the Perinthatta anorthosite.

Ezhimala igneous complex is spatially more close to the Perinthatta anorthosite. Compared to the Perinthatta anorthosite, Ezhimala igneous complex is smaller and therefore in no way it is possible for the Ezhimala gabbro to be the source for the plagioclases in the Perinthatta anorthosite. Moreover, plagioclases in these two plutons are very much different in their composition and zoning. Plagioclases in Perinthatta anorthosite (oligoclase in composition) do not show zoning while those of Ezhimala gabbro are highly calcic (labrodorite) and zoned and this point to different kinds of magma for these two plutons.

The primitive mantle normalized trace element patterns of the most mafic member of the anorthositic suite is compared with averages of Ezhimala gabbro and the diorites of Karikkottakkari and Adakkathod in figure 6.44. It is seen that the pattern for the anorthositic rock cut across those of others confirming that the anorthosites are not co-magmatic with other rocks.
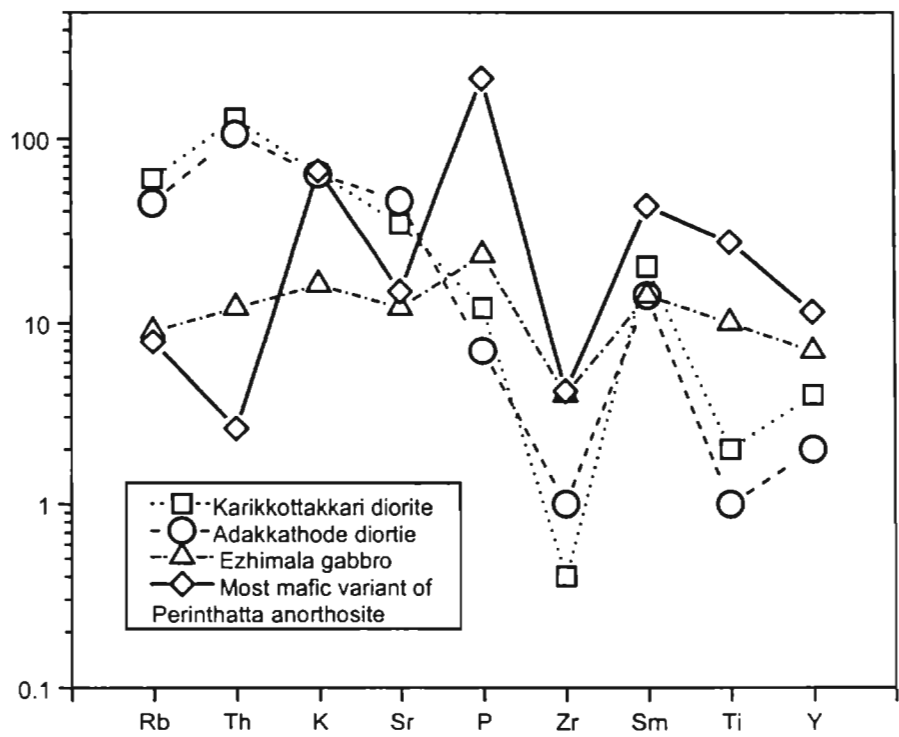
Fig. 6.44   Comparison of primitive mantle-normalized trace element patterns of diorites and Ezhimala gabbro with that of the most mafic variant of Perinthatta anorthosite

The similarity between anorthosite and the associated igneous complex lies in their general alkalinity. All the plutons associated with Bavali lineament are somewhat alkaline in nature. The origin of alkalinity especially of the Perinthatta anorthosite has already been discussed (section 5.4.1, chapter 5). This common alkalinity of the plutons along a linear stretch may be regarded as due to taphrogenetic magmatism during Pan-African time as most of these plutons are assumed to be of that age.

•   •   •

Summary

The present work deals with the petrogenesis of Perinthatta anorthosite based on its field, petrographic and geochemical aspects. As the pluton is seen emplaced in the poly-deformed and metamorphosed rocks of the northern part of Kerala, the study incorporates analyses of structural and metamorphic aspects of the region. A brief study on the series of mafic to felsic plutons seen spatially associated with the Perinthatta anorthosite is also carried out to understand their possible petrogenetic link with the anorthosite. The conclusions arrived at from the study are summarized below.

Analysis of the structure of the northern part of Kerala indicates that the WNW-ESE trending Bavali shear zone is the major structural feature in the area. The presence of different generations of penetrative planar structures and the imprints of three generations of folding in the rocks of the region reveal its poly-deformed nature. A comparison of the structural elements along the western, central and eastern sectors of the Bavali shear zone indicates similar structural evolution in all the three sectors but with slight differences in the inferred stress fields and localized differential response depending on the nature of the affected rocks. The main episode of shearing took place between the second and third generations of folding.

The amphibolite facies metamorphism recorded in gneisses along the Bavali shear zone was later to the F_1 folding episode while the F_2 folds are later to this metamorphism. Granulite facies metamorphism postdates F_2. The shear zone is dipping towards southwest and the kinematic indicators along it indicates a dextral sense of shearing and a dip-slip movement. The Perinthatta anorthosite is on the up-thrown block and is essentially a post-tectonic intrusion.

Based on the interpretation of metamorphic aspects of the rocks of the northern Kerala, four distinct provinces are identified and their P-T conditions during peak metamorphism and corresponding crustal depths could be inferred. The crustal segments exposed on either side of the Bavali shear zone represents two levels of the crust, the northern block exposing the deeper portion.

The northern granulite province in which the Perinthatta anorthosite is emplaced represents the lower part of the thick Proterozoic crust as the exposed rocks were subjected to granulite facies metamorphism at a crustal depth of ~35km. From the negligible difference between the estimated metamorphic pressures corresponding to the core and rim compositions of the phases in the granulites, a near-uniform high pressure all over this province is inferred and thus it could be envisaged that this crustal segment remained for a considerably longer period under peak metamorphic regime.

The anorthositic rocks display compelling field evidences suggestive of their intrusive nature. Petrographic analysis indicates that the Perinthatta plulton is essentially made up of dioritic anorthosite and anorthosite with subordinate amount of anorthositic diorite. Textural and mineralogical characteristics of the anorthositic rocks reveal the cumulate nature of the pluton.

The major element geochemistry of the anorthositic rocks shows that they are analogous to massif type anorthosite occurring elsewhere in the world but for the slightly higher content of alkalies, especially Na_2O, in them. The trace and rare earth element concentrations in the anorthositic rocks confirm the cumulate nature inferred from the petrography of the rocks. REE based modelling of parental melt indicates that the anorthositic cumulates were derived from a magma of soda-rich intermediate chemistry characterized by about 100 times chondritic REE abundances with no Eu anomaly and slightly fractionated

chondrite-normalized REE pattern probably derived by the partial melting of a granulitic or eclogitic source.

The mafic mineral assemblage of the anorthositic rocks points to their crystallization in a dehydrating environment. Exsolution texture in the phases and the temperature estimates based on the mineral chemistry indicate a high initial temperature of the melt and a prolonged cooling history for the Perinthatta pluton. Barometric studies from the chemistry of the coexisting minerals of anorthositic rocks indicate that the rocks solidified at a crustal depth of ~20 km. Isotope data points to the Pan-African age and the composite nature of the intrusive. It further suggests a mantle source for the anorthositic rocks.

Petrological study of the associated plutons of the Perinthatta anorthosite reveals that these rocks represent neither the complimentary residual liquid after the formation of the anorthositic rocks nor the parental liquid for the anorthosite pluton and that they are not genetically related to the Perinthatta anorthosite. The similarity between the Perinthatta anorthosite and the associated plutons lies in their common alkalinity which may be regarded as the key aspect of the taphrogenetic magmatism during Pan-African time in the region.

● ● ●

(iii)

Bibliography

Abbot, D.H. and Hoffman, S.E. 1984. Archaean plate tectonics revised. 1. Heat flow, spreading rate and age of subducting oceanic lithosphere and their effects on the origin and evolution of continents. Tectonics, vol. 4, pp. 429-448.

Agrawal, S. 1995. Discrimination between Late-Orogenic, Post-Orogenic and Anorogenic granites by major element compositions. Jour. of Geology, v. 103, pp. 529-537.

Anil Kumar, P.S., Nair, M.M. and Varma, A.D.K. 1992. Studies on the acid intrusives of Kannur and Wynad districts, Kerala. Rec. Geol. Surv. India, v. 125(5), pp. 124-129.

Arth, J.G. 1976. Behaviour of trace elements during magnetic processes - a summary of theoretical models and applications. Jour. Res. U.S. Geol. Survey, v.4, pp.41-47.

Ashwal, L.D. 1982. Proterozoic anorthosite massifs: a review. In: D. Walker and I.S. Mc Callum (Eds.) Workshop on magmatic processes of early planetary cursts: magma oceans and stratiform layered intrusions. Lunar Planet Inst. Tech. Rep. 82-01, Lunar Planet Inst., Houston, pp. 40-42.

Ashwal, L.D. 1982. Mineralogy of mafic and Fe- Ti oxide-rich differentiates of the Marcy anothosite massif, Adirondacks, New york. American Mineralogist, v. 67, pp.14-27.

Ashwal, L.D. 1993. In: Anorthosites. Springer- Verlag Berlin Heidelberg, p. 422.

Ashwal, L.D. and Seifert, K.E. 1980. Rare earth element geochemistry of anorthosite and related rocks from the Adirondacks, N.Y. and other massif-type complexes. Geol. Soc. Am. Bull., 91, 105-107, pp. 659-684.

Ashwal, L.D. and Wooden, J.L. 1985. Sm-Nd isotopic studies of Proterozoic anorthosites: systematics and implications. In: Tobi AC, Touret JLR (eds) The deep Proterozoic crust in the North Atlantic provinces. NATO ASI Ser C, 158, Reidel, Dordrecht, pp 61-73.

Balachandran, V., Chandrasekhar, Nambiar, A.R. and Adiga, K.S. 1980. Geology o parts of Kakankote State Forest, Mysore District, Karnataka. Geol. Surv. Ind. Progress Report for Field Season 1979-80.

Balaram, V. 1991. Determination of rare earth elements in geological samples by Inductively Coupled Plasma Mass Spectrometry. Jour. Indian Che. Soc., v. 63, pp. 600-603.

Barker, F. 1979. Trondhjemites: definition, environment and hypothesis of origin. In: F. Barker (Ed.) Trondhjemites, Dacites and related rocks. Elsevier, Amsterdam, pp. 1-12.

Bartlett, J.M., Harris, N.B.W., Hawkesworth, C.J. and Santosh, M. 1995. New isotope constraints on the crustal evolution of South India and Pan-African grnulite metamorphism. Mem. Geol. Soc. India, No.34, pp. 391-397.

Berg, J.H. 1977. Dry granulite mineral assemblages in the contact aureoles of the Nain complex, Labarador. Contrib. Mineral Petrol. 64, pp. 33-52.

Berman, R.G. 1991. Thermobarometry using multi-equilibrium calculations: A new technique with petrological applications. Canadian Minerlogist, v. 29, pp. 833-855.

Bernard-Griffiths, J., Jahn, B.M. and Sen, S.K. 1987. Sm-Nd isotopes and REE geochemistry of Madras granulites: an introductory statement. Precambrian Res., v. 37, pp. 343-355.

Bhushan, S.K., Bhaskar Rao, B., Parthasarathy, R. and Nambiar, C.G. 1988. Geochemistry and genesis of meta-anorthositic rocks near Innukurti, Mellore district, Andhra Pradesh, South India. Neues Jahrbuch Miner. Abh, v. 159, pp. 153-164.

Bickle, M.J. 1978. Heat loss from the Earth: A constraint on the Archaean tectonics from the relationships between geothermal gradients and the rate of plate production. Earth Planet. Sci. Let., vol. 40, pp. 301-315.

Brynton, W.V. 1984. Cosmochemistry of the rare earth elements; Meteorite studies. In P. Henderson (Ed.) Rare Earth Element Geochemistry (Elsevier), pp. 63-144.

Buddington, A.F. 1939. Adirondack igneous rocks and their metamorphism. Geol. Soc. Am. Memoir, 7, pp. 343.

Buddington, A.F. 1975. Anorthosite-bearing complexes: classification and parental magmas. In; Studies in Precambrian, Dept. of Geology, University of Bangalore, India, pp. 115-141.

Campbell, I.H. and Jarvis, G.I. 1984. Mantle convection and early crustal evolution. Precamb. Res., vol.26, pp.15-56.

Cawthorn, R.G. and Collerson, K.D. 1974. The Recalculation of pyroxene end member parameters and the estimation of ferrous and ferric iron content from electron microprobe analysis. American Mineralogist, v. 59, pp. 1203-1208.

Chacko, T., Lamb, M. and Farquhar, J. 1996. Ultra-high temperature metamorphism in the Kerala Khondalite Belt, In: M. Santosh, M. Yoshida (Eds.) The Archaean and Proterozoic terrains in southern India within East Gondwana. Gondwana Research Group, Mem. 3, pp. 157-165.

Choudhary, A.K., Harris, N.B.W., Van Calteran, P. and Hawkesworth, C.J. 1992. Pan-African charnockite formation in Kerala. Geol. Mag. , v. 129, pp. 257-264.

Cox, K.G., Bell, J.D. and Pankhurst, R.J. 1979. The interpretation of igneous rocks. London: Allen and Unwin.

Currie, K.L. 1989. New ideas on an old problem: the peralkaline rocks. In: C. Leelanandam (Ed.), Alkaline Rocks. Mem. Geol Soc. India, no.15, pp.117-136.

De Waard D. and Wheeler. E.P. 1971. Chemical and petrologic trends in anorthositic and associated rocks of the Nain massif, Labrador. Lithos 4: 367-380.

De Waard D, Duchesne JC. and Michot J. 1974. Anorthosites and their environment. In: Belliere J, Duchesne J.C. (eds.) Geologie des domaines cristallins. Cent Soc Geol Belg, Liege, pp 323-346.

Drury, S.A. and Holt, R.W. 1980. The tectonic framework of the South Indian craton: a reconnaissance involving LANDSAT imagery. Tectonophysics, v.65, pp. T1-T15.

Drury, S.A., Harris, N.B.W., Holt, R.W., Reeves-smith, G.J. and Wightman, R.T. 1984. Precambrian tectonics and crustal evolution in South India. Jour. Geology, v. 92, pp. 1-20.

Duchesne, J.C. and Demaiffe, D. 1978. Trace elements and anorthosite genesis. Earth. Planet. Sci. Letters, v. 38, pp. 249-272.

Eby, N.G. 1992. Chemical subdivision of the A-type granitoids: Petrogenetic and tectonic implications. Geology, v. 20, pp. 641-644.

Eklund, O., Frojdo, S. and Lindberg, B. 1994. Magma mixing, the petrogenetic link between anorthositic suits and rapakivi granites, Aland, SW Finland. Mineralogy and Petrology, vol. 50, pp. 3-19.

Ellis, D.J. 1980. Osumilite-Saphirine-quartz-granulite from Enderby land Antarctica: P-T conditions of metamorphism, implications for garnet-cordierite equilibria and the evolution of the deep crust. Contrib. Mineral. Petrol., v.74, pp. 201-210.

Emslie, R.F. 1970 The geology of the Michikamau intrusion, Labrador. Geol. Surv. Can. Pap, 68-57, pp.85.

Emslie, R.F. 1978. Anorthosite massifs, rapakivi granites, and late Proterozoic rifting of North America. Precambrian Res., v. 7, pp. 61-98.

Emslie, R.F. 1980. Geology and petrology of the Harp Lake Complex, Central Labrador: an example of Elsonian magmatism, Geol.Surv. Canada. Bull. 293. p. 136.

Emslie, R.F. 1985. Proterozoic anorthosite massifs. In: A. Tobi, J.L.R. Touret (Eds.) The Deep Proterozoic Crust in the North Atlantic provinces. NATO ASI Ser C, 158. Reidel, Dordrecht, pp.39-60.

Emslie, R.F., Hamilton, M.A. and Theriault, R.J. 1994. Petrogenisis of a mid-proterozoic anorthosite-mangerite-charnokite-granite (AMCG) complex: isotopic and chemical evidence from the Nain plutonic suite. Jour. Geol., v.102, pp.539-558

Gopalakrishna, K., Sugavanan, E.B. and Rao, V.V. 1975. Are there rocks older than Dharwars? A reference to rocks of Tamil Nadu. Indian Mineralogist, v.16, pp.1-11.

Gopinathan, V., Lakshmeesha, B. and Gopinath, K.S. 1996. Geology and geochemistry of the Perinthatta monzonite-magerite anorthosite intrusion, Kannur district, Kerala state, India. Gondwana Research Group Misc. Publ. No.4 (M. Santosh and M. Yoshida, Eds.), pp. 26-27.

Gordon, T.M. 1992. Generalized thermobarometry: Solution of the inverse chemical equilibrium problem using data for individual species. Geochim. Cosmochim. Acta, v. 56, pp. 1793-1800.

Gresens, R.L. 1978. Evaporites as precursors of massif anorthosite. Geology, 6, pp. 46-50.

Gromet, L.P. and Dymek, R.F. 1982. Petrological and geochemical characterization of the St. Urbane anorthosite massif, Quebec; Summary of initial results. In: Walker, D, McCallum,I.S (Eds.). Workshop on magmatic processes of early planetary crust: magma oceans and stratiform layered intrusions. Lunar Planet Inst. Tech. Rep, 82-01, Lunar Planet. Inst, Houston, pp. 72-74.

Hansen, E.C. 1983. The granulite-grade metamorphism in southern Karnataka, south India: the role of the fluid phase. Unpublished Ph.D thesis.

Hansen, E.C., Newton, R.C. and Janardhan, A.S. 1984. Fluid inclusions from the amphibolite facies gneiss to charnockite progression in Southern Karnataka, India: Direct evidence concerning the fluids of granulite metamorphism. Jour. Meta. Geol., vol. 2, pp. 249-264.

Harris, N.B.W., Holt, R.W. and Drury, S.A. 1982. Geobarometry, geothermometry, and Late Archean geotherms from the granulite facies terrain of south India. Jour. Geology, v. 90, pp. 509-527.

Harris, N.B.W., Taylor, P.N. and Santosh, M. 1994. Crustal evolution in south India: constraints from Nd isotopes. Jour. Geol., v. 102, pp. 139-150.

Haselton, H.T., Hovis, G.L., Hemingway, B.S. and Robie, R.A. 1983. Calorimetric investigations of the excess entropy of mixing in analbite-sanidine solid solutions: lack of evidence for Na, K short-range order and implications for two – feldspar thermometry. American Mineralogist, v.68, pp. 398-413.

Henderson, P. 1983. (Ed.). Rare Earth Element geochemistry. Elsevier.

Herz, N and Force, E.R. 1984. Rock suites in Grenvillian terrane of the Roseland district, Virginia, Part 1. Lithologic relations. In: Bartholomew MJ (ed.) The Grenville Event in the Appalachians and related topics. Geol Soc Am Spec Pap 194: 187-214.

Hibbard, M.J. 1991. Textural anotomy of twelve magma mixed granitoid systems. In:Didier, J, Barbarian (eds.) Enclaves and granite petrology. Dev. in Petrol., v. 13. Elsevier, Amsterdam, p.625.

Holland, T.H. 1900. The charnockite series: a group of Archaean hypersthene rocks in Peninsular India. Mem. Geol. Surv. India., v. 28(2), pp. 117-249.

Holm, P.E. 1985. The geochemical fingerprinting of different tectoniomagmatic environments using hygromagmatophile element abundances of tholeiitic basalts and basaltic andesites. Chem. Geol., v. 51, pp. 303-323.

Hunt, T.S. 1863. In: Logan, W.E., Murray, A., Hunt, T.S. and Billings, E. (Eds.). Geology of Canada, report of progress from its commencement to 1863. Geol. Surv. Canada, Report Progress, p. 22.

Huppert, H.E. and Sparks, R.S.J. 1988. The generation of granitic magmas by intrusion of basalt into continental crust. Jour. Petrol., v.29, pp. 599-624.

Janardhan, A.S., Newton, R.C. and Smith, J.V. 1979. Ancient crustal metamorphism at low P_{H_2O} : Charnockite formation at Kabbaldurga, South India. Nature, v. 278, pp. 511-514.

Janardhan, A.S. and Wiebe, R.A. 1985. Petrology and geochemistry of the Oddanchatram anorthosite and associated basic granulites, Tamil Nadu, South India. Jour. Geol.Soc. India, v.26, pp. 163-176.

Janardhan, A.S. 1989. Granulite facies rocks of southern Karnataka: mode of origin and their relation to the Dharwar Craton. Abs. in Structure and Dynamics of the Indian Lithosphere. NGRI, Hyderabad., pp. 90-91.

Janardhan, A.S., Jayananda, M. and Shankara, M.A. 1994. Formation and tectonic evolution of granulites from the Biligiri Rangan and Niligiri hills, S. India: geochemical and isotopic constraints. Jour. Geol. Soc. India, vol. 44, pp. 27-40.

Jayananda, M., Janardhan, A.S., Sivasamudram, P. and Peucat, J.J. 1995. Geochronologic and isotopic constraints on grnulite formation in the Kodaikanal area, southern India. In: India and Antarctica during Precambrian (Eds. M. Yoshida and M. Santosh), Geol. Soc. India. Mem. No. 34, pp. 373-390.

Jayananda, M. and Peucat, J-J. 1996. Geochronological framework of southern India. In: Gondwana Research Memoir No.3: The Arhaean and Proterozoic Terrains in Southern India within East Gondwana (Eds. M. Santosh and M. Yoshida). pp. 53-75.

John Kurian, P., Radhakrishna, M., Nambiar, C.G. and Murthy, B.V.S. 1999. Interpretation of gravity field over the Perinthatta anorthosite, Northern Kerala. Jour. Geol. Soc. India, v. 54, pp. 483-490.

Kaila, K.L., Roy Chowdhury, K., Reddy, P.R., Krishna, V.G. Hari Narain, Subbotin, S.I., Sollogub, V.B., Chekunov, A.V., Kharetchko, G.E., Lazarenko, M.A. and Ilehenko, T.V. 1979. Crustal structure along Kavali-Udupi profile in the Indian peninsular shield from deep seismic sounding. Jour. Geol. Soc. India, v. 20, pp. 307-33.

Kanungo, D.N., Chetty, T.R.K. and Mallikarjuna Rao, J. 1986. Anorthosites and associated rocks of Nellore-Gudur, South India. Jour. Geol. Soc. India, v. 27, pp. 428-439.

Katz,M.B. 1978. Tectonic evolution of the Archaean Granulite facies belt of Sri Lanka and South India. Jour. Geol. Soc. India, v. 19, no. 5, pp. 185-205.

Krishanaraj, N.S., Janardhan, A.S. and Basavalingu, B. 1994. Garnet-Kyanite bearing pelitic and associated mafic granulites along Jalsoor-Mercara shear zone: evidence for deep burial and later uplift. Jour. Geol. Soc. India, v. 44, pp. 617-625.

Krishna Brahmam, N. 1993. Gravity in relation to crustal structure, palaeosutures and seismicity of southern India. Geol. Soc. India. Memoir, v.25, pp. 165-201.

Kumar, M., Dasgupta, S. and Mukhopadhyay, S. 1984. The Bengal anorthosite and the associated rocks, Bankura district, West Bengal. Geol. Surv. India Special Publ. No.12, pp. 191-197.

Kushiro. I. 1980. Viscosity, density, and structure of silicate melts at high pressures, and their petrological applications. In: Hargraves RB (ed) Physics of magmatic processes. Princeton Univ Press, Princeton NJ, pp 93-120.

Kushiro I, and Fujii T. 1977. Floatation of plagioclase in magma at high pressures and its bearing on the origin of anorthosite. Proc Jpn Acad Ser B 53: 262-266.

Lahiri, T.C., Nambiar, A.R. and Reddy, U.S. 1975. Reports on geological mapping and geochemical sampling for precious metals in parts of Attapadi area, Palghat district, Kerala. Rec. Geol. Surv. India, F S 1975-76.

Le Bas, M.J., Le Maitre, R.W., Streckeisen, A. and Zanettin, B. 1986. A chemical classification of volcanic rocks based on the total alkali-silica diagram. Jour. Petrol., v. 27, pp. 745-750.

Leelanandam C., 1987 Proterozoic anorthosite massifs: an overview. Indian Jour. Geol., v. 59, No.3, pp. 179-194.

Leelanandam C. and Narsimha Reddy M. 1985. Petrology of the Chimalpahad anorthosite complex, Andhra Pradesh, India. Neues Jahrb Mineral Abh 153: 91-119.

Leelanandam, C. and Reddy, M.N. 1988. Precambrian anorthosites from peninsular India—problems and perspectives. Ind. Jour. Geol., v. 60, No.2, pp. 111-136.

Leelanandam, C. 1997. The Khondapalli layered complex, Andhra Pradesh, India: a synoptic overview. Gondwana Research, v. 1, No.1, pp.114.

Mahabaleshwar, B. and Peucat, J.J. 1988. 2.9. b.y. Rb-Sr age granulite facies rocks from Satnur-Halagur- Sivasamudram area of Southern Karnataka, South India. Jour. Geol. Soc. India, v. 32, pp. 461-467

Mahabaleshwar, B., Jayananda, M., Peucat, J.J. and Shadakshara Swamy, N. 1995. Archaean high grade gneiss complex from Satnur-Halagur-Sivsamudram areas, Karnataka, South India: Petrogenesis and crustal evolution. Jour. Geol. Soc. India, v. 45, pp. 33-49.

Mahadevan, T.M. 1964. The origin of the charnockite suite of rocks forming part of the Western Ghats in Kerala, India. Proc. Int. Geol. Congress 22nd Session, No.13, pp. 87-96.

Mahadevan, T.M. 1994. Deep continental structure of India: a review. Geol. Soc. India, Memoir No. 28, p. 569.

Martin, H. 1986. Effects of steeper Archaean geothermal gradients on geochemistry of subduction zone magmas. Geology, vol. 14, pp. 753-756.

Mason, B and Moore, C.B. 1982. Principles of Geochemistry. 4th Edn. John Wiley and Sons, New York. 344p.

McBirney, A.R. and Hunter, R.H. 1995. The cumulate Paradigm Reconsidered. Jour. Geol., v. 103, pp. 114-122.

Mc Carthy, T.S, Hasty, R.A. 1976. Trace element distribution patterns and their relationship to the crystallization of granitic melts. Geochim. Cosmochim. Acta, v. 40, pp. 1351-1358.

Middlemost, E.A.K. 1975. The basalt clan. Earth Planet. Sci. Lett., v.11,pp.337-364.

Miyashiro, A. 1973. The Troodos ophiolitic complex was probably formed in an island arc. Earth Planet Sci. Letters., v. 19, pp. 218-224.

Mohan, A. and Jayananda, M. 1999. Metamorphism and isotopic evolution of Granulites of southern India: Rererence to Neoproterozoic crustal evolution. Gondwana Research, v.2, No.2,pp.251-262.

Morse, S.A. 1982. A partisan review of Proterozoic anorthosites. Am. Mineral., v. 67, pp. 1087-1100.

Mukherjee, S. De, S.K. and Bhaumick, T. 1984. Geology of the nepheline syenites occurring in the area around Kushunda, Purulia, v. 114, pp. 59-62.

Mukherjee, A., Bhattacharya, A. and Chakraborty, S.C. 1986. Convergent phase equilibria at the massif anorthosite-granulite interface near Bolangir, Orissa, India and thermal evolution of a part of the Indian shield. Precamb. Res., v. 34, pp. 69-104.

Naha, K and Srinivasan, R. 1996. Nature of the Moyar and Bhavani shear zones, with a note on its implication on the tectonics of the southern Indian Precambrian shield. Proc. Indian Acad. Sci. (Earth Planet. Sci.)., v.105, No.2, pp. 173-189.

Nair, M.M., Vidyadharan, K.T., Pawar, S.D., Sukumaran,P.V. and Murthy, Y.G.K. 1976. The structural and stratigraphic relationship of the schistose rocks and associated igneous rocks of the Tellicherry – Manantoddy area, Cannanore district, Kerala. Ind. Mineralogist, v. 16, pp. 89-100.

Nair, M.M., Pawar, S.D., Vidyadharan, K.T. and Senthiappan, M. 1980. Vengad Group of Kerala -- An equivalent of the Dharwars of South India. Proc. Sym. on Geology and Geomorphology of Kerala, Spl. Publ. No.5, Geol. Surv. India. pp. 9-13.

Nair, M.M. and Vidyadharan, K.T. 1982. Rapakivi granite of Ezhimala complex and its significance. Jour. Geol. Soc. India, v. 23, pp. 46-51.

Nair, M.M. and Nair, P.K.R. 1997 Charnockite formation in North Kerala- new stratigraphic evidence. Indian jour. Earth Sci., v.24, Nos. 1-2, pp. 15-20.

Nair, N.G.K. and Santosh, M. 1984. Petrochemistry and tectonic significance of the Peralimala alkali granite, Cannanore district, Kerala. Jour. Geol. Soc. India, v. 25, pp. 35-44.

Nair, N.G.K., Soman, K., Santosh, M., Arakelyants, M.M. and Golubyev, V.N. 1985. K-Ar ages of three granite plutons from north Kerala. Jour. Geol. Soc. India, v.26, pp. 674-676.

Nambiar, A.R. 1976. Report on the geological mapping and geochemical exploration for precious metals in parts of Attapadi area, Palghat district, Kerala. Rec. Geol. Surv. India, Field Season 1976-77.

Nambiar, A.R. 1987. Mineralogy and geochemistry of adakkathodu gabbro massif from the bavali fault zone, north Kerala. Rec. Geol. Surv. India, pp-16-24.

Nambiar, A.R., Vidyadharan, K.T. and Sukumaran, P.V. 1982. Petrology of anorthosites of Kerala. Rec. Geol. Surv. India, v. 114, pt. 5, pp.60-70.

Nambiar, C.G. 1987. Geochemistry and genesis of charnockites and associated rocks from northern Kerala. Unpub. Ph.D thesis submitted to Indian Institute of Technology, Bombay. p. 191.

Nambiar, C.G., Bhaskar Rao, B. and Fedkin, V.V. 1989. Geothermobarometric studies on the granulites of northern Kerala. Current Trends in Geology – XII, Metamorphism, Ophiolites and Orogenic belts: Ed. P.S. Salkani, pp. 53.

Nambiar, C.G., Bhaskar Rao, B., Parthasarathy, R. and Fed'kin, V.V. 1992. Geochemistry and genesis of charnockites and associated gneisses from northern Kerala, India. In: High-Grade Metamorphics (Ed. A. Barto-Kyriakids). Theophrastue Pub. S.A., Greece, pp. 187-215.

Nambiar, C.G. and Devarajan, M.K. 1993. On the probable subjacent extension of Perinthatta anorthosite body. Proc. 80th Ind.Sci. Cong. (Abs.), pt.3, pp.2

Nambiar, C.G., Radhakrishna, M., Soney, K.P. and John Kurian, P. 1999. Nature and evolution of Precambrian lower crustal segments associated with Bavali lineament and Wynad schist belt. Final Technical Report, DST project, pp.120.

Narayanaswami, S. 1976. Structure and Tectonics of the Archaean crystalline rocks of Kerala. Proc. Symp. on Geology an Geomorphology of Kerala (Abstract), Geol. Surv. Inidia.

Naqvi, S.M. and Rogers, J.J.W. 1983. Eds. Precambrian of South India. Mem. Geol. Soc. India. v. 4, pp. 1-575.

Naqvi, S.M. and Rogers, J.J.W. 1987   Precambrian Geology of India, Oxford University Press. p.223.

Newton, R.C, Smith,J.V. and Windley, B.F. 1980. Carbonic metamorphism, granulites and crustal growth. Nature, v.288, pp.45-50.

Odom, A.L. 1982. Isotope age determinations of rock and mineral samples from the Kerala district of India. Final Report (unpublished), UN Case 81.

Papezik, V.S. 1965. Geochemistry of some Canadian anorthosites. Geochim. Cosmochim. Acta., 29, pp. 673-709.

Pearce, J.A., Harris, N. B.W. and Tindle, A.G. 1984. Trace element discrimination diagrams for the tectonic interpretation of granitic rocks. Jour. of Petrology, v. 25, part 4, pp. 956-983.

Perkins, D. and Newton, R.C., 1981. Charnockite geobarometers based on coexisting garnet-pyroxene-plagioclase-quartz. Nature, v. 292, pp. 144-146.

Peucat, J.J., Vidal, P., Bernard-Griffiths, J. and Condie, K.C. 1989. Sr, Nd and Pb isotope systematics in the Archaean low to high grade transition zone of southern India: Syn-accretion vs post accretion granulites. Jour. Geol., v. 97, pp. 537-550.

Philpotts., A.R. 1968. Parental magma of the anorthosite-mangerite suite. In: Isachsen Y.W. (ed.) Origin of anorthosite and related rocks. NY State Mus Sci Serv Mem 18: 207-212.

Philpotts. A.R. 1981. A model for the generation of massif-type anothosites. Can Mineral 19: 233-253.

Philpotts, A.R. 1990. Principles of Igneous and Metamorphic Petrology. Prentice hall, New Jersey, 498p.

Phinney, W.C. and Norrison, D.A. 1990. Partition coefficients for calcic plagioclase: implications for Archaean anorthosites. Geochim. Cosmochim. Acta, v.54, pp.1639-1654.

Pichamuthu, C.S. 1961. Transformation of Peninsular gneiss into charnockite in Mysore state, India. Jour. Geol. Soc. India, v. 2, pp. 49-49.

Poldervaart, A. and Hess, H.H. 1951. Jour. Geol., v. 59, pp. 472.

Powell, R. 1985. Geothermometry and geobarometry : A discussion. Jour. Geol. Soc. London, v. 142, pp. 29-38.

Powell, R. and Holland, T. 1994. Optimal geothemometry and geobarometry. American Minerlogist, v. 79, pp. 120-133.

Radhakrishna, B.P. and Ramakrishnan, M. 1990. Archaean greenstone belts of South India – Bellur Rama Rao volume. Mem. Geol.Soc. India, v.19, p.497

Radhakrishna, B.P., Ramakrishnan, M. and Mahabaleswar, B. 1990. Granulites of South India - Pichamuthu volume, Mem. Geol. Soc. India., v. 17, p.502.

Radhakrishna, B.P. 1993. (Ed.) Continental crust of South India. Memoir 25, Geological Soc. India. p. 379.

Radhakrishna, T. and Mathew, J. 1995. Oxygen isotopes and mantle sources of the mafic dykes in the South Indian high-grade terrain. In: Dyke Swarms of Peninsular India, Mem. 33, Geol. Soc. India. pp. 133-147

Radhakrishna, T., Pearson, D.G. and John Mathai 1995. Evolution of Archaean southern India lithospheric mantle: a geochemical study of Proterozoic Agali-Coimbatore dykes. Contrib. Mineral. Petrol.

Raith, M., Rasse, P., Ackermand, D. and Lal, R.K. 1983. Regional geothermobarometry in the granulite facies terrane of South India. Transactions of the Royal Society o Edinburgh: Earth Sciences, 73, pp. 221-244.

Raith, M., Henget., Nagel, B., Bhattacharya, A. and Srikantappa, C., 1988a. metamorphic conditions in the Nilgiri granulite terrane and the adjacent Moyar and Bhavani shear zones: A reevaluation. Jour. Geol. Soc. India, No.1, v. 31, pp. 112-113.

Raith, M., Klatt, E., Spiering, B., Srikantappa, C. and Stahle, H.J. 1988b. Gneiss-charnockite transformation at Kottavattam, southern Kerala (India). Jour. Geol. Soc. India, v. 31, No.1, pp. 114-115.

Raith, M., Srikantappa, C., Ashamanjari, K.G. and Spiering, B. 1990. The granulite terrain of Niligiris (southern India): Characterization of high grade metamorphism. In: Granulites and crustal evolution. (Eds) D. VIELZEUF and Ph. Vidal Kuwer Academic Publishers, pp. 339-365.

Rajesh, H.M., Santosh, M., Osani, Y., Veno, T. and Yoshida, M. 1998. Pigeonite exsolution in pyroxene phenocrysts from a massive anorthosite in South India-Implication for petrogenesis. Indian Mineralogist, v. 32, pp. 30-31.

Rameshwar Rao, D. and Narayana, B.L. 1996. Enderbites and associatec gneissic rocks of Dharmapuri area, Tamil Nadu, India. In: The Archaean and Proterozoic Terrains of Southern India Within East Gondwana (M. Santosh and M. Yoshida (Eds.) Gondwana Research Group, Mem. No. 3, pp. 167-183.

Ramsay, J.G. 1967. Folding and fracturing of rocks. McGraw Hill, New York, p.568.

Rasse, P., Raith, M., Ackermand, D. and Lal, R.K. 1986. Progressive metamorphism of mafic rocks from greenschist to granulite facies in the Dharwar craton of south India. Jour. Geology, vol.94, pp. 261-282.

Ravindrakumar, G.R. 1986. The petrology and geochemistry of massif anorthosites and gabbros of the Bavali fault zone, North Kerala. Proc. Ind. Acad. Sci. (Earth Planet. Sci.), v. 95, pp. 117-130.

Ravindrakumar, G.R. and Sinha-Roy, S. 1985. Field relations and geochemistry of Peralimala syenite pluton, north Kerala. Ind. Mineralogist, v. 26, pp. 33-41.

Ravindrakuamr,. G.R. and Chacko, T. 1994. Geothermobarometry of mafic granulites and pelites from Palaghat gap, south India: petrological evidence for isothermal uplift and rapid cooling. Jour. Met. Geol., v. 12, pp. 479-492.

Ravindrakuamr, G.R. and Chacko, T. 1994. Geothermobarometry of mafic granulites of Manantoddy, North Kerala. Jour. Geol. Soc. India, v. 33, No. 2, pp. 132-139.

Ravindrakumar, G.R. and Srikantappa, C. 1987. Mineral and whole rock chemistry and P-T conditions of metamorphism of metapelites of Manantoddy, northern Kerala. Proc., 6th Indian geological congress, Roorkee, pp. 103-109.

Santosh, M., Iyer, S.S., Vasconcellos, M.B.A. and Enzweiler, J. 1989. Late Precambrian alkaline plutons in southwest India: geochronologic and rare earth element constriants on Pan-African magmatism. Lithos, v. 24, pp. 65-79.

Santosh, M. and Nair, N.G.K. 1983. Granite-molybdenite association in Kerala in relation to taphrogenic metallogeny. Proc. Indian Acad. Sci. (Earth Planet. Sci.), v. 92(3), pp. 297-310.

Santosh, M., Nair, N.G.K., Pande, K. and Gopalan, K. 1986. Rb-Sr geochronology of the Ambalavayal granite, Kerala. Jour. Geol. Soc. India, v. 27, pp. 309-312.

Santosh, M., Kagami, H. and Nanda-Kumar, V. 1992. Pan-African granulite formation in East Gondwana: geochronologic (Sm-Nd and Rb-Sr) and petrogenetic constraints. Bull. Ind. Geol. Assoc., v.25, pp.1-10.

Sarkar, A. and Bose, M.K. 1978. Observations on the Kadavur igneous complex, Tiruchirapalli, Tamil Nadu. Ind. Jour. Earth Sci., v. 5, pp.194-199.

Sinha-Roy, S. and Ravindrakumar, G.R. 1985. Pseudotachylites of the Bavali fault zone, Cannanore district, North Kerala. Jour. Geol. Soc. India, v. 26, pp. 182-190.

Sinha-Roy, S. and Ravindrakumar, G.R. 1986. Geochemistry of the gabbro-tonalite-trondhjemite-granite suite of the Ezhimala pluton, north Kerala. Jour. Geol. Soc. India, v. 27, pp. 325-337.

Silver, L.T. 1968. A geochronologic investigation of the Adirondack Complex, Adirondack Mountains, New York. In: Y.W. Isachsen (Ed.) Origin of anorthosite and related rocks. NY State Mus. Sci. Serv. Mem., 18, pp. 233-252.

Sparks, R.S.J., Marshall, L.A. 1986. Thermal and mechanical constraints on mixing between mafic and silicic magmas. Jour. Vol. Geotherm. Res., v.29, pp. 99-124.

Srikantappa, C.1996. The Nilgiri block. In: The Archaean and Proterozoic Terrains of Southern India Within East Gondwana (M. Santosh and M. Yoshida (Eds.) Gondwana Research Group, Mem. No. 3, pp. 185-222.

Stormer, J.C. 1975. A practical two-feldspar geothermometer. American Mineralogist, v. 60, pp. 667-674.

Streckeisen, A. 1976. To each plutonic rock its proper name. Earth. Sci. Rev., 12, pp. 1-33.

Subramaniam, A.P. 1956. Petrology of the anorthosite-gabbro massif at kadavur, Madras, India. Geol. Mag., v. 93, pp. 287-300.

Sun, S.S. and McDonough, W.T. 1989. Magmatism in the ocean basins. A.D. Sanders and M.J. Norry (Eds.). Geol. Soc. Amer. Spec. Publ., No. 42, pp. 313-345.

Swami Nath, J., Ramakrishnan, M. and Vishwanathan, M.N. 1976. Dharwar Stratigraphic Model and Karnataka Craton Evolution. Rec. Geol. Surv. India. v.107, pp. 149-179.

Tak, M.W. 1983. Significant contribution of the Landsat-1 data in the study of the anorthosite body of Bolangir district, Orissa. Geol. Surv. India Misc. Publ. 48., pp. 67-73.

Thornton, C.P. and Tuttle, O.F. 1960. Chemistry of Igneous rocks: 1. Differentiation Index: Amer. Jour. Sci., v. 258,pp. 664-668.

Touret, L.R.J. 1988. Nature and interpretation of fluid inclusions in granulites. Jour. Geol. Soc. India, v. 31, No.1, pp.158-160.

Unnikrishnan-Warrier, C., Yoshida, M., Kagami, H. and Santosh, M. 1995. Sm-Nd and Rb-Sr mineral isochron ages of Madras charnockite, and an evaluation of garnet geochronometry in granulites. Mem. Geol.Soc. India, No. 34, pp. 399-412.

Unnikrishnan-Warrier, C., Santosh, M. and Yoshida, M. 1995. First report of Pan-African Sm-Nd and Rb-Sr mineral isochron ages from regional charnockites of southern India. Geol. Mag. 132(3), pp.253-260.

Upton, B.G.J. 1971. Melting experiments on chilled gabbros and syenogabbros. Carniegie Inst. Wash Year Book, 70, pp. 112-118.

Upton, B.C.J. 1974. The alkaline province of south-west Greenland. In: Sorenson, H. (ED.) The Alkaline Rocks. John Wiley & Sons, London, pp.221-238.

Varadan, G.N. and Venkataramana, B. 1976. Occurrence of granophyre at Ezhimala in Cannanore district, Kerala. Indian Minerals, v. 30, pp. 96-97.

Vidyadharan, K.T., Sukumaran, P.V and Nair, M.M. 1977. Report on the detailed study of anorthosites around Perinthatta, Cannanore district, Kerala. Unpublished Report. Geol. Surv. India. Field season 1976-1977.

Vidyadharan, K.T., Sukumaran, P.V and Nair, M.M. 1977 A note on the occurrence of anorthosite near Perinthatta, Taliparamba taluk, Cannanore district, Kerala. Jour. Geol. Soc. India, v. 18, pp. 519-520.

Wager, L.R., Brown, G.M, and Wadsworth, W.J. 1960. Types of igneous cumulates. Jour. Petrology, v.1, pp. 73-85.

Wells, P.R.A., 1977. Pyroxene thermometry in simple and complex systems. Contrib. Mineral. Petrol., v.62, pp. 129-139.

Whalen J.B, Currie K.L, and Chappell B.W. 1987. A-type granites: geochemical characteristics, discrimination, and petrogenesis. Contrib Mineral Petrol 95: 407-419.

Winkler, H.G.F. 1987. Petrogenesis of metamorphic rocks. 5th edition, Springer-Verlag. P. 348.

Wilson, M. 1989. Approximate range of D values for the partitioning of trace elements between common rock-forming minerals and liquids of basic – intermediate compositions. In: Igneous Petrogenesis – a global tectonic approach. Unwin Hyman, London. pp. 418-421.

Wood. B.J. 1974. Solubility of alumina in orthopyroxene coexisting with garnet. Contrib. Mineral. Petrol., v, 46, pp. 1-15.

Xue, S. and Morse, S.A. (1993).   Geochemistry of the Nain massif anorthosite, Labrador: Magma diversity in five intrusions.   Geochim. Cosmochim. Acta, v. 57, pp. 3925-3948.

Appendix - I

This appendix gives a brief description of the localities referred to in the thesis. The information starts with the number of the location (S1, S2 etc.) and the latitude and longitude in the parentheses. This is followed by the name of the area and and its accessibility is given (in most cases) by indicating the approximate distance from a nearby township. This is followed by the rock type present in the area. The last line gives the number of samples collected from the location.

S1 (Lat. 12° 9' 20" and Long. 75° 17' 30")
Porakkunnu quarry. 7km south of Aravanhal on Aravanchal-Mathamangalam road.
Anorthositic diorite.
S-1/A and S-1/B

S2 (Lat. 12° 9' 10" and Long. 75° 17' 40")
Very near to location S1
Dioritic anorthosite
S-2/A

S3 (Lat. 12° 10' and Long. 75° 16' 40")
Vattappara quarry. 5km from Kuttur on Kuttur-Perinthatta road.
Anorthosite
S-3/A, S-3/3, AN-3/A, AN-3/B

S4 (Lat. 12° 9' 50" and Long. 75° 16' 50")
1km east of location S3.
Anorthosite.
S-4/A, AN-4/A.

S5 (Lat. 12° 10.6' and Long. 75° 18')
Thandanat quarry 2 km east Thandanat junction from Aravanchal-Porakkunnu road.
Mafic granulite
S-5

S6 (Lat. 12° 13.5' and Long. 75° 19')
Peringom
Very near to Peringom Post Office
Mafic granulite with crude gneissocity
S-6/A

S7 (Lat. 12° 13' and Long. 75° 20')
Peringom
½ km south of Peringom Junction along Peringom-Mathamangalam road.
Mafic granulite
S-7

S9
Peingom
50 m south of the location L-7
Mafic granulite
S-9

S11 (Lat. 12° 8' and Long. 75° 16')
Eramam. 3km from Eramam junction towards Kuttur.
Dioritic anorhosite
S-11/D

S12 (Lat. 12° 9' 10" and Long. 75° 14' 30")
Alakkad. 4km from Mathil junction towards south.
Dioritic anorthosite
S-12/C, S-12/F, S-12/L, S-12/T.

S15 (Lat. 12° 9' and Long. 75° 19')
Kulikappuram
3km NE of Kuttur on Kuttur-Peruvamba road
ated charnockite
S-15/P

S21 (Lat. 12° 12' and Long. 75° 14' 30")
Alappadamba. 3km from Mathil junction towards north.
Dioritic anorthosite
S-21/1

S22 (Lat. 12° 13' 40" and Long. 75° 14')
Alappadamba. 2km west of location S21.
Dioritic anorthosite.
S-22.

L25 (Lat. 12° 0' and Long. 75° 35.7')
Road side quarry along Irikkur-Blathur road
(Nearly 2km south of Kalliyad Ganapathi temple)
Charnockite
P-25

L36 (Lat. 12° 4' and Long. 75° 30.2')
Nidiyenga
About 5km north of Srikandapuram
Charnockite
P-36

L44 ((Lat. 12° 4' and Long. 75° 31')
4km NNE of Srikantapuram on Nidiyenga-Kuttumukam road
Felsic charnockitic gneiss
P-44

L45 (Lat. 12° 4' and Long. 75° 42')
Kuttuppuzha
A road cutting at Kuttuppuzha junction
Weathered gneiss with pegmatite
P-45

L46 (Lat. 12° 5.5' and Long. 75° 33')
Chemberi
A hill top SW of Chemberi on Nidiyenga Chemberi road
Gneissic charnockite
P-46

L50 (Lat. 12° 5.5' and Long. 75° 40.3')
Mattara
100 m east of Mattara junction
charnockite
P-50

L51 (Lat. 12° 4.8' and Long. 75° 39.7')
Mattara
300 m SW of Mattara junction
Charnockite
P-51/1

S19 (Lat. 11° 54.33' and Long. 75° 37')
Sivapuram. Palukachipara quarry.
Syenite
S-19/1

S23 (Lat. 12° 3' and Long. 75° 12.5')
Ramanthali. Quarry in the eastern slope of Ezhimala.
Granophyre
S-23/1

S25 (Lat. 12° 2.3' and Long. 75° 12.7')
Ramanthali. Quarry very near to the location S23.
Granophyre
S-25/1

S 33 (Lat. 12° 1.5' and Long. 75° 13.2')
Kakkampara. Quarry in the southern slope of Ezhimala.
3km towards west from Ettikkulam.
Gabbro.
S-33/A

S 34 (Lat. 12° 1.4' and Long. 75° 13.2')
Kakkampara. SW slope of Ezhimala
Granophyre
S-34/1

S36 (Lat. 12° 1.7' and Long. 75° 13.3')
Kakkkampara. A well cutting. 100 m north of the location S33.
Very coarse grained gabbro.
S-36/A

S 38 (Lat. 12° 1' and Long. 75° 13.2')
Kakkampara. Rock exposure along the beach.
Gabbro
S-38/A

S40 (Lat. 12° 40' and Long. 75° 13')
Kakkampara. An exposure along the beach.
Gabbro
S40/A

S 48 (Lat. 12° 2' and Long. 75° 13')
A quarry 1km north of Palakkod on Palakkod Payyanur road.
Leuco gabbro
S-48/A, S-48/B

S 49 (Lat. 12° 2.2' and Long. 75° 13.3')
A quarry 1km north of location S48.
Gabbro
S-49/A, S49/B

S50, S51, S52, and S53 (Lat. 12° 2.9' and Long. 75° 12')
Quarries near Kuunaru on the eastern slope of Ezhimala hills.
Gabbro
S-51/A, S-52/A, S-53/A and S-53/B.

S 54 (Lat. 12° 3.9' and Long. 75° 12')
Quarry along the northern flank of Ezhimala hills.
Granite.
S-54/B. S-54/C

S57 (Lat. 12° 0.2" and Long. 75° 45.15')
Karikkottakkari. Quarry very near to Karikkottakkari junction.
Diorite
S-57/A

S61 (Lat. 12° 0.5' and Long. 75° 45.33')
200 m northeast of Karikkottakkari junction.
Diorite
S-61/A

S62 (Lat. 12° 0.8' and Long. 75° 45.5')
500m northeast of Karikkottakkari junction along the karikkottakkari-Anapandi
road.
Diorite
S-62/A

S63 (Lat. 12° 0.45' and Long. 75° 45')
200m west of Karikkottakkari junction.
Diorite
S-63/A, S-63/B

S67 (Lat. 12° 1' and Long. 75° 44.55')
1km SW of Anapandi on Anapandi-Karikkottakkari road.
Diorite
S-67/A, S-67/B

S74 (Lat. 11° 54.7' and Long. 75° 37.15')
Vellilode quarry. 1km east of Sivapuram on Sivapuram-Kakkengad road.
Syenite
S-74/A

S75 (Lat. 11° 54.8' and Long. 75° 37.33')
200m east of location S74 on on Sivapuram-Kakkengad road.
Pink syenite
S-75/A

S77 (Lat. 11° 55.15' and Long. 75° 39')
Alayachi. 9km from Kakkengad on Kakkengad-Sivapuram road
Foliated syenite
S-77/A

S79 (Lat. 11° 55.15' and Long. 75° 38.7')
Kunduthod. 10km from Kakkengad on Kakkengad-Sivapuram road
Foliated syenite
S-79/A

S80 (Lat. 11° 53.8' and Long. 75° 36.5')
Maruvanchery. Very near to Sivapuram.
Pink syenite
S-80/A

S81 (Lat. 11° 53.9' and Long. 75° 36.33')
Kathirode. 100 m northwest of location S81
Syenite
S-81/A, S-81/B

S90 (Lat. 12° 2' and Long. 75° 12')
Quarry along the western slope of Ezhimala hills inside the Naval Academy.
Pink Granophyre
S-90/A

S95 (Lat. 12° 1.5' and Long. 75° 11.5')
200m west of north gate of Ezhimala Naval Academy.
Pink granophyre.
S-95/A

S101 (Lat. 11° 55.5' and Long. 75° 51')
500m NNE of Adakkathod junction.
Diorite
S-101/A, S-101/B, S-101/C

S103 (Lat. 11° 55.5' and Long. 75° 50')
Kannanchira. Very near to Adakkathod
Diorite
S-103/A, S-103/B, S-103/C

Appendix –II

Foliation readings collected for the structural study of this thesis:

WESTERN SECTOR

Location	Foliation reading
B-7	N80/ subvertical
B-8	N80/ subvertical
B-9	N75/ subvetical
B-10	N265/ 75 due NNW
B-10	N75/ subvertical
B-11	N83/ subvertical
B-12	N75/ 70 due NNW
C-2	N225/ 75 due NW
C-3	N253/ 75 due NW
C-3	N248/ 55 due NW
N-19	N104/ 70 due NE
N-19	N123/ 66 due NE
N-19	N290/ 71 due NE
N-20	N263/ 70 due NW
N-20	N260/ 83 due NNW
N-20	N104/ 62 due NNE
N-20	N89/ 72 due N
N-20	N84/ 72 due N
N-26	N75/ 71 due NW
N-26/A	N276/74 due NNE
N-27	N293/ 76 due NNE
N-27	N291/ subvertical
N-28	N96/ 76 N
N-29	N107/ 71 due NNE
N-30	N104/ 80 due NNE
N-31	N270/ 82 due S
N-31	N296/ 50 due SW
N-32	N77/ 44 due SE
N-33	N60/ 69 due SE
N-34	N90/ 62 N
N-35	N267/ 77 due NW
N-36	N272/ 55 due S
N-37	N282/ 75 due SW
N-37	N282/ 82 due NE
N-37	N270/ 68 S
N-38	N93/ 84 due N

N-39	N102/ 72 due NNE
	N260/ 82 due S

CENTRAL SECTOR

Z-1	N81/ 51 due S
Z-1	N79/ 64 due N
B-1	N84/ 69 due N
B-1	N80/ subvertical
B-2	N110/ 70 due NNE
B-4	N90/ subvertical
B-5	N285/ subvertical
B-7	N80/ subvertical
B-8	N80/ subvertical
B-9	N75/ subvertical
B-10	N265/ 75 due N
B-10	N75/ subvertical
B-11	N83/ suvertical
N-16	N103/ 76 due NE
N-17	N120/ 85 due SW
N-17	N286/ 86 due SW
N-17	N290/ 87 due NE
N-17	N117/ 75 due SW
N-17	N103/ 65 due SW
N-18	N102/ 74 due SW
N-18	N315/ 75 due SW
N-18	N110/ 64 due SW
N-18	N96/ 74 due N
N-18	N85/ 69 N
N-18	N93/ 72 N
N-22	N198/ 62 SE
N-23	N339/ 72 due WSW
N-25	N183/ 43 due E
N-40	N275/ 80 due N
N-40	N288/ 53 due NE
N-40	N270/ 62 due N
N-40	N97/ 78 due N
N-41	N285/ 86 due NNE
N-42	N296/ 87 due NE
N-43	N125/ 71 due SSW
N-44	N110/ 88 due SW
N-45	N136/ subvertical
N-45	N100/ 85 due S
N-46	N305/ 70 due SW
N-47	N118/ 76 due NE

EASTERN SECTOR

Z-4	N312/ 85 due NE
Z-4	N125/ 71 due NE
Z-4	N129/ 70 due NE
Z-7	N118/ subvertical
Z-9	N117/ 80 due SSW
Z-10	N140/ 68 due WSW
Z-11	N170/ 78 due E
Z-11	N343/ 79 due E
D-1	N110/ 62 due SW
D-1	N116/ 68 due SW
D-2	N115/ 75 due SW
D-	N115/ 78 due SW
D-4	N87/ 65 due S
D-4	N150/ subvertical
D-5	N335/ 78 due SW
Y-2	N321/ 87 due SW
Y-2	N327/ 85 due SW
Y-4	N135/ 75 due SW
Y-5	N143/ 64 due WSW
Y-5	N292/ subvertical
Y-8	N295/ 73 due NE
Y-9	N285/ 45 due NE
Y-9	N300/ 69 due NE
Y-10	N340/ 76 due NE
Y-11	N73/ 72 due SSE
Y-12	N80/ 78 due S
Y-12	N25/ 60 due NW
N-13	N283/ 75 due NE
N-14	N138/ 73 due NE
N15	N275/ 86 due S

Appendix – III

This appendix gives the expansion of abbreviations used in the thesis:

qtz - Quartz

plg   Plagioclase

bio - biotite

gt - garnet

hbl   hornblende

cpx - clinopyroxene

opx - orthopyroxene

pyx - pyroxene

En   Enstatite

Fs   Ferrosilite

Wo - Wollastonite

WR - Whole rock